# Investigating the role of hepcidin and iron homeostasis in mycobacterial infection




Rachel Kandt
Brasenose College
University of Oxford

A thesis submitted for the degree of
*Doctor of Philosophy*

Trinity 2015

Word count: ~36,000

**Investigating the role of hepcidin and iron homeostasis in mycobacterial infection**

Rachel Kandt, Brasenose College

Thesis submitted for the degree of Doctor of Philosophy in Clinical Medicine

Trinity Term 2015

## Abstract

Tuberculosis, caused by *Mycobacterium tuberculosis* (*M.tb)* is one of the world's most prevalent infectious diseases. The quest for an effective vaccine and an immune correlate of protection are on going. Previous literature reports links between the iron status of the host and disease severity, but the underlying mechanisms are not clear. Here, a murine model of *M.tb* infection was used to determine the effect of *M.tb* infection on the expression of hepcidin and other genes involved in the regulation of iron homeostasis. Female BALB/c and C57BL/6 mice were infected with *M.tb* Erdman via aerosol. Change in expression of iron-responsive genes was measured by liver qRT-PCR. Bacterial burden was determined in organ homogenates. The effect of iron deficiency on disease outcome was also investigated, where mice fed an iron-deficient or control diet were infected with *M.tb.* To determine whether hepcidin has a role in disease outcome, *Hamp1*$^{-/-}$ mice were also infected with *M.tb.* In the time course experiments, changes in hepcidin kinetics post-*M.tb* infection were observed, which were likely regulated by BMP/SMAD and not IL-6/JAK-STAT signalling. In the iron-restricted diet experiments, iron deficiency did not reproducibly affect bacterial burden. Moreover, deletion of *Hamp1* did not affect outcome of *in vivo M.tb* infection. The data in this thesis indicate that iron homeostasis is altered during *M.tb* infection, but that altering host iron homeostasis by inducing iron deficiency or deleting the hepcidin gene does not compromise the host's ability to control infection.

# Declaration

I hereby declare that all work presented in this thesis is original. All experimental work and data analyses for the work presented here were conducted by the author, with the exception of the following list.

I gratefully acknowledge the help of the following persons:

Elena Stylianou for her help in all the mouse challenge experiments presented in this thesis, as well as in the *in vitro* assays in presented in Chapter 5.

Kristin Griffiths, Hazel Poyntz and Lucy Eddowes for their help with the mouse challenge experiments presented in Chapter 3.

Youlia Beglov for her help in the challenge experiments in Chapters 4 and 5

Lisa Stockdale and Dr Vivek Naranbhai for their help in the iron diet challenge experiments presented in Chapter 5.

Dr Paulo Bettencourt for his help with the *in vitro* experiments in Chapter 5.

OCHRe at the John Radcliffe Hospital in Oxford who processed and prepared the histological sections and stains in Chapters 4 and 5.

Dr Sophie Vaulont developed the *Hamp1*$^{-/-}$ mice used in Chapter 4 and heterozygous breeding pairs were provided by Andy McKie of Kings' College, London.

George Warimwe for his advice on the statistical analyses.

The Sir Richard Stapley Educational Trust for their generous donation towards my second year university fees.

# Acknowledgements

First and foremost I would like to thank my supervisor Professor Helen McShane for her support and guidance throughout my project. Furthermore, I could not have progressed this far without the input of Dr Hal Drakesmith. Secondly, the work in this thesis would not have been possible without Elena Stylianou, who has encouraged and supported me throughout my DPhil, both in and out of the lab. I would also like to thank Lisa Stockdale, Youlia Beglov, Kristin Griffiths and Hazel Poyntz for their help during the challenge experiments. Thanks to Matt O'Shea and Rachel Tanner for their thoughts on the *in vitro* work. Thanks also to the Drakesmith group for their help with the iron side of things and to the rest of the TB group for their support. The animal experiments would not have been possible without the help of the FGF staff.

Thanks to Serena Ding, Natasha Perks, and anyone else in Brasenose HCR who supported me over the last 4 years, as well as my oldest friend Laura Marsden. To my Mum and Dad, for adopting me and giving me a new chance at life. Thank you for pushing me and making me aspire to do things such as a DPhil at Oxford, you are the reason I am who I am today and I would not have had these opportunities without you. Not forgetting my twin, Matt, for the constant stream of insults. Finally, thanks to Ben Bronselaer for encouraging me to do insane bike rides and half marathons to keep me focused during those final few months. You kept a smile on my face even on the toughest days.

# Table of contents

Abstract....2

Declaration....3

Acknowledgements....4

Table of contents....5

List of figures....13

List of tables....17

List of abbreviations....18

1 Introduction....24

1.1 Tuberculosis....24

1.1.1 Overview....24

1.1.2 Global control of TB disease over the years....26

1.1.3 Pathogenesis and immunology of TB infection....28

1.1.4 Symptoms and diagnosis....36

1.1.5 Treatment and drug resistance....37

1.1.6 Vaccination against TB....39

1.1.7 Animal models of TB....42

1.2 Iron....45

1.2.1 Background....45

1.2.2 Systemic iron homeostasis....46

1.2.3 Cellular iron homeostasis ..... 60

1.3 Iron and TB ..... 63

1.3.1 Human studies on TB and iron ..... 63

1.3.2 Animal studies on M.tb and iron homeostasis ..... 63

1.3.3 In vitro studies ..... 64

1.3.4 TB and hepcidin ..... 64

1.3.5 The role of iron in innate immunity ..... 68

1.3.6 Bacterial iron homeostasis as a potential novel target for anti-tubercular agents and vaccines ..... 71

1.4 Aims of the project ..... 72

1.5 Experimental approaches ..... 73

2 Materials and Methods ..... 75

2.1 Animals ..... 75

2.1.1 Mice ..... 75

2.1.2 *Hamp1* $^{-/-}$ mice ..... 75

2.1.3 Animal welfare ..... 75

2.1.4 Custom mouse diets ..... 76

2.1.5 Anaesthesia ..... 76

2.1.6 BCG vaccination ..... 76

2.1.7 Intranasal BCG infection ..... 77

2.1.8 Aerosol *M.tb* infection ..... 77

2.1.9 Extraction of blood for haematological analyses ..... 78

2.1.10 Tail bleeds ..... 78

2.1.11 Analysis of blood/serum products ..... 78

2.1.12 Extraction of organs for qRT-PCR ..... 79

2.1.13 Harvesting of spleen, livers and lungs for histology ..... 79

2.1.14 Histopathological techniques ..... 79

2.1.15 Organ homogenisation and plating for CFU ..... 80

2.1.16 Genotyping of *Hamp1*$^{-/-}$ mice ..... 80

2.1.17 Quantitative real-time PCR (qRT-PCR) ..... 82

2.2 Mycobacteria ..... 85

2.2.1 BCG Pasteur ..... 85

2.2.2 *M.tb* ..... 85

2.2.3 Culture of BCG in liquid broth ..... 85

2.2.4 Freezing down BCG Pasteur stocks ..... 85

2.3 In vitro and ex vivo assays ..... 86

2.3.1 Splenocyte and BCG co-culture experiments ..... 86

2.3.2 THP-1 and BCG co-culture experiments ..... 87

2.3.3 Mycobacterial Growth Inhibition (MGIT) Assays ..... 88

2.4 Statistical analyses ..... 92

3 The effect of mycobacterial infection on murine iron homeostasis ..... 94

3.1 Introduction ..... 94

3.2 Evaluation of the effect of *M.tb* infection on the expression of genes involved in iron homeostasis ..... 96

3.2.1 *M.tb* aerosol infection in mice results in infection of lungs, spleen and liver. BCG vaccination reduces bacterial burden in all three organs. ..... 97

3.2.2 *M.tb* infection affects the expression of genes involved in iron homeostasis ..... 98

3.3 The effect of *M.tb* on hepcidin kinetics in time course studies in BALB/c mice ..... 103

3.3.1 *M.tb* burden increases in lungs and spleen from 24 hours post-infection ..... 103

3.3.2 Hepcidin fluctuates post-infection ..... 106

3.3.3 Changes in hepcidin expression post-*M.tb* infection may be regulated by BMP signalling ..... 106

3.3.4 A role for hypoxia in regulation of hepcidin in TB? ..... 107

3.3.5 Roles for other molecules involved in iron homeostasis ..... 108

3.3.6 Expression of proinflammatory cytokines is altered post-infection ..... 113

3.4 Time course infection studies in C57BL/6 mice ..... 115

3.4.1 Dissemination of *M.tb* occurs earlier in BCG-vaccinated mice 115

3.4.2 Hepcidin fluctuates post-M.tb infection in C57BL/6 mice and is likely regulated by the BMP/SMAD signalling pathway ..... 117

3.4.3 Involvement of other genes involved in iron homeostasis post-*M.tb* infection in C57BL/6 mice ..... 120

3.4.4 Expression of genes encoding inflammatory cytokines increases in unvaccinated mice post-infection ..... 124

3.5 Effect of BCG vaccination of the expression of genes involved in iron homeostasis ..... 127

3.5.1 BCG vaccination and *M.tb* infection have similar effects on hepcidin kinetics ..... 127

3.6 Discussion ..... 131

4 Investigating the effect of *Hamp1* gene deletion in murine *M.tb* infection 140

4.1 Introduction ..... 140

4.2 Characterisation of the *Hamp1*$^{-/-}$ mouse model ..... 142

4.2.1 Confirmation of genotype by gel electrophoresis and qRT-PCR ..... 142

4.2.2 Observations in the abdominal cavities of Hamp1$^{-/-}$ mice ..... 143

4.2.3 Haematological parameters ..... 144

4.2.4 Confirmation of genotype by qRT-PCR ..... 147

4.2.5 Tissue iron accumulation ..... 148

4.3 *M.tb* infection in *Hamp1*$^{-/-}$ mice ..... 149

4.3.1 Deletion of *Hamp1* does not affect outcome of M.tb infection 149

4.3.2 Gene expression analyses ..... 150

4.4 Discussion..... 156

5 Consequences of dietary iron restriction on susceptibility to mycobacteria in mice ..... 166

5.1 Introduction ..... 166

5.2 The effect of altering iron availability on growth of BCG *in vitro* .. 167

5.2.1 Optimisation of mycobacterial growth inhibition assays ..... 167

5.2.2 Mycobacterial growth inhibition tube (MGIT) assay ..... 169

5.3 Haematological characterisation of the iron-deficient mouse model . 171

5.3.1 Dietary iron restriction alters haematological parameters ..... 171

5.3.2 Dietary iron restriction affects the expression of genes involved in iron homeostasis ..... 174

5.3.3 Dietary iron restriction affects splenic iron accumulation..... 179

5.4 The effect of dietary iron restriction on BCG infection ..... 180

5.4.1 Experimental outline ..... 180

5.4.2 Dietary iron restriction does not affect growth of BCG in this in vitro infection model..... 180

5.4.3 Haematological parameters are altered by BCG infection ..... 181

5.4.4 Gene expression analyses ..... 184

5.5 The effect of dietary iron restriction on *M.tb* infection – pilot experiment ..... 188

5.5.1 Experimental outline ..... 188

5.5.2 Mice fed an iron-restricted diet control *M.tb* as well as mice fed a control diet ..... 189

5.5.3 The effect of dietary iron restriction on post-*M.tb* infection gene expression analyses ..... 190

5.6 Does a diet containing 18ppm of ferric iron induce iron deficiency? 193

5.6.1 Experimental outline ..... 193

5.6.2 Switching mice to a diet containing 18ppm may reverse iron deficiency induced by severe dietary iron restriction ..... 193

5.7 The effect of dietary iron restriction on *M.tb* infection: experiment 1196

5.7.1 Experimental outline ..... 196

5.7.2 Dietary iron restriction reduces *M.tb* growth ..... 197

5.7.3 Gene expression analyses ..... 197

5.7.4 Gene expression analyses: genes involved in immune reponse 203

5.8 The effect of dietary iron restriction on *M.tb* infection: repeat ..... 205

5.8.1 Experimental outline ..... 205

5.8.2 Dietary iron restriction did not affect the growth of *M.tb in vivo* .....206

5.8.3 Post-*M.tb* infection gene expression analyses ..... 207

5.8.4 Proinflammatory cytokine expression in *M.tb*-infected iron deficient mice ..... 212

5.9 Discussion ..... 214

6 Conclusions and future directions ..... 223

7 Appendix ..... 231

8 References ..... 234

# Table of figures


Figure 1.1 Estimated TB prevalence from 1990-2014.....27

Figure 1.2 Pathogenesis of TB disease.....28

Figure 1.3 A tuberculous granuloma.....36

Figure 1.4 Intestinal iron absorption.....47

Figure 1.5 Recyling of iron by macrophages.....51

Figure 1.6 Regulation of systemic iron homeostasis by hepcidin.....54

Figure 1.7 Regulation of hepcidin synthesis.....56

Figure 1.8 Regulation of hepcidin transcription by inflammation and iron..59

Figure 1.9 The IRE/IRP regulatory system.....61

Figure 3.2.1 CFU burden in unvaccinated and BCG-vaccinated mice post-*M.tb* infection.....98

Figure 3.2.2 The effect of *M.tb* infection and BCG vaccination on the expression of genes involved in iron homeostasis.....102

Figure 3.3.1 CFU time course in *M.tb*-infected mice.....105

Figure 3.3.2 Hepatic gene expression analyses in post-*M.tb* infection time course.....112

Figure 3.3.3 Immune gene expression analyses in the liver in a post-*M.tb* infection time course.....114

Figure 3.4.1 CFU time course in *M.tb*-infected C56BL/6 mice.....116

Figure 3.4.2 Hepatic gene expression analyses in post-*M.tb* infection time course..... 123

Figure 3.4.3 Immune gene expression analyses in liver in a post-*M.tb* infection time course ..... 126

Figure 3.5.1 Hepatic gene expression analyses in C57BL/6 mice post-BCG vaccination..... 130

Figure 4.2.1 Confirmation of genotype by PCR ..... 142

Figure 4.2.2 Initial observations in *Hamp1*$^{-/-}$ abdominal cavity..... 143

Figure 4.2.3 Full blood counts in *Hamp1*$^{-/-}$ mice and controls..... 146

Figure 4.2.4 Confirmation of genotype by qRT-PCR..... 147

Figure 4.2.5 Iron deposition in *Hamp1*$^{-/-}$ mice ..... 148

Figure 4.3.1 Aerosol infection of *Hamp1*$^{-/-}$ mice with *M.tb* ..... 150

Figure 4.3.2 Gene expression in livers of *Hamp1*$^{-/-}$ mice challenged with *M.tb.* ..... 155

Figure 5.2.1 *In vitro* BCG killing assays ..... 169

Figure 5.2.2 *In vitro* mycobacterial growth inhibition assays..... 170

Figure 5.3.1 Haematological parameters in mice fed an iron-deficient diet .. 174

Figure 5.3.2 The effect of dietary iron restriction on gene expression ..... 178

Figure 5.3.3 Perls staining of lungs, liver and spleen sections of mice fed an iron-deficient or control diet ..... 179

Figure 5.4.1 Experimental design: BCG infection of iron-deficient mice ..... 180

Figure 5.4.2 Bacterial burden in iron-deficient mice infected with BCG..... 181

Figure 5.4.3 The effect of dietary iron restriction in BCG infection on haematological parameters ..... 184

Figure 5.4.4 Expression of genes involved in regulation of iron homeostasis, post BCG *i.n.* infection ..... 188

Figure 5.5.1 Pilot iron diet experimental design..... 189

Figure 5.5.2 Effect of restricting dietary iron availability on susceptibility to *M.tb.* ..... 190

Figure 5.5.3 Effect of restricting dietary iron availability on gene expression post-*M.tb* infection..... 192

Figure 5.6.1 Diet switching experimental outline ..... 193

Figure 5.6.2 The effect of switching from 4-18ppm diet on the expression of genes involved in iron metabolism. ..... 195

Figure 5.7.1 Infection of iron-deficient mice with *M.tb* – experimental outline ..... 196

Figure 5.7.2 Infection of iron-deficient mice with aerosolised *M.tb*..... 197

Figure 5.7.3 The effect of restricting dietary iron availability in *M.tb* infection on the expression of genes involved in iron metabolism. ..... 202

Figure 5.7.4 Effect of restricting dietary iron availability in *M.tb* infection on the expression of genes encoding pro-inflammatory cytokines.. 204

Figure 5.8.1 Infection of iron-deficient mice with *M.tb* – experimental outline ..... 206

Figure 5.8.2 Infection of iron-deficient mice with aerosolised *M.tb* - repeat..... 207

Figure 5.8.3 Gene expression analyses in iron-deficient mice infected with *M.tb*. ..... 211

Figure 5.8.4 Effect of restricting dietary iron availability in *M.tb* infection on the expression of genes encoding pro-inflammatory cytokines:repeat. ..... 213

# List of tables

Table 1 List of inventoried TaqMan Gene Expression Assays (Applied Biosystems) used in qRT-PCR. ..... 84

Table 2 Table of Reagents ..... 232

Table 3 Table of solutions ..... 233

# List of abbreviations:

| | |
|---|---|
| ABC | ATP-binding cassette |
| ACO2 | mitochondrial aconitase 2 |
| Ag85A | antigen 85A |
| Ag85B | antigen 85B |
| APC | antigen-presenting cell |
| ATP | adenosine triphosphate |
| B2M | β-2 microglobulin |
| BCG | Bacille Calmette-Guérin |
| BMP | bone morphogenetic protein |
| BSL3 | biosafety level 3 |
| bTB | bovine tuberculosis |
| cDNA | complementary DNA |
| CD | cluster of differentiation |
| CFP | culture filtrate protein |
| CFU | colony forming units |
| CTL | cytotoxic lymphocyte |
| CXCL | C-X-C chemokine ligand |
| CXCR | C-X-C chemokine receptor |
| DC | dendritic cell |
| DC SIGN | dendritic cell-specific intracellular adhesion molecule – grabbing non-integrin |
| dCytB | duodenal cytochrome B |

| | |
|---|---|
| DFO | desferroxamine |
| DMT1 | divalent metal transporter 1 |
| DNA | deoxyribonucleic acid |
| DOTS | directly-observed therapy short course |
| ELISA | enzyme-linked immunosorbant assay |
| ELISpot | enzyme-linked immunosorbant spot |
| EM | environmental mycobacteria |
| EPI | expanded program on immunisation |
| EPO | erythropoietin |
| ERFE | erythroferrone |
| ESAT-6 | early secreted antigenic target 6 |
| FAC | ferric ammonium citrate |
| GSK | GlaxoSmithKline |
| HAMP | hepcidin antimicrobial peptide |
| HCP-1 | haem carrier protein-1 |
| HCT | haematocrit |
| HFE | hereditary haemochromatosis protein |
| HGB | haemoglobin |
| HJV | haemojuvelin |
| HIV | human immunodeficiency virus |
| HO-1 | haem oxygenase-1 |
| *i.d.* | *intradermal* |
| IFN-$\gamma$ | interferon gamma |
| IGRA | interferon gamma release assay |
| *i.n.* | *intranasal* |

| | |
|---|---|
| iNOS | inducible nitric oxide synthase |
| IRAK | interleukin-1 receptor associated kinase |
| IRE | iron-responsive element |
| IRP | iron regulatory protein |
| *i.v.* | *intravenous* |
| JAK | janus activated kinase |
| LIP | labile iron pool |
| *L.monocytogenes* | *Listeria monocytogenes* |
| LPS | lipopolysaccharide |
| ManLAM | mannosylated lipoarabinomannan |
| MCH | mean cell haemoglobin |
| MCHC | mean cell haemoglobin concentration |
| MCV | mean cell volume |
| MDR-TB | multi-drug resistant TB |
| MHC | major histocompatibility complex |
| *M. bovis* | *Mycobacterium bovis* |
| mRNA | messenger RNA |
| *M.smegmatis* | *Mycobacterium smegmatis* |
| *M.tb* | *Mycobacterium tuberculosis* |
| MVA | modified vaccinia virus ankara |
| NF-kB | nuclear factor kappa beta |
| NHP | non-human primate |
| NK | natural killer |
| NO | nitric oxide |
| NRAMP | natural resistance-associated macrophage protein |

| | |
|---|---|
| PAMP | pathogen-associated molecular pattern |
| PAS | p-amino salicylic acid |
| PBS | phosphate buffered saline |
| PCBP1 | poly (rC)-binding protein 1 |
| PCR | polymerase chain reaction |
| PLT | platelets |
| PMA | phorbol myristate acetate |
| PPD | purified protein derivative |
| ppm | parts per million |
| PRR | pattern recognition receptor |
| RBC | red blood cell |
| RD | region of difference |
| RDW | red cell distribution width |
| RNA | ribonucleic acid |
| RNI | reactive nitrogen intermediates |
| ROI | reactive oxygen intermediates |
| RNA | ribonucleic acid |
| qRT-PCR | quantitative real time polymerase chain reaction |
| *s.c.* | *sub cutaneous* |
| SIV | simian immunodeficiency virus |
| STAT | signal transducer and activator of transcription |
| *S.typhi* | *Salmonella typhi* |
| TB | tuberculosis |
| TCR | T cell receptor |
| TDR-TB | totally drug resistant tuberculosis |

| | |
|---|---|
| TFR1 | transferrin receptor 1 |
| Th | T helper |
| TLR | toll-like receptor |
| TMPRSS6 | transmembrane protease, serine 6 |
| TNF-α | tumour necrosis factor |
| TST | tuberculin skin test |
| UTR | untranslated region |
| *V. Vulnificus* | *Vibrio vulnificus* |
| WBC | white blood cell |
| WHO | World Health Organisation |
| WT | wild type |
| XDR-TB | extensively-drug resistant tuberculosis |
| ZN | Ziehl-Neelsen |

# Introduction

# 1 Introduction

## 1.1 Tuberculosis

### *1.1.1 Overview*

Tuberculosis (TB) is the second leading cause of death worldwide by an infectious agent, causing over 1 million deaths per annum [1]. It is estimated that one third of the world's population (around 2 billion people) is latently infected with the causative agent, *Mycobacterium tuberculosis (M.tb),* but 90% of infected people are not at risk of developing active disease since they develop an immune response that successfully contains the bacteria within a granuloma. Currently, the only licensed TB vaccine is BCG, which was developed by Calmette and Guérin nearly a century ago [2]. This vaccine was produced by serial passage of a *Mycobacterium bovis* (*M.bovis)* isolate until it was no longer virulent. However, BCG provides variable efficacy worldwide. Therefore, research to find a more effective vaccine is paramount. Primary infection with *M.tb* leads to active disease in approximately 10% of those infected, and the chance of reactivation from latent disease to active disease in a healthy individual is 5 to 10% [3]. It is as yet unclear why some people are at risk of developing active disease and some are not. One example of the varying susceptibility to TB disease is the accidental administration of live *M.tb* instead of BCG vaccine to German infants in 1926. Whilst the majority of these children became very ill, some of them appeared to be unaffected [4].

Immune-deficiency caused by infection with human immunodeficiency virus (HIV), poor nutrition, old age, and alcohol, are risk factors for the most common form of TB disease, pulmonary TB, which accounts for 70% of TB cases [5]. TB causes up to a quarter of HIV/AIDS related deaths [6]. Consequently, TB is endemic in areas with high incidence of HIV such as Asia and Africa, but immigration is also leading to spread throughout more western countries and into Europe. In addition, drug non-compliance has resulted in the emergence of multi-, extensively- and totally-drug resistant TB (MDR-TB, XDR-TB and TDR-TB, respectively). Drug-resistant strains develop as a result of drug non-compliance due to the lengthy treatment regime. MDR-TB is defined as TB disease caused by strains of *M.tb* resistant to the two most commonly used drugs for treatment of TB, isoniazid and rifampicin [1]. XDR-TB can be defined as disease cause by a strain of *M.tb* that is resistant to the two aforementioned drugs, in addition to fluoroquinolone and any second-line injectable drug. Cases of TDR-TB have been described as infection with strains that do not respond to any drugs currently known to treat TB. Worryingly, a total of 92 countries had reported at least one case of XDR-TB by 2013 and around 10% of these countries had more than ten cases in one year [1]. In addition to the economic burden of drug-resistant TB, emergence of totally drug resistant strains could be potentially devastating worldwide. Accordingly, the World Health Organisation (WHO) has just adopted a post-2015 plan to eliminate TB as a global epidemic by 2035 [7]. The aims of the plan are to change how countries organise their TB prevention programs, as well to increase research into new drugs, diagnostic tools, and to continue the quest to find an effective vaccine.

### *1.1.2 Global control of TB disease over the years*

The discovery of *M.tb* by Robert Koch in 1882, followed by the discovery of tuberculin in 1890, BCG in 1921, and the first anti-tuberculous drugs in 1943, led to a decrease in TB mortality rates in the early to mid 20$^{th}$ century. For example, mortality rates in the Netherlands decreased dramatically from 2000/100, 000 in 1901 to 10 in every 100,000 in 1903 [8]. In 1974, BCG was included in the Expanded Program on Immunisation (EPI) schedule.

Despite the decline in TB seen at the beginning of the 20$^{th}$ century, in the 1980s, the onset of the AIDs/HIV pandemic led to an increase in TB, which placed a large strain on public health. In 1991, the WHO set up a strategy to control TB, the directly observed therapy short-course (DOTS) strategy, with the aim of decreasing global TB burden. This strategy focuses on effective diagnosis of active TB, and directly observed treatment in order to reduce drug-resistant cases. The DOTS strategy is cost-effective and reduces TB mortality. Since 2000, the Stop TB Partnership has been issuing five and ten year global plans to raise awareness of TB and to prevent global spread of the disease. The first plan, which covered 2001-2005 aimed to improve research and development, as well as focusing on areas where TB is most endemic. This plan focused on the expansion of the DOTS strategy and the emergence of drug-resistant strains of TB, as well as TB in HIV infection. In 2006, the partnership launched the Global Plan to Stop TB 2006-2015 at the World Economic Forum. This $56 billion plan represented a three-fold increase in investment into TB control compared with the 2001-2005 plan, a success in itself. In addition, this plan was designed to work in combination with the objectives of the Millennium

Development Goals for TB, set by the United Nations, in order to reach the target of halving TB prevalence and deaths from 1990 levels by 2015, as illustrated in Figure 1.1. Between 2011 and 2015, a third Stop TB plan was set up with the primary aim of improving treatment and the development of new diagnostic tests. Finally, as mentioned above, the WHO created a post-2015 strategy with the aim of elimination TB as a global epidemic by 2035. The newest Stop TB plan, the Global Plan to Stop TB 2016-2020, aims to make global TB efforts more ambitious over the coming years, primarily by changing the way the TB programs are currently run, and by increasing research and development in order to reach the goals set in the WHO post-2015 Global TB Strategy.

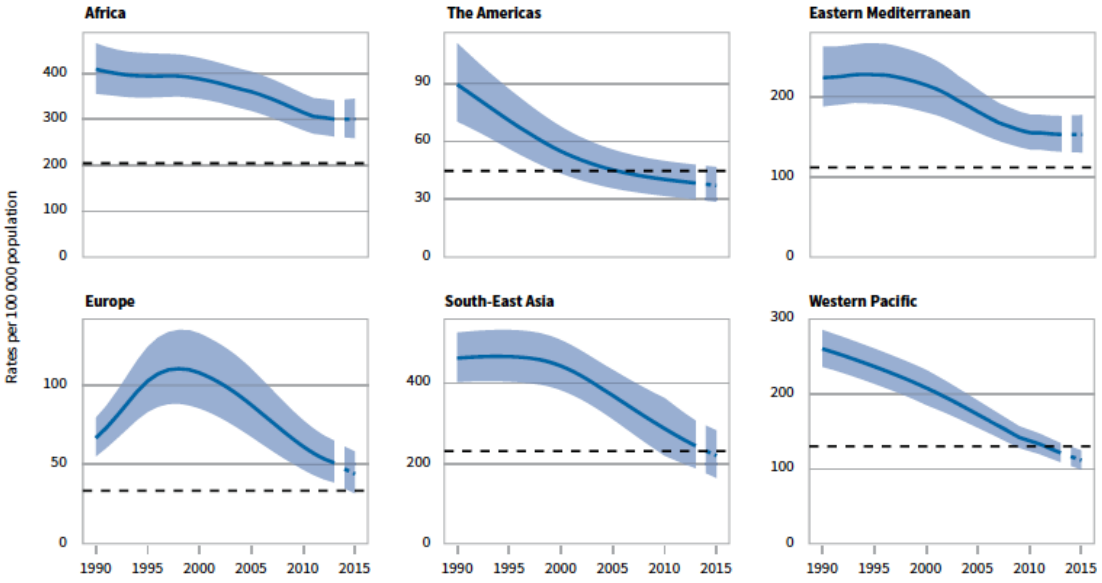


**Figure 1.1 Estimated TB prevalence from 1990-2014.** Shaded areas represent uncertainty bands, with horizontal dashed lines representing the Stop TB target which is a 50% reduction in the 1990 rates by 2015. Dashed lines within the uncertainty bands represent projected rates up to 2015. Taken from [7]

### 1.1.3 *Pathogenesis and immunology of TB infection*

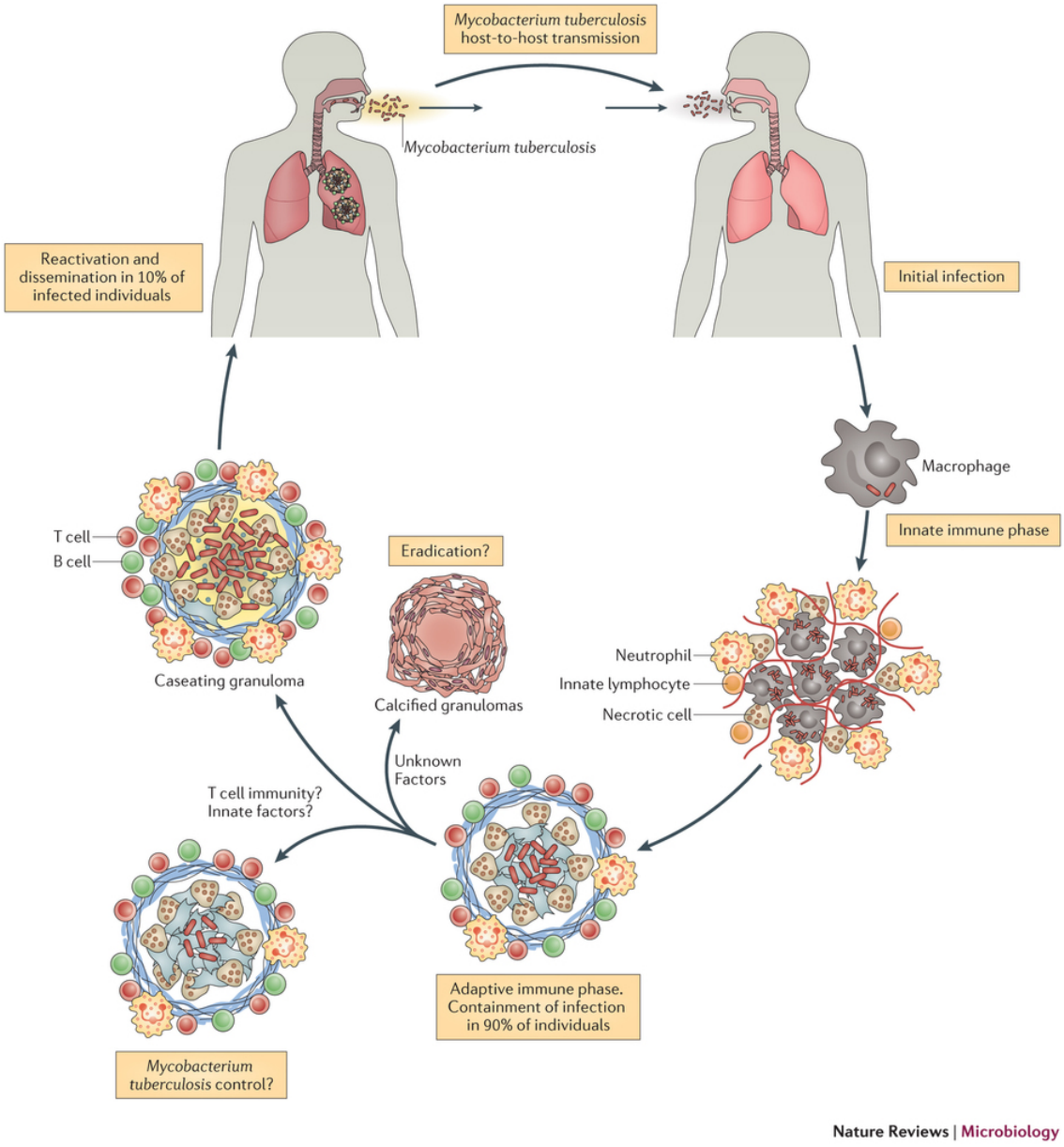


**Figure 1.2 Pathogenesis of TB disease.** An individual is infected with TB when they inhale aerosolised droplets containing *M.tb* bacilli, which have been generated by an individual with active TB disease (by coughing, for example). Following inhalation of the bacilli, an innate immune response occurs characterised by the recruitment of inflammatory cells to the lung. Bacteria disseminate in DCs to the mediastinal lymph node, where antigenic peptide is presented to T cells, triggering the proliferation of antigen-specific T cells, and their recruitment to the lungs. Here, a number of immune cells including T cells, B cells, activated macrophages, and epitheloid cells join to form granuloma. In the majority of cases (90%), effective containment of bacilli within granuloma results in latent *M.tb* infection, which is asymptomatic. However, a small percentage of people will then go on to develop active disease, which can lead to break down of the granuloma and resultant release of bacilli. These can then be transmitted to new individuals via coughing. Taken from Nunes-Alves et al; Nature Reviews Microbiology 12 (4), 289-99 (2014) [9].

#### *1.1.3.1 Pathogenesis*

TB is caused by aerosol infection with the acid-fast, rod-shaped bacillus *M.tb* [10]. Transmission occurs through the inhalation of infected droplets expelled (by coughing, for example) from a patient with active pulmonary TB. *M.tb* is a slow growing organism, with a replication time of approximately 20 hours [11]. It has a complex cell wall, making it very robust and difficult to treat. The thick layer of hydrophobic mycolic acids making up most of the cell wall increase resistance to degradation by lysosomal enzymes, which are released by infected host cells. Based on experimental models, TB pathogenesis can be split into 4 well-defined stages (illustrated in Figure 1.2):

1. Inhalation of *M.tb* into the airways and alveoli, followed by phagocytosis by resident alveolar macrophages.
2. Recruitment of inflammatory cells such as neutrophils, dendritic cells (DCs) and monocytes, in response to secretion of IL-12 and IL-18 by alveolar macrophages.
3. Control of mycobacterial replication. Activation of an adaptive immune response results in an influx of antigen-specific T cells and the formation of granuloma, which contain *M.tb* during latent infection.
4. Post-primary TB. 10% of individuals infected with latent *M.tb* infection eventually develop active disease as a result of mycobacterial persistence combined with break down of granuloma, leading to dissemination of the bacteria.

#### *1.1.3.2 Innate immune response*

The pathogenesis of TB disease is well reviewed by Zuniga et al [12] and O'Garra et al [5]. Inhalation of *M.tb* bacilli into the lungs stimulates an innate immune response characterised by an influx of phagocytic cells such as resident alveolar macrophages, neutrophils, DCs and natural killer (NK) cells, which are thought to be the first line of defence against *M.tb.* NK cells bind to damaged or infected cells, releasing cytotoxic granules on their surface in order to induce apoptosis and killing of *M.tb.* The killing capacity of these innate immune cells often influences the outcome of infection. Mycobacterial killing is often mediated by antimicrobial effector functions of macrophages, such as the release of reactive oxygen species (ROS) and reactive nitrogen intermediates (RNI).

Identification of *M.tb* by the host is through the recognition of pathogen-associated molecular patterns (PAMPs), which are components of pathogens, such as mycolic acid in the *M.tb* cell wall, lipopolysaccharide (LPS), or bacterial RNA and DNA. PAMPs are recognised by specialised host cell receptors known as pattern recognition receptors (PRR), such as mannose receptors, which induce phagocytosis of *M.tb* [13]. Toll like receptors (TLRs) are a family of PRRs present on or within antigen presenting cells (APCs). TLR2, TLR4, and TLR9 have been shown to be particularly important in *M.tb* detection [4, 14]. For example, TLR4 is the receptor for a heat shock protein 60/65, which is secreted by *M.tb.* TLR4-deficient C3H/HeJ mice are more susceptible to *M.tb* than controls, as LPS recognition by TLR4 regulates the induction of pro-inflammatory cytokines [15]. The myeloid differentiation factor 88 (Myd88)/IRAK signalling pathway is activated by activated TLRs, leading to

the activation of transcription factor NFkB and subsequent transcription of inflammatory cytokines [16, 17].

Following recognition by macrophages and monocytes, *M.tb* is phagocytosed into a phagosome. Normally, the bacteria-containing phagosome would fuse with a lysosome, forming a phagolysosome, in which the bacteria are degraded by intralysosomal acidic hydrolases. However, *M.tb* is able to evade destruction within the phagosome. It is able to inhibit phagosome maturation and phagolysosome fusion, inhibiting acidification, thereby prolonging its survival. The exact process by which *M.tb* can do this has been investigated extensively and it is thought that *M.tb* inhibits the recruitment of late endosomal protein Rab7, which is involved in the formation of lysosomes [18] (reviewed in [13]). Inhibition of phagosome maturation not only inhibits killing of *M.tb,* but also impairs the presentation of antigen on major histocompatibility complex (MHC) II molecules on the cell surface (MHC proteins are proteins expressed on the surface of immune cells which are involved in recognition of antigen by T cells). Persistence of *M.tb* as a result of inhibition of phagolysosome fusion can be overcome by autophagy of host cells. Autophagy is a process by which a cell is able to clean up surplus or damaged components by sequestering them into an autophagosome for degradation. It has recently been shown to play a role in the elimination of *M.tb* during the innate immune response, and is stimulated by IFN-$\gamma$ in *M.tb* infected macrophages [19]. *M.tb* is also able to induce apoptosis of host cells [20].

Cytokines play an important role in the recruitment of immune cells to the site of infection. Once peripheral immune cells such as monocytes, neutrophils and

DCs have been recruited to the site of infection, *M.tb* that have not been killed in the first stage of infection are able to infect new cells and grow logarithmically. Infected cells secrete antimicrobial peptides, chemokines, and cytokines such as TNF-α and IL-6, which aid in the formation of granuloma. Some bacterial killing occurs here, since TNF-α stimulates apoptosis of infected cells. TNF-α, which is released by macrophages, neutrophils, DCs and T cells, mediates early inflammatory responses, primarily by stimulating release of IL-1 and IL-6. TNF-α is also involved in control of *M.tb* growth, as well as maintenance of granuloma. Studies in TNF-α gene-disrupted mice have revealed the importance of TNF-α in *M.tb* infection. Mice treated with anti-TNF-α antibody, or with TNF-α gene disruption have increased susceptibility to mycobacterial infection [21, 22]. Moreover, a five-fold increase in reactivation of latent *M.tb* infection has been observed in humans treated with anti-TNF therapy for rheumatoid arthritis [23], illustrating the importance of this cytokine in the control of latent infection [22].

DCs are specialised APCs involved in linking innate and adaptive immune responses. They also express PRRs to aid in recognition and uptake of *M.tb,* including the unique DC-specific intracellular adhesion molecule-grabbing non-integrin (DC-SIGN) receptor, which binds to mannosylated lipoarabinomannan (ManLAM) on *M.tb.* Infected DCs migrate to draining lymph nodes of the lung 8-12 days post-infection, under the influence of IL-12(p40)/IL-12(p70), CCL19 and CCL21. Here, they present antigenic peptide to naïve $CD4^+$ T cells to initiate an adaptive immune response.

#### *1.1.3.3 Adaptive immune response*

If the innate immune response is not sufficient enough to control an invading pathogen, initiation of an adaptive immune response occurs, resulting in the activation of cells involved in the adaptive immune response. Development of an effective adaptive immune response is vital for inhibition of *M.tb* replication and for the formation of granuloma.

In order to develop effector T cell responses, *M.tb* must disseminate to the lymph nodes, often in migrating DCs via the upregulation of CCR7 [24]. Naïve T cells are those that have not yet encountered any foreign antigen. They often encounter foreign antigen in the lymph nodes, where APCs present *M.tb* antigens on an MHC molecule. There are 2 classes of MHC molecules involved in presentation of antigen, class I and class II MHC. Antigen that is present in the cytosol of host cells is presented to $CD8^+$ T cells on MHC class I molecules. Class II MHC molecules bind to peptides obtained from cellular vesicles, and present to $CD4^+$ T cells [25]. Since *M.tb* is located inside the phagosome, the majority of antigen presentation occurs via class II MHC, predominantly inducing a $CD4^+$ T cell response [26]. Interestingly, it has also been shown that *M.tb* is able to perforate the phagosomal membrane, potentially releasing antigenic peptide into the cytoplasm so it can enter the class I processing pathway, to be presented to $CD8^+$ T lymphocytes [27]. Glycolipid antigens from the *M.tb* cell wall are presented by APCs in the CD1 family, which present antigen via CD1 molecules to CD1-restricted cells ($\alpha\beta$ T cells lacking CD4 and CD8 receptors), mounting an important part of host immune response against *M.tb*.

In order to differentiate, as well as being activated by antigen presented on APCs, T cells must receive a second signal by co-stimulatory molecules [28]. Co-stimulatory molecules such as B7 and CD40 on the APC, must bind to CD28 and CD40L respectively, on T cells. Co-stimulation combined with the release of IL-2 from the activated T cell results in the proliferation of these antigen specific T cells. Naïve $CD4^+$ cells can develop into T helper 1 (Th1), T helper 2 (Th2), T helper 17 (Th17) or regulatory T (Treg) cells. In *M.tb* infection, T cells activated by the adaptive immune system are generally of the helper T cell type. This is because activated DCs secrete IL-12, which induces IFN-γ secretion in natural killer (NK) cells. Priming of $CD4^+$ T cells in the presence of IL-12 and IFN-γ leads to differentiation into a Th1 cell. A Th1, rather than a Th2 response, is critical for protection against TB [11]. There is a wealth of evidence showing that $CD4^+$ T cells are critical in the control of *M.tb*, the prime example being increased risk of TB disease in HIV infection, which is characterised by a reduction in $CD4^+$ T cells [29]. Once activated, T cells migrate to the lungs around 15-18 days post-infection [30].

Evidence shows that $CD8^+$ T cells are also important in *M.tb* infection [31, 32]. $CD8^+$ effector cells are cytotoxic lymphocytes (CTL), which are able to kill host cells through Fas ligand dependent and independent mechanisms. Differentiated $CD8^+$ T cells migrate to the lungs, where they encounter antigen presented on class I MHC [32]. They produce IFN-γ and TNF-α, but can also release cytotoxic enzymes such as perforin and granzymes, which damage host cells by inducing apoptosis. The role of IFN-γ in *M.tb* infection has been extensively studied, as it is critical in the regulation of T cell responses during *M.tb*

infection. Stimulated by IL-12, IFN-γ is released from $CD4^+$ and $CD8^+$ T cells, as well as NK cells, where it activates macrophages and induces further cytokine production in order to reduce mycobacterial replication [5]. It also activates bactericidal factors such as inducible nitric oxide synthase (iNOS), leading to the production of RNI. In support of this, IFN-γ knockout mice are more susceptible to *M.tb* infection [33], and humans with defective IFN-γ-related genes are more susceptible to environmental mycobacteria (EM) [23]. Once activated, antigen-specific T cells migrate to the lungs in a chemokine-dependent manner. Chemokines such as CCL2, CCL3, CCL5, CXCL8 and CXCL10 are also critical in the recruitment of cells to the site of infection, for the formation of granuloma [34, 35]. Granuloma are characterised by aggregation of activated T cells and infected macrophages containing the *M.tb*, which, if stable, may result in a latent *M.tb* infection. These granuloma are the hallmark of effective containment of latent *M.tb* infection.

A final stage of pathogenesis occurs if the host immune system fails to control bacterial growth. Around 10% of those infected with latent *M.tb* infection will progress to this stage. In reactivation, caseous necrosis begins to occur in the previously protective granuloma. Cells are no longer able to contain *M.tb* so it escapes to the extracellular environment and may spread to other parts of the lung and be further disseminated throughout the body. In addition, damage of nearby bronchi may result in transmission of infectious aerosol droplets by the infected individual through coughing [12].

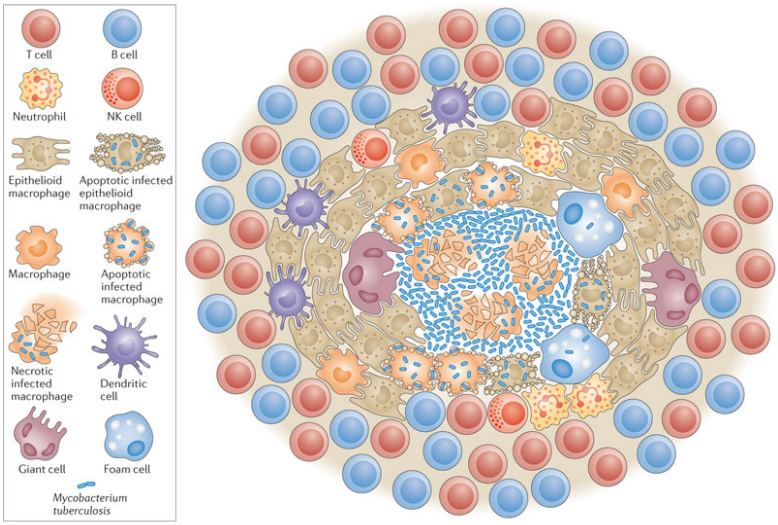


**Figure 1.3 A tuberculous granuloma.** The granuloma is a highly organised aggregate of epitheloid macrophages, which can fuse into multinucleated giant cells or differentiate into foamy macrophages, the latter of which often accumulate at the rim of the necrotic centre of the granuloma. Foam cells and multinucleated giant cells often do not contain bacteria, as bacteria are mostly present in the central necrotic regions of the granuloma near the dying macrophages. The granuloma also contains other cell types such as neutrophils, DCs, B cells, T cells, NK cells and fibroblasts, which are surrounded by epithelial cells at the edge of the granuloma. From Ramakrishan; Nature Reviews Immunology 12, 352-366 (2014) [36]

### *1.1.4 Symptoms and diagnosis*

Symptoms of active TB disease include night sweats, fever, anorexia, lethargy and cough with bloody sputum. Rapid and accurate diagnosis of TB is critical in order to reduce disease transmission. However, a large proportion of suspected cases are in endemic countries with low income where funding is not available for advanced diagnostic tests. A range of diagnostic tests are currently available, although some of these tests are not definitive. Active TB disease can be diagnosed by culture or sputum microscopy, where acid-fast bacilli are stained by Ziehl-Neelsen (ZN) staining, although the latter cannot distinguish drug sensitivity. The WHO have recently endorsed the XPert MTB/RIF automated PCR-based test, which detects both presence of *M.tb* in sputum, as

well as rifampicin resistance. This test is the fastest yet, giving results in just a few hours, however global deployment is currently limited by cost [37]. For diagnosis of latent *M.tb* infection, in the traditional tuberculin skin test (TST), purified protein derivative (PPD), a mixture of antigens of *M.tb*, is injected intradermally, and the response to these antigens is measured several days later. The size of the swelling predicts the patient's likelihood of being infected with *M.tb.* However, this test is unable to distinguish between *M.tb* infection and BCG vaccination, as some of the antigens in PPD are also present in the BCG vaccine. Other, more specific diagnostic tools include the interferon (IFN)–γ release assays (IGRAs), such as the T-Spot, or enzyme linked immunosorbant assays (ELISAs), such as Quantiferon ELISAs, both of which measure the amount of IFN-γ released in response to a range of relatively *M.tb*-specific antigens (early secretory antigenic target-6 (ESAT-6), culture filtrate protein-10 (CFP-10), and additional TB7.7 in the Quantiferon). IGRAs are not confounded by BCG vaccination or exposure to EM since the antigens in the IGRA are not present in BCG or most EM. However, IGRAs are more expensive and technical than TSTs.

### *1.1.5 Treatment and drug resistance*

The aims of TB treatment are to 1) cure the disease in order to improve quality of life for the patient, 2) reduce transmission of *M.tb* to others, 3) prevent relapse of TB and 4) prevent the spread of drug resistant TB.

The course of treatment for TB is dependent on whether a patient has active or latent *M.tb* infection, and their degree of risk of activation of that latent

infection [38]. Following a diagnosis of active pulmonary TB, a standard 6-month course of antibiotics is recommended by the WHO [39]. This regime compromises an intensive 2-month course of first line drugs isoniazid, rifampicin, pyrazinamide and ethambutol, followed by isoniazid and rifampicin for a further 4 months. Treatment of drug-sensitive TB has a high success rate if medication is taken correctly, with cure rates of 90-95% [40]. Therefore, in order to prevent non-compliance and emergence of drug-resistant strains, this regime should be administered under the DOTS strategy, where patients must be observed taking their medication [41]. Non-compliance not only occurs due to the lengthy duration of treatment, but also because the drugs have unpleasant side effects such as hepatotoxicity. As has already been mentioned, the global problem of TB disease is also confounded by the emergence of drug-resistant strains of *M.tb.* The fast spontaneous mutation rate of *M.tb*, as well as patients not complying with treatment have contributed to this [42]. According to the WHO Global Drug Resistance Surveillance Project conducted between 2002 and 2007, 17% of new cases had resistance to at least one of the usual anti-tuberculous drugs, and 3.3% of TB cases in 2009 were MDR [38]. As described above, MDR-TB is defined as *M.tb* which is resistant to the two most commonly used drugs for treatment of TB, isoniazid and rifampicin [43]. Average treatment for MDR-TB is for two years, and consists of up to 10 drugs and continued treatment for months after the patient is smear negative to ensure complete clearance of the bacterium. XDR-TB is TB disease with a strain of *M.tb* which is resistant to the two aforementioned drugs, in addition to fluoroquinolone and any second-line injectable drug. Therefore, XDR-TB is extremely difficult to treat and has stimulated research into new anti-tuberculous drugs.

### *1.1.6 Vaccination against TB*

One key strategy to reduce the incidence of TB is prophylactic immunisation. Alternatively, a therapeutic or post-exposure vaccine could be useful for the infected population as an alternative or adjunct to antibiotic treatment. BCG was developed by Calmette and Guérin by the serial passage of an *M.bovis* isolate until it lost the region of difference (RD)-1 locus, responsible for virulence [2]. BCG was first administered as an oral vaccine in 1921 [44]. Today, it is given intradermally (*i.d.)* usually in the upper arm, resulting in a pus-filled lesion at the vaccination site until it heals and forms a scar, which is useful evidence of vaccination status. Since the discovery of BCG, a number of clinical trials have evaluated the global efficacy of the vaccine, which ranges between 0 and 80% depending on geographical location. Efficacy against pulmonary disease seems to be lowest in areas where disease is more prevalent, such as sub-Saharan Africa, and in those countries with closer proximity to the equator. One explanation of the variable efficacy of BCG is that people living in areas with decreased efficacy also have increased exposure to EM, which may interfere with the protective mechanisms of BCG, as prior exposure to mycobacterial antigens may induce mycobacterial immunity and therefore immunity against the vaccine itself [44]. It has also been suggested that differences in vaccine strain or storage, nutritional factors, genetics factors or maternal immunology might also affect vaccine efficacy. However, there has been no evidence thus far to conclude that any of these account for a substantial component of the varying efficacy of BCG.

Although BCG provides variable efficacy against pulmonary TB, which is the greatest cause of TB-related morbidity and mortality worldwide [45], it does confer some protection against disseminated TB and TB meningitis in infants, which is why it is still given to infants in epidemic areas as part of the WHO EPI schedule [46]. Babies born to HIV-positive mothers should not be vaccinated until their HIV status is known. Vaccine efficacy can wane with age but re-vaccination of adolescents who were vaccinated at birth has been shown to be ineffective [47, 48].

Since BCG already offers some protection against mycobacterial disease, it is likely that a novel TB vaccine would be designed to include BCG in an improved strategy, either by developing an improved strain of BCG, or by boosting BCG-induced immunity [49]. Developing a new vaccine is difficult since we do not fully understand the nature of protective immunity. All the candidates currently in development aim to induce cellular immunity, since a cellular immune response is required to protect against TB disease [2]. There are 15 vaccines currently in different stages of clinical trials which is a vast improvement on none ten years prior to that [2]. There are two approaches to TB vaccine development. The first is to modify the current BCG vaccine or perhaps even modify another mycobacterial species, in order to increase its efficacy. One way of modifying BCG is to produce recombinant BCG strains. rBCG30 is a vaccine that over-expresses the 30kDa major secreted antigen from *M.tb.* Another way to modify BCG is to generate a strain that targets immune processing pathways. One example is BCG expressing listeriolysin from *Listeria monocytogenes (L.monocytogenes)* [50]. This vaccine increases acidification of

the phagosome, thereby resulting in endosomal escape of antigen into the cytoplasm, presentation via Class I MHC, and the induction of antigen-specific $CD8^+$ T cell responses. Another promising vaccine candidate is MTBVAC, which is a live attenuated strain of *M.tb* with deleted *phoB* and *fadD26* genes, which are key virulence factors. This vaccine is the first using a live attenuated strain of *M.tb* to enter clinical trials, and confers pre-clinical protection superior to BCG [51].

The second, potentially complementary approach is to use the current BCG vaccine (or modified BCG) as a prime for a booster in the form of a protein vaccine combined with an adjuvant, or a viral vector. Viral vectors can also be used to boost BCG vaccines, since viruses induce strong cellular immunity. One viral vector-based vaccine, which was developed within the Jenner Institute at the University of Oxford, is MVA85A. This vaccine is a Modified Vaccinia virus Ankara (MVA) expressing antigen 85A, a protein of the highly immunodominant antigen 85A complex of *M.tb.* The viral vector, MVA, is highly attenuated and is very safe. In pre-clinical studies, boosting BCG with MVA85A improved protection in mouse, guinea pig, bovine and non-human primate (NHP) models of *M.tb* infection [52-58]. It has been recently tested as a BCG prime-MVA85A boost in South African infants [59]. The vaccine was well tolerated and induced modest cellular immune responses, but unfortunately provided no efficacy against *M.tb* infection or TB disease when compared to controls. This trial highlights the challenges in TB vaccine development as well as the urgent need for better preclinical and clinical models for vaccine evaluation, prior to committing to large, expensive field efficacy trials.

### *1.1.7 Animal models of TB*

Since it is unethical to challenge humans with *M.tb*, our best option to research disease pathogenesis and for testing TB vaccine candidates is to use animal models. Despite there being no perfect model available, it is important that comparisons still continue to be made between a range of animal models and humans in order to maximise our understanding of the underlying mechanisms of the host-pathogen interaction, and therefore the factors determining TB disease pathogenesis [5]. The mouse aerosol challenge model has been invaluable in its contribution to our current understanding of TB disease pathogenesis and the protective efficacy of TB vaccines [60, 61]. In addition, a wealth of immunological reagents is available for mice. Other animal models can be used, such as guinea pigs, rabbits and cattle and these animals have immune responses comparable to those seen in human *M.tb* infection. For example, there is evidence of IFN-γ, TNF-α and IL-2 production from $CD4^+$ and $CD8^+$ T cells in these models post-infection [62]. Unfortunately, there is a limited range of reagents available for guinea pigs, rabbits and cattle, and in addition, housing them within BSL (biosafety level) 3 containment is costly compared to mice [63]. NHPs are usually used as a last efficacy test for vaccine and drug candidates before they enter human clinical trials.

Robert Koch was the first to use the mouse model of *M.tb* infection when he showed that inoculation with *M.tb* induced lesions similar to those seen in human disease [64]. Although the relevance of mouse models is debated, humans and mice share 85% of their genome, with many genes involved in disease control being shared by the two species [65]. The most commonly used

strains for *M.tb* infection studies are the relatively resistant C57BL/6 and BALB/c strains, since they are able to contain bacteria and therefore chronic infection can be monitored. Moreover, the BCG vaccine reduces *M.tb* lung CFU by around 1-2 logs in these strains, highlighting the usefulness of this model in vaccine efficacy testing. However, mouse pathology post-infection varies considerably from that observed in humans, so they are perhaps not a good model of latent *M.tb* infection. Infected mice develop granuloma-like structures, which are poorly organised, not as complex as human granuloma, and do not develop caseating necrosis [66]. Death occurs due to expansion of the granuloma with immune cells reducing surface area for gas exchange [67]. Additionally, there is no distinction between latent and active disease in mice since the bacterial loads remain high but somewhat controlled throughout the course of infection. Other strains of mice such as CBA, DBA/2 and C3H are more susceptible to infection than C57BL/6 and BALB/c strains. Differences in susceptibility have long been attributed to genetic variation, highlighting the role of genetic variation on disease outcome in humans [68, 69]. The I/St strain eventually succumbs to disease, developing necrotic granulomas, which may be more representative of human disease [70, 71]. Therefore, C57BL/6 and BALB/c mice may be more relevant for studying the immune response to *M.tb*, while the more sensitive strains such as CBA may be more suitable for studying the development of pathology and active disease in relation to human disease. Genetically-altered mice have also proven to be a powerful tool in identifying the immune factors essential for control of *M.tb*. IFN-$\gamma$ knockout mice, for example, are unable to control growth of *M.tb* and rapidly succumb to infection [33]. Despite its limitations, the mouse model is still a useful challenge model,

but the strain of mouse should be chosen according to the aspect of disease being studied.

Guinea pigs are highly susceptible to *M.tb* infection and therefore provide another useful animal model of TB. They were the first animal model used by Koch in order to show that a microorganism was the aetiological agent of TB [72]. Guinea pigs develop pathological features more comparable to human disease than mice do, as they develop granuloma and caseous necrosis similar to humans [66], however liquefaction does not occur in this species. As a result, guinea pigs have been used as a gold standard for testing drugs and biological agents against *M.tb*, as well as by Calmette et al for the pre-clinical testing of the BCG vaccine [73, 74]. The major limitation of the guinea pig model is the limited range of immunological reagents available, although this is improving.

Rabbits represent another useful animal model of TB disease. They are thought to develop lung pathology most similar to humans, since they form granuloma with liquefied cavities in the centre, like those observed in humans [66]. Moreover, a spectrum of disease has been observed in rabbits infected with a range of strains of *M.tb.* Thus, they provide an excellent model for investigating many stages of human disease [75]. NHPs are probably the best animal model of *M.tb* since they develop extensive caseous necrosis with liquefaction of granuloma and cavity formation, which is very similar to human disease [76, 77]. In addition, susceptibility to *M.tb* is reduced by BCG vaccination, and different breeds have different degrees of susceptibility, once again highlighting the role of genetic variation in disease outcome. Research on Simian Immunodeficiency Virus (SIV) has aided the development of a wide range of reagents for NHPs.

However, using NHPs as a model of TB disease is limited since they are difficult to contain, expensive to maintain, and also require high security facilities [62].

## 1.2 Iron

### *1.2.1 Background*

Iron, which is one of the most abundant elements on earth, is essential for almost all organisms, including Mycobacteria, with the exception of a few such as the *Lactobacillus* family, for example [78]. It is a vital co-factor for many enzymes involved in key cellular processes such as DNA synthesis and respiration, as well as being involved in reactions involving energy production and oxidative phosphorylation due to its key role in electron transport. In these redox reactions, iron readily switches between its oxidised, ferric ($Fe^{3+}$) form and its reduced, ferrous ($Fe^{2+}$) form. In addition, iron is necessary for defence against pathogens, where free ferrous iron ($Fe^{2+}$) donates an electron, catalysing the production of reactive oxygen species (ROS) or hydroxyl radicals by Haber-Weiss and Fenton chemistry, respectively. Whilst these free radicals are important in defence against pathogens, they can also be highly toxic to the host, since free radicals are capable of causing significant toxicity to host cell membranes and nucleic acids. Therefore, free iron is extremely reactive and toxic and regulation of iron homeostasis in order to limit iron availability to both host and pathogen and prevent toxicity is paramount [79]. It is critical that organisms have strict and complex control mechanisms for iron acquisition, storage, transport and utilisation [80]. For example, under normal conditions, iron is usually bound to iron transport and storage proteins such as transferrin,

ferritin and lactoferrin [81]. As a result, pathogens must compete with their host for iron whilst ensuring they do not acquire toxic amounts of this metal. Therefore iron must be strictly regulated on both a systemic and a cellular level.

### *1.2.2 Systemic iron homeostasis*

Human iron requirement is dependent on the amount absorbed from the diet, the amount recycled from senescent erythrocytes, how much is utilised for erythropoiesis (the process requiring the most iron), as well as by how much is lost. Since adults lose less than 1% of their iron stores daily, this can be replaced using dietary iron sources. An average male has about 3-4g of iron in his body, whereas women only have 2-3g due to smaller iron reserves as a consequence of iron loss during menstruation and lower haemoglobin concentrations.

Recovery of iron from damaged or senescent erythrocytes is the major source of iron, not absorption from the diet. The majority of iron in the body is stored as haem iron inside haemoglobin in erythrocytes, which usually totals up to 2g. In contrast, plasma only contains up to 3mg of iron, bound to plasma storage protein, transferrin, which transports $Fe^{3+}$ iron to the bone marrow for erythropoiesis.

Human erythrocytes live around 120 days before they are degraded by macrophages in the spleen and liver, releasing the iron back to transferrin for transport back to the bone marrow. Iron recycling produces up to 25mg of iron-transferrin per day. Some iron can also be stored in liver hepatocytes or macrophages inside iron storage proteins. Humans are unable to increase iron excretion, even in cases where intake and storage become excessive. Therefore,

regulating the relatively small amount of iron absorbed through the intestine is critical in maintaining iron homeostasis [78].

### *1.2.2.1 Intestinal iron absorption*

A small amount (up to 2mg) of dietary ferric ($Fe^{3+}$) iron is absorbed per day, primarily through duodenal enterocytes [78]. In this process, iron is transported through the apical membrane of the enterocytes, translocated through the cell, and released basolaterally into the bloodstream to be loaded onto apo-transferrin, as summarised in Figure 1.4. In humans, two forms of iron are absorbed intestinally: haem iron and non-haem iron. Haem is the major source of iron in diets rich in red meats, providing around two-thirds of the dietary iron supply of the body [78]. The process by which haem is transported into the cytoplasm is controversial. There are currently two candidate haem transporters, the first being haem carrier protein 1 (HCP1), and the second is haem-responsive protein gene-1 [79]. Haem is translocated into enterocytes and then degraded by haem-oxygenase (HO1) in order to release $Fe^{2+}$ into the cell.

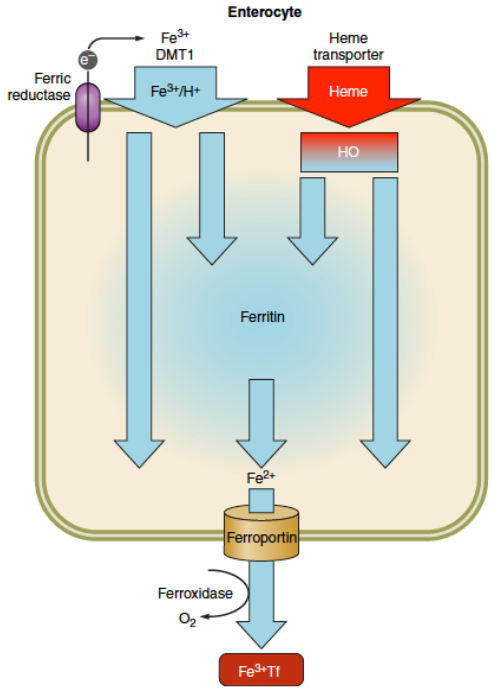


**Figure 1.4 Intestinal iron absorption.** Uptake of iron at the apical brush border of enterocytes occurs through DMT1 or through an unknown haem importer. $Fe^{3+}$ iron must be reduced to $Fe^{2+}$ iron by ferric reductases before being transported into the cytoplasm by DMT1. Excess intracellular iron is stored in the iron storage protein ferritin, and a small amount remains in the LIP. Before transport through the basolateral membrane, $Fe^{2+}$ iron is oxidised to $Fe^{3+}$ by ferroxidases hephaestin and ceruloplasmin prior to export through the iron exporter, ferroportin. Taken and adjusted from [79].

#### *1.2.2.2 Intracellular iron transport by DMT1*

Non-haem iron is transported into the cell via divalent cation transporter DMT1, which is located on the brush-border membrane of duodenal enterocytes [82]. Since DMT1 can only transport ferrous iron, ferric iron must be reduced prior to import by a ferric reductase such as duodenal cytochrome B (dcytB). DMT1 is an integral membrane protein consisting of 12 transmembrane domains with cytoplasmic termini [83, 84]. It is essential for iron homeostasis as it is also critical in the delivery of iron from transferrin into the cytoplasm, particularly in erythrocyte precursors. Mouse studies have confirmed the essential role of DMT1 in dietary iron acquisition, since mice with mutant *Dmt1* have severe iron-deficiency anaemia [85]. Mutations in human DMT1 result in microcytic anaemia as a result of erythrocyte precursors being unable to utilise transferrin-bound iron, as well as inhibiting uptake of dietary iron in enterocytes [86].

#### *1.2.2.3 Iron storage proteins: ferritin*

Once inside the cell, iron that is not immediately required for metabolic purposes can be stored inside a ubiquitous iron binding storage protein, ferritin. The majority of iron is stored inside macrophages of the reticuloendothelial system (in particular, kupffer cells) and in hepatocytes. Delivery of ferrous iron to ferritin occurs through cytoplasmic chaperones such as poly (rC)-binding protein 1 (PCBP1), but the process by which iron exits from ferritin, and transits to the iron exporter ferroportin, is unknown. Ferritin is a very large (450kDa) protein composed of subunits of either H- or L-type ferritin. A group of 24 subunits combine to form a spherical apoferritin polypeptide shell, capable of storing up to 4500 iron molecules in an inner ferric iron core [87]. Ratios of

these 2 subunits differ according to tissue type and can change rapidly in response to a number of stimuli and changes in conditions. Ferritin sequesters iron in a non-toxic form, therefore playing an important role in iron homeostasis [88]. Indeed, loss of H-Ferritin (encoded by the *Fth* gene) in mice results in embryonic lethality [89], and conditional disruption of *Fth* results in tissue damage as a consequence of loss of liver iron storage [90]. Storage of excess iron inside ferritin is not only critical in preventing toxicity, but also for the controlled delivery of iron to exporters on the basolateral membrane. Expression of ferritin is primarily regulated by the concentration of intracellular iron, but can also be regulated by inflammation and hypoxia. Excess iron results in the post-transcriptional up-regulation of ferritin via the Iron Responsive Element/Iron Regulatory Protein (IRE/IRP) network, which will be discussed in more detail later on. Conversely, iron depletion results in reduced ferritin expression, in order to release stored iron back into the labile iron pool [91]. An excess of iron exceeding apo-ferritin availability can lead to deposition of iron adjacent to ferritin, known as haemosiderin. Serum ferritin correlates with iron stores in most conditions [92, 93], but not during infection and inflammatory conditions, where serum ferritin may be high in the absence of high iron stores.

#### *1.2.2.4 Iron export: ferroportin*

Once inside the cell, dietary iron can also be exported from duodenal enterocytes into the bloodstream. This is mediated by ferroportin, the sole known mammalian iron exporter, in conjunction with copper-containing ferroxidases including hephaestin and ceruloplasmin, which oxidise ferrous iron back to ferric iron [94, 95]. Ferroportin, encoded by the FPN1 gene in humans

and *Fpn1* in mice, is highly expressed at all sites involved in the transfer of iron to plasma, namely duodenal enterocytes, placental cells and macrophages. It is also expressed to a certain extent in hepatocytes, but at much lower levels that in macrophages. It regulates how much dietary iron enters the circulation. Complete loss of ferroportin in zebra fish results in embryonic lethality, unless rescued by iron injections. However, these fish are still iron deficient and unable to regulate iron absorption [96]. Loss of ferroportin in mice also renders them embryonically lethal, with conditional intestinal deletions resulting in mucosal iron retention and hypochromic anaemia. Moreover, disruption of the ferroportin gene in humans results in the iron overload disorder haemochromatosis. These studies confirm that regulation of ferroportin is critical for maintaining systemic iron homeostasis in order to prevent iron overload, deficiency disorders, or infectious disease. The expression of ferroportin is regulated post-translationally by the peptide hormone hepcidin, and also post-transcriptionally by iron through the IRE/IRP network, which will be discussed later.

#### *1.2.2.5 Iron recycling in macrophages*

As mentioned above, the main source of iron in the body comes from the recycling of senescent erythrocytes by macrophages, and not from the absorption of dietary iron. This process is summarised in Figure 1.5. Up to 70% of iron in the body is stored inside haemoglobin in erythrocytes. Human erythrocytes live for around 120 days before they are degraded by macrophages in the spleen and liver, releasing the iron back to transferrin for transport back to the bone marrow. Haemoglobin is critical for transport of oxygen around the

body. Ferric ($Fe^{2+}$) iron is stored inside the haem group of haemoglobin, which consists of a porphyrin ring of 4 pyrrole molecules, linked by methene bridges [97]. The phagocytosis of senescent erythrocytes into phagolysosomes results in the break down of the effete erythrocyte, releasing haem, which is subsequently degraded by HO1. This frees $Fe^{2+}$ iron into the cytoplasm either for storage inside ferritin, or for export by ferroportin at the basolateral membrane of the macrophage.

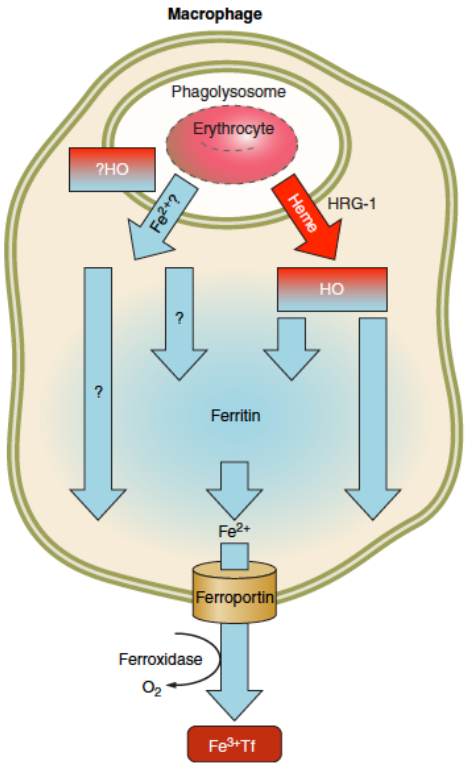


**Figure 1.5 Recycling of iron by macrophages.** Senescent erythrocytes are phagocytosed by macrophages in the reticuloendothelial system. Once in the phagolysosome, they are degraded by proteolysis and the haem is degraded by HO1, releasing iron into the cell, either for storage in ferritin or export through ferroportin. From [79].

### *1.2.2.6 Extracellular iron transporters*

After ferric iron is released from cells, it normally binds to transferrin, a plasma iron carrier with a high affinity for iron. Saturation of plasma transferrin with iron is a useful indicator of systemic iron homeostasis. Transferrin is an 80kDa glycosylated protein composed of a single polypeptide chain of 680-700 amino acids, forming 2 non-cooperative iron-binding sites each capable of binding 1

iron atom. Apo-transferrin (transferrin not bound to iron) binds to iron and then delivers it to cells by binding to its specific cell-surface receptor, transferrin receptor (TfR). This mediates the internalisation of the transferrin-iron complex by receptor-mediated endocytosis into an acidic lysosome, releasing the iron into the cytoplasm. Transferrin receptor (TfR), encoded by the TFRC gene in humans and *Tfrc* in mice, is a transmembrane protein made up of two 90kDa subunits, joined by a disulphide bond. In order to facilitate internalisation of the complex, phosphorylation by a $Ca^{2+}$-calmodulin-protein kinase C complex is necessary. Once iron has been released, the apo-transferrin is released back into the plasma via DMT1 and the transferrin receptor is recycled back to the cell surface. Any iron that has been released inside the cell by transferrin can be used in the synthesis of haem for erythropoiesis, or stored inside iron storage proteins. The non-redundancy of transferrin is evidenced by the severe iron overload observed in atransferrinemia in mice and humans [98, 99]. TFRC is regulated post-transcriptionally by the IRE/IRP network. There is also a second transferrin receptor, transferrin receptor 2, which is involved in sensing extracellular iron availability.

#### *1.2.2.7 Labile iron pool (LIP)*

When intracellular iron is not stored in ferritin, it forms a pool of accessible and redox-active iron, which only accounts for a small percentage of cellular iron content. This pool likely contains iron in both the $Fe^{2+}$ and $Fe^{3+}$ forms, which appears to be complexed by a range of ligands. This free iron can catalyse the production of highly toxic hydroxyl radicals via Haber-Weiss and Fenton chemistry. Therefore, the LIP must be kept to a minimum, through the

transcriptional, post-transcriptional and post-translational regulation of the key proteins in involved in the maintenance of iron homeostasis.

#### *1.2.2.8 Hepcidin – the master regulator of iron metabolism*

As mentioned earlier, the regulation of ferroportin and therefore the absorption of dietary iron is critical in the maintenance of systemic iron homeostasis, since we are unable to regulate excretion of iron. Ferroportin expression is post-translationally regulated by hepcidin antimicrobial peptide (HAMP). Hepcidin, which was discovered in 2000 in human urine, is a small (25 amino acid) peptide hormone [100]. The 84aa pre-pro-peptide is produced in the liver prior to cleavage and release in its 25aa, mature form [100, 101]. It is known to be the master regulator of iron homeostasis, since it binds to ferroportin, resulting in its internalisation, degradation, and subsequent inhibition of iron export from macrophages and hepatocytes [102]. The regulation of systemic iron homeostasis by hepcidin is summarised in Figure 1.6.

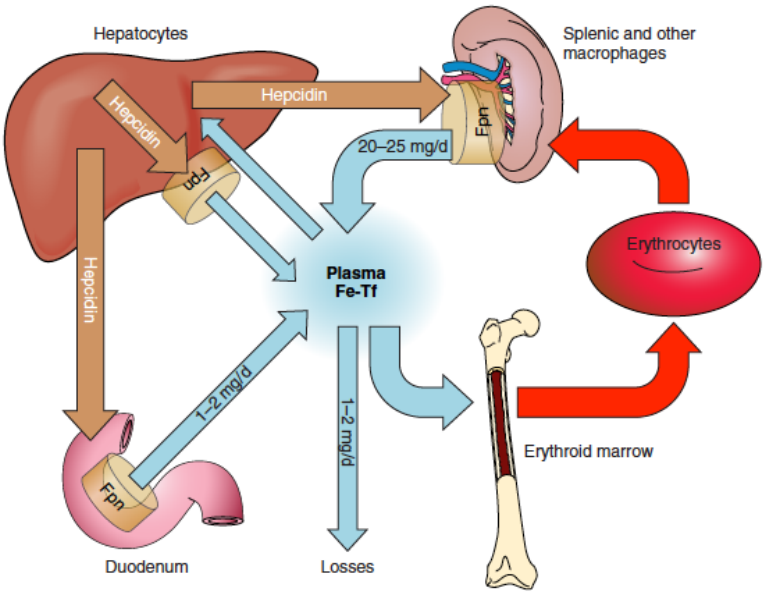


**Figure 1.6 Regulation of systemic iron homeostasis by hepcidin.** Dietary iron is absorbed from the duodenum, after which it is released and circulates in the blood bound to plasma transferrin, where it is used by red blood cells for erythropoiesis. The majority of iron is recycled in macrophages, which break down iron from effete erythrocytes and release it again. Excess iron is stored in ferritin in the liver to prevent toxicity. Hepcidin regulates transferrin iron levels by degrading ferroportin, inhibiting iron release from macrophages and enterocytes. Hepcidin synthesis is negatively regulated by increased erythropoietic activity and positively by increased iron stores. Iron bound to transferrin is indicated in blue, iron in erythrocytes in red. Iron flow regulated by hepcidin is indicated in blue. From [79].

High hepcidin results in degradation of ferroportin, resulting in reduction of dietary iron absorption through duodenal enterocytes, reduction of iron release from recycled erythrocytes in macrophages that have phagocytosed and degraded erythrocytes, and release of iron stores from hepatocytes. As a consequence, hepcidin-induced reduction of serum iron levels may be protective against blood-borne pathogens such as malaria, but paradoxically may be beneficial to pathogens whose preferred niche is the iron-loaded macrophage [103]. Low hepcidin results in high ferroportin expression leading to high levels of circulating iron due to increased dietary iron uptake, and iron release with little iron storage inside macrophages [104]. Disruption of the gene encoding hepcidin, as well as many of the genes involved in the control of hepcidin,

results in severe tissue iron overload in both species due to iron redistribution, demonstrating the lack of redundancy in this pathway [105-107]. Over-expression of hepcidin on the other hand can cause iron-deficiency anaemia. Most mammals have a single hepcidin gene. In humans, hepcidin is encoded by the hepcidin antimicrobial peptide (HAMP) gene. However, mice possess 2 hepcidin genes, *Hamp1* and *Hamp2*, which are located on the same region on mouse chromosome 7 [108, 109]. However, evidence suggests that *Hamp2* is not involved in iron metabolism since mice over-expressing this gene do not develop iron deficiency anaemia like mice over-expressing *Hamp1* [110]. Interestingly, fish have up to 7 Hamp genes, but only one of these in any one species appears to regulate hepcidin, the rest being antimicrobial. Evidence for the lack of redundancy of hepcidin in the control of iron homeostasis has been observed in mouse models and in human disease. Over expression in mice results in iron deficiency anaemia [111, 112], whereas *Hamp1*$^{-/-}$ mice over-absorb iron, resulting in systemic iron overload, with a paradoxical reduction in macrophage iron stores. Interestingly, the phenotype in *Hamp1*$^{-/-}$ mice is similar to that observed in human hereditary haemochromatosis, which will be discussed in more detail later [105, 112, 113].

*1.2.2.8.1 Regulation of hepcidin*

Hepcidin synthesis is modulated by a number of factors: iron overload, erythropoietic activity, inflammatory stimuli, hypoxia, and anaemia [107, 114], summarised in Figure 1.7 and in further detail at the signalling level in Figure 1.8.

*Positive regulation of hepcidin*

*Iron*

Iron abundancy (in the form of plasma iron or stored iron) induces secretion of hepcidin by hepatocytes, the primary cell secreting this peptide, thereby reducing dietary iron absorption, and release of iron from macrophages and hepatocytes.

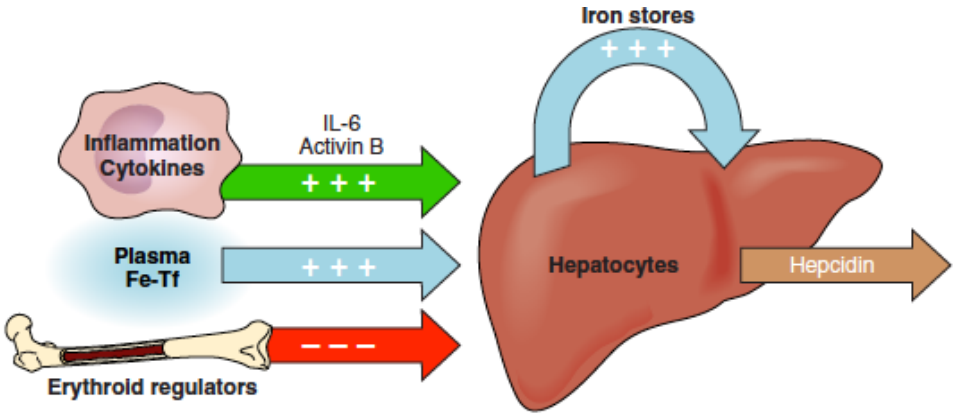


**Figure 1.7 Regulation of hepcidin synthesis.** A number of factors influence the synthesis of hepcidin in hepatocytes. Inflammation (green) and iron stores plus iron transferrin (blue) induce hepcidin synthesis, whilst erythroid regulators (red) inhibit hepcidin synthesis. From [79].

The key pathway for the regulation of hepcidin transcription is the Bone Morphogenetic Protein (BMP) pathway with its canonical SMAD pathway, as evidenced by the induction of hepcidin by multiple BMPs [115, 116]. In support of this, the hepcidin promoter contains a number of BMP-response elements, and SMAD4 ablation results in hepcidin ablation [117]. BMPs bind to BMP receptors and induce oligomerisation of the serine/threonine receptor kinases, leading to phosphorylation of SMAD1/5/8. This results in the partnering of SMADs with their common signalling transducer, SMAD4, followed by

translocation to the nucleus. A number of BMPs are able to induce hepcidin expression. However, Bmp6 is the key ligand for the BMP receptor in mice, since disruption of the *Bmp6* gene results in severe iron overload as a result of reduced hepcidin production [118, 119]. In order to regulate hepcidin expression in response to iron levels, intracellular and extracellular iron sensors are required. Transferrin receptors 1 and 2, haemojuvelin (HJV), holo transferrin, hereditary haemochromatosis protein (HFE) and BMP6 all induce hepcidin through this pathway. HJV is a BMP co-receptor and therefore induces hepcidin transcription. Mutations of HJV in humans are the primary cause of juvenile haemochromatosis [106], and cause severe iron overload in mice [120].

It is not yet clear how extracellular iron sensors communicate with the BMP pathway in order to regulate hepcidin transcription. It is likely that TfR1 and TfR2 combined with HFE function as extracellular iron sensors, by sensing the levels of holotransferrin (diferric transferrin). Binding of HFE to TfR1 is competitively inhibited by holotransferrin, so with increasing levels of iron and therefore higher concentrations of holotransferrin, HFE is displaced by holotransferrin and then HFE binds and stabilises TfR2. The BMPR complex is then able to stimulate hepcidin transcription through an unknown pathway. Intracellular iron sensors involved in regulation of hepcidin transcription are currently unknown.

*Inflammation*

Hepcidin is also induced in hepatocytes by a wide range of infectious stimuli. IL-6 induces hepcidin expression via the Janus Kinase (JAK)- signal transducer and activator of transcription 3 (STAT3) pathway [121]. It binds to its

receptor, IL-6 receptor alpha and gp130, inducing receptor dimerisation, activating the associated JAKs, which then phosphorylate themselves and the receptor, enabling binding of STATs. Dimerised STATs are then able to translocate to the nucleus to regulate hepcidin transcription.

*Inhibition of hepcidin*

As mentioned earlier, hepcidin is negatively regulated by anaemia and hypoxia. In a mouse model, anaemia induced by phenyl hydrazine or repeated phlebotomies results in down-regulation of hepcidin mRNA [107]. Increased erythropoietic activity or haemorrhage also suppresses hepcidin induction, ensuring increased iron availability for the synthesis of haemoglobin and erythropoiesis. This is regulated by a recently discovered hormone, erythroferrone (ERFE), which is produced by erythroblasts in response to erythropoietin (EPO) [122].

When iron stores are decreased, another potential iron sensor, transmembrane protease, serine 6 (TMPRSS6), a serine protease, acts to inhibit hepcidin expression by cleaving HJV to soluble HJV (sHJV), thereby inhibiting BMP-induced hepcidin transcription. Mutations in TMPRSS6 in both mice and humans result in over-stimulation of hepcidin and subsequent anaemia as a consequence of the trapping of iron inside macrophages.

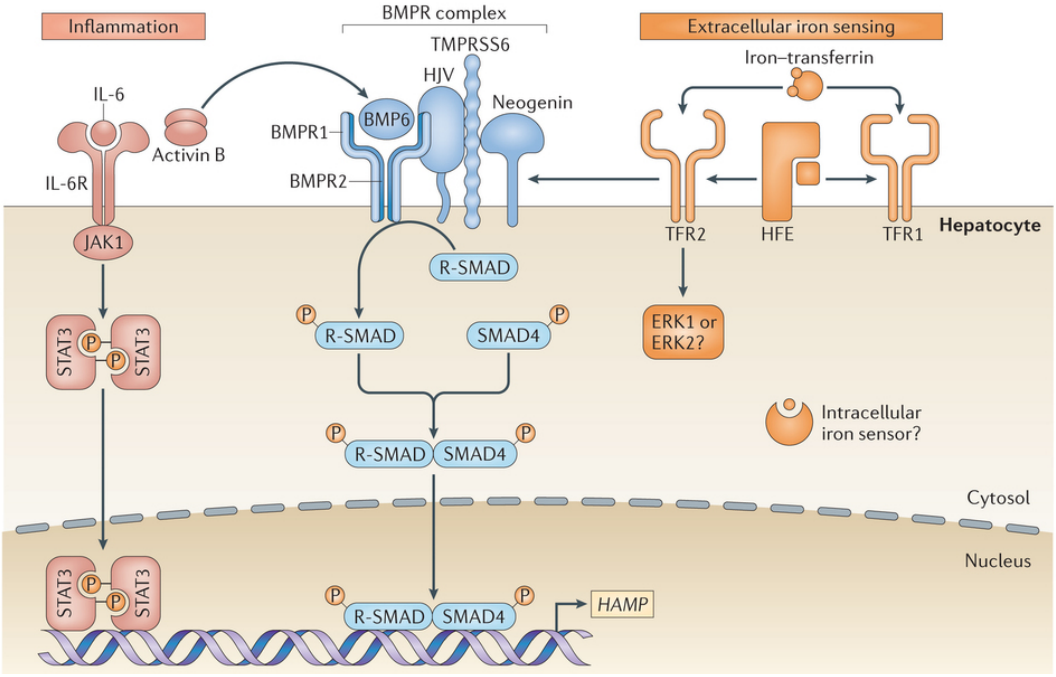


**Figure 1.8 Regulation of hepcidin transcription by inflammation and iron.**
The primary regulators of hepcidin transcription are the SMAD and STAT3 pathways, through iron-related and inflammatory signals, respectively. The BMP/SMAD pathway is induced by interaction of BMPs (in particular BMP6) with heterodimeric BMP receptor subunits (BMPR1 and 2), resulting in oligomerisation of receptor kinases, and subsequent phosphorylation of SMAD1/5/8. Phosphorylated SMADs partner with their common signalling transducer, SMAD4 and translocate to the nucleus to induce hepcidin transcription. TMPRSS6 is a negative regulator of BMPR signalling, acting by cleaving HJV. HFE associated with TFR1 is displaced by holotransferrin, resulting in HFE binding and stabilizing TFR2, which results in induction of hepcidin transcription via BMP through an as yet unknown mechanism. In inflammation, hepcidin transcription is also induced by the binding of IL-6 to its receptor, IL-6R, and induction of the JAK/STAT3 pathway. It is likely that activin B also signals through the BMPR pathway. Reprinted with permission from Ganz et al, Nature Reviews Immunology 15 (8), 2015 [123]

In hypoxia, suppression of hepcidin increases iron availability to the bone marrow, possibly in part through the induction of hypoxia inducible factor (HIF) HIF1-α which induces TMPRSS6, thereby cleaving HJV and inhibiting hepcidin production via inhibition of BMP/SMAD signalling [124, 125], although this has not been widely reproduced. More recent research points to regulation of hepcidin in hypoxia through upregulation of EPO and consequently ERFE.

### *1.2.3 Cellular iron homeostasis*

In addition to regulation of systemic iron homeostasis, it is essential that the expression of iron acquisition, storage, transport, and export proteins is tightly regulated, in order to prevent cell toxicity by excess iron. Intracellular iron homeostasis is regulated post-transcriptionally by the IRE/IRP system (Figure 1.9) [78]. This system happens to be one of the best-characterised post-transcriptional regulatory systems in vertebrates [126]. It is regulated by the binding of two cytoplasmic hairpin-like responsive proteins, IRP1 and IRP2, to iron responsive elements (IREs), which are conserved cis-regulatory mRNA motifs located on the un-translated regions (UTRs) of mRNA encoding critical iron regulatory proteins [127]. IREs have been found in a total of 15 mRNAs, encoding proteins for iron acquisition, storage, utilisation and export. The mRNAs encoding H- and L-ferritin, ferroportin, and mitochondrial aconitase 2 (ACO2) all have 5' UTRs containing a single IRE (Figure 1.2.6). TFR1 mRNA contains multiple IREs in its 3' UTR, and the mRNA for DMT1 contains a single IRE in its 3' UTR. The location of the IREs determines how these genes are regulated by iron availability [128, 129]. IRPs exist in 2 confirmations, depending on circulating iron levels. Under low iron conditions, IRP1 and IRP2 bind to IREs in either the 5' or 3' UTR of target mRNA. There are two mechanisms involved. IRPs binding to single 5' UTR IREs inhibit translation, whereas IRPs binding to multiple 3' UTR IREs increase mRNA stability and prevent degradation, leading to translation [78]. In iron rich cells, IRPs are unable to bind to IREs due to the assembly of an iron-sulphur cluster in IRP1, which converts it into a cytosolic aconitase. In addition, IRP2 undergoes proteasomal degradation. The involvement of TFR1, DMT1 and FPN1 in

systemic iron homeostasis represents cross talk between systemic and cellular iron homeostasis.

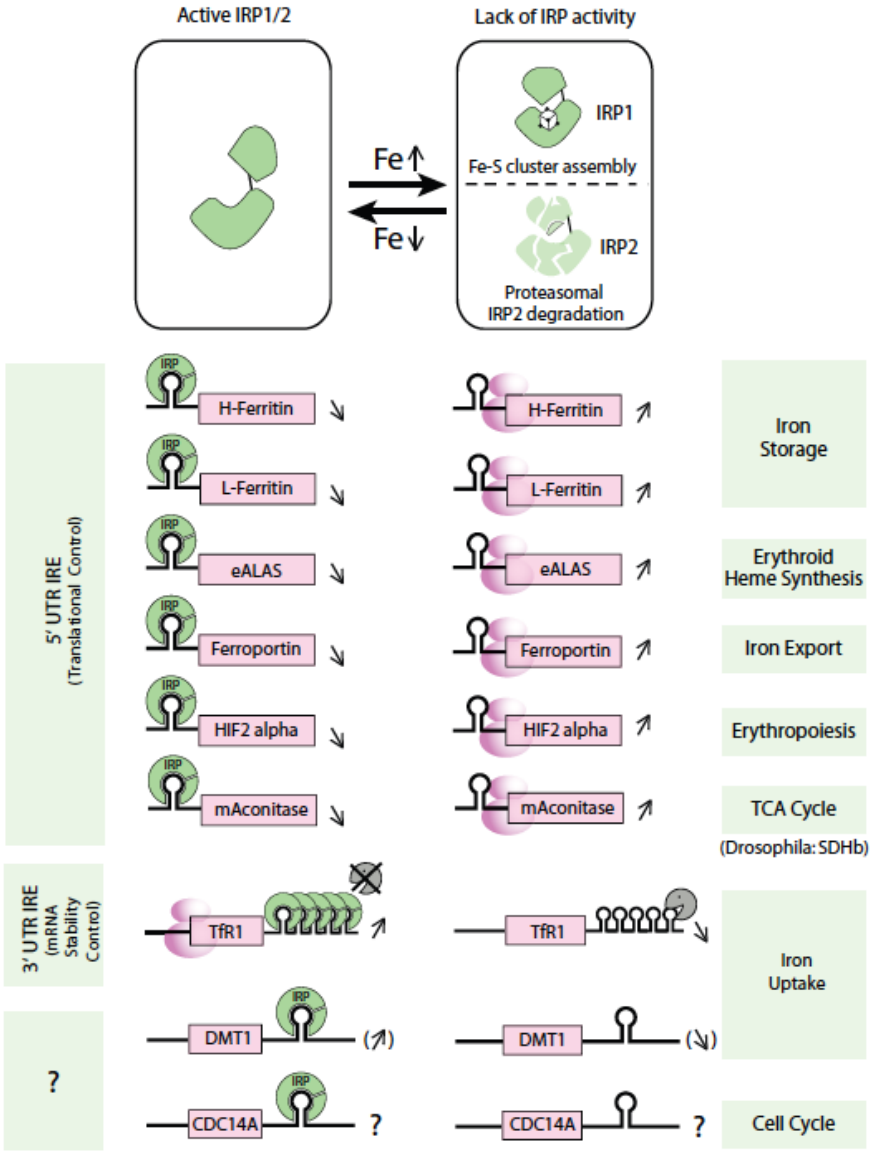


**Figure 1.9 The IRE/IRP regulatory system.** IRPs interact with IREs in order to regulate expression of proteins involved in iron acquisition, storage, transport, and export. In iron-deficient conditions, the iron-sulphur cluster in IRP1 is unstable, allowing IRP1 to bind to IREs, mediating translational repression of mRNAs with IREs in the 5' UTR and therefore reducing protein levels. Conversely, mRNAs with 3' UTRs are stabilised. This prevents cleavage of *TFR1* mRNA. In iron-rich conditions, the iron-sulphur cluster in IRP1 stabilises it and IRP2 is degraded. IRP1, which now functions as a cytosolic aconitase, can no longer bind to 5' UTRs and repress translation. Expression of mRNAs with 3' UTRs, such as *DMT1* is repressed, and *TFR1* mRNA is degraded. From [78].

### *1.2.4 Iron-related disorders*

Since iron metabolism is so tightly regulated, disruption of homeostasis, for example by mutation of hepcidin, hepcidin targets or other regulatory proteins results in iron-related disorders, which are relatively common. Hereditary haemochromatosis is a primary genetic disorder of iron homeostasis, in which excessive absorption of dietary iron results in toxic tissue iron accumulation. The primary cause of hereditary haemochromatosis is a deficiency in hepatic hepcidin production, which cannot be counterbalanced because humans are unable to excrete iron effectively. Insufficient hepcidin production results in increased ferroportin expression, allowing uncontrolled absorption of dietary iron and therefore increased serum iron levels, as well as excessive release of iron from stores, leading to iron loading of parenchymal cells. The most common cause of adult haemochromatosis is an autosomal recessive C282Y mutation of the HFE gene, situated on the short arm of chromosome 6 [130]. Juvenile haemochromatosis, which is relatively rare, is usually caused by mutations in the hepcidin or hemojuvelin. Other forms may be due to mutations in ferroportin, rendering it resistant to hepcidin [131].

Patients with iron loading anaemias such as β-thalassemia develop severe iron overload, even though they are anaemic. Anaemia occurs due to defective beta-globin production in erythroid precursors, resulting in ineffective erythropoiesis and resultant anaemia with suppression of hepcidin likely via enhanced production of erythroferrone. The hepcidin suppression then leads to excessive dietary iron absorption

## 1.3 Iron and TB

### *1.3.1 Human studies on TB and iron*

Iron availability to both host and pathogen can determine the outcome of infection, and the virulence of many pathogens can be enhanced by iron. Iron plays a critical role in TB since it is essential for the survival and replication of *M.tb* both *in vivo* and *in vitro*, but also influences host immune responses against invading pathogens. In humans, iron overload can exacerbate TB disease, as evidenced by a number of studies. In the 19$^{th}$ century, Dr. Armand Trousseau, a French clinician, was the first to recognise exacerbation of TB disease following treatment of anaemic TB patients with iron supplements. Higher TB disease incidence has also been associated with African iron overload [132]. More recently, associations have been found between pulmonary TB and higher serum iron parameters [133]. Moreover, iron status may help to predict treatment failure and mortality associated with TB [134]. Therefore, it is especially important that clinicians treating patients with TB (or other infectious diseases) and anaemia consider that administration of iron supplements may have severe consequences.

### *1.3.2 Animal studies on M.tb and iron homeostasis*

In support of human data, a number of animal studies support the concept that the iron status of the host is of paramount importance in *M.tb* infection. For example, mice deficient in β-2 microglobulin (B2M) have severe tissue iron overload and are more susceptible to *M.tb* than wild-type mice since β-2 microglobulin is involved in the regulation of cellular iron uptake by HFE (HFE requires B2M to fold correctly). Mice deficient in B2M also have no functional

$CD8^+$ T cells because classical MHC I proteins also require B2M to fold correctly, which could explain why they are more susceptible to *M.tb.* However, treatment with the iron chelator lactoferrin reverses the increase in susceptibility, whereas the same treatment in mice deficient in MHC Class I (which also have defective $CD8^+$ T cells) does not. It is therefore likely that increased susceptibility to *M.tb* observed in B2M knockout mice is a result of iron overload caused by B2M knockout rather than an effect of disruption of $CD8^+$ T cell functionality. Correspondingly, increased dietary iron availability, or parenteral iron administration also enhances growth of mycobacteria *in vivo* [135, 136]. In contrast, iron chelation results in inhibition of murine *M.tb* growth [135].

### *1.3.3 In vitro studies*

Studies into iron and mycobacteria were first conducted around 50 years ago, on *Mycobacterium smegmatis (M.smegmatis),* a non-pathogenic mycobacteria [137]. The bacterium was shown to undergo a number of metabolic changes in iron-deficient medium. The addition of iron experimentally almost always results in enhanced mycobacterial growth, and the addition of iron chelators, such as desferroxamine (DFO), reduce growth.

### *1.3.4 TB and hepcidin*

Despite strong evidence that iron availability affects outcome of TB disease, investigations into hepcidin and its involvement in TB disease are limited [138]. Firstly, *in vivo* data suggest that hepcidin may have antimicrobial properties against *M.tb*, however this was likely using concentrations of hepcidin much higher than occur physiologically [104, 139]. Moreover, hepcidin was found to be

stimulated *in vitro* by components of *M.tb* [139], which is not surprising since infectious stimuli have been previously shown to induce hepcidin induction [140]. Correspondingly, a study of HIV-associated TB by Kerkhoff et al found that serum hepcidin concentrations increased with mycobacterial burden [141], and hepcidin was also shown to be an independent predictor of mortality [138]. In support of this, a recent study in the Gambia observed that treatment of TB resulted in normalisation of hepcidin concentrations combined with resolution of associated anaemia, indicating that TB is likely the cause of increased hepcidin, leading to anaemia. In another study by Minchella et al [142], higher hepcidin and ferritin were associated with increased risk of early progression to pulmonary TB in close household contacts. Interestingly, low plasma transferrin at the time of exposure was also risk factor, which is not surprising since transferrin represents a host iron withholding mechanism.

In extracellular infections, the induction of hepcidin resulting in the sequestration of iron inside cells away from invading pathogens is likely a protective mechanism. However, paradoxically, this may provide an iron source for pathogens that reside intra-cellularly, such as *M.tb*, and may explain the associations between increased risk of TB in patients with higher hepcidin levels. Therefore, hepcidin induction by *M.tb* infection may actually worsen disease outcome by effectively providing the pathogen with increased iron. Correspondingly, elevated hepcidin at the time of HIV diagnosis has also been found to be associated with TB, as iron redistribution into the macrophage favours co-infection with intracellular pathogens [143]. As previously

mentioned, raised intracellular iron levels also impact on macrophage effector mechanisms important in the control of intracellular bacteria.

### *1.3.4.1 Mycobacterial iron homeostasis*

#### *1.3.4.1.1 Iron acquisition systems*

Mycobacteria compete for host iron sources such as haem, lactoferrin, transferrin and ferritin via the production of high affinity iron chelators, known as siderophores, which are critical for survival of mycobacteria inside macrophages [144, 145]. Transferrin traffics to the *M.tb*-infected phagosome, so *M.tb* can access iron with its siderophores when the phagosome fuses with vesicles full of $Fe^{3+}$-transferrin [146]. Growth of *M.tb* in human serum is inhibited as a result of the iron-witholding action of transferrin [147], and this can be reversed by the addition of exogenous siderophores [148]. The *mbt* genes encode proteins involved in siderophore biosynthesis [149]. The mutation of *mbtB* renders *M.tb* unable to produce any siderophores and impairs growth in iron-deficient media [149]. *M.tb* produces two classes of siderophores. The lipophilic siderophores carboxymycobactin and exochelin can both be secreted and therefore scavenge iron from extracellular sources [150]. In addition, *M.tb* produces a lipophobic siderophore, mycobactin, which remains cell-associated, facilitating iron transport into the cell, or serving as a short-term iron storage molecule in the bacterial cell intra envelope. $Fe^{3+}$ siderophore complexes are actively taken up into *M.tb* via an ATP-binding cassette (ABC) transporter, IrtAB. Disruption of the genes encoding this transporter dramatically affects, but does not completely eliminate bacterial replication, both in culture and *in vivo* [81]. Once $Fe^{3+}$ is inside the bacterial envelope, it is reduced to $Fe^{2+}$ by a

ferri-reductase prior to transport across the cell membrane, where it can then be used directly as required, or stored inside cytoplasmic bacterial iron storage proteins, BfrA, a ferritin-like protein, or bacterioferritin (BfrB), in order to prevent iron-mediated toxicity [150]. The importance of these iron storage proteins has recently been highlighted in a study by Pandey et al [151], where *M.tb* strains with these genes disrupted were generated. The strain lacking ferritin (BrfA) was strongly attenuated compared with the wild-type H37Rv strain, most likely as a consequence of iron-mediated toxicity. This strain was also more susceptible to antibiotics, which is relevant in the development of potential new therapeutic targets against *M.tb*. Of note, the ferritin mutant strain may also present a potential TB vaccine candidate, since vaccination of mice with this strain leads to vaccine-induced protection against virulent *M.tb* comparable with BCG [152].

*1.3.4.1.2 Transcriptional regulation of iron homeostasis by M.tb*

In order to prevent iron deficiency, or toxicity as a result of excess intracellular iron, bacteria are able to sense intracellular iron levels and transcriptionally regulate the expression of genes involved in iron uptake, storage and transport. Analysis of changes in *M.tb* gene expression in iron-rich and iron-replete medium revealed 155 iron-regulated genes. One of these, IdeR (iron dependent transcriptional regulator), is critical for the regulation of iron uptake in *M.tb*. In fact, deletion of the IdeR gene confirms that IdeR is indispensable for *M.tb*. Depending on iron availability, IdeR is able to repress or activate transcription of iron-responsive genes such as siderophores or iron storage proteins, which is likely determined by the location of the IdeR binding site within the promoter

[81]. This system bears some resemblance to the human intracellular IRE/IRP network, although gene expression is regulated at a transcriptional, rather than a post-transcriptional level.

### *1.3.5 The role of iron in innate immunity*

Strict regulation of host iron homeostasis is not only critical in the prevention of host toxicity, but can also influence the outcome of infection, as it is involved in the host protective immune response [153]. As mentioned earlier, hepcidin is often induced during blood-borne infections, presumably in order to sequester iron inside macrophages away from extracellular pathogens. Accordingly, hepcidin induction during malarial infection is protective as it results in the re-distribution of iron into macrophages [154]. Paradoxically, hepcidin induction may enhance iron availability for intracellular pathogens, worsening disease outcome [123].

It is becoming increasingly likely that the regulation of iron homeostasis in response to infection is determined by the location of the pathogen [155], as intra-macrophage iron content may significantly affect the outcome of intracellular infections. Iron negatively affects the anti-microbial functions of macrophages by inhibiting pathways regulated by IFN-γ, reducing their ability to control intracellular pathogens such as *Mycobacteria and Salmonella* [156-158]. Moreover hepcidin deficiency in a mouse model of hereditary haemochromatosis may reduce growth of intracellular bacteria such as *M.tb* as consequence of reduced intra-macrophage iron content [159]. Decrease of intracellular iron may a) reduce infection by limiting iron availability to the

pathogen and b) stimulate release of anti-microbial cytokines such as TNF-α and inducible nitric oxide synthase (iNOS) [155]. In an intracellular infection, such as *M.tb,* it is possible that the post-translational modification of ferroportin by hepcidin is over-ridden by IFN-γ-induced induction of iNOS which leads to the production of nitric oxide (NO) and subsequent activation of Nrf2, a transcription factor which stimulates ferroportin transcription [155]. As a consequence, iron export is increased, resulting in a reduction of intramacrophage iron, which may be detrimental to intracellular pathogens residing in macrophages. In support of this, increased ferroportin expression and iron export has been observed in macrophages infected with *Salmonella typhimurium (S.typhi)* [160]. Moreover, exogenous hepcidin enhances intracellular growth of *Chlamydia psittaci, trachomatis* and *Legionella pneumophila,* and *Leishmania amazonensis* parasites induce hepcidin to prevent export of macrophage iron, thereby promoting replication [161, 162]. Increased ferroportin expression has also been observed in mycobacteria-containing phagosomes [163]. These studies support the hypothesis that the export of iron from inside the cell is a defence mechanism against intracellular bacteria. In addition, a number of other host defence mechanisms against infection involve the regulation of iron metabolism.

#### *1.3.5.1 NO*

It has already been mentioned that NO plays a role in the control of ferroportin expression. It binds to the transcription factor Nrf2, increasing its binding affinity for the ferroportin promoter, thereby increasing ferroportin expression and export of iron from the cell [164]. In addition, it also affects cellular iron

homeostasis by increasing IRP binding to reduce ferritin transcription, resulting in release of iron from the cell.

#### *1.3.5.2 NRAMP1*

Natural resistance-associated macrophage protein-1, or NRAMP1, is an integral membrane protein of macrophage phagosomes. It is encoded by the NRAMP1 gene in humans and *Nramp1* in mice. It transports divalent cations across the phagosomal membrane, the direction of which is controversial, but there is increasing evidence that it removes iron from the macrophage phagosome, into the cytoplasm, where it is then transported out of the cell by ferroportin, resulting in reducing iron availability for intracellular pathogens (reviewed in [[160, 165, 166]). In support of this, a number of human studies support a link between an NRAMP1 polymorphisms and increased susceptibility to *M.tb* disease [167]. Moreover, disruption of *Nramp1* in mice confers susceptibility to intracellular infections, including *Mycobacteria.* In addition to the removal of iron from the bacteria-containing phagosome, NRAMP1 also strengthens the formation of immune effector pathways with anti-microbial effects, such as TNF-α and NO formation. It also has an involvement in the production of lipocalin-2 (LCN2), which also plays a role in reducing iron availability for *M.tb.*

#### *1.3.5.3 Lipocalin-2*

LCN2 is a protein secreted by a number of cells including macrophages [168]. It binds to salicylate-derived siderophores, which are organic iron chelators produced by bacteria in order to scavenge iron from their environment [153]. Therefore, it is able to withhold iron from invading pathogens. *Lcn2*$^{-/-}$ mice are

more susceptible to infections than wild-type controls, and addition of recombinant LCN2 dramatically reduces growth of *M.tb* in culture [169, 170]. Since these pathways are important for defence against intracellular pathogens, one of the anti-microbial roles of the pro-inflammatory cytokine, IFN-γ, is to regulate the expression of NO, NRAMP and LCN2 in order to restrict iron availability for microbes. Moreover, activation of human monocytes by IFN-γ results in reduced cell surface TfR expression and IFN-γ also reduces iron macrophage acquisition from holotransferrin [171, 172]. IFN-γ is also a key component of the immune response against *M.tb*, so therefore, the importance of IFN-γ in *M.tb* infection may be partly due to its anti-microbial role in the induction of these pathways, in order to reduce iron availability for *M.tb*.

### *1.3.6 Bacterial iron homeostasis as a potential novel target for anti-tubercular agents and vaccines*

In light of the newly emerging antibiotic-resistant strains of *M.tb* and the importance of iron regulation for the bacterium, drugs that interfere with bacterial iron homeostasis may have potential as anti-tubercular agents. Interestingly, the method of action of one of the oldest drugs for treatment of TB, p-amino salicylic acid (PAS), is most likely through inhibition of mycobactin synthesis, thereby preventing *M.tb* from scavenging iron from the host [173]. Inhibition of MbtA, required by *M.tb* for synthesis of siderophores, inhibits the growth of *M.tb* in iron-restricted media [174], so presents another target for anti-tuberculous drugs [175]. Additionally, it might also be possible to target IdeR protein to circumvent *M.tb* infection, since it is indispensible for the pathogen. Moreover, as already mentioned above, attenuated strains of *M.tb*

that have had their iron acquisition or storage genes altered may be useful novel vaccine candidates [152]. In addition, management of dietary iron intake may be critical in regulating disease outcome. It is therefore of utmost importance that research in these areas continues, since it may offer some promising targets for treatment and prevention of TB disease and *M.tb* infection.

## 1.4 Aims of the project

The virulence of many pathogens, as well as the host immune response, is affected by iron availability. The role of iron in mycobacterial growth has been studied in detail, and recently, a few studies have looked at the role of hepcidin in HIV-associated TB disease. However, investigations into the role of hepcidin in *M.tb* infection remain limited. Therefore, the aims of this project were to investigate the role of hepcidin and iron homeostasis in *M.tb* infection by:

a) Determining the effect of *in vivo M.tb* and BCG infection on the expression of hepcidin and other genes involved in iron homeostasis in BALB/c and C57BL/6 mice
b) Determining the effect of BCG vaccination on the expression of hepcidin and other genes involved in iron homeostasis
c) Determining the effect of hepcidin deficiency on susceptibility to *in vivo M.tb* infection using a *Hamp1*$^{-/-}$ mouse model
d) Determining the effect of dietary iron deficiency on susceptibility to *in vivo M.tb* infection
e) Determining the effect of increasing or decreasing iron availability on mycobacterial growth *in vitro*

## 1.5 Experimental approaches

In Chapter 3, the effect of *M.tb* infection on hepatic *Hamp1* expression was studied in both BALB/c and C57BL/6 mice, at a range of time points post-infection. qRT-PCR was also used to quantify the expression of other genes involved in iron homeostasis. The effect of BCG vaccination on these parameters was also investigated in C57BL/6 mice.

In Chapter 4, a *Hamp1*-deficient mouse strain was used to determine the effect of hepcidin deficiency on outcome of *M.tb* infection. *Hamp1*$^{+/-}$ animals were obtained from Dr. Sophie Vaulont and Dr. Andy McKie and bred in our animal facility in Oxford to produce *Hamp1*$^{-/-}$ offspring. This model was characterised by histological analyses, as well as by the measurement of haematological parameters and gene expression.

In Chapter 5, an iron-deficient mouse model was used to determine the effect of iron deficiency on *M.tb* and BCG infection. Iron deficiency was induced by feeding mice an iron-deficient diet. This model was characterised by assessment of haematological parameters, iron deposition and gene expression prior to infection studies.

# Materials and Methods

# 2 Materials and Methods

## 2.1 Animals

### *2.1.1 Mice*

For the first three experiments, female BALB/c mice (Harlan Laboratories, U.K.) were used. In all subsequent experiments, C57BL/6OlaHsd (Harlan Laboratories, U.K.) were used, with the exception of the gene-deleted mouse experiments. Mice were generally purchased at 6 to 8 weeks of age and rested for one week prior to commencement of procedures.

### *2.1.2 Hamp1$^{-/-}$ mice*

For the *Hamp1*$^{-/-}$ mouse experiments, 2 breeding pairs heterozygous for the *Hamp1* mutation were a gift from Dr. Sophie Vaulont (INSERM, Paris, France). *Hamp1* was disrupted by replacement of exons 1, 2 and part of 3 with a hygromycin resistance cassette via classic homologous recombination in embryonic stem (ES) cells, as described in [113]. Mice were on a C57BL/6 J129 background and were bred in our facility at the Wellcome Trust Centre for Human Genetics, Oxford. Breeding pairs were mated after 8 weeks of age and litters weaned at 3 weeks. Pups were then separated by gender and genotyped. Females were used for experiments.

### *2.1.3 Animal welfare*

All procedures were performed under PPL 30/2889 and PIL 30/9756 granted by the UK Home Office. Mice were kept in individually ventilated cages within a specific pathogen free facility. All housing and procedures were in compliance

with the 'Code of Practice for the Housing and Care of Animals used in Scientific Procedures' and followed the 'Guidance on the Operation of the Animals (Scientific Procedures) Act 1989'. All mice were culled by cervical dislocation at termination of experiments.

### *2.1.4 Custom mouse diets*

Custom diets were manufactured by Harlan Teklad (Madison, US) to contain either 4 parts per million (ppm) or 18ppm of iron in the form of ferric citrate. A control diet was also manufactured identical to the iron deficient diet with the exception that it contained 200ppm of iron, similar to the standard diet used in our facility. Diets were irradiated but designed so that enough nutritional value was retained post-irradiation.

### *2.1.5 Anaesthesia*

For cardiac bleeding and ear tagging, mice were anaesthetised with 2-4% isofluorane and oxygen (2L/min) in air. Post-cardiac puncture, which is a terminal procedure, mice were culled by cervical dislocation. Post-ear tagging, mice were monitored for full recovery from anaesthetic.

### *2.1.6 BCG vaccination*

BCG Pasteur was grown in house in 7H9 Broth (BD, UK) with 0.05% Tween 80 (Sigma Aldrich, UK). Mice were vaccinated with ~4x$10^5$ CFU of BCG Pasteur (PHE, UK) in PBS injected subcutaneously (*s.c.)* into the base of the tail using a U-100 29G syringe in a volume of 100µl. Mice were restrained for this procedure using a tail restrainer.

### *2.1.7 Intranasal BCG infection*

Mice were lightly anaesthetised and scruffed before 50µl containing $5x10^6$ CFU of BCG Pasteur was pipetted drop by drop into the nostrils of the mouse.

### *2.1.8 Aerosol M.tb infection*

Mice were transferred to the category three (CL3) suite within the animal facility and loaded into nose-only restrainers. Mice were exposed to aerosolised *M.tb* Erdman KO1 (TMC107) (BEI Resources, Manassas, USA) using a Biaera AeroMP-controlled nebuliser (Biaera technologies, Hagerstown, USA) contained within a Category Level 3 TCOL isolator (Total Containment Oxford Limited, Oxford, UK) maintained under negative pressure with respect to the atmosphere. The exposure time was 10 minutes, followed by a 5 minute purge cycle at an airflow of 12L/min and pressure of 20psig. Mice were then removed from the restrainers and transferred to cages within the CL3 suite. The challenge process was monitored using the Biaera aeroMP controller. During the cycle, *M.tb* was collected in the impinger (containing PBS and 0.01% Tween 80) and was then plated onto Middlebrooks 7H10 agar to confirm successful challenge. Infectious dose was also verified by quantifying bacterial burden in 2 mice, 24 hours post-infection.

For time course and initial iron restriction experiments, *M.tb* was prepared at a dose of $5x10^6$ CFU/ml in sterile PBS, resulting in infection with 100-200 CFU in the lungs 24 hours post-challenge. All animals in HAMP1$^{-/-}$ infection experiments and final iron-deficient diet experiments were infected with a lower concentration of $1x10^6$ CFU/ml, with 50-100 CFU observed in the lungs 24 hours post-infection.

### *2.1.9 Extraction of blood for haematological analyses*

Mice were anaesthetised with 2-4% isofluorane and oxygen (2L/min) in air and maintained on this until the procedure was complete. Once anaesthetised in an anaesthetic chamber, mice were laid in the supine position. The rib cage was suppressed gently on either side to raise up the chest cavity in order to locate the heart. A BD Microlance 3 26G x 5/8" syringe with a 1ml BD barrel was then inserted horizontally into the heart and held steady for blood removal, after which ~100µl of blood was immediately transferred into a BD Microtainer™ tube containing di-potassium EDTA (BD, UK) and mixed several times to inhibit clot formation. The remainder (500-800µl) was transferred to a 1.5ml eppendorf tube and left in the fridge overnight. The next day it was spun at 14,000 RPM for 10 minutes and the top serum layer was removed and separated into another eppendorf for storage at -80°C until analysis.

### *2.1.10 Tail bleeds*

Where blood was required in a non-terminal procedure, mice were placed in a heat box at 38°C until tail veins were vasodilated. They were then transferred to a restrainer and a small nick was made in the tail vein using a scalpel blade. Drops of blood were then squeezed into the BD Microtainer™ tube and mice were monitored for cessation of bleeding. No more than 100µl of blood was taken.

### *2.1.11 Analysis of blood/serum products*

Blood collected in BD Microtainer™ tubes was analysed for haematological parameters using a Pentra ABX machine. The machine uses 70µl of sample.

*2.1.12 Extraction of organs for qRT-PCR*

Immediately following sacrifice, the median lobe of the liver was removed, avoiding the gall bladder. The inferior edge of this lobe was sliced and cut into 3 small segments around 2mm x 2mm with a sterile scalpel and then transferred into 1ml of RNALater RNA Stabilisation Reagent (Qiagen) and stored at 4°C until required. The remainder of this lobe was sliced into 3 chunks, placed in a 1ml cryovial and snap frozen in liquid nitrogen. After removal of samples from liquid nitrogen, they were transported on dry ice until transfer to -80°C.

*2.1.13 Harvesting of spleen, livers and lungs for histology*

Mice were culled by cervical dislocation. The spleen and the median lobe of the liver were aseptically removed and transferred to a 50ml falcon tube containing 10mls of 10% Neutral Buffered Formal (NBF). To harvest lungs, the body cavity was opened up to expose the trachea. A nick was then created in the top of the trachea using a scalpel. A BAL tube attached to a 2ml syringe containing 1ml of 10% NBF was then gently inserted into the trachea and the lungs were then flushed with NBF. Lungs were then removed and placed in 10% NBF.

*2.1.14 Histopathological techniques*

Tissue was fixed overnight in 10% NBF. Samples were then transferred to 70% EtOH to start the dehydration process. Paraffin-embedded tissue sectioning, and Perl's staining (for non-haem iron) were performed by the Oxford Centre for Histopathology Research (OCHRe) (JR Hospital, Oxford).

*2.1.15 Organ homogenisation and plating for CFU*

At each time point, mice were sacrificed and organs were aseptically removed and placed in 1ml of sterile PBS in Precellys® (Stretton Scientific) CK28-R 2ml re-enforced ceramic homogenizing tubes containing 2.8mm ceramic beads. Organs were then homogenised for 20s at 5500rpm in a Precellys 24 homogeniser (Stretton Scientific). At 24 and 48 hour time points, lungs were plated out neat in 100µl on 7 plates per animal. At all other time points, lungs from unvaccinated animals were plated out at $1x10^{-2}$, $1x10^{-3}$ and $1x10^{-4}$ dilutions. In vaccinated animals, they were plated out at $1x10^{-1}$, $1x10^{-2}$ and $1x10^{-3}$ dilutions. Spleens were plated at $1x10^{-1}$, $1x10^{-2}$ and $1x10^{-3}$ or neat and $1x10^{-1}$ and $1x10^{-2}$. 30µls of each dilution was plated onto a third of a plate, in duplicate. CFU was counted 4 weeks after plating.

All agar plates were made in house with 20mls of 7H10 or 7H11 agar (Sigma) with Middlebrooks's OADC enrichment (Becton Dickinson).

*2.1.16 Genotyping of Hamp1$^{-/-}$ mice*

*2.1.16.1 DNA extraction*

To determine the genotype of the *Hamp1* mice bred in our facility, ear punches were collected in RNAse-free eppendorfs and stored at -20°C unless processed immediately. The ear punch was cleaned with 70% EtOH between each mouse. To extract the DNA, eppendorfs were spun at 9000xg for 1 minute and 20µl of ear punch buffer containing 1mg/ml proteinase K was added to each sample and incubated at 55°C for 20 minutes. Samples were then vortexed to break up tissue and incubated on a shaking heater for a further 20 minutes at 55°C. Proteinase K was inactivated by addition of 180µl RNAse-free water to each

sample which was then heated to 99°C for 5 minutes. After cooling, samples were stored at -20°C until required. Custom-made lyophilised oligonucleotides from Sigma Aldrich (forward WT: Int1F 5'GGGCTGTAGAGGTTCTGCTG-3', Reverse: EX 3R 5'AACAGATACCACACTGGGAA-3', forward KO: ko1 rcB 5'GCCTGAAGAACGAGATCAGC-3') were diluted to a final concentration of 160nM per reaction. The PCR reaction was performed using a GoTaq Flexi DNA polymerase kit (Promega) with dNTPs from a High Capacity RNA-to-cDNA kit (Applied Biosystems), following the manufacturer's protocol. Separate WT and KO reactions were performed, using the same reverse primer.

The PCR cycle was as follows:

| | | | |
|---|---|---|---|
| Primary denature | 94°C | 4 minutes | |
| Denature | 94°C | 30 seconds | Repeat x 35 |
| Anneal | 54°C | 30 seconds | |
| Extension | 72°C | 40 seconds | |
| End | 72°C | 5 minutes | |

PCR products were stored at -20°C until required.

*2.1.16.2 Agarose gel electrophoresis*

Mouse DNA samples were analysed by 1% agarose gel electrophoresis (100V, 45 minutes). Agarose was melted in 1xTAE buffer, with DNA stained using SYBR safe (Life Technologies). PCR products were visualized on a transilluminator, and sized relative to a GeneRuler 1kb DNA Ladder (Life Technologies). WT reactions amplify a 586 base pair (bp) product and KO reactions amplify a 260bp product.

### *2.1.17 Quantitative real-time PCR (qRT-PCR)*

#### *2.1.17.1 RNA extraction and reverse transcription*

RNA was extracted from mouse tissue using an RNEasy Plus Mini Kit (Qiagen) following manufacturer's protocols. Liver tissue stored in 1ml RNAlater RNA Stabilisation Reagent (Qiagen) was homogenized in 600µl RLT buffer (with 1% betamercaptoethanol) in Precellys® 1.5ml tubes (Stretton Scientific). Samples were homogenised in a Precellys®24 at 5000rpm for 2 x 10 seconds with a 10 second break between. The standard RNA extraction protocol was then followed.

#### *2.1.17.2 Reverse transcription*

RNA was diluted in RNAse-free water so each reaction contained <2mg per 20µl reaction prior to reverse transcription using a High Capacity cDNA Reverse Transcription Kit (Applied Biosystems), to convert RNA to cDNA as follows: A 2x reverse transcription mastermix was prepared on ice with the following (per reaction): 2µl of 10 x RT buffer, 0.8µl of 25 x dNTP mix (100mM), 2µl of 10 x RT random primers, 1µl of Multiscribe reverse transcriptase and 4.2µl of RNAse-free water, to a total volume of 10µl of master mix per reaction. The reaction mix was vortexed and pulsed briefly in a microfuge before 10µl was added to 0.1ml PCR tubes. 10µl of diluted template RNA was added and tubes were vortexed and spun briefly before being placed in a thermocyler. The reverse transcription cycle was as follows: 10 minutes at 25°C, 120 minutes at 37°C, 5 seconds at 85°C and then 4°C until cDNA was frozen at -20°C until required.

*2.1.17.3 Quantitative real-time PCR (qRT-PCR)*

Hepatic gene expression was quantified by qRT-PCR using TaqMan Gene Expression Assays (Applied Biosystems) (Table 1) diluted 1:10 in TaqMan Gene Expression Master mix (Applied Biosystems), following manufacturer's protocols. cDNA was diluted in the required volume of RNAse-free water to 2.5ng/μl per reaction so input concentration was the same for each sample. In each well of the reaction plate (MicroAmp Fast Optical 96-well Reaction Plates, 0.1ml, Applied Biosystems), 5.5μl of diluted assay was added, followed by 4.5μl of diluted cDNA, to a total of 10μl per well. Technical duplicates were performed. Plates were sealed before being centrifuged briefly and run on an Applied Biosystems StepOnePlus Real Time PCR system. Reactions were performed in duplicate and analysed by calculating change in gene expression relative to an endogenous control (*Hprt1*), using the formula $2^{-}\Delta$Ct.

| Protein | Gene Symbol | TaqMan Gene Expression Assay Code | Notes |
|---|---|---|---|
| **Activin A** | *Inhba* | Mm00434339_m1 | |
| **Activin B** | *Inhbb* | Mm03023992_m1 | |
| **Bone morphogenetic protein 6** | *Bmp6* | Mm01332882_m1 | |
| **Carbonic anhydrase 9** | *Car9* | Mm00519570_m1 | |
| **Ferritin light chain** | *Ftl* | Mm03030144_g1 | |
| **Ferritin heavy chain** | *Fth* | Mm00850707_g1 | |
| **Ferroportin 1** | *Fpn1* | Mm00489837_m1 | |
| **Fibrinogen alpha chain** | *Fga* | Mm00802584_m1 | |
| **Haem oxygennase 1** | *Ho1* | Mm00516005_m1 | |
| **Hepcidin 1** | *Hamp1* | Mm00519025_m1 | |
| **Hprt-1** | *Hprt1* | Mm01545399_m1 | |
| **Inhibitor of DNA Binding 1** | *Id1* | Mm00775963_g1 | Endogenous control |
| **Interferon gamma** | *Ifng* | Mm01168134_m1 | |
| **Interleukin-6** | *Il-6* | Mm99999064_m1 | |
| **Lipocalin 2** | *Lcn2* | Mm01324470_m1 | |
| **Nramp1** | *Nramp1* | Mm00443045_m1 | |
| **Serum amyloid A1** | *Saa1* | Mm00656927_g1 | |
| **Transferrin receptor** | *Tfrc* | Mm00441941_m1 | |
| **Tumour necrosis factor-alpha** | *Tnfa* | Mm00443258_m1 | |

**Table 1. List of inventoried TaqMan Gene Expression Assays (Applied Biosystems) used in qRT-PCR.**

## 2.2 Mycobacteria

### *2.2.1 BCG Pasteur*

BCG Pasteur was grown in house in 7H9 broth (PHE, UK) containing 0.05% Tween 80, as described below.

### *2.2.2 M.tb*

*M.tb* Erdman strain KO1 was provided by BEI Resources, Manassas, USA. Stocks were provided as frozen suspensions at a concentration of $7.4x10^7$ CFU/ml or $5.2x10^7$ CFU/ml but always diluted in sterile PBS to $5x10^6$ or $1x10^6$ CFU/ml for aerosol infections.

### *2.2.3 Culture of BCG in liquid broth*

Middlebrooks 7H9 media was made up as per manufacturer's instructions (10% ADC supplement and 0.05% Tween 80 (no glycerol)). 5ml of Middlebrooks 7H9 was added to a sterile 15ml universal tube, which was then inoculated with 5ml of BCG seed stock and incubated at 37°C in a shaking incubator for 5 days. In parallel, a negative control was set up containing 10ml of 7H9 medium without BCG. After 5 days the optical density (OD) of the culture was measured on a spectrophotometer at 600nm. For preparing BCG for freezing stocks, an $OD_{600}$ of 0.4 was optimal.

### *2.2.4 Freezing down BCG Pasteur stocks*

Cultures with an $OD_{600}$ of around 0.4 were transferred into 50ml Falcon tubes and centrifuged at 3000rpm for 30 minutes at RT. Supernatant was then discarded and the pellet was re-suspended in 30ml of sterile PBS. The culture was then spun again on the same settings. BCG for seed stocks was frozen down

in 7H9 medium and BCG for vaccinations was frozen down in sterile PBS. All were frozen in 1ml aliquots and kept at -80°C.

## 2.3 *In vitro* and *ex vivo* assays

### *2.3.1 Splenocyte and BCG co-culture experiments*

Naïve murine splenocytes were co-cultured in a range of conditions (exogenous iron, iron chelator or hepcidin) in order to determine the effect of alteration of iron availability on intracellular growth of BCG. Splenocytes were prepared as described below for the MGIT assays. 5000 CFU of BCG in 20µl was added to each sample in 1.5ml micro tubes along with 500µl containing $1x10^6$ splenocytes, in duplicate. Ferric ammonium citrate (FAC) was added at 250µg/ml, desferroxamine (DFO) at 50µM, and hepcidin peptide at 0.5µM. Control tubes without cells but with the same conditions were also set up. All samples were then rotated for 96 hours at 37°C.

After 96 hours, tubes were spun at 12,000 RPM for 5 minutes and the supernatant poured off. Splenocytes were lysed by the addition of 1ml of sterile $dH_2O$ to release intracellular BCG. Samples were then vortexed and left for 5 minutes at RT. This was repeated three times, followed by another spin at 12,000 RPM for 10 minutes. Supernatants were poured off and pellets re-suspended in 500µl 7H9. Samples were then plated neat, 1 in 10 and 1 in 100 on Middlebrooks 7H10 agar plates, which were then incubated at 37°C. Colonies were counted after 3 weeks to quantify bacterial growth by CFU.

### *2.3.2 THP-1 and BCG co-culture experiments*

#### *2.3.2.1 THP-1 monocyte culture*

The THP-1 monocytic cell line was a gift from Lucy Eddowes (Weatherall Institute of Molecular Medicine, Oxford, UK). Cells were cultured at a maximum concentration of $1x10^6$/ml in vented cell culture flasks in RPMI with 1% Penicillin/Streptomycin, 1% L-Glutamine and 10% FCS at incubated at 37°C in humidified air containing 5% $CO_2$.

#### *2.3.2.2 Seeding of THP-1 cells*

THP-1 cells were seeded and differentiated in 24-well cell culture plates at $5x10^5$/ml in 1ml with 20nM PMA and incubated at 37°C or 24 hours. The next day, PMA was removed and cells received 1ml of fresh media containing either FAC at a concentration of 250μg/ml or DFO (both Sigma) at 50μM for 24 hours.

#### *2.3.2.3 BCG infection*

After a 24 hour incubation with or without iron or chelator, media was removed and cells were infected with 500μl of BCG in media containing the usual concentrations of FAC or DFO for 4 hours. After 4 hours, 1ml of PBS was added to all wells to wash off extracellular BCG and 1ml of fresh media with FAC or DFO was added for the remaining time points. Media was replaced every day, with fresh FAC or DFO where required.

#### *2.3.2.4 Plating for bacterial burden via micro CFU*

At each time point (4h, 24h, 48h and 6 days post-BCG) BCG was plated for quantification of bacterial burden by micro CFU. Firstly, media was removed from the well and 1ml of PBS was added to wash off any extracellular BCG. Following removal of PBS, 300µl of lysis buffer (1% igepal in sterile water) was gently added and mixed very well in each well. Dilutions of lysed cell mixes were prepared at 0, $10^{-1}$, $10^{-2}$ and $10^{-3}$ in a 96-well U-Bottom plate. 5µls drops of each dilution were then plated in duplicate on a square Middlebrooks agar plate. Plates were then allowed to dry and were wrapped in foil at 37°C for 1 week before counting.

### *2.3.3 Mycobacterial Growth Inhibition (MGIT) Assays*

#### *2.3.3.1 Assay overview*

This assay measures the *in vitro* ability of the cell type in question to inhibit growth of mycobacteria. It was developed as an alternative to *in vivo* challenge, as it can be used to assess immunogenicity in samples taken pre-and post-vaccination. The tubes used in this assay contain Middlebrooks 7H9 media. At the bottom of the tube is an oxygen-quenched fluorochrome. During bacterial growth, oxygen inside the tube is utilised and carbon dioxide is excreted, resulting in activation of the fluorochrome, which fluoresces under UV light. The MGIT machine monitors fluorescence every hour and once a tube reaches a certain level of fluorescence, it becomes "positive". Therefore, the time to positivity (TTP) is proportional to bacterial growth.

In this thesis, bacteria were inoculated directly into MGIT tubes in a range of conditions, or firstly co-cultured with THP-1 cells, as described below. To validate the MGIT assay, splenocytes from BCG-vaccinated and unvaccinated mice were also used, since BCG-vaccinated mice inhibit bacterial growth better than unvaccinated mice.

#### *2.3.3.2 Preparation of spleens for validation experiment*

Spleens were aseptically removed from mice and placed in 1ml of sterile PBS. They were then mashed in a 6-well plate using the blunt end of a 1ml syringe and RPMI containing 10%FCS, 1% P/S and 1% L-glut to wash the syringe. Samples were then put through a cell strainer and mashed again before being transferred to a 50ml falcon tube and the volume was topped up to 15ml. Samples were left at RT for 30 minutes to allow antibiotics to act, followed by centrifugation at 1500rpm for 10 minutes. Supernatants were then poured off and pellets re-suspended in RPMI + 10% FCS and 1% L-Glut without P/S, in order to wash off the antibiotics, before spinning again. Supernatants were poured off and the pellets were re-suspended in 5ml of RPMI with HEPES + 10% FCS+1% L-Glut. Cells were then counted using a CasyCounter and concentrations adjusted to a final concentration of $2x10^6$/ml so that 500ul contained 1 million cells. For each spleen, 500µl containing 1 million cells was then transferred to two (duplicate) 1.5ml cryovials.

#### *2.3.3.3 Preparation of BCG Pasteur*

BCG Pasteur frozen down in 7H9 was thawed, sonicated twice for 1 minute and placed on ice for 1 minute between each sonication. It was then diluted in RPMI HEPES + 10% FCS + 1% L-Glut so that 100µl contained the pre calculated

inoculum volume from the titration stock. Each sample then received 100µl of BCG/media master mix on top of the 500µl to a final volume of 600µl per cryovial. Tubes were subsequently placed in a rotating rack at 37°C for 96 hours.

#### *2.3.3.4 Preparation of M.tb*

*M.tb* Erdman was thawed and sonicated twice for 1 minute (placed on ice for 1 minute between each sonication for cooling). It was then diluted into a master mix so the correct inoculum volume was present in 100µl for each sample, the same as just described for the BCG stock.

#### *2.3.3.5 Set up of positive control tubes*

Positive control tubes were set up on day 0 of the MGIT assay. To set up control tubes, one vial of MGIT OADC broth was re-suspended in MGIT PANTA antibiotic medium. Three MGIT tubes were then supplemented with 800µl of this medium. 500µl from the third, supplemented MGIT tube was added to the other two and 100µl of the master mix containing the mycobacteria was added to the two control tubes. Tubes were then mixed and placed directly in the BACTEC MGIT 960 machine.

#### *2.3.3.6 Processing of samples after 96 hours*

BACTEC MGIT tubes for the required number of samples were supplemented with 800µl of MGIT PANTA antibiotic medium mixed with MGIT OADC enrichment broth. Samples were removed from the incubator and centrifuged at 12,000rpm for 5 minutes. Supernatants were carefully discarded and cells were lysed in 1ml of sterile water before being transferred to supplemented BACTEC

MGIT tubes. Tubes were then placed in the BACTEC 960 machine and incubated at 37°C until they became positive.

#### *2.3.3.7 Titration of bacterial stocks*

The dose of bacteria required for inoculation of positive controls and each sample tube was calculated for an ideal time to positivity (TTP) of 6.5 days. The correct inoculum to achieve this is calculated by titrating the BCG beforehand and producing a standard curve with the equation y = mLn(x)+c where m=gradient, x = inoculum, y = TTP and c = y-intercept. This was calculated for each stock of bacteria used. To titrate the mycobacteria, 6 x 10-fold serial dilutions of each stock were done in MGIT 7H9 media supplemented with the PANTA antibiotics/OADC enrichment broth mix. MGIT tubes were inoculated in duplicate with 500µl of diluted bacteria or neat stock before being placed in the BACTEC 960 machine. For each dilution, stock was also plated on Middlebrooks 7H10 agar plates in order to quantify bacterial burden by CFU.

#### *2.3.3.8 Calculating net growth from raw MGIT data*

All positive tubes are given a TTP (time to positivity) value by the BACTEC 960 machine. Net growth is calculated from the TTP values for matched duplicates by converting to an inoculum volume, which is calculated based on the titration curve for each bacterial stock. The equation TTP= mLn (x) + c could be rearranged in order to find x=EXP((y-c)/m) (TTP set to an optimum of 156 hours). Inoculum volume in µl could then be converted to CFU count (based on estimated CFU/ml by plating) and $\log_{10}$ transformed. The change in net growth was calculated as sample $\log_{10}$ CFU – control $\log_{10}$ CFU.

#### *2.3.3.9 Using MGIT assays to determine how altering iron availability affects BCG growth*

MGIT assays were also set up using THP-1 monocytes incubated for 4 days with BCG in a range of conditions. THP-1 monocytes were cultured beforehand as detailed in section 2.4.2.1 prior to addition of $1x10^6$ cells per cryovial in 500ul. The correct BCG inoculum volume in a further 100ul of media was then added. This BCG master mix was made up to have FAC added to a final concentration in the tube ranging from 10-5000μg/ml or DFO added between 1-10,000μM. Tubes were subsequently placed in a rotating rack at 37°C for 96 hours. Assays were also set up by adding BCG and the above concentrations of FAC and DFO directly to MGIT tubes. All samples were prepared in duplicate.

## 2.4 Statistical analyses

Statistical analyses were performed in GraphPad Prism 6. All data sets were tested for normality with the normality tests offered by Prism. Where 2 groups were compared, Mann-Whitney tests were performed. Where two or more groups were compared, multiple Mann-Whitney tests were performed with Bonferroni corrections for multiple comparisons. Correlations were either Spearman Rank correlations or Pearson correlations, depending on whether data followed Gaussian distribution. Where two factors were being compared, two-way ANOVAs were performed with Bonferroni post-tests for multiple comparisons. Significance was taken as $p=<0.05$ where $p=<0.05$, $p=<0.01$, $p=<0.001$ and $p<0.0001$ are represented by *, **, *** and ****, respectively.

# Chapter 3

# 3 The effect of mycobacterial infection on murine iron homeostasis

## 3.1 Introduction

Iron is vital for the growth of *M.tb* but also for the growth and immune function of the host organism since it is able to interfere with host anti-microbial effector mechanisms [176]. Therefore, a delicate balance between iron availability to the host and the pathogen exists. There is increasing evidence that iron availability is differentially regulated by the host, depending on whether a pathogen resides extracellularly or intracellularly. Increased hepcidin expression has been associated with extracellular pathogens, and reduced hepcidin expression has been associated with intracellular pathogens [177, 178]. Furthermore, intramacrophage iron content may significantly affect the outcome of intracellular infections. For example, iron negatively affects the anti-microbial functions of macrophages by inhibiting pathways regulated by IFN-γ, reducing their ability to control intracellular pathogens such as *Mycobacteria* and *Salmonella* [156-158]. Decrease of intracellular iron can a) reduce infection by limiting iron availability to the pathogen and b) stimulate release of anti-microbial cytokines such as TNF-α and iNOS [155].

A number of human studies suggest that iron supplementation may be linked to poorer disease outcomes in TB [133, 145, 179, 180]. In addition, iron overload in a mouse model has been linked to increased disease severity [179, 181] and the iron-overloaded B2M knockout mouse succumbs to disease more rapidly.

Treatment of the iron overload in B2M knockout mice reverses the increase in susceptibility, but does not affect $CD8^+$ T cell knockout mice. This confirms that the increased susceptibility to infection seen in B2M knockout mice is related to iron overload, and is not a result of the B2M knockout affecting $CD8^+$ T cell functionality [135, 145]. Interestingly, recent studies have highlighted a relationship between the iron regulatory peptide hepcidin and TB disease; high hepcidin has been linked to increased risk of mortality associated with TB disease [141].

The role of hepcidin and iron homeostasis in controlled *in vivo* murine *M.tb* infection has not been previously investigated. Since the mechanisms of pathogenesis of *M.tb* infection are not yet clear, it is important to investigate novel pathways that might be relevant and could be used as a therapeutic target, such as iron homeostasis in the host or the pathogen. For example, if intramacrophage iron content is important in control of *M.tb,* it may be possible to manipulate this therapeutically as a way of treating TB disease.

To investigate this further, I examined the effect of *M.tb* infection on iron homeostasis in a murine aerosol *M.tb* infection model. I firstly investigated how *M.tb* infection affects the expression of genes involved in iron homeostasis in BALB/c mice. Then I went on to look at kinetics of these genes post-infection. In this DPhil project, I also used a hepcidin knockout mouse strain on a C57BL/6 background. Although it is well documented that C57BL/6 and BALB/c mice are similarly resistant to *M.tb* [70], I had not looked at hepcidin kinetics post-infection in C57BL/6 mice. There is evidence in the literature that genetic background affects systemic iron parameters [182, 183]. To investigate

this, I also infected C57BL/6 mice and performed gene expression analyses, as well as quantification of bacterial burden, to compare to the previous experiment in BALB/c mice.

Aims of this chapter:

- Determine the effect of *M.tb* infection on the expression of hepcidin and other genes involved in iron homeostasis
- Determine the kinetics of expression of hepcidin and other genes involved in iron homeostasis post-*M.tb* infection
- Determine whether BCG vaccination affects the expression of hepcidin and other genes involved in iron homeostasis
- Compare responses in BALB/c and C57BL/6 mice to determine whether there are strain differences in the expression of genes involved in iron homeostasis

## 3.2 Evaluation of the effect of *M.tb* infection on the expression of genes involved in iron homeostasis

To explore the effect of BCG vaccination and *M.tb* infection on iron homeostasis, in particular on hepcidin gene expression, eight week old BALB/c mice were left unvaccinated (control mice) or were vaccinated *s.c.* with $4x10^5$ CFU of BCG and infected 10 weeks later with ~100 CFU of aerosolised *M.tb* (Figure 3.2.1A). Four weeks later, the experiment was terminated and lungs, spleen and liver were homogenised to quantify bacterial burden (CFU). Uninfected and unvaccinated, and uninfected and vaccinated groups were

included as controls and were harvested at the same time point. For all animals, gene expression was quantified in the median lobe of the liver, since hepatic hepcidin mRNA levels have been shown to correlate with serum hepcidin levels and iron stores [109, 184].

### *3.2.1 M.tb aerosol infection in mice results in infection of lungs, spleen and liver. BCG vaccination reduces bacterial burden in all three organs.*

Bacterial colonies were observed in lung, spleen, and liver homogenates, 4 weeks post-infection (Figure 3.2.1 B-D). As expected, BCG vaccination significantly reduced the bacterial burden in lungs ($p=0.0002$), spleen ($p=0.0003$), and liver ($p=0.0022$) of vaccinated compared to unvaccinated mice.

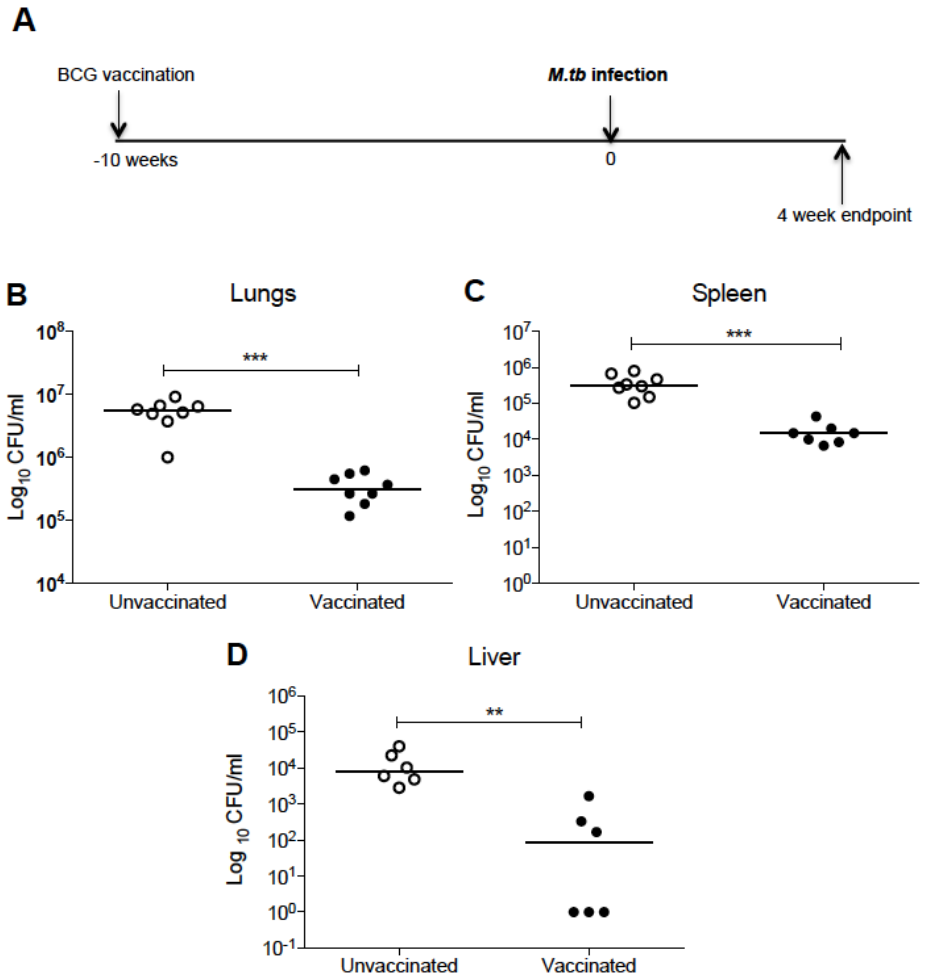


**Figure 3.2.1 CFU burden in unvaccinated and BCG-vaccinated mice post-*M.tb* infection.** BALB/c mice were vaccinated with BCG 10 weeks prior to infection with *M.tb*. Uninfected controls were also included, and the experiment was terminated 4 weeks post-infection (A). Lungs (B), spleen (C) and liver (D) were homogenised and plated out for quantification of bacterial growth by CFU. Open circles represent unvaccinated animals, closed circles represent vaccinated animals. N=8 per group. All statistical analyses were Mann-Whitney tests where * p≤0.05, ** p≤0.01 *** p=≤0.001 **** p=≤0.0001

### *3.2.2 M.tb infection affects the expression of genes involved in iron homeostasis*

In our pilot infection studies (data not shown), post-*M.tb* infection *Hamp1* (the gene encoding hepcidin) expression was significantly higher in BCG-vaccinated mice than in unvaccinated mice, indicating that higher hepcidin might be a protective mechanism of BCG vaccination. However, no uninfected control groups were included in this experiment, so it is possible that differences in

bacterial load between unvaccinated and vaccinated mice might be confounding this data. In this repeat infection, *Hamp1* mRNA expression was compared in uninfected and infected mice (Figure 3.2.2A). *Hamp1* expression was significantly higher in BCG-vaccinated mice compared to unvaccinated mice post-infection (p=0.0025) but no difference was observed between unvaccinated and vaccinated mice in the uninfected controls. When comparing vaccinated groups, uninfected mice had a similar level of *Hamp1* mRNA as the *M.tb* infected mice, but hepcidin was down-regulated in the unvaccinated mice post-infection (p=0.0293). This implies a down-regulation of hepcidin in the unvaccinated mice post-infection, rather than an up-regulation induced by BCG vaccination itself. Moreover, it is likely that the difference observed between unvaccinated and vaccinated mice is due to differences in bacterial load since BCG vaccination reduces CFU by around 1 log.

In this *M.tb* infection experiment, differences in levels of *Fpn1* (the gene encoding ferroportin) between vaccinated-infected and unvaccinated-infected mice, but not uninfected mice, were observed (Figure 3.2.2B) (p=0.0148), indicating that reduced bacterial burden as a result of BCG vaccination likely affects the expression of *Fpn1*, probably through altered hepcidin expression.

To investigate whether SMAD or STAT3 pathways might be influencing hepcidin expression 4 weeks post-challenge, I quantified the expression of other genes that are induced by these two pathways. I hypothesised that since TB induces inflammation and release of IL-6 [185], hepcidin expression during *M.tb* infection might be regulated by the inflammatory JAK/STAT3 pathway. However, the gene encoding fibrinogen alpha chain (*Fga*), which is STAT3-

dependent, did not correlate with *Hamp1* message (Figure 3.2.2F). Furthermore, expression of *Il6*, which is known to induce hepcidin via the inflammatory JAK/STAT3 pathway, although higher in unvaccinated animals, did not correlate with *Hamp1* mRNA (data not shown). *Id1*, a BMP target gene, was also quantified but did not correlate with *Hamp1* either (Figure 3.2.2E). These data suggest that neither of these two pathways are responsible for the suppression of *Hamp1* seen in *M.tb* infected mice.

I then investigated whether hypoxia may play a role in the observed hepcidin suppression, since it is known to suppress hepcidin expression [107, 125, 186, 187]. Interestingly, the expression of a marker gene for hypoxia, carbonic anhydrase 9 (*Car9*) was significantly higher in unvaccinated infected mice than uninfected controls (p=0.0007, Figure 3.2.2C), and correlated inversely with *Hamp1* (r=-0.6882, p=0.0032, Figure 3.2.2G). The potential role of hypoxia was further suggested by a strong positive correlation between *Car9* and lung CFU (r=0.8079, p=0.0002) (Figure 3.2.2H). Moreover, expression of the gene encoding haem oyxgenase 1 (*Ho1*), which is induced by oxidative stress, was also significantly raised in unvaccinated, infected mice (p=0.0007) (Figure 3.2.2.D).

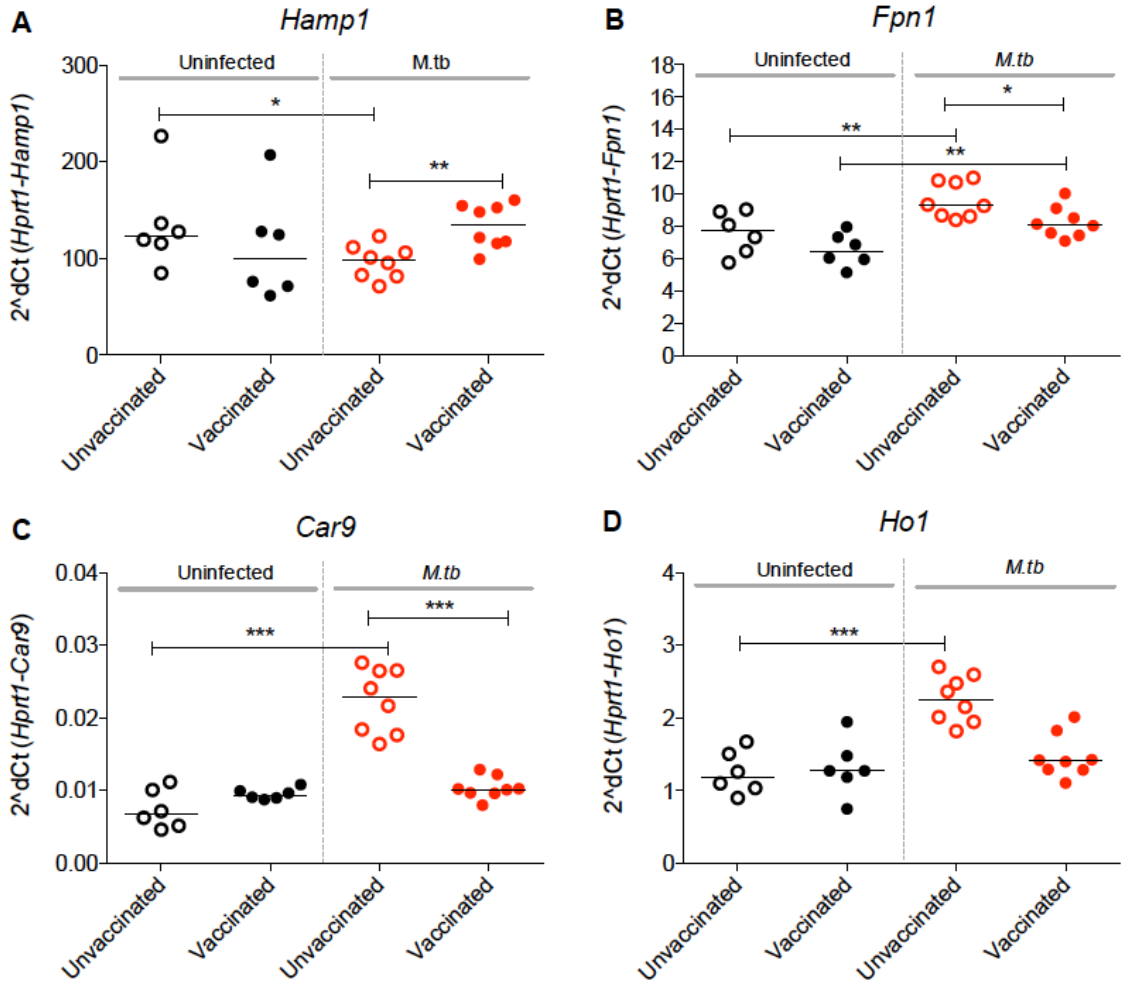
A
Hamp1
Uninfected
M.tb
2^dCt (Hprt1-Hamp1)
300
200
100
0
*
**
Unvaccinated
Vaccinated
Unvaccinated
Vaccinated
B
Fpn1
Uninfected
M.tb
2^dCt (Hprt1-Fpn1)
18
16
14
12
10
8
6
4
2
0
**
*
**
Unvaccinated
Vaccinated
Unvaccinated
Vaccinated
C
Car9
Uninfected
M.tb
2^dCt (Hprt1-Car9)
0.04
0.03
0.02
0.01
0.00
***
***
Unvaccinated
Vaccinated
Unvaccinated
Vaccinated
D
Ho1
Uninfected
M.tb
2^dCt (Hprt1-Ho1)
4
3
2
1
0
***
Unvaccinated
Vaccinated
Unvaccinated
Vaccinated

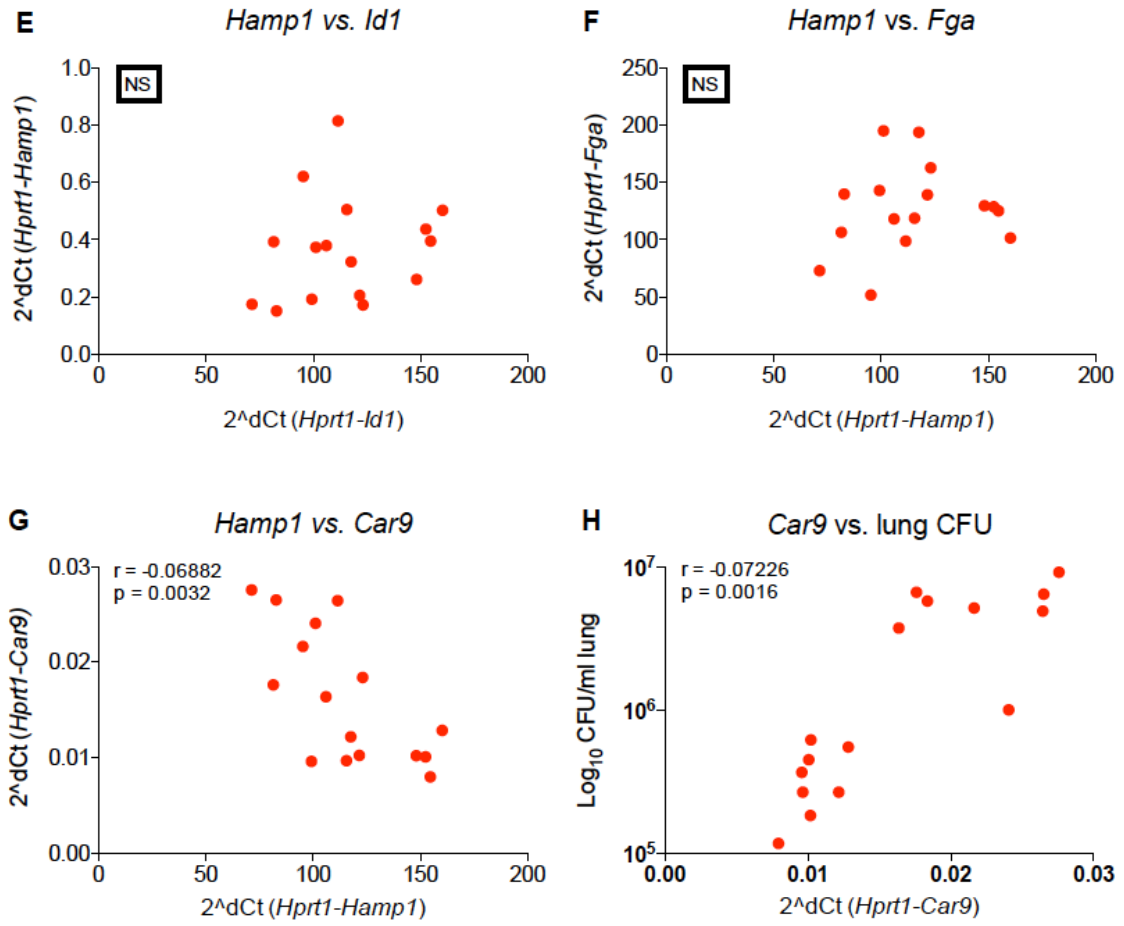


**Figure 3.2.2 The effect of *M.tb* infection and BCG vaccination on the expression of genes involved in iron homeostasis.** BALB/c mice were vaccinated with BCG 10 weeks prior to infection with *M.tb*. Unvaccinated and uninfected controls were also included, and the experiment was terminated at 4 weeks post-infection. Hepatic gene expression analyses for *Hamp1* (A), *Fpn1* (B), *Car9* (C), and *Ho1*(D) was performed for all animals including uninfected controls. Correlations with *Hamp1* were performed for *Id1*, *Fga* and *Car9* (E, F and G, respectively) as well as for *Car9* with lung CFU (H). Open circles represent unvaccinated animals, and closed circles represent vaccinated animals. Black symbols represent uninfected animals and red symbols represent infected animals. All analyses were Mann-Whitney tests corrected for multiple comparisons where * p≤0.05, ** p≤0.01 *** p=≤0.001 **** p=≤0.0001. n=6 for uninfected groups, n=8 for infected groups.

## 3.3 The effect of *M.tb* on hepcidin kinetics in time course studies in BALB/c mice

I have shown that hepcidin gene expression was suppressed in unvaccinated but not BCG-vaccinated mice 4 weeks post-*M.tb* infection, and that suppression was possibly induced by hypoxia. Moreover, this suppression was not seen in uninfected animals, possibly as they were not hypoxic. I next investigated the kinetics of hepcidin expression post-*M.tb* infection to determine whether hepcidin might be induced earlier post-infection. BCG-vaccinated and unvaccinated BALB/c mice were infected with *M.tb* and animals were taken down at 1, 2, 7, and 28 days post-infection. Uninfected controls (unvaccinated and vaccinated) were also taken down the day before infection (D0), as well as at D28 (Figure 3.3.1A). Liver was taken from all animals for qRT-PCR analysis, and lung and spleen homogenates from infected animals were plated out to quantify bacterial burden.

### *3.3.1 M.tb burden increases in lungs and spleen from 24 hours post-infection*

In our infection experiments, 2 animals are normally taken down 24 hours post-infection in order to confirm successful infection and to quantify infection dose. However, we have not previously looked at growth in lungs and spleen between D1 and D28 post-infection. In this experiment, around 100 CFU/ml of bacteria was observed in the lungs one day post-infection, with no differences seen between groups (Figure 3.3.1B). However, no bacteria were observed in the spleens of the majority of animals this early on, with the exception of a few of the vaccinated animals (Figure 3.3.1C). One week post-infection, bacteria were

present in the spleen, indicating dissemination occurs between D1 and D7 post-infection. Interestingly, at D7, vaccinated animals had a significantly higher bacterial burden in their spleens than unvaccinated animals ($p=0.0395$), although no difference was observed in the lungs. This is the opposite of what is seen at D28 in both lungs and spleen, where bacterial burden is the highest, and vaccinated mice have ~1 log lower bacterial burden than unvaccinated mice ($p=0.0395$ and $p=0.0316$, respectively), again confirming that the BCG reduces bacterial burden.

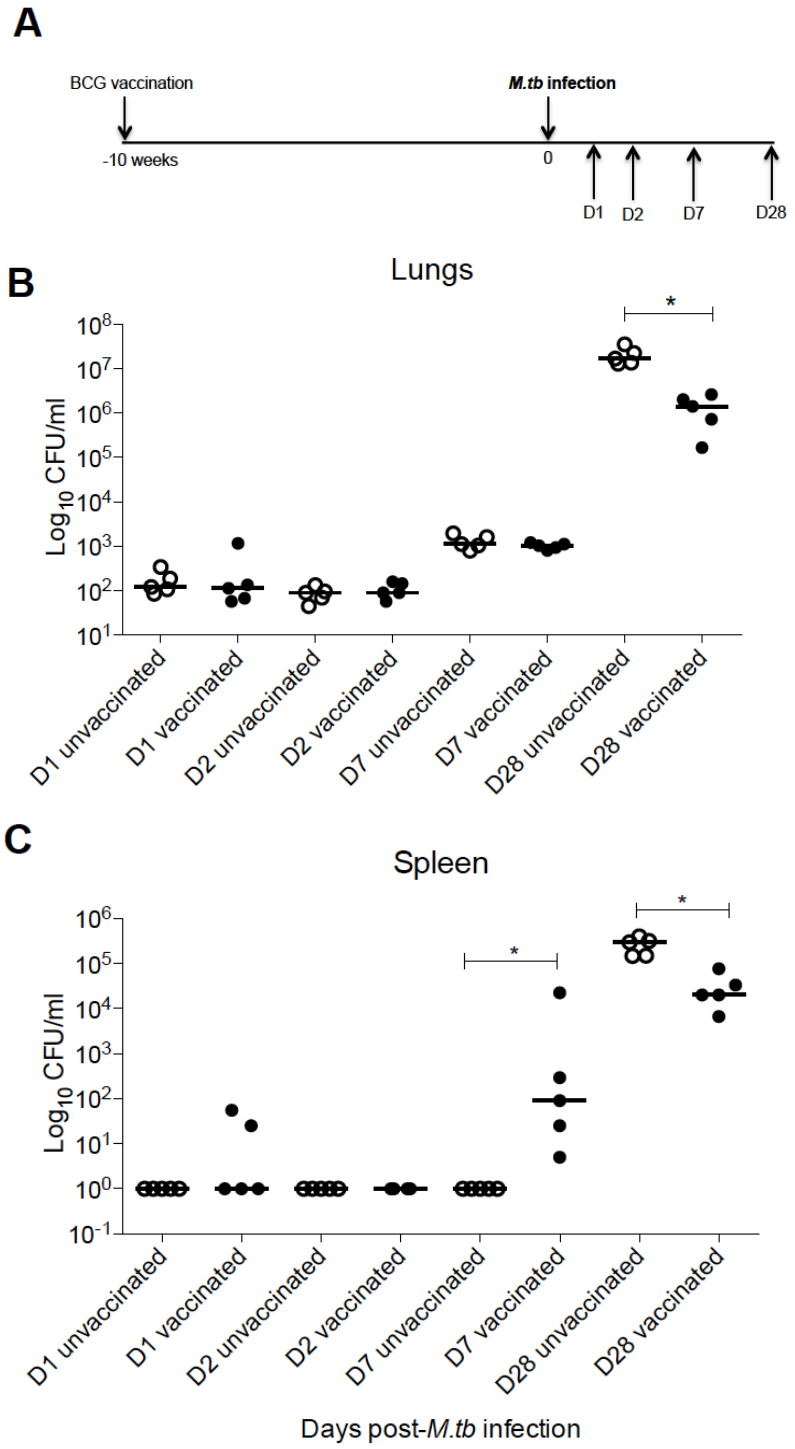


**Figure 3.3.1 CFU time course in *M.tb*-infected mice.** BALB/c mice were vaccinated with BCG. Ten weeks later, animals were infected with *M.tb* via aerosol. Animals were sacrificed at D1, D2, D7 and D28 following infection (A). Organs were harvested for quantification of bacterial burden (CFU) as shown for lungs (B) and spleen (C). Unvaccinated animals are represented by open circles and vaccinated animals by closed circles. A Kruskal-Wallis test was performed on all groups ($p = <0.0001$), followed by Mann Whitney tests to compare groups at each time point, with Bonferroni corrections for multiple comparisons. *, **, *** and **** represent $p \leq 0.05$, $p \leq 0.01$, $p = \leq 0.001$ and $p = \leq 0.0001$, respectively. n=5 animals per group

### *3.3.2 Hepcidin fluctuates post-infection*

*Hamp1* expression fluctuated post-infection in both unvaccinated and BCG-vaccinated mice (Figure 3.3.2A). In agreement with previous data, at 28 days post-infection, *Hamp1* mRNA was significantly lower in unvaccinated mice compared to vaccinated mice (p=0.0316) (Figure 3.3.2B). *Hamp1* mRNA was also reduced in the unvaccinated-infected mice compared with their uninfected controls (p=0.0316), indicating that infection reduced expression of *Hamp1*. No differences were observed between vaccinated groups pre- and post-infection, confirming that hepcidin suppression was not affected by BCG vaccination itself, and most likely is a result of reduced bacterial burden in the vaccinated animals. However, *Hamp1* did not correlate with lung CFU (Figure 3.3.2Q), suggesting that the observed suppression of *Hamp1* in the unvaccinated infected mice may not be directly related to bacterial burden.

### *3.3.3 Changes in hepcidin expression post-M.tb infection may be regulated by BMP signalling*

Previously I did not observe a relationship between *Hamp1* expression and markers of BMP/SMAD or JAK/STAT signalling. However, with a larger group of animals and a wider range of timepoints post-infection, a positive correlation between *Hamp1* mRNA and *Id1* mRNA (r=0.5603, p=0.0002) (Figure 3.3.2O) was seen across all timepoints, consistent with findings that the BMP pathway regulates hepcidin mRNA transcription [121]. This correlation was still evident when groups were split into unvaccinated and vaccinated animals, so was not an effect of the observed *Hamp1* suppression in unvaccinated mice (data not shown). Consistent with my previous data, no correlation was observed between

*Fga* and *Hamp1* (Figure 3.3.2P), suggesting there is no role of the inflammatory JAK/STAT3 pathway in the regulation of *Hamp1* transcription during *M.tb* infection.

### *3.3.4 A role for hypoxia in regulation of hepcidin in TB?*

Despite the correlation seen between *Hamp1* and *Id1* (Figure 3.3.2O), and the significant drop in *Hamp1* in unvaccinated mice at 4 weeks post-infection (Figure 3.3.2B), BCG vaccination did not affect the overall expression of *Id1* mRNA over the time course. This could indicate that the BMP pathway is not solely responsible for regulating *Hamp1* mRNA. To investigate whether hypoxia might be implicated in the regulation of hepcidin post-*M.tb* infection. I looked at expression of *Car9*.

Time post-infection had a significant effect on *Car9* mRNA levels, with levels increasing gradually post-infection in both unvaccinated and vaccinated mice (Figure 3.3.2G; p=<0.0001). When compared with the uninfected controls, *M.tb*-infected mice had significantly raised *Car9* mRNA (p=0.0316), but no differences were observed between vaccinated groups (Figure 3.3.2H). Interestingly, although correlations were previously seen between *Car9* and *Hamp1* mRNA levels when only looking at D28 post-infection, no correlation was seen over the whole time course (Figure 3.3.2R). However, as illustrated in Figure 3.3.2S, a weak positive correlation between liver *Car9* mRNA levels and lung CFU was found in unvaccinated animals (which had higher bacterial burden) (r=0.4991, p=0.0012).

I also looked at another marker of hypoxia, *Ho1*, which showed similar changes to *Car9* post-infection (Figure 3.3.2I and J). As with *Car9*, hepatic expression of *Ho1* mRNA increased with time post-challenge in both unvaccinated and vaccinated mice (p=<0.0001), with significant increases being observed between D7 and D28 in both unvaccinated and vaccinated animals (p=0.0079 and p=0.0159, respectively). The increase in expression of *Car9* and *Ho1* with increased bacterial burden implies that the pathology caused by *M.tb* infection might result in hypoxia. However, since *Car9* did not correlate with *Hamp1* (Figure 3.3.2R), it is unlikely that hypoxia is influencing hepcidin expression. Moreover, despite the observed increases in *Ho1* in the time course plot, when compared to uninfected controls, no differences were observed.

### *3.3.5 Roles for other molecules involved in iron homeostasis*

I also measured the expression of *Lcn2*, the gene encoding antimicrobial peptide lipocalin 2, which functions by binding bacterial siderophores in order to reduce iron availability for invading pathogens [170, 188]. Post-*M.tb* infection, *Lcn2* expression peaked at D1 in both unvaccinated and vaccinated mice and was not significantly different between groups. The increase was only significant between D0 and D1 in the unvaccinated mice (Figure 3.3.2M; p=0.00037). Two days post-infection, *Lcn2* had returned to baseline, consistent with previous findings [188]. No differences were observed when comparing infected animals to uninfected controls at D28 (Figure 3.3.2N).

I also quantified the expression of *Nramp1,* the gene encoding divalent metal transporter Nramp1, an abundantly expressed phagosomal protein, which has

been associated with increased resistance to a number of infections, including *M.tb*. It likely functions by transporting iron from inside the phagosome into the cytoplasm for export, ultimately reducing intracellular iron availability for intracellular pathogens [189]. Expression of hepatic *Nramp1* increased significantly post-infection in the unvaccinated mice, with expression at D28 being significantly higher than all earlier timepoints (Figure 3.3.2K) ($p=<0.0001$ for all). Consistent with this finding, at D28, *Nramp1* was significantly higher in infected unvaccinated animals than in uninfected controls (Figure 3.3.2L; $p=0.0316$). This is not surprising since *Nramp1* is induced by infectious stimuli and IFN-$\gamma$, which is also produced post-*M.tb* infection [190]. Moreover, *Nramp1* correlated positively with lung CFU (Figure 3.3.2T, $r=0.6064$, $p=<0.0001$). Finally, *Nramp1* is known to induce the expression of *Lcn2* in order to restrict iron availability to the pathogen [191]. However, no correlations were observed between the two (data not shown).

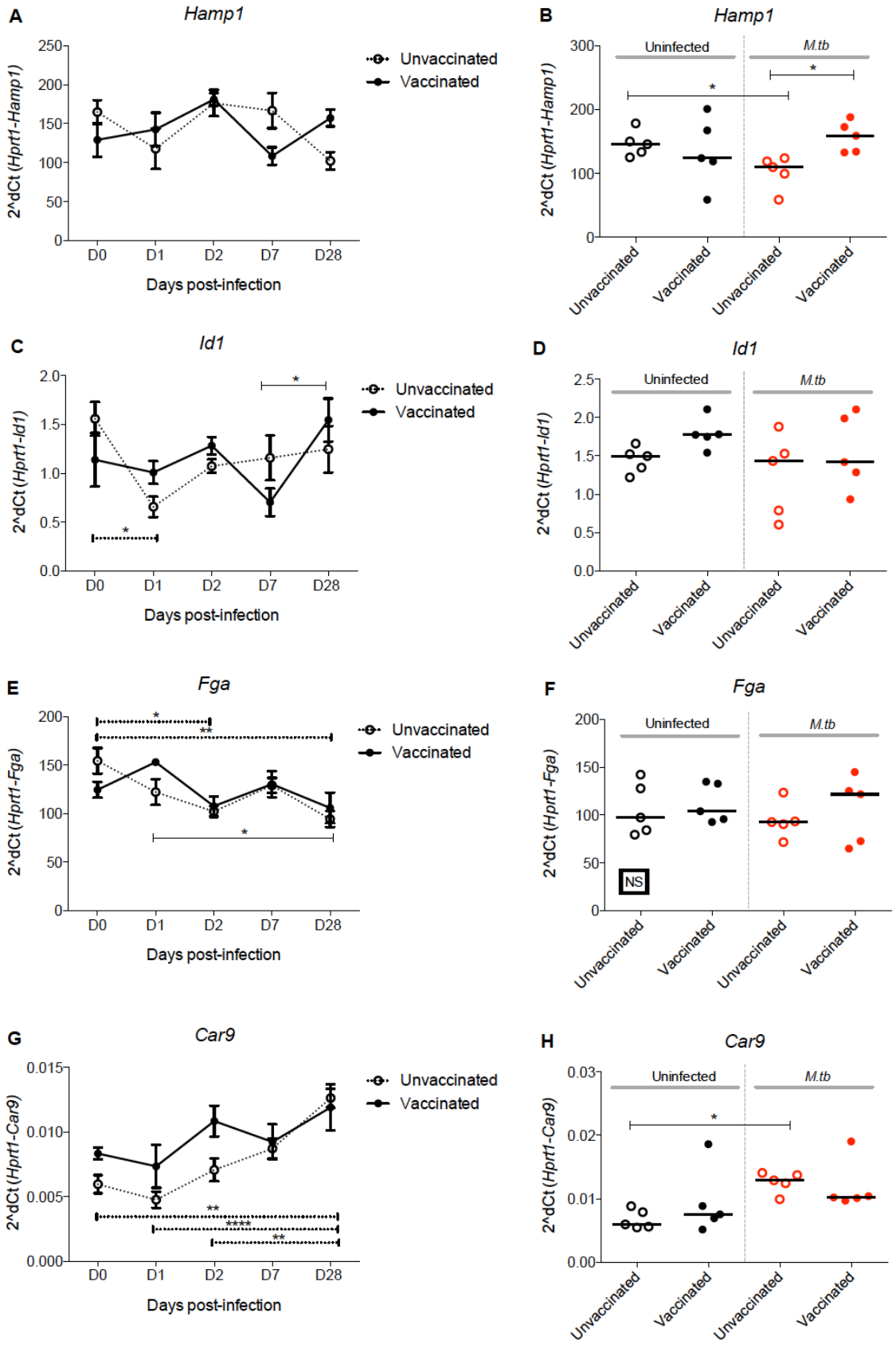
A
Hamp1
2^dCt (Hprt1-Hamp1)
Unvaccinated
Vaccinated
D0
D1
D2
D7
D28
Days post-infection
B
Hamp1
2^dCt (Hprt1-Hamp1)
Uninfected
M.tb
Unvaccinated
Vaccinated
C
Id1
2^dCt (Hprt1-Id1)
D
Id1
E
Fga
2^dCt (Hprt1-Fga)
F
Fga
NS
G
Car9
2^dCt (Hprt1-Car9)
H
Car9

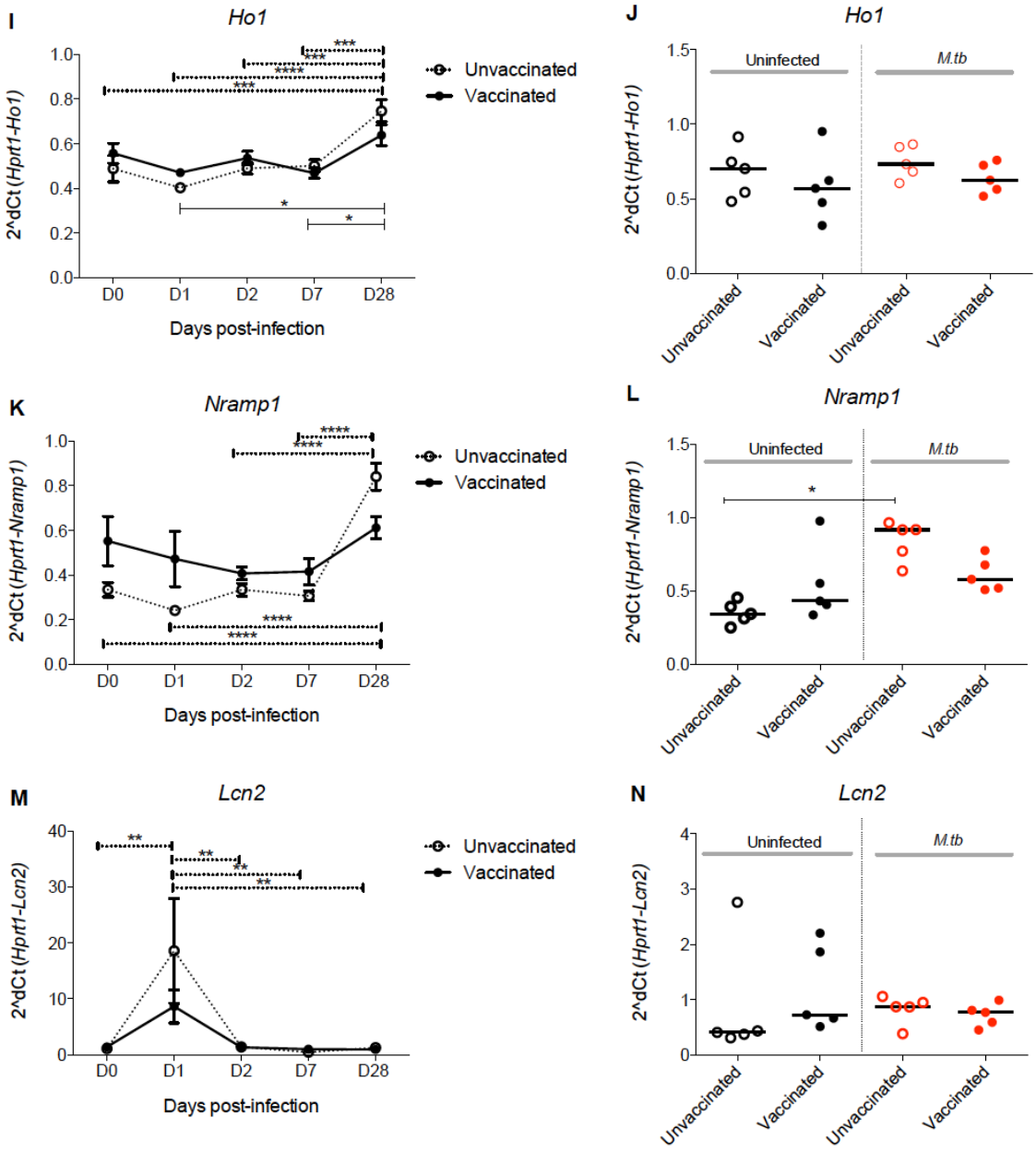
I
Ho1
2^dCt (Hprt1-Ho1)
Days post-infection
D0
D1
D2
D7
D28
Unvaccinated
Vaccinated
J
Ho1
Uninfected
M.tb
2^dCt (Hprt1-Ho1)
Unvaccinated
Vaccinated
K
Nramp1
2^dCt (Hprt1-Nramp1)
L
Nramp1
M
Lcn2
2^dCt (Hprt1-Lcn2)
N
Lcn2

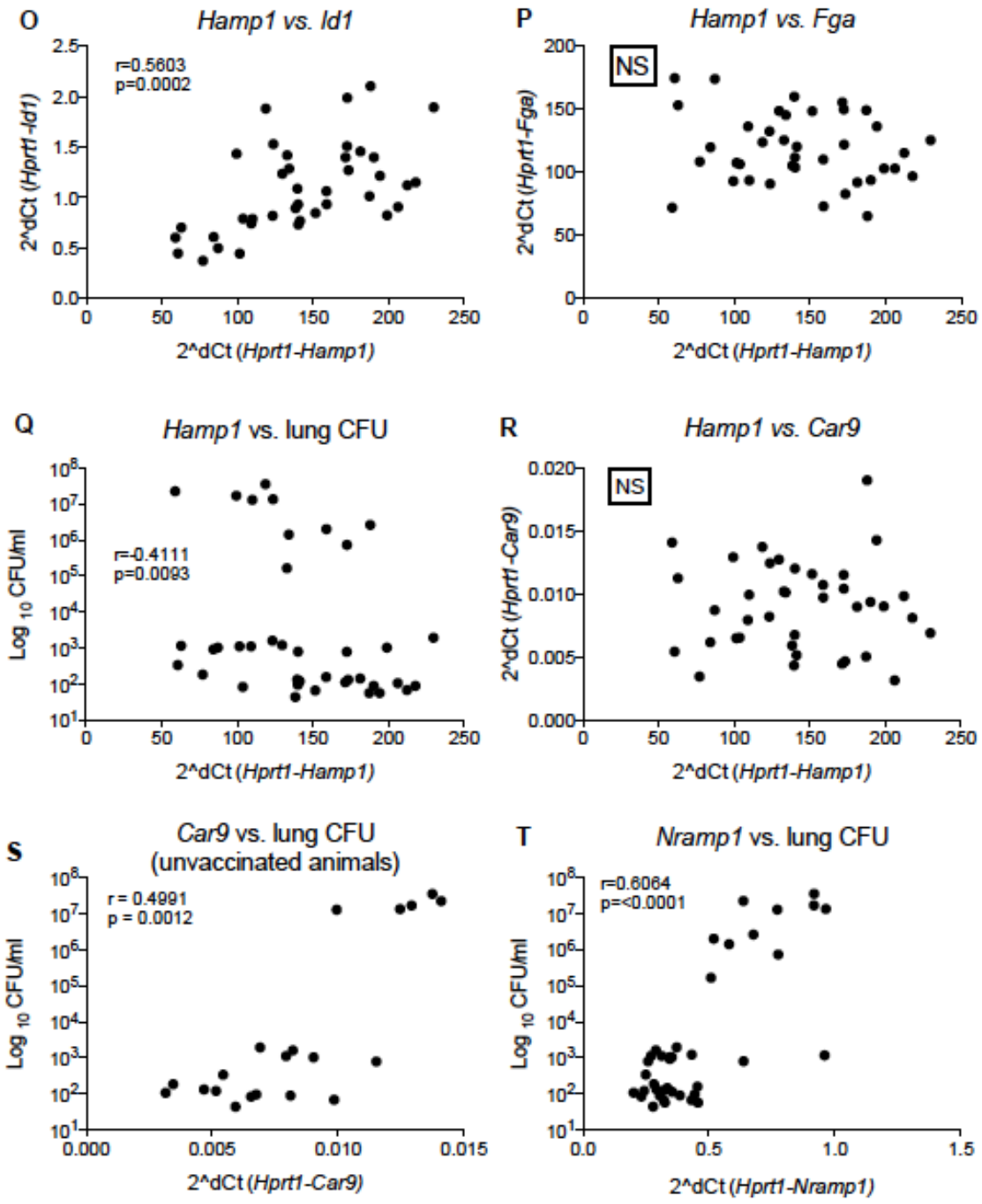


**Figure 3.3.2 Hepatic gene expression analyses in post-*M.tb* infection time course.** BALB/c mice were vaccinated with BCG. Animals were infected 10 weeks later with *M.tb* via aerosol. Uninfected animals were also taken down at D0 and D28. Hepatic gene expression analyses are shown for *Hamp1* (A), *Id1* (C), *Fga* (E), *Car9* (G) *Ho1* (I) *Nramp1* (K), and *Lcn2* (M), with their respective comparisons to uninfected controls at D28 in B, D, F, G, J, L and N. Correlations are also shown for *Hamp1* with *Id1* (O), *Hamp1* and *Fga* (P), *Hamp1* with lung CFU (Q), *Hamp1* with *Car9* (R), *Car9* with lung CFU (S), and *Nramp1* with lung CFU (T). Two-way ANOVAs were performed for time courses with Bonferroni post tests, Mann Whitneys corrected for multiple comparisons in uninfected control comparisons, and all correlations were Spearman correlations. *p≤0.05 ** p≤0.01 *** p=≤0.001 **** p=≤0.0001. n=5 per group.

### *3.3.6 Expression of proinflammatory cytokines is altered post-infection*

In the unvaccinated animals, liver *Tnfa*, *Il6* and *Ifng* mRNA levels increased between D7 and D28 post-infection, with significantly higher *Tnfa* and *Ifng* expression seen at D28 (p=0.00317 for all) (Figure 3.3.3A and E), consistent with the previous infection experiment. These changes were not observed in the vaccinated animals, perhaps due to reduction in bacterial burden as an effect of vaccination (Figure 3.3.3 A and E). At D28, *Tnfa* and *Il6* did not differ between uninfected mice and infected mice. Therefore, although it is well characterized that these two cytokines are released following *M.tb* infection, quantification of liver expression does not highlight increases post-infection. However, hepatic *Ifng* mRNA expression correlated with lung CFU (Figure 3.3.3G) (p=0.0007, r=0.5192). Furthermore, when comparing infected animals to uninfected controls at D28 (Figure 3.3.3F), *Ifng* mRNA levels were significantly higher in unvaccinated infected mice than in their uninfected controls, but no differences were observed between vaccinated groups (Figure 3.3.3F).

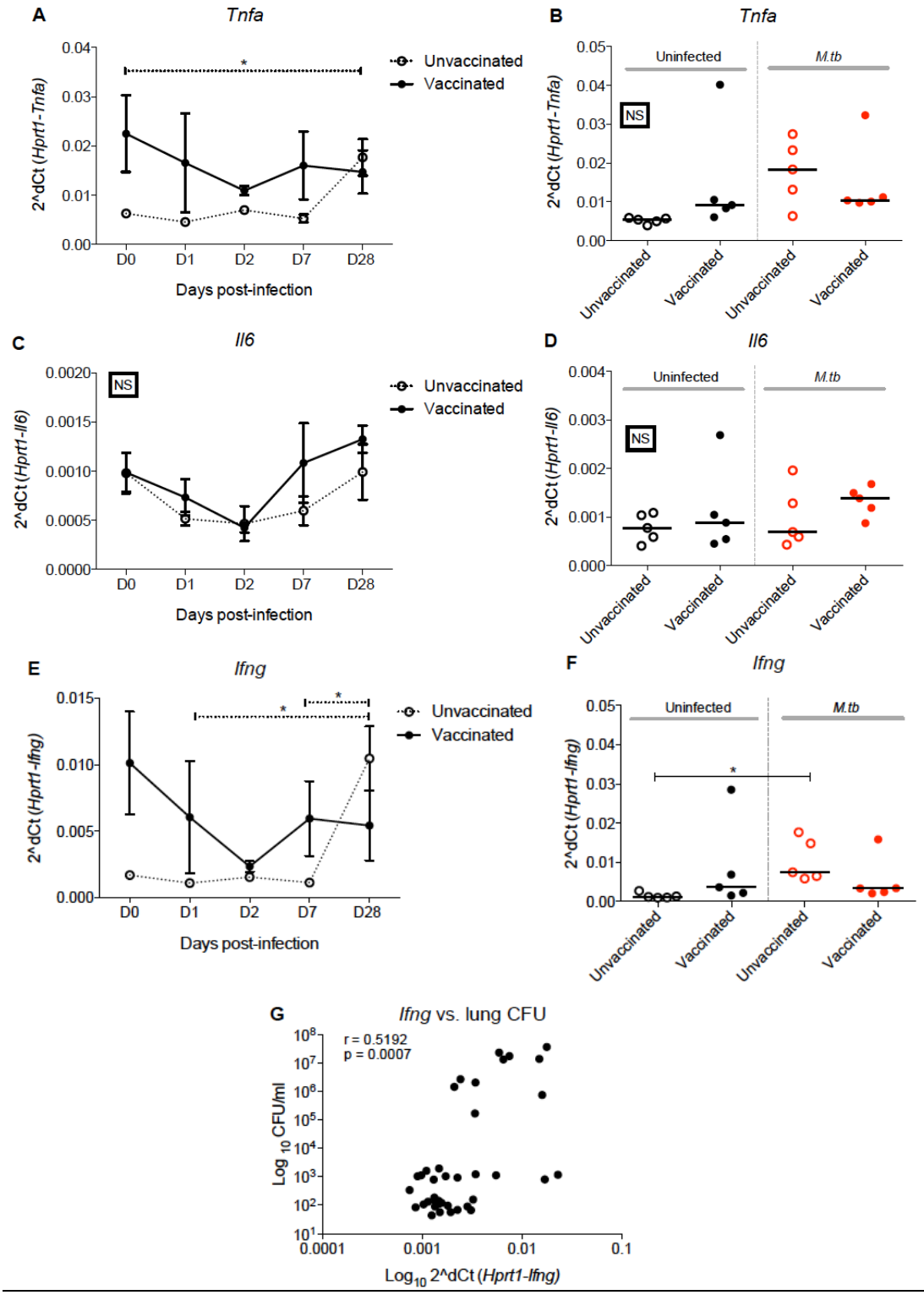


**Figure 3.3.3 Immune gene expression analyses in the liver in a post-*M.tb* infection time course.** BALB/c mice were vaccinated with BCG. Animals were infected 10 weeks later with *M.tb* via aerosol. Uninfected animals were also taken down at D0 and D28. Hepatic gene expression analyses are shown for *Tnfa* (A), *Il6* (C) and I*fng* (E), with their respective comparisons with uninfected controls at D28 in (B, D and F). A Spearman correlation between *Ifng* and lung CFU is shown in G. Two-way ANOVAs with Bonferroni post tests were performed for time courses, and Mann-Whitney tests with Bonferroni corrections for multiple comparisons were done to compare groups to uninfected controls where *p≤0.05 ** p≤0.01 *** p=≤0.001 **** p=≤0.0001. n=5 per group.

## 3.4 Time course infection studies in C57BL/6 mice

Since I also planned to use a hepcidin-deficient mouse on a C57BL/6 J129 background in this project, I also wanted to look at kinetics of genes involved in iron homeostasis in C57BL/6 mice in order to confirm there are no major differences between these two strains. C57BL/6 mice were vaccinated with BCG 10 weeks prior to infection with *M.tb* and taken down at 1, 7, 14, 28 and 56 days post-infection (Figure 3.4.1A). Five unvaccinated and five vaccinated mice were taken down at each timepoint, with uninfected controls (unvaccinated and vaccinated) for D0 (baseline), D28 and D56. Lung and spleen homogenates were used to quantify bacterial growth, and gene expression analyses were done in the liver.

### *3.4.1 Dissemination of M.tb occurs earlier in BCG-vaccinated mice*

Bacterial colonies were observed in lung homogenates from 1 day post-infection, with BCG-induced protection evident from 28 days post-infection (Figure 3.4.1B, p=0.0395). Peak bacterial burden was reached 14 days post-infection, with a median of $2.2 \times 10^6$ CFU in the lungs of unvaccinated mice. Bacterial load then began to decrease as animals began to control the infection. BCG-induced protection was still observed 56 days post-infection (p=0.0395). Bacteria were undetectable in the spleen until 7 days post-infection, when ~100 CFU were detected in the vaccinated mice (none in the unvaccinated group) (Figure 3.4.1C) (p=0.0395). By 14 days post-infection, there was no difference in CFU counts between the two groups. BCG-induced protection was evident from D28 (p=0.0395) and still present at D56 post infection, although not significant.

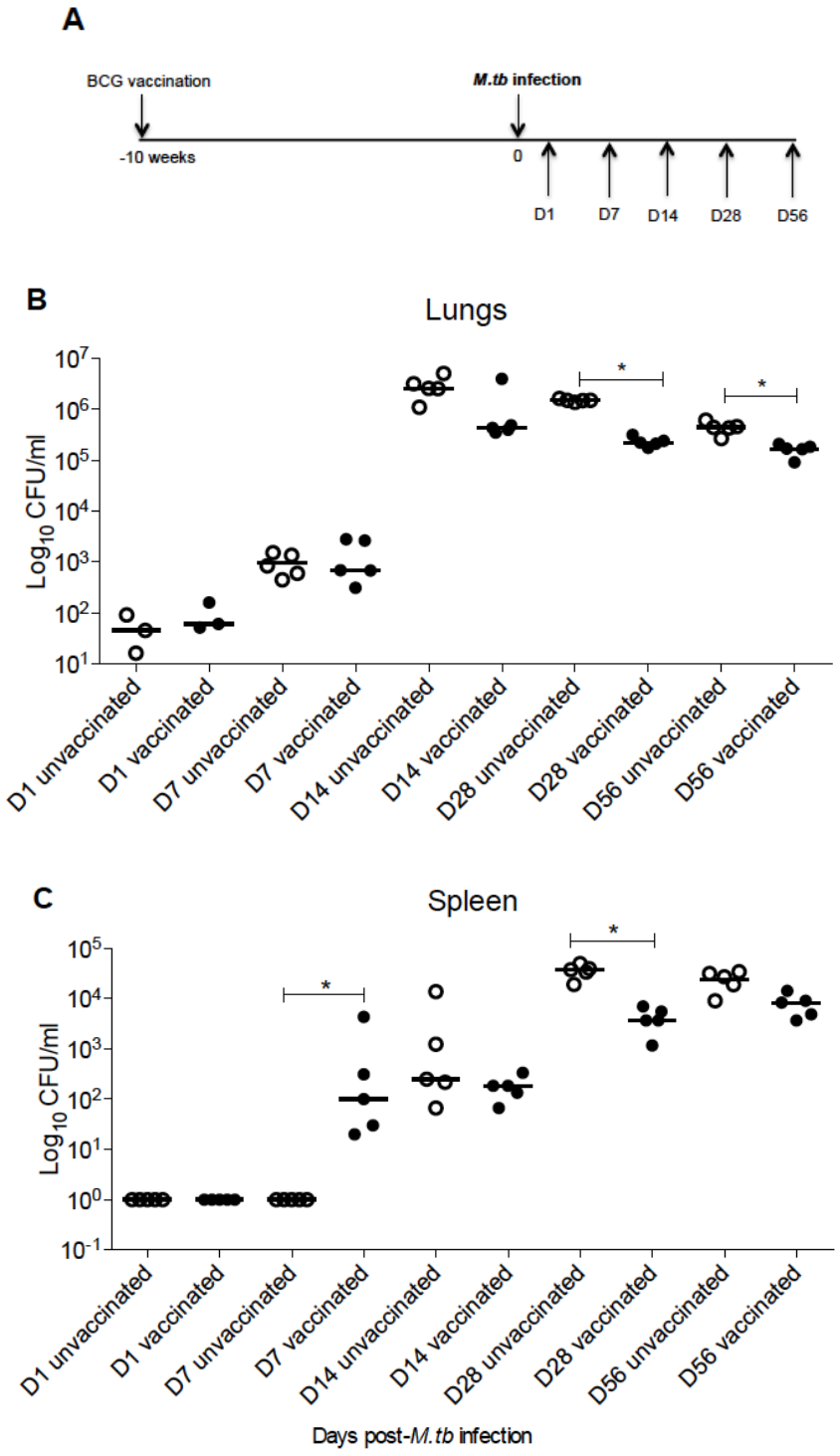


**Figure 3.4.1 CFU time course in *M.tb*-infected C57BL/6 mice.** Ten weeks post-vaccination, animals were infected with aerosolised *M.tb*. Animals were sacrificed at D1, D7, D14, D28 and D56 following infection, as well as D0 pre-infection for baseline (A). Organs were harvested for quantification of bacterial burden as shown for lungs (B) and spleen (C). Unvaccinated animals are represented by circles and vaccinated animals by squares. N = 5 animals per group. A Kruskal Wallis test was performed on all groups (p = <0.0001), followed by Mann Whitney tests with Bonferroni corrections for multiple comparisons where required. *p≤0.05 ** p≤0.01 *** p=≤0.001 **** p=≤0.0001

### *3.4.2 Hepcidin fluctuates post-M.tb infection in C57BL/6 mice and is likely regulated by the BMP/SMAD signalling pathway*

In this time course, I looked at trends in *Hamp1* mRNA expression after *M.tb* infection in C57BL/6 mice. *Hamp1* gene expression was affected by time post-infection and also vaccination status (p=0.0026 and p=0.0033, respectively) (Figure 3.4.2A). In both unvaccinated and vaccinated mice, *Hamp1* mRNA dropped from baseline (D0) initially following infection, peaking at D7 in the vaccinated mice, and later, at D14 in the unvaccinated mice, before dropping back to levels similar to those observed at baseline (D0) (Figure 3.4.2A). This is comparable to the previous infection in BALB/c mice, indicating similarities in the control of iron homeostasis post-*M.tb* infection between the two mouse strains. At D28, *Hamp1* message was reduced in the unvaccinated mice (p=0.0018), but not in the vaccinated mice, compared with baseline. By D56 however, this was no longer significant. This could be a result of the reduction in bacterial burden by D56 (Figure 3.4.1), or alternatively, it could be because of an emerging adaptive immune response [192].

There was no significant difference in *Hamp1* mRNA expression between unvaccinated and vaccinated groups at D28 or D56 post-infection, contrary to my findings in BALB/c mice. At D28, there is a trend towards reduced *Hamp1* expression in the infected unvaccinated mice, compared with uninfected controls, which was significant prior to conservative corrections for multiple comparisons. At D56, *Hamp1* was significantly suppressed in the unvaccinated infected mice when compared with the uninfected controls, but it was not in the vaccinated mice (Figure 3.4.2B; p=0.0316). However, at D56, uninfected BCG-

vaccinated mice had significantly lower *Hamp1* expression than their vaccinated controls (p=0.0316), consistent with the theory that hepcidin may be reduced by vaccination in order to restrict intracellular iron availability as a protective mechanism.

In the BALB/c time course experiment, *Fpn1* mRNA was not quantified. However, in this infection in C57BL/6 mice, *Fpn1* message increased steadily post-infection, becoming significantly higher at D28 compared with D0 in the unvaccinated mice (p=0.0001), and by D56 compared with D0 in the BCG-vaccinated mice (p=0.0226) (Figure 3.4.2 C+D). Statistical analyses indicate *Fpn1* expression was affected by both timepoint post-infection (p=<0.0001) and by vaccination (p=0.0084). Since hepcidin targets ferroportin for degradation, it is not surprising that hepcidin correlates inversely with ferroportin (Figure 3.4.2L, r=-0.3181, $r^2$=0.1012, p=0.0244). Furthermore, at D56, infected unvaccinated mice had raised *Fpn1* message compared with uninfected controls, although this was not significant after correcting for multiple comparisons (Figure 3.4.2D) . This is the opposite of the observed decrease in *Hamp1* mRNA at this timepoint, thus fitting with hepcidin regulating *Fpn1* expression, and that *M.tb* infection results in decreased hepcidin expression accompanied by increased *Fpn1* expression, possibly as a way of depriving the intracellular pathogen of iron as a protective response.

Considering the induction of hepcidin following most infections is regulated via the JAK/STAT3 pathway, I wanted to confirm that the BMP/SMAD pathway and not JAK/STAT3 signalling is responsible for regulation of *Hamp1* post-*M.tb* infection. As seen before, *Hamp1* mRNA levels correlated weakly with *Id1*

mRNA (Figure 3.4.2K, r=0.5064, p=0.0002), but not with *Il6* (Figure 3.4.3F), suggesting that the BMP/SMAD pathway is likely to be the main regulator of liver hepcidin induction. This time, however, *Hamp1* correlated weakly with *Fga* (Figure 3.4.2O, r=0.3402, $r^2$=0.1157, p=0.0168). However, statistical analyses indicate that *Fga* expression was not affected by time post-infection, but was by vaccination (p=0.0251). When splitting the data, *Fga* did not correlate with *Hamp1* in only the unvaccinated mice, but *Id1* did.

Moreover, I also quantified the expression of the gene encoding activin B, *Inhbb*, which is induced by inflammatory stimuli. Activin B has been shown to induce hepcidin expression via BMP/SMAD signalling in the context of LPS-induced inflammation [193]. However, *Inhbb* mRNA expression was overall unaffected by time post-*M.tb* infection, but was by vaccination (p=0.0020). Expression of *Inhbb* was significantly reduced in vaccinated mice between D0 and D28 (Figure 3.4.2F). Furthermore, *Hamp1* expression correlated inversely with expression of pro-inflammatory cytokines *Tnfa* and *Ifng* (Figure 3.4.3B+D). This, combined with the fact the expression of *Il6*, which is known to induce hepcidin via inflammatory JAK/STAT3 signalling, did not change over the time course, and did not correlate with *Hamp1* (Figure 3.4.3F) suggests that the inflammatory pathway is unlikely to play a role in the regulation of hepcidin post-*M.tb* infection.

Interestingly, *Car9* expression increased post-infection in the unvaccinated mice, and correlated positively with *Hamp1* (Figure 3.4.2M; r=0.5185, p=0.0001), contrary to findings in the previous time course. It is evident from my data that *Car9* is higher in mice with higher bacterial burdens, since *Car9* also correlates

positively with lung CFU (Figure 3.4.2N; r=0.3087, p=0.0292). In this time course, the additional group at D56, where bacterial burdens are higher could explain the discrepancy between correlations seen in this experiment and the previous ones in the BALB/c mice, where there was an additional earlier timepoint, where burdens were lower.

### *3.4.3 Involvement of other genes involved in iron homeostasis post-M.tb infection in C57BL/6 mice*

Similar to the previous time course in BALB/c mice, *Nramp1* increased post-infection in both unvaccinated and BCG-vaccinated mice, peaking at D14 in the vaccinated mice and D28 in unvaccinated mice (Figure 3.4.2G; p=0.0030 D0-D14 BCG-vaccinated mice, p=<0.0001 D0-D28 unvaccinated mice). Expression of *Nramp1* was also significantly higher in the BCG-vaccinated mice between D1 and D28, highlighting that the early induction of *Nramp1* might be a protective mechanism of the BCG vaccine. *Nramp1* correlated positively with lung CFU (r=0.05433, p=<0.0001 Figure 3.4.2P) suggesting that its expression increases with bacterial burden. *Nramp1* expression also correlates positively with *Ifng* mRNA (r=0.9016, p=<0.0001 Figure 3.4.3H), consistent with findings that *Nramp1* drives accelerated inflammatory responses, as it promotes secretion of inflammatory cytokines such as IFN-γ and TNF-α [189, 194].

In the previous time course study in BALB/c mice, *Lcn2* mRNA peaked at 24 hours post-infection and rapidly returned back to baseline, consistent with findings in a previous study in BCG-infected mice [188]. Although not statistically significant, a similar increase was seen at 1 day post-infection

(Figure 3.4.2H). Interestingly, however, 7 days post-infection, *Lcn2* mRNA levels increased to a peak at D28 in the unvaccinated mice (p=0.0309 D0-D28 unvaccinated mice) and D14 in the vaccinated mice, highlighting potential differences in *Lcn2* expression between BALB/c and C57BL/6 mice. At D7 and D14, BCG-vaccinated mice had significantly higher levels of *Lcn2* mRNA than unvaccinated mice, and the peak *Lcn2* level in vaccinated mice is likely between D14 and D28, suggesting a potential protective mechanism of BCG may be to induce these responses earlier.

I then went on to look at the expression of the iron storage proteins light and heavy chain ferritin (encoded by *Ftl* and *Fth*, respectively). Quantification of ferritin message by real time PCR is not necessarily reflective of true ferritin levels, as it is also regulated post-transcriptionally [88]. Post-*M.tb* infection, I observed changes in the expression of both *Ftl* and *Fth* mRNA. Time post-infection and vaccination affected expression of both *Ftl* (Figure 3.4.2I; p=<0.0001 and p=0.0133, respectively) and *Fth* (Figure 3.4.2J; p=<0.00001 and p=0.0293, respectively). Overall, *Ftl* mRNA significantly decreased post-infection in the unvaccinated, but not BCG-vaccinated mice (p=0.00076 D0-D28, p=0.0002 D0-D56). In contrast, *Fth* mRNA decreased significantly in both unvaccinated and vaccinated mice between baseline (D0) and D28 (Figure 3.4.2J; p=0.0063 and p=0.0006, respectively). Furthermore, I found a strong inverse correlation between *Ifng* and *Ftl* mRNA in the unvaccinated mice (r=-0.6777, p=0.00002, data not shown), consistent with studies showing IFN-γ negatively regulates ferritin expression in order to decrease intracellular iron availability [166].

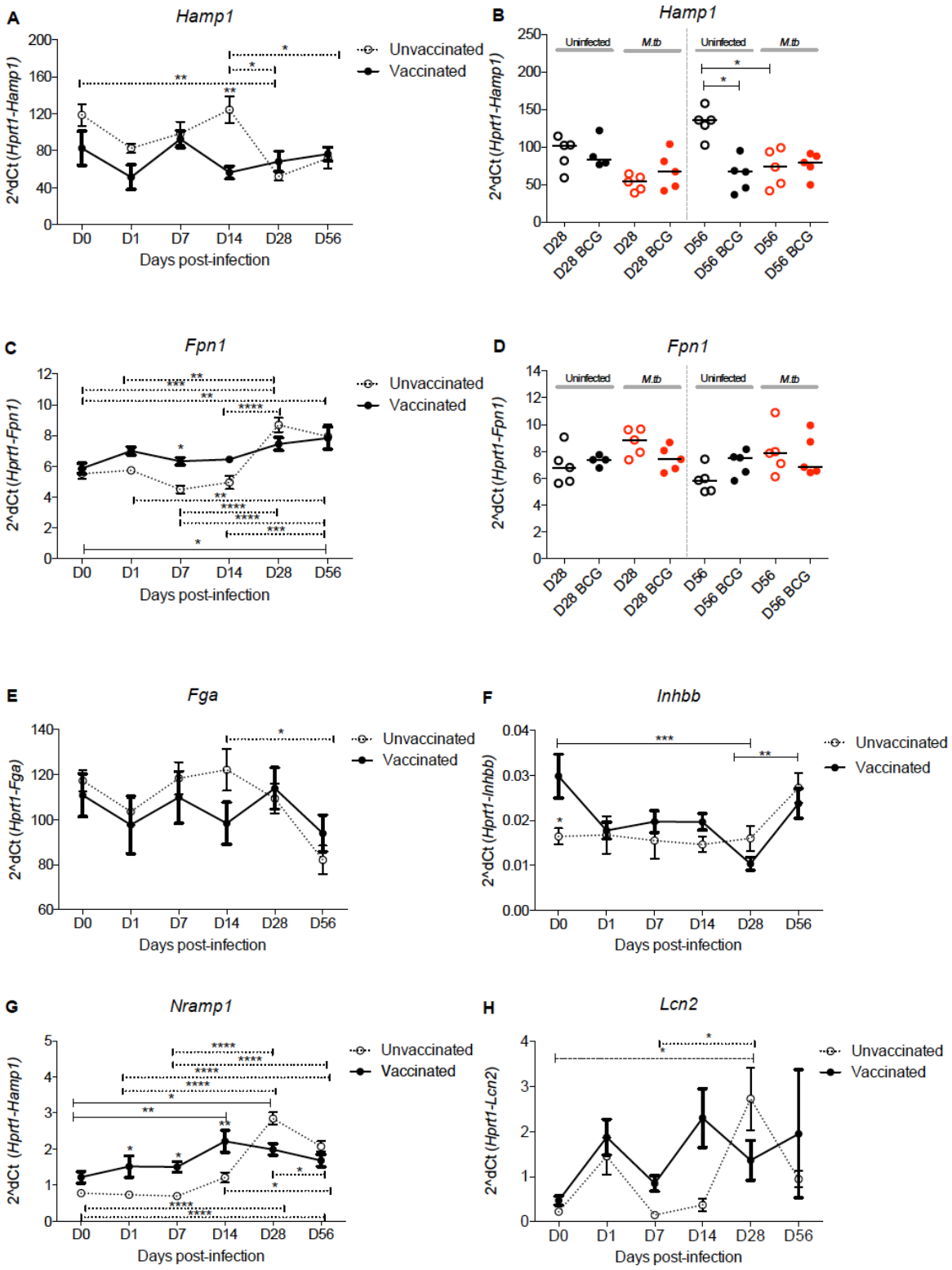
A
Hamp1
2^dCt (Hprt1-Hamp1)
Days post-infection
Unvaccinated
Vaccinated
B
Hamp1
Uninfected
M.tb
D28
D28 BCG
D56
D56 BCG
C
Fpn1
2^dCt (Hprt1-Fpn1)
D
E
Fga
2^dCt (Hprt1-Fga)
F
Inhbb
2^dCt (Hprt1-Inhbb)
G
Nramp1
2^dCt (Hprt1-Hamp1)
H
Lcn2
2^dCt (Hprt1-Lcn2)

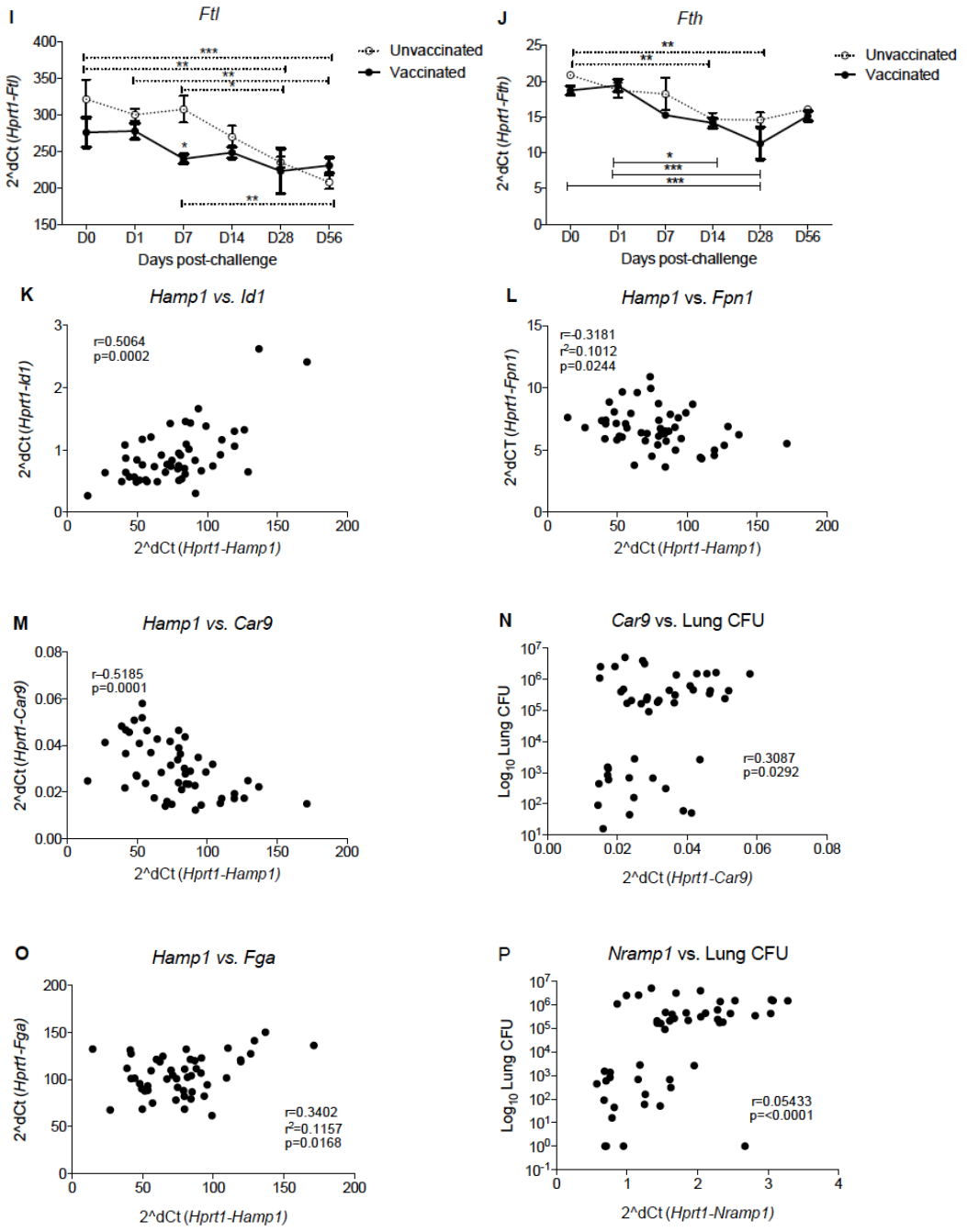


**Figure 3.4.2 Hepatic gene expression analyses post-*M.tb* infection.** Mice were vaccinated with BCG 10 weeks before infection with *M.tb*. Animals were taken down at D1, D7, D14, D28 and D56 post-infection. Uninfected controls were taken down at D0, D28 and D56 (B and D). Gene expression is shown for *Hamp1* (A), *Fpn1* (C), *Fga* (E), *Inhbb* (F), *Nramp1* (G), *Ftl* (H), *Fth* (I), *Ifng* (H), with uninfected controls for *Hamp1* and *Fpn1* in B and D, respectively. Correlations are *Hamp1* vs. *Id1* (K), *Hamp* vs. *Fpn1* (L), *Hamp* vs. *Car9* (M), *Car9* vs. lung CFU (N), *Hamp* vs. *Fga* (O) and *Nramp1* vs. lung CFU (P). Statistical analyses for time courses were 2-way ANOVAs with Bonferroni post-tests for multiple comparisons where *p≤0.05 ** p≤0.01 *** p=≤0.001 **** p=≤0.0001. n=5 per group. Comparisons to uninfected controls were by Mann-Whitney tests, and correlations by Spearman rank. Dotted lines, dotted bars and empty circles indicate data for unvaccinated mice, and full lines and full circles, data for BCG-vaccinated mice.

### *3.4.4 Expression of genes encoding inflammatory cytokines increases in unvaccinated mice post-infection*

In the previous time course in BALB/c mice, I quantified hepatic expression of pro-inflammatory cytokines TNF-α and IFN-γ, finding them both to be up-regulated in unvaccinated mice between baseline (D0) and D28 post-infection. A similar trend was observed in C57BL/6 mice. *Ifng* expression was affected by time post-*M.tb* infection (Figure 3.4.3A, p=<0.0001), but not by BCG vaccination. A significant increase was observed between D0 and the peak *Ifng* level at D28 (p=<0.0001), which was followed by a significant reduction back down to baseline by D56 (p=0.0106). A similar pattern was observed for *Tnfa*. Expression was affected by time post-*M.tb* infection (Figure 3.4.3C, p=0.0010) but BCG vaccination did not affect expression. In the unvaccinated mice, *Tnfa* mRNA gradually increased post-infection, peaking at D28 (p=0.0007 between D0 and D28), with levels returning back to baseline by D56 (Figure 3.4.3C). Although BCG vaccination did not significantly affect levels of *Tnfa* and *Ifng* mRNA, the significant increases evident in only the unvaccinated groups may highlight earlier immune responses in the vaccinated mice. This corroborates my findings that bacterial dissemination occurs more quickly in vaccinated mice (Figures 3.3.1B and 3.4.1B). Interestingly, *Hamp1* correlates inversely with both *Ifng* and *Tnfa*, suggesting that inflammation is unlikely to be inducing *Hamp1* expression (Figure 3.4.3B, r=-0.5076, p=0.0002 and Figure 3.4.4D, r=-0.3904, o=0.0051, respectively). Moreover, *Il6* expression was unaffected by infection or BCG vaccination (Figure 3.4.3E), and did not correlate with *Hamp1* (Figure 3.4.3F). *Ifng* also correlated positively with lung CFU (Figure 3.4.3G,

r=0.4046, p=0.0036). In addition, *Nramp1* strongly correlated with *Ifng* mRNA (Figure 3.4.3H, r=0.9016, p=<0.0001).

To further investigate whether severity of infection might alter hepcidin expression, I correlated *Hamp1* with lung CFU. No correlation was found (Figure 3.4.2L). However, *Hamp1* did correlate inversely with *Ifng* (Figure 3.4.3B) (r=-0.5076 and p=0.0002), indicating that stronger immune responses may be associated with reduced hepcidin expression.

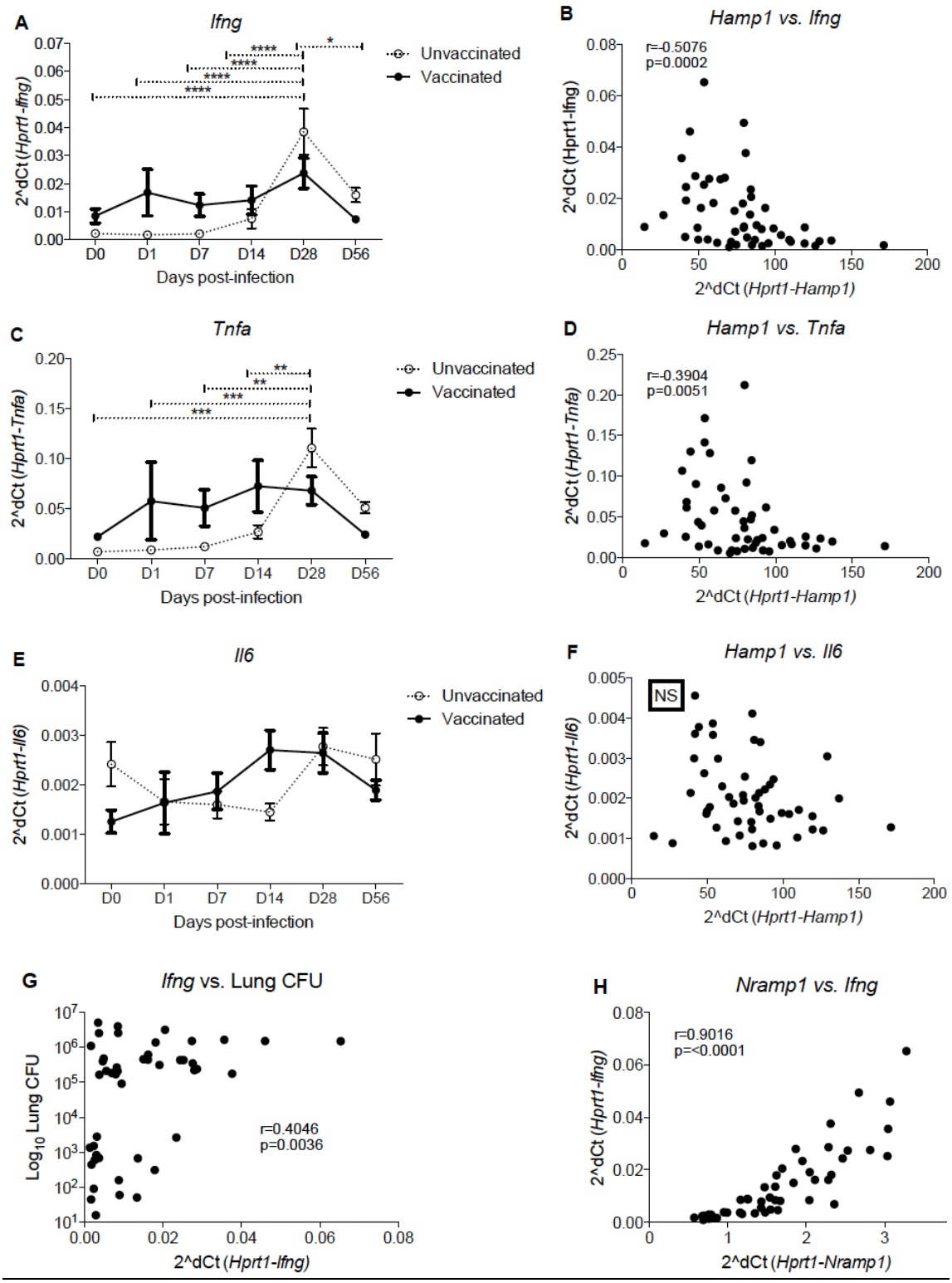


**Figure 3.4.3 Immune gene expression analyses in liver in a post-*M.tb* infection time course.** C57BL/6 mice were vaccinated with BCG. Animals were infected 10 weeks later with *M.tb* via aerosol. Uninfected animals were taken down at D0 (baseline), D28 and D56. Hepatic gene expression analyses are shown for *Ifng* (A), *Tnfa* (C) and *Il6* (E). Correlations between *Hamp1* and *Ifng*, *Tnfa* and *Il6* are shown in B, D and F, respectively. Correlations between *Ifng* and lung CFU are shown in G, and *Nramp1* and *Ifng* in H. Two-way ANOVAs with Bonferroni post tests were performed for time courses, Mann Whitney tests corrected for multiple comparisons in uninfected control comparisons, and all correlations were Spearman correlations. *p≤0.05 ** p≤0.01 *** p=≤0.001 **** p=≤0.0001. n=5 per group.

## 3.5 Effect of BCG vaccination of the expression of genes involved in iron homeostasis

So far in this chapter I have looked at the effect of *M.tb* infection on the expression of hepcidin and other genes involved in iron homeostasis, at a range of timepoints, and then I looked at whether these genes were expressed differently in BCG-vaccinated mice compared to unvaccinated mice. I then went on to determine the effect of BCG vaccination on gene expression. As BCG is a live attenuated strain of *M.bovis,* my hypothesis was that vaccination with BCG would have similar effects on gene expression to *M.tb* infection. Moreover, if BCG vaccination has any long-term effects on expression of these genes, it may affect iron homeostasis during subsequent infection. C57BL/6 mice were vaccinated with BCG and were taken down at D0 (pre-vaccination), D1, D2, D7 and D14 post-vaccination.

### *3.5.1 BCG vaccination and M.tb infection have similar effects on hepcidin kinetics*

Although not significant, hepcidin kinetics post-BCG vaccination were similar those seen post-*M.tb* infection (Figure 3.5.1A), peaking at D7 and then dropping back to baseline. Interestingly, *Fpn1* expression peaked at D14 post-vaccination, similar to what was observed at D28 in unvaccinated mice after *M.tb* infection (Figure 3.5.1B; p=0.0451 D2-D14, Kruskal Wallis p=0.0186) which is expected when hepcidin drops back to baseline. These data indicate that the response immediately following either BCG vaccination or *M.tb* infection is to transiently reduce hepcidin expression followed by a return to

baseline, which occurs to coincide with an adaptive immune response. As with *Hamp1*, no significant differences were observed in *Id1* expression post-vaccination, however, a similar trend towards a peak at D7 was seen, and the two correlated positively (r=0.434, p=0.034) (Figure 3.5.1H), consistent with my previous data. No changes in the expression of *Bmp6* were observed either. I also measured the expression of *Saa1*, the gene encoding serum amyloid protein 1, a major acute phase protein. Serum amyloid protein 1 is secreted by the liver following stimulation by pro-inflammatory cytokines such as TNF, which I have also shown to be induced followed BCG vaccination (Figure 3.5.1) [195-197]. *Saa1* mRNA was transiently induced following vaccination (p=0.0325), peaking at D1 (p=0.0159) and dropping back down by D7 (D1-D7 p=0.0159), likely as part of the inflammatory response to the vaccine. *Saa1* is a JAK/STAT3 dependent gene, so is a good measure of induction of this pathway. This suggests that in the case of BCG vaccination, similar to in *M.tb* infection, the BMP/SMAD pathway is likely the main regulator of hepatic hepcidin induction.

Since *M.tb* infection induces IFN-γ and TNF-α, these were also quantified post-BCG vaccination to see whether a similar level of induction was seen. As expected, BCG vaccination resulted in increases in the hepatic expression of both *Ifng* and *Tnfa* expression (p=0.0099 and p=0.0093, respectively) (Figure 3.5.1E+F), as expected, although the levels were lower in comparison to those following *M.tb* infection. These data indicate that BCG vaccination itself does not, at least in the short term, have any significant effects on the expression of hepcidin. However, peak responses to BCG vaccination do not occur until 10-12

weeks post-vaccination [52]. Therefore, some of these genes measured here may peak much later on and these results may not be representative of peak changes in iron homeostasis induced post-vaccination. A longer time course study might be more appropriate.

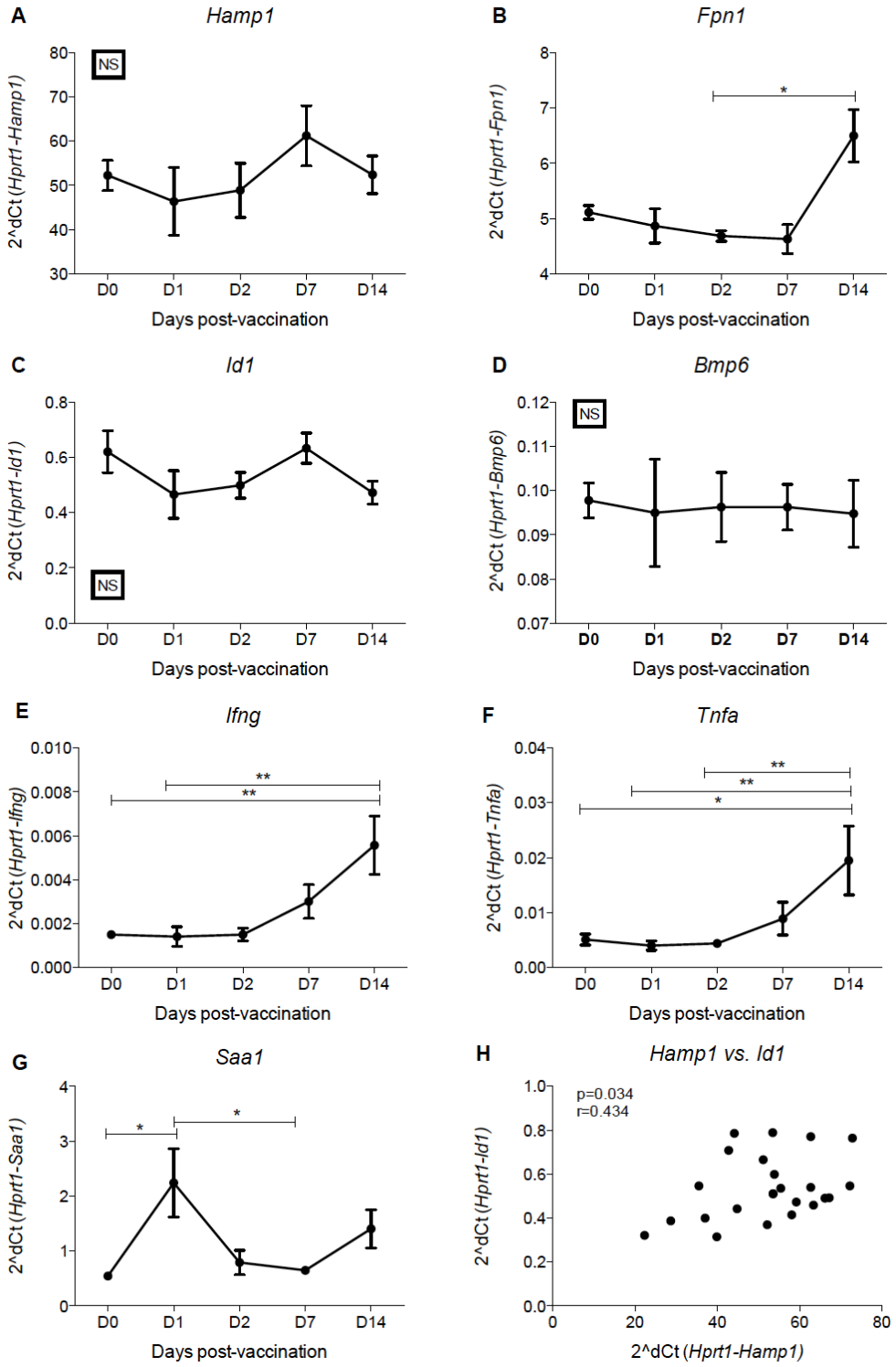


**Figure 3.5.1 Hepatic gene expression analyses in C57BL/6 mice post-BCG vaccination.** C57BL/6 mice were vaccinated with BCG Pasteur and taken down at D0 (unvaccinated), D1, D2, D7 and D14 post-vaccination. Hepatic gene expression analyses are shown here for *Hamp1* (A), *Fpn1* (B), *Id1* (C), *Bmp6* (D), *Ifng* (E), *Tnfa* (F), *Saa1* (G) and correlations for *Hamp1* vs. *Id1* are shown in H. Correlations are Spearman Rank correlations. A Kruskal Wallis test was done to compare timepoints, with Mann-Whitney tests and Bonferroni adjustment for multiple comparisons where required. N=5 per group. *p≤0.05 ** p≤0.01 *** p=≤0.001 **** p=≤0.0001.

## 3.6 Discussion

Key findings for this chapter:

- Hepatic hepcidin mRNA is down-regulated 4 weeks after aerosol *M.tb* infection in both BALB/c and C57BL/6 mice (possibly leading to reduced degradation of ferroportin)
- Ferroportin is up-regulated post-infection, which may increase export of iron from the macrophage
- Nramp1 is up-regulated post-infection, which may result in export of iron from the *M.tb*-containing phagosome and may therefore be a protective mechanism
- Ferritin is also down-regulated, which may result in release of iron from stores for export from the macrophage
- Hepcidin correlates with markers of BMP/SMAD signalling and not inflammatory JAK/STAT3 signalling, despite induction of pro-inflammatory cytokines, making it likely that the observed down-regulation of hepcidin post-infection is due to inhibition of BMP/SMAD signalling via an unknown mechanism
- Ultimately, this combination of changes in gene expression may lead to increased export of iron from the *M.tb*-infected phagosome, resulting in reduced iron availability for the pathogen. Therefore, reduction of hepcidin may be protective.

The purpose of the experiments described in this chapter was to determine whether *M.tb* infection affects the expression of hepcidin and other genes

involved in iron homeostasis, and therefore whether hepcidin has a role in the response post-infection. In addition, I wanted to investigate whether BCG vaccination has an effect on iron homeostasis pre- and post-infection, and if so whether this might highlight any potential protective mechanisms of the vaccine. Finally, since I decided to repeat my experiments in C57BL/6 mice because the hepcidin-deficient mice were on a C57BL/6 background, I wanted to determine whether there were any significant differences between these two strains that would provide me with further insights into how potential differences in iron homeostasis between the strains might affect mycobacterial susceptibility.

It is well documented that there is an important interaction between immune function and iron homeostasis [155], and that host iron status can affect disease outcome. In addition, there is increasing evidence that iron availability is differentially regulated depending on the location of the pathogen [155, 166]. Firstly, the *M.tb* infection time course data shown here illustrate that hepatic *Hamp1* mRNA fluctuates post-*M.tb* infection, in both unvaccinated and vaccinated mice. However, in contrast with previous *in vitro M.tb* infection studies in macrophages, hepcidin was not induced to a high level post-infection [104]. In fact, it was significantly down-regulated in the unvaccinated mice 4 and 8 weeks post-infection. Moreover, in some experiments, in the uninfected controls, BCG-vaccinated mice already had reduced levels of *Hamp1* compared to the unvaccinated mice, indicating that suppression of *Hamp1* might be a protective mechanism of BCG vaccination. An explanation for the more severe suppression of *Hamp1* observed in the unvaccinated mice could be that down-

regulation may be dependent on severity of infection. BCG vaccination reduces bacterial burden by around 1 log, therefore hepcidin is not down-regulated to the same scale as in the unvaccinated mice. Quantification of hepcidin at the protein level would confirm reduction post-*M.tb* infection.

Previous studies provide evidence for a strong induction of hepcidin following a range of extracellular infections, as well as following stimulation with inflammatory mediators [104, 140]. However, hepcidin induction during intracellular infection may not be protective given that it results in the redistribution of iron into macrophages, where intracellular pathogens such as *M.tb* may reside [103]. In support of this, recent studies in humans indicate that high hepcidin is a risk factor for TB disease [141]. Therefore, the reduction in hepcidin I have observed post *M.tb* infection may highlight a potential protective mechanism.

Here I have shown the significant up-regulation of genes encoding pro-inflammatory cytokines IFN-γ and TNF-α post-*M.tb* infection, without a concomitant induction of *Hamp1* expression. This is consistent with findings that the host response to intracellular infection may be to reduce macrophage iron availability, irrespective of inflammation [155-157]. In support of this, inverse correlations between *Hamp1* and *Ifng* mRNA were found. Since *M.tb* resides in macrophage phagosomes [198] and is able to access iron from cytoplasmic iron sources or by complexing with endosomes to access iron bound to transferrin receptor [145], increased hepcidin and resultant iron loading inside the macrophage is likely to be detrimental to the host. Although alveolar macrophages are not directly involved in iron recycling and storage like splenic

macrophages, they do express ferroportin since they play a critical role in scavenging iron from inhaled air pollution particles in order to protect lungs from oxidative damage, and are therefore able to respond to hepcidin [199]. Therefore, the suppression of hepcidin with concomitant increase in ferroportin expression that I have observed post-*M.tb* infection may function to reduce alveolar macrophage iron content in order to inhibit mycobacterial growth. In support of this, non-typhoidal *Salmonella* (NTS), another intracellular pathogen, grows less well when hepcidin is lower, probably due to reduced iron availability inside the macrophage [157]. Moreover, I observed increased *Nramp1* mRNA expression post-*M.tb* infection. Induction of *Nramp1* has previously been shown as a protective immune mechanism, and there is increasing evidence that its function is to remove $Fe^{2+}$ from inside the phagosome, thereby restricting iron availability for pathogens [191, 200]. Correspondingly, *Nramp1* polymorphisms have been associated with increased susceptibility to *M.tb* [201, 202].

I also observed reductions in both heavy and light chain ferritin post-infection, and this was more significant in unvaccinated mice. This is consistent with findings by Thom et al [80], who also found that ferritin is suppressed by inflammatory cytokines such as TNF-α . Decreased ferritin expression could result in release of iron for export by ferroportin in order to decrease iron availability for *M.tb.* Alternatively, there is evidence that ferritin suppresses immune functions by decreasing free iron [203]. Therefore, ferritin may be down regulated post-*M.tb* infection in order to release iron required for protective immune responses, such as the production of NO, and for T cell proliferation.

There is evidence in the literature that hepcidin induction by a range of infections and infectious stimuli is mediated via IL-6 via the induction of the inflammatory JAK/STAT3 pathway [121, 204, 205]. However, here I have shown that changes in hepcidin expression post-*M.tb* infection correlate with *Id1*, a marker of BMP/SMAD signalling. Moreover, correlations between the canonical JAK/STAT3-dependent gene, *Fga*, were only observed in one experiment. In this experiment, despite observing a weak positive correlation between *Fga* and *Hamp1*, no other indicators of inflammation correlated positively with *Hamp1.* In fact, hepatic *Ifng* and *Tnfa* mRNA correlated inversely with *Hamp1*, and *Il6* mRNA was not induced post-*M.tb* infection in any of the experiments in this chapter (nor did it correlate with *Hamp1).* Therefore, it is more likely that the BMP/SMAD pathway is the main regulator of hepcidin expression in *M.tb* infection. Interestingly, I also found evidence of increased expression of *Car9*, a marker gene of hypoxia, highlighting a potential role of hypoxia in the observed suppression of hepcidin post-*M.tb* infection. The mechanism by which hypoxia is able to inhibit hepcidin is controversial, but is likely through HIFs, particularly HIF-1α**,** which may inhibit hepcidin through inhibition of the BMP/SMAD pathway by induction of TMPRSS6, a HJV cleaving enzyme [125], which disrupts BMP/SMAD signalling. However, in moderate hypoxia, erythropoietin (EPO) mRNA should be detectable in the liver [206], and I was unable to detect any at the timepoints where *Car9* mRNA was the highest. Moreover, in early

experiments, liver TMPRSS6 transcripts were unaffected by *M.tb* infection (data not shown in this thesis). Therefore, even if the induction of *Car9* is suggestive of hypoxia, it is unclear whether it would be severe enough to interfere with hepcidin expression, although this could support the observed down-regulation of hepcidin in these experiments, which is likely regulated through the BMP/SMAD pathway. Further work needs to be done to confirm whether inhibition of the BMP/SMAD pathway is causing the reduction in hepcidin observed in my *M.tb* infection time courses.

Secondly, in the *M.tb* infection experiments, at the later timepoints, there was a trend towards uninfected BCG-vaccinated mice having reduced liver *Hamp1* expression compared to the unvaccinated uninfected mice, suggesting that BCG vaccination may reduce hepcidin expression. Since BCG vaccination effectively represents infection with attenuated *M.bovis*, it might induce a similar response to that seen post-*M.tb* infection, but to a reduced scale since it is not as virulent. This was tested in a post-vaccination time course in uninfected mice, and no significant changes in the 14 days immediately following vaccination were found, although trends were similar to those seen post-*M.tb* infection. Expression of *Fpn1* had started to increase by D14, indicating that reduced hepcidin might be seen after this timepoint, or that *Fpn1* is induced independently of hepcidin. Once again, this induction of *Fpn1* is likely to be a protective mechanism to deprive intracellular pathogens of iron. Peak immune responses to BCG vaccination are not observed until 10-12 weeks post-

vaccination, so it might be useful to repeat this timecourse up to 12 weeks post-vaccination [52].

Thirdly, bacterial burden was quantified at every timepoint post-infection and in both BALB/c and C57BL/6 mice, bacteria could be quantified earlier in the vaccinated mice than in the unvaccinated mice. This earlier dissemination of *M.tb* can be compared to the earlier dissemination from lungs to spleen evident in more resistant mouse strains, compared with more susceptible ones [24]. Earlier dissemination has been correlated with earlier induction of immune responses against mycobacteria, therefore the earlier dissemination seen in BCG-vaccinated mice could highlight a protective mechanism of the vaccine [24].

I also wanted to determine whether there were any major differences between the two mouse strains used in these experiments in terms of expression of genes involved in iron homeostasis. These two strains are both fairly resistant to *M.tb*, with similar levels of bacterial burden seen post-infection [70], consistent with our findings. BALB/c mice have higher serum iron parameters than C57BL/6 mice [183] and interestingly, have been found to be more susceptible than C57BL/6 mice to *intravenous (i.v.)*, but not aerosol *M.tb* infection [207, 208]. A possible explanation for this is that raised serum iron parameters in the BALB/c mice during *i.v.* infection increases iron availability for the pathogen and therefore increases bacterial growth. However, since their liver *Hamp1* mRNA levels are comparable to those in C57BL/6 mice, intracellular iron content might be similar and during aerosol infection with resultant intramacrophage infection, these two strains might have comparable susceptibility to *M.tb*. Or, if the intracellular iron content of these two strains

does differ, perhaps small changes are not enough to affect the growth of *M.tb.* Comparison of intramacrophage iron levels in these two strains could confirm this.

To summarise, in this chapter I have shown that liver hepcidin mRNA fluctuates post-*M.tb* infection and is eventually reduced post-infection in unvaccinated but not BCG-vaccinated mice. It is likely that the BMP/SMAD signalling pathway is regulating hepcidin expression post-*M.tb* infection, although further work needs to be done to clarify this. The reduction in hepcidin expression was accompanied by raised *Fpn1* and *Nramp1*, which may function to reduce macrophage iron content as a protective mechanism against *M.tb.* It is also possible that BCG vaccination itself might induce a similar response, since in some experiments there is a trend towards vaccinated mice having reduced hepcidin compared to unvaccinated mice, before infection with *M.tb.* These data emphasise the ability of the host to redistribute iron in order to restrict availability to *M.tb.* It is likely that these changes are based on the location of the invading pathogen, so in this case focus on reduction of iron in the *M.tb*-containing macrophages. Further work needs to be done to confirm whether macrophage iron is reduced post-infection, and whether or not this is protective, since it may highlight a useful therapeutic target for treatment of TB disease.

# Chapter 4

# 4 Investigating the effect of *Hamp1* gene deletion in murine *M.tb* infection

## 4.1 Introduction

Data generated in the previous chapter suggest that *M.tb* infection in mice leads to down-regulation of *Hamp1* mRNA. One explanation for this is that down-regulation of hepcidin leads to increased ferroportin expression, resulting in export of iron from inside the macrophage as an attempt to restrict iron availability to mycobacteria. This is consistent with evidence that the host responds to intracellular infections by modulating iron metabolism in order to reduce intracellular iron content [140, 155, 166, 177, 178]. In contrast, previous literature indicates that *in vitro M.tb* infection stimulates the production of hepcidin [209]. Moreover, a number of recent studies in HIV-infected humans have found that high hepcidin is a risk factor for development of TB, and is a predictor of mortality [141], although it is unclear whether higher hepcidin is a cause or effect of TB disease. It is possible that increased hepcidin seen in these studies is beneficial to the pathogen and not the host, perhaps due to increased intracellular iron content as a consequence of raised hepcidin concentrations. Therefore, the hypothesis was that hepcidin deficiency may be protective against *M.tb.*

To investigate this further, *Hamp1*$^{+/-}$ mice were bred to generate *Hamp1*$^{-/-}$ mice and littermate controls (*Hamp1*$^{+/+}$ and *Hamp1*$^{+/-}$ mice).

*Hamp1*$^{-/-}$ mice are viable, but develop extensive iron overload, a phenotype similar to that seen in human hereditary haemochromatosis [113]. They present with increased serum iron and ferritin, extreme iron accumulation in the liver, and excess non-haem iron in the lung [113]. In the liver, iron tends to accumulate in centrolobular areas rather than in resident macrophages (kupffer cells), where sparing is seen. In contrast, splenic iron is decreased, with sparing observed in the macrophages. In hepcidin deficiency, splenic macrophages and kupffer cells do not store iron, but are constantly importing and exporting iron. Most other cell types are massively iron overloaded in this genotype.

Since *Hamp1*$^{-/-}$ mice have multivisceral iron overload with excess non-haem iron present in the lungs, one might hypothesise this would increase *M.tb* growth. However, I hypothesised that if alveolar macrophages (where *M.tb* resides) are iron-spared like splenic macrophages and kupffer cells, this may impact on *M.tb* growth. In support of this hypothesis, one study has shown that monocyte-derived macrophages from patients with haemochromatosis are iron-depleted and are therefore better able to control *M.tb* [159]. Therefore, my hypothesis was that hepcidin-deficient mice would control *M.tb* infection better than wild type controls due to a reduction in intramacrophage iron availability.

Aims of this chapter:

- To characterise the *Hamp1*$^{-/-}$ mouse model by:
  a) quantification of haematological parameters
  b) assessment of tissue iron accumulation

- Investigate the role of hepcidin in *M.tb* infection by infecting *Hamp1*$^{-/-}$ mice with *M.tb*
- Determine the effect of hepcidin deletion in *M.tb* infection on genes involved in regulation of iron metabolism

## 4.2 Characterisation of the *Hamp1*$^{-/-}$ mouse model

### *4.2.1 Confirmation of genotype by gel electrophoresis and qRT-PCR*

PCR and gel electrophoresis was done prior to all experiments in order to confirm genotype. An example gel is shown in figure 4.2.1.

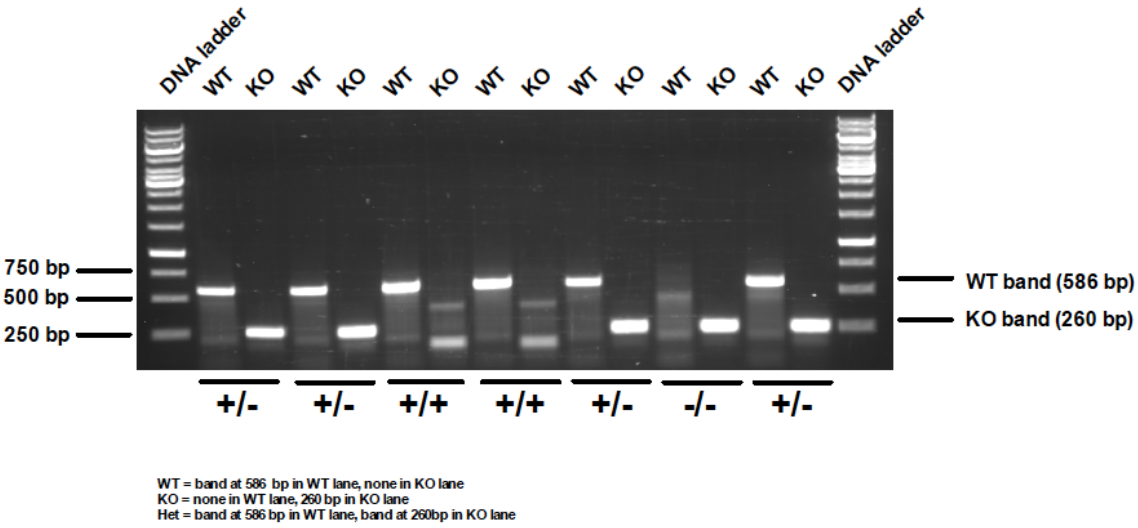


**Figure 4.2.1 Confirmation of genotype by PCR.** Presence of *Hamp1* DNA was detected in mouse ear tissue and confirmed by running PCR products on a 1% agarose gel to confirm genotype. A sample of 7 animals is shown.

### *4.2.2 Observations in the abdominal cavities of Hamp1$^{-/-}$ mice*

Figure 4.2.2 illustrates the immediate observations when dissecting a hepcidin knockout mouse. On the left (Figure 4.2.2A) is the *Hamp1*$^{-/-}$ mouse, which has clearly bronzed pancreas compared to the wild type on the right (Figure 4.2.2B). Bronzing is an effect of excess iron, and was observed to a certain degree in all *Hamp1*$^{-/-}$ mice, but it was markedly darker in the older mice, which eventually lose weight and have to be culled. Liver cirrhosis was also evident and more severe in older animals, probably due to increased liver iron accumulation.

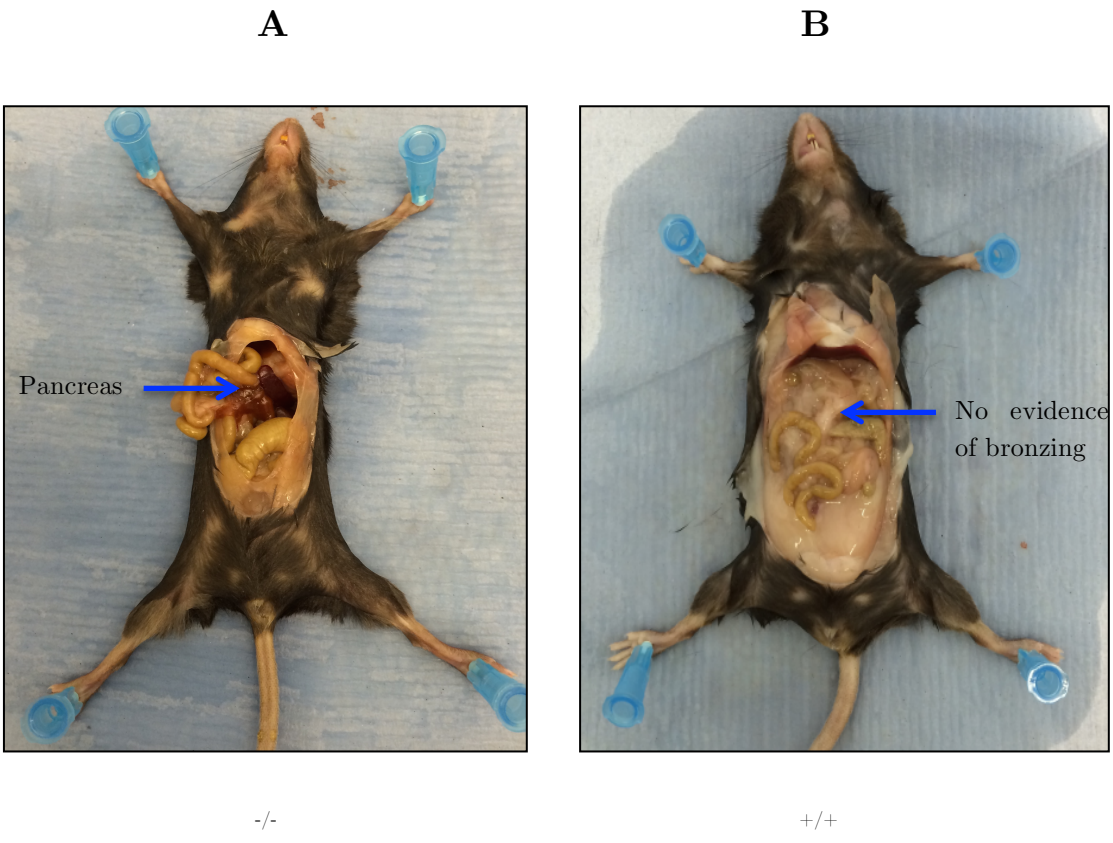


**Figure 4.2.2 Initial observations in *Hamp1*$^{-/-}$ abdominal cavity.** *Hamp1*$^{-/-}$ and wild type mice were culled by cervical dislocation and dissected via incision in the abdominal cavity prior to being photographed. The *Hamp1*$^{-/-}$ mouse is depicted on the left in **A**, with a C57BL/6 wild type on the right (**B**)

### *4.2.3 Haematological parameters*

To determine the effect of *Hamp1* gene deletion on haematological parameters, 5 *Hamp1*$^{-/-}$, 5 *Hamp1*$^{+/-}$ and 5 *Hamp1*$^{+/+}$ wild type littermate controls were bled for full blood count analyses. Mice were culled by cervical dislocation and liver was taken for qRT-PCR analyses to confirm genotype.

In figure 4.2.3, some full blood count parameters differed between *Hamp1*$^{-/-}$, *Hamp1*$^{+/-}$, and wild type (*Hamp1*$^{+/+}$) mice. Parameters relating to blood iron content indicated higher levels of iron in the *Hamp1*$^{-/-}$ mice. Haemoglobin concentration (HB), mean cell volume (MCV) and mean cell haemoglobin (MCH) were all significantly higher in the hepcidin-deficient compared to the wild type mice (Figure 4.2.3B, D and E). Interestingly, MCH was also significantly higher in the heterozygous mice than the wild type mice, which may mean these mice have an intermediate phenotype. Red blood cell count (RBC), haematocrit (HCT), mean cell haemoglobin concentration (MCHC), platelets (PLT) and red cell distribution width (RDW) all remained unchanged. No differences were observed in white blood cell proportions (white cell count, lymphocyte %, monocyte %, neutrophil %, eosinophil % and basophil %) (Figure 4.2.3I-N) between *Hamp1*$^{-/-}$ and wild type mice. Therefore, deletion of the *Hamp1* gene significantly altered haematological parameters relating to increased iron stores, but did not have an effect on white blood cell differentials.

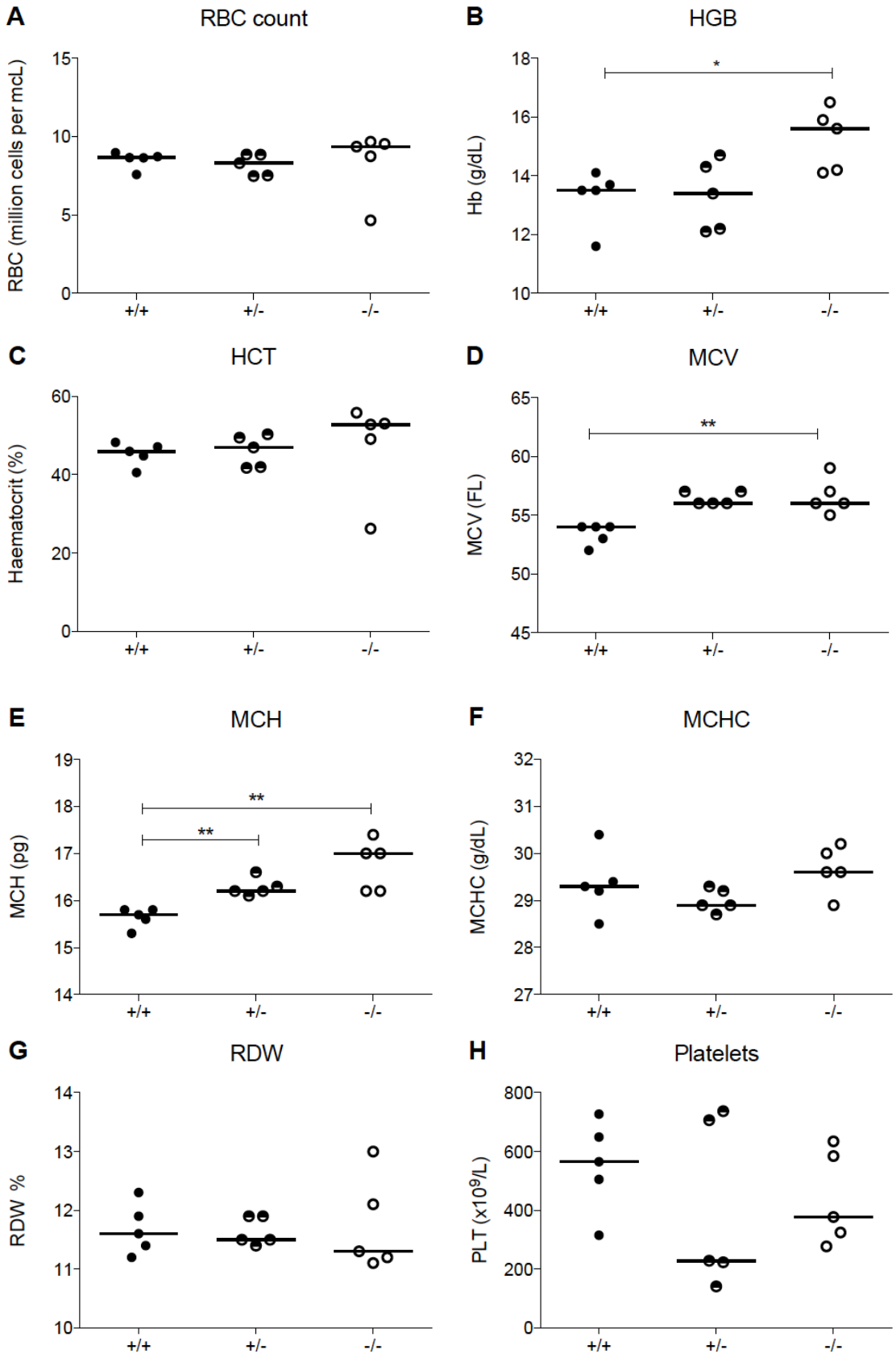
A
RBC count
RBC (million cells per mcL)
15
10
5
0
+/+
+/-
-/-
B
HGB
Hb (g/dL)
18
16
14
12
10
*
C
HCT
Haematocrit (%)
60
40
20
0
D
MCV
MCV (FL)
65
60
55
50
45
**
E
MCH
MCH (pg)
19
18
17
16
15
14
**
**
F
MCHC
MCHC (g/dL)
32
31
30
29
28
27
G
RDW
RDW %
14
13
12
11
10
H
Platelets
PLT (x10⁹/L)
800
600
400
200
0

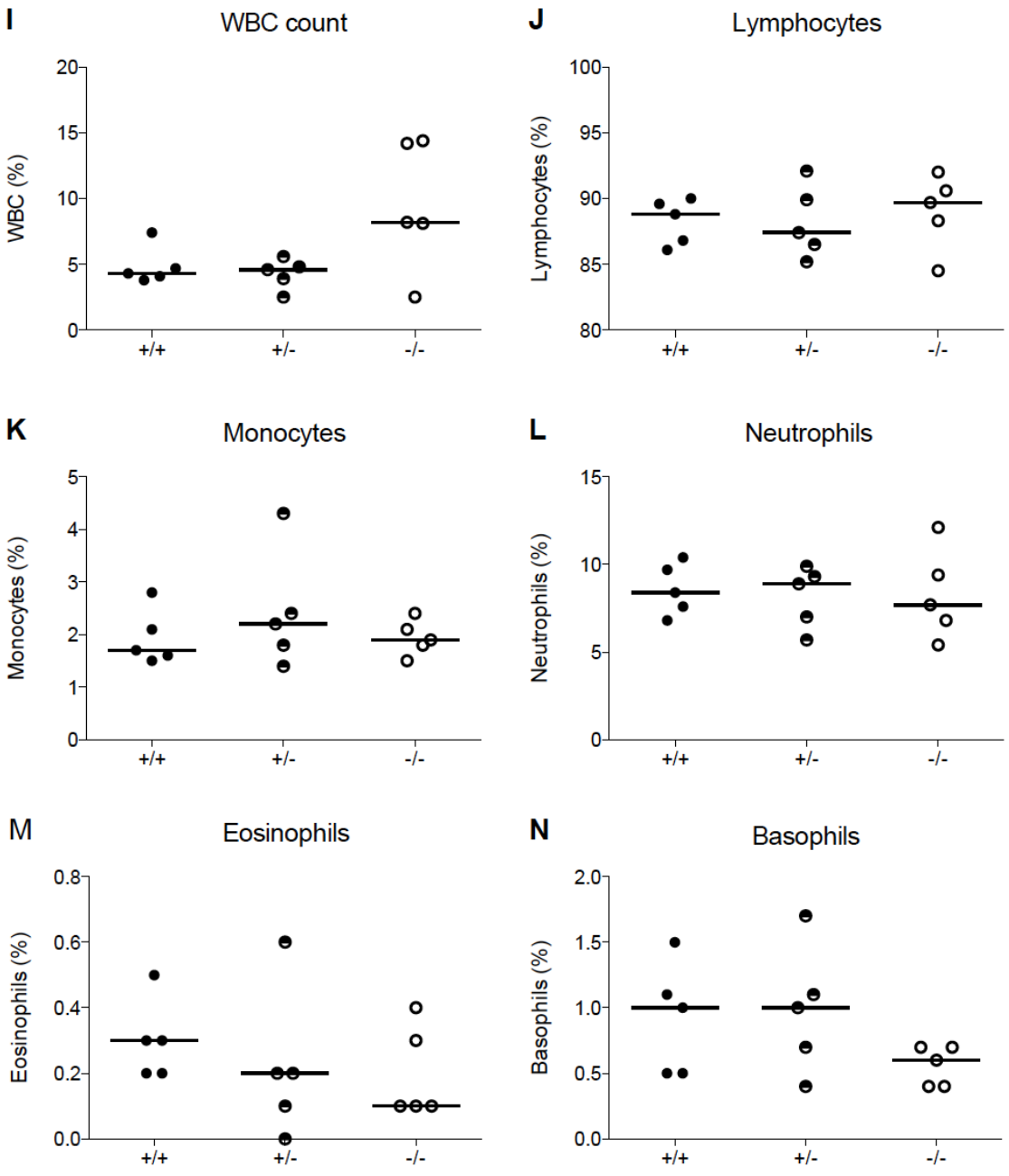


**Figure 4.2.3 Full blood counts in *Hamp1*$^{-/-}$ mice and controls.** Blood was collected via cardiac puncture from hepcidin deleted, heterozygous and wild type littermate control mice for analysis on an ABX Pentra 60 instrument. Data are plotted for RBC count (A), haemoglobin concentration (B), haematocrit (C), mean cell volume (D), mean corpuscular haemoglobin (E), mean corpuscular haemoglobin concentration (F), red cell distribution width (G), platelet count (H), white cell count (I), % lymphocytes (J), monocytes (K), neutrophils (L), eosinophils (M) and basophils (N). Statistical analyses were Mann-Whitney tests adjusted for multiple comparisons. Wild type animals are represented by full circles, heterozygotes by half circles, and hepcidin-deficient animals by empty circles. N=5 animals per group. *p≤0.05 ** p≤0.01 *** p=≤0.001 and **** p=≤0.0001.

### *4.2.4 Confirmation of genotype by qRT-PCR*

In addition to gel electrophoresis, genotype was confirmed at the termination of the experiment by qRT-PCR. In the mice used for measurement of haematological parameters and quantification of tissue iron accumulation by histology, hepatic *Hamp1* expression was significantly reduced in the *Hamp1*$^{-/-}$ mice compared to the wild type or heterozygous mice (p=0.0316 for both), confirming the genotyping technique was accurate (Figure 4.2.4). Interestingly, *Hamp1* expression looks higher in the control mice than the heterozygous mice, which may indicate a potential intermediate phenotype.

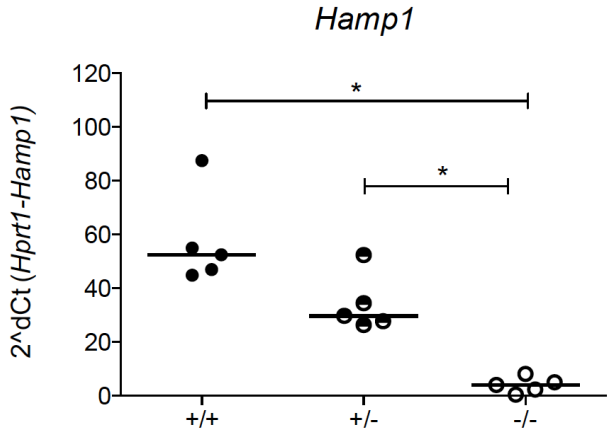


**Figure 4.2.4 Confirmation of genotype by qRT-PCR.** Hepatic *Hamp1* gene expression was quantified by qRT-PCR with a *Hamp1* TaqMan Assay. Full circles represent wild type controls, half circles heterozygous animals and empty circles represent *Hamp1*$^{-/-}$ animals. Mann Whitney tests with Bonferroni corrections for multiple comparisons were performed to compare groups. N=5 animals per group. Average age 5 months. *, **, *** and **** represent p≤0.05, p≤0.01, p=≤0.001 and p=≤0.0001, respectively.

### *4.2.5 Tissue iron accumulation*

To determine the effect of *Hamp1* deficiency on tissue iron distribution, 5 *Hamp1*$^{-/-}$ mice and 5 wild type littermate controls were culled by cervical dislocation. Lungs, liver and spleen were prepared for histology and stained for iron by Perl's staining. Excess non-haem iron was observed in the lungs and liver of the *Hamp1*$^{-/-}$ mice, while iron sparing was seen in the spleen, compared to the wild type controls (Figure 4.2.5), consistent with the literature [113]. In the liver, iron was concentrated more in the periportal areas but is also spread out over centrilobular areas.

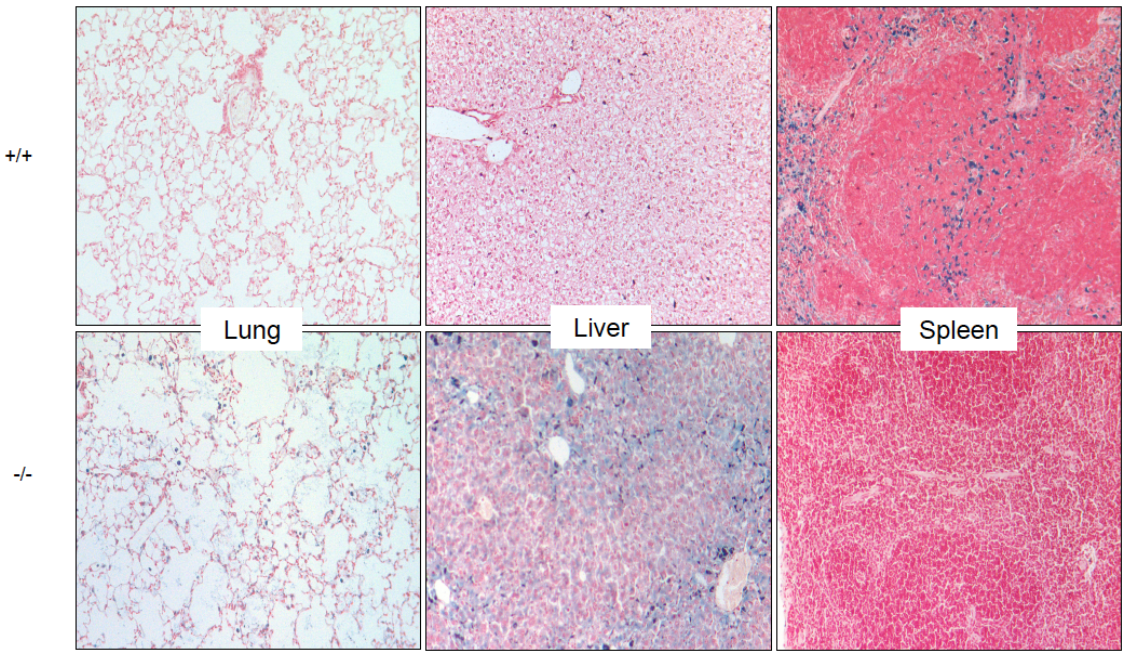


**Figure 4.2.5 Iron deposition in *Hamp1*$^{-/-}$ mice.** Perl's' staining of murine lung, liver and spleen sections. Typical sections are shown at an original magnification of x10. Non-haem ferric iron stains blue

## 4.3 *M.tb* infection in *Hamp1*$^{-/-}$ mice

### *4.3.1 Deletion of Hamp1 does not affect outcome of M.tb infection*

Female *Hamp1*$^{-/-}$ mice were infected with 50-100 CFU of *M.tb* via aerosol and bacterial burden was quantified in lungs and spleen 4 weeks post-infection. As illustrated in Figure 4.3.1A and B, no significant differences were observed between *Hamp1*$^{-/-}$, *Hamp1*$^{+/-}$ and wild type controls, in either lung or spleen (median CFU $8.1x10^6$, $5.3x10^6$ and $8.0x10^6$ for wild type, *Hamp1*$^{+/-}$ and *Hamp1*$^{-/-}$ mice, respectively). No weight loss was observed post-challenge in any of the groups. Median weights were higher at D27 (27 days post-challenge) compared to D0 (day of challenge) in all groups (19.5g to 20.3g in $^{+/+}$, 20.6g to 22.1g in $^{+/-}$ and 20.6g to 22.45g in $^{-/-}$) with wild type mice reaching significance ($p=0.0020$) (Figure 4.3.1C). This indicates that despite the altered iron metabolism and severe iron overload of the knockout mice, deletion of the hepcidin gene did not have a significant effect on susceptibility to *M.tb* infection.

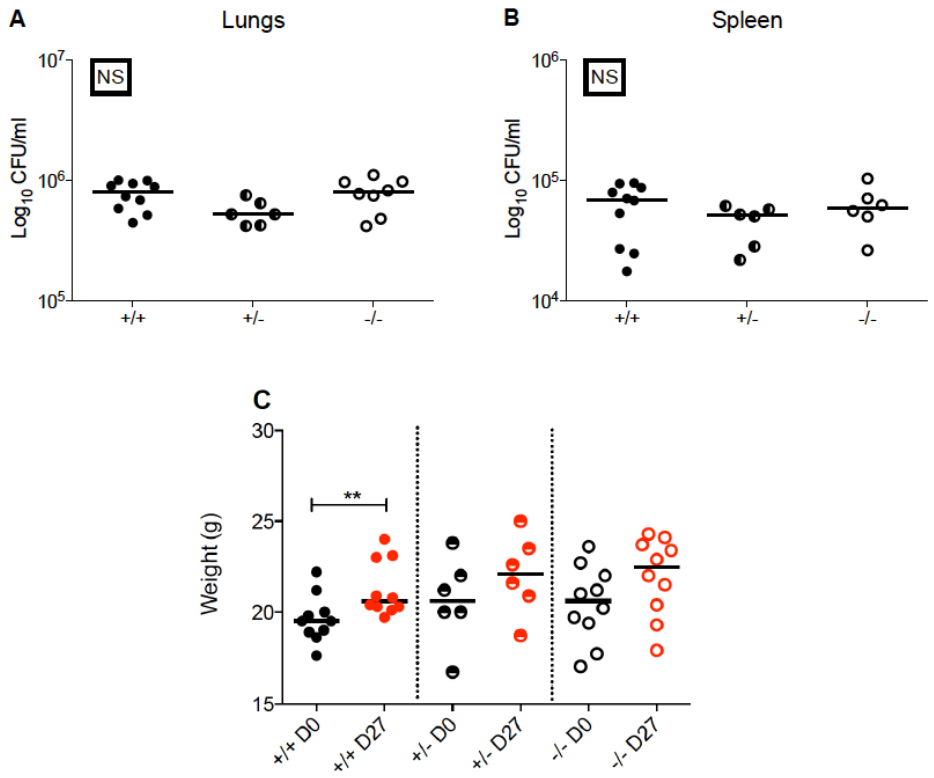


**Figure 4.3.1 Aerosol infection of *Hamp1*$^{-/-}$ mice with *M.tb*.** Mice were infected with *M.tb* and culled 4 weeks later. CFU was quantified in lung (**A**) and spleen (**B**) homogenates. Wild type mice are represented by closed circles, *Hamp1*$^{+/-}$ mice by half circles and *Hamp1*$^{-/-}$ mice by open circles. A Kruskal-Wallis test was performed for the three groups (p=0.1177 for lung, p=0.3734 for spleen), followed by Mann-Whitney tests to compare each group. N=10 for wild type and HAMP1$^{-/-}$ groups and n=6 for *Hamp1*$^{+/-}$. Weights before and after infection are illustrated in (**C**), with black circles indicating pre-challenge weights and red circles indicating weights 4 weeks post-infection. Wilcoxon matched pairs tests were done to compare pre and post infection, and Mann-Whitney tests to compare groups. All analyses were performed in Prism 6. *p≤0.05 ** p≤0.01 *** p=≤0.001 **** p=≤0.0001. The average age of animals was 12 weeks

### *4.3.2 Gene expression analyses*

Liver *Hamp1* expression was significantly reduced in the *Hamp1*$^{-/-}$ (p=<0.0003) and *Hamp1*$^{+/-}$ (p=0.0006) mice compared with wild type controls, confirming that the *Hamp1*$^{-/-}$ mice do have their hepcidin gene deleted (although this was already confirmed by genotyping) (Figure 4.3.2A). No significant difference was observed between heterozygous and wild type mice, although some of the wild

type mice did have higher *Hamp1* expression (although overall not significant), so an intermediate phenotype cannot be ruled out.

Expression of the gene encoding ferroportin, *Fpn1*, was significantly higher in the *Hamp1*$^{-/-}$ mice (p=0.0156) (Figure 4.3.2B), which is not surprising since hepcidin is knocked out in these mice and is therefore unable to bind to and induce degradation of ferroportin protein. Although not significant, there is a trend towards higher *Fpn1* mRNA expression in the heterozygous mice, consistent with the slight, but not significant reduction in *Hamp1* seen in the *Hamp1*$^{+/-}$ mice compared with the wild types.

Hepcidin is regulated by iron via the BMP/SMAD signalling pathways, and by inflammation via the JAK/STAT3 inflammatory pathways [210]. Since hepcidin is regulated by iron through the BMP/SMAD signalling pathway, I wanted to investigate whether this pathway is involved in the regulation of iron homeostasis in *Hamp1*$^{-/-}$ mice. Therefore, I quantified hepatic expression of *Id1* and *Bmp6* mRNA 4 weeks post-*M.tb* infection. *Id1* mRNA expression was significantly higher in the *Hamp1*$^{-/-}$ mice compared with wild type (p=<0.0003) and *Hamp1*$^{+/-}$ mice (p=0.0090) (Figure 4.3.2C), consistent with the role of the BMP signalling pathway in the regulation of iron homeostasis. *Hamp1*$^{+/-}$ mice also had significantly higher *Id1* gene expression than the wild type controls (p=0.0225), indicating at least at the signalling level, that these animals may have slightly altered iron homeostasis compared with wild type animals. This is consistent with the observed trend (although not significant) of *Hamp1* being slightly lower in the *Hamp1*$^{+/-}$ mice when compared with wild type animals (Figure 3.4.2A). Therefore, this is consistent with findings in the

characterisation data that heterozygous mice might, at least on a signalling level, have an intermediate phenotype in terms of gene expression when compared with wild type animals.

When analysing all groups together, *Id1* (a marker of BMP/SMAD signalling) correlated inversely with *Hamp1* expression (Spearman R=-0.6752, p=0.0002) (Figure 4.3.2D). Since there is no hepcidin in the *Hamp1*$^{-/-}$, the resulting iron overload is likely leading to an unsuccessful attempt to induce hepcidin transcription via the BMP/SMAD pathway, and this explains the high expression of *Id1* (Figure 4.3.2C). Although not significant, *Bmp6* is slightly higher in the knockout group (Figure 4.3.2E), in line with involvement of the BMP/SMAD signalling pathway in the knockout mice.

I also quantified the expression of *Tfrc*, the gene encoding transferrin receptor protein 1, which transports iron bound transferrin and therefore iron into cells, thereby regulating iron homeostasis [123]. *Tfrc* mRNA levels were significantly higher in the *Hamp1*$^{-/-}$ mice compared with the *Hamp1*$^{+/-}$ animals (Figure 4.3.2F**,** p=0.0225, median=0.158 in *Hamp1*$^{-/-}$ mice and 0.114 in the *Hamp1*$^{+/-}$ mice). This was not significant when comparing *Hamp1*$^{-/-}$ and wild type controls, although *Tfrc* was trending towards being higher in the *Hamp1*$^{-/-}$ mice. This is surprising since *Tfrc* normally correlates inversely with intracellular iron content, and *Hamp*$^{-/-}$ mice have iron-overloaded livers, as evidenced in Figure 4.2.5.

The expression of ferritin, the iron storage protein, is positively regulated by iron through the IRE/IRP iron regulatory system [88]. Here, I measured

expression of *Ftl*, encoding ferritin light chain, and *Fth*, which encodes ferritin heavy chain [88]. *Ftl* was significantly increased in the *Hamp1*$^{-/-}$ mice compared with wild type controls and *Hamp1*$^{+/-}$ mice, which was as expected due to their iron-overloaded phenotype (Figure 4.3.2G p=<0.0003 and p=0.0051, respectively). Conversely, expression of *Fth* mRNA was reduced in *Hamp1*$^{-/-}$ mice (Figure 4.3.2F, p=0.0051). Since ferritin is also post-transcriptionally regulated, not much can be inferred from this data, although in some cases, an increase in ferritin mRNA has been seen in response to iron [88, 211]. In addition, ferritin-L chain is predominantly expressed in the liver and spleen, whereas ferritin-H chain is predominantly expressed in the heart and kidney, so the expression of *Ftl* here is more likely reflective of liver ferritin protein [212]

No changes in expression of genes encoding pro-inflammatory cytokines IL-6, TNF-α or IFN-γ were observed between groups, highlighting a possible lack of effect of hepcidin knockout on immune function, consistent with findings that the deletion of hepcidin does not affect proportions of immune cells as seen in the full blood count data, and also that it has no effect on susceptibility to *M.tb.*

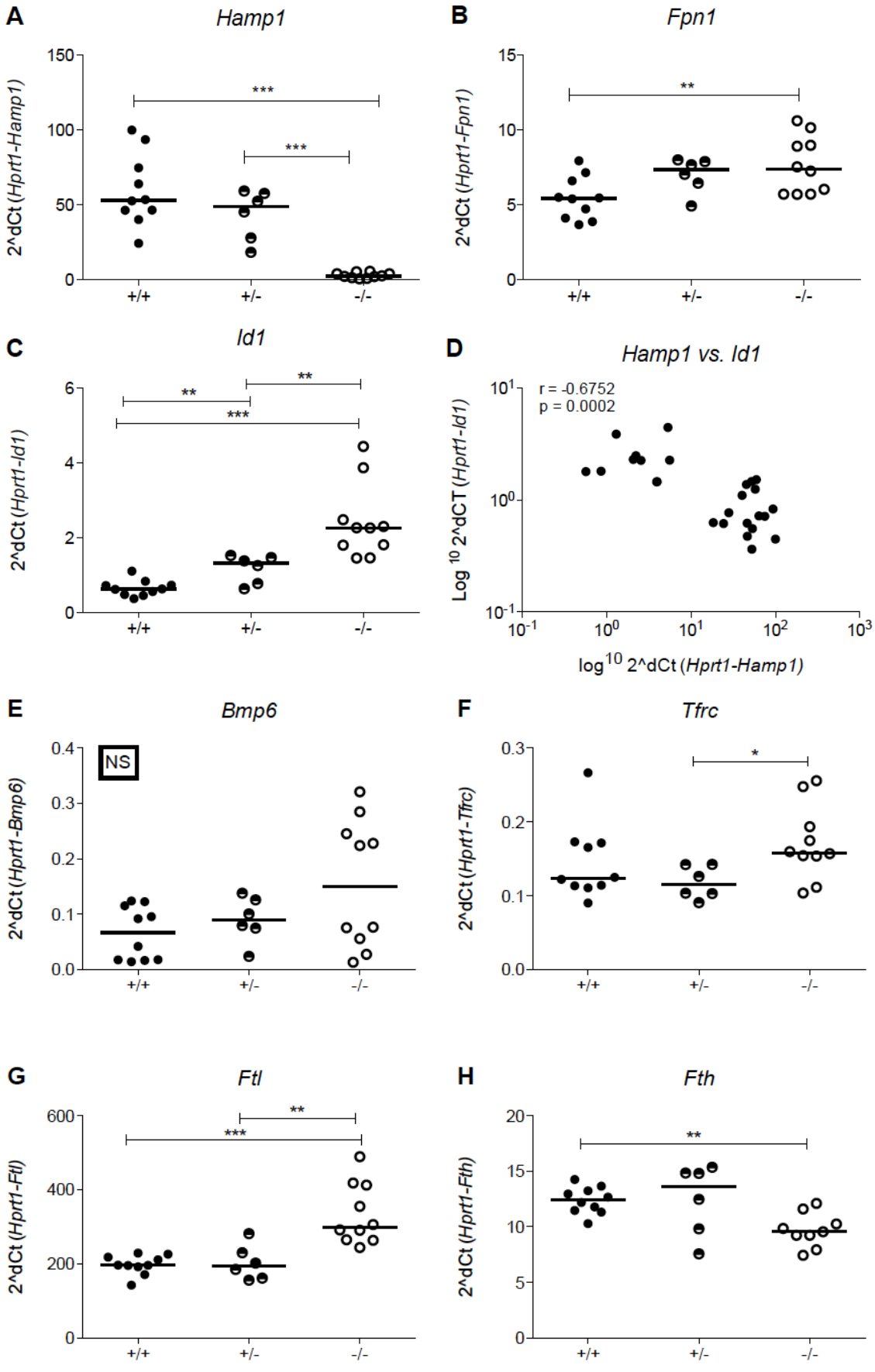
A
Hamp1
2^dCt (Hprt1-Hamp1)
150
100
50
0
***
***
+/+
+/-
-/-
B
Fpn1
2^dCt (Hprt1-Fpn1)
15
10
5
0
**
+/+
+/-
-/-
C
Id1
2^dCt (Hprt1-Id1)
6
4
2
0
**
**
***
+/+
+/-
-/-
D
Hamp1 vs. Id1
r = -0.6752
p = 0.0002
Log 10 2^dCT (Hprt1-Id1)
log 10 2^dCt (Hprt1-Hamp1)
E
Bmp6
2^dCt (Hprt1-Bmp6)
0.4
0.3
0.2
0.1
0.0
NS
+/+
+/-
-/-
F
Tfrc
2^dCt (Hprt1-Tfrc)
0.3
0.2
0.1
0.0
*
+/+
+/-
-/-
G
Ftl
2^dCt (Hprt1-Ftl)
600
400
200
0
**
***
+/+
+/-
-/-
H
Fth
2^dCt (Hprt1-Fth)
20
15
10
5
0
**
+/+
+/-
-/-

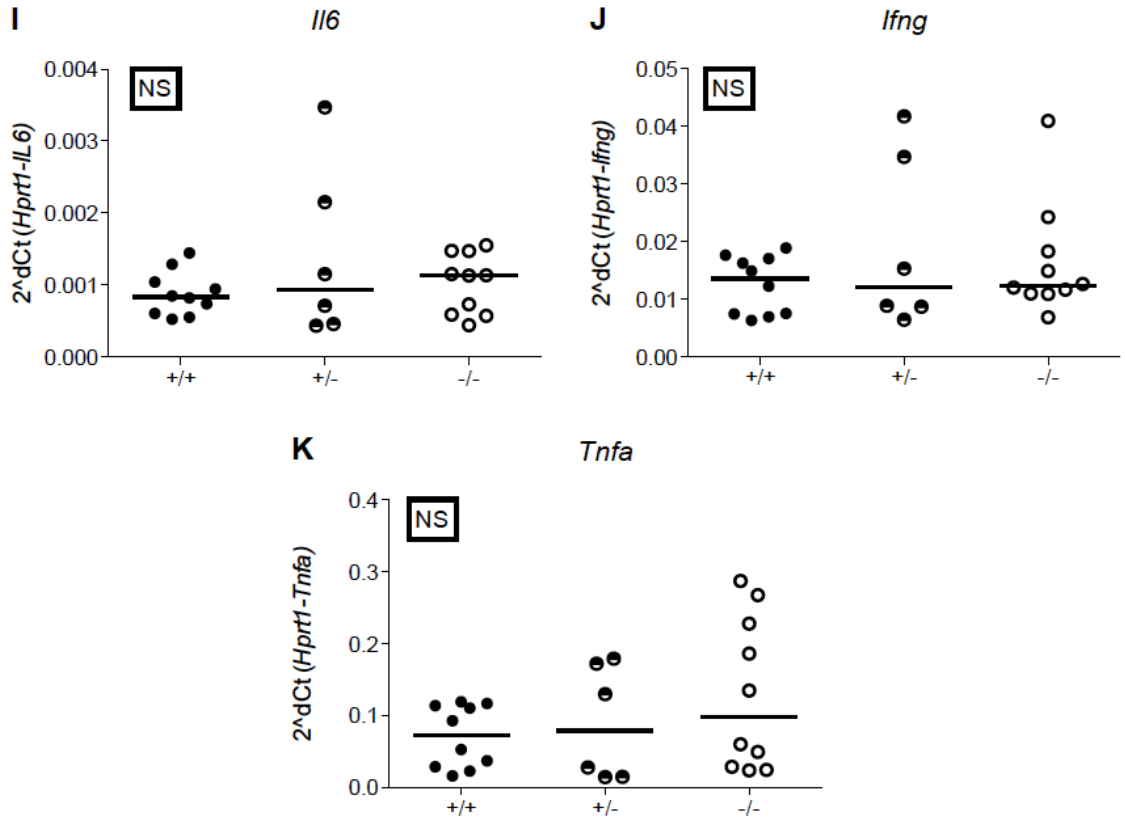


**Figure 4.3.2 Gene expression in livers of *Hamp1*$^{-/-}$ mice challenged with *M.tb*.** Hepatic gene expression is shown for *Hamp1* (**A**), *Fpn1* (**B**), *Id1* (**C**), *Bmp6* (**E**), *Tfrc* (**F**), *Ftl* (**G**), *Fth* (**H**), *Il6* (**I**), *Ifng* (**J**) and *Tnfa* (**K**) were performed using qRT-PCR. Values are expressed as 2^-ΔCt of the gene of interest relative to the housekeeping gene, *Hprt1*. Wild type mice are represented by closed circles, *Hamp1*$^{+/-}$ by half circles, and *Hamp1*$^{-/-}$ mice by open circles. Mann-Whitney tests with Bonferroni corrections for multiple comparisons were performed to compare groups. *p≤0.05 ** p≤0.01 *** p=≤0.001 **** p=≤0.0001.

## 4.4 Discussion

Key findings for this chapter:

- Hepcidin deletion in mice results in an iron-overloaded phenotype, with altered tissue iron distribution and haematological parameters (consistent with published data)
- Hepcidin deletion did not affect susceptibility to infection with *M.tb*

The aim of this chapter was to determine whether deletion of the hepcidin 1 gene and the resultant iron overload have a significant effect on murine *M.tb* infection. In Chapter 3, I showed that hepcidin mRNA levels fluctuate considerably post-*M.tb* infection, with evidence of hepcidin down regulation and ferroportin induction at later time points, potentially highlighting restriction of macrophage iron as a protective mechanism against *M.tb* infection or at least as a host response to infection. Recent literature highlights that hepcidin may be an independent risk factor in TB disease, as it has been found to be a predictor of mortality in TB disease [138, 141]. The mechanisms involved have not been studied in detail, and it is unclear whether a) hepcidin is merely an acute phase marker which is consequently higher in those patients with more severe disease and b) whether hepcidin is a cause or effect of worsening disease outcome [138]. It is possible that hepcidin may worsen TB disease outcome by degrading ferroportin, resulting in the redistribution of iron stores, and increasing iron availability in macrophages for intracellular pathogens that target this cell type.

*Hamp1*$^{-/-}$ mice have multivisceral iron overload with a phenotype somewhat comparable to severe hereditary haemochromotosis [113], so could also be a

useful model to determine whether systemic iron overload worsens disease outcome, as has been found in published studies [133, 179]. Although *Hamp1*$^{-/-}$ mice are severely iron overloaded, they have iron sparing in spleen and liver macrophages due to overexpression of ferroportin, which exports iron from the cell. Intramacrophage iron content may play a role in the outcome of intracellular infections by influencing bacterial growth, but also by affecting the host immune response. For example, iron inhibits pathways regulated by IFN-γ in macrophages, inhibiting their anti-microbial functions and reducing their ability to control *Mycobacteria and Salmonella* infections [156-158]. As a result, perturbations in iron availability affect host immune function. For example, macrophages from patients with hereditary haemochromatosis have decreased iron acquisition which impairs *M.tb* growth [159]. My hypothesis was that deletion of the *Hamp1* gene in mice might be protective against *M.tb* infection, since macrophage iron concentration is reduced, which may inhibit *M.tb* growth.

Firstly, I characterised the *Hamp1*$^{-/-}$ mouse model. A number of haematological parameters, such as haemoglobin concentration, were indicative of iron overload. These data are consistent with another study by Lesbordes-Brion et al [113]. However, in this study, these parameters returned back to normal levels by 6 months of age, so perhaps larger differences would have been seen in mice of a younger age (the age at which animals were infected with *M.tb).* It would also be useful to quantify serum iron parameters such as serum ferritin and transferrin receptor. Moreover, tissue iron staining provided evidence of iron overload in the lungs and liver, with iron sparing in the spleen. These findings were consistent with previous findings, as well as haematological data [113].

Secondly, to determine whether *Hamp1* deletion and resultant impaired iron homeostasis affected susceptibility to mycobacteria, I infected mice lacking *Hamp1* with *M.tb*. Surprisingly, no differences were observed in the bacterial burdens of either lungs or spleens of *Hamp1*$^{-/-}$ compared to wild type animals post-infection. It is therefore unlikely that *Hamp1* gene deletion has an impact on outcome of *M.tb* infection. Weight loss can be used as a measure of disease progression in animals with a susceptible phenotype, however, *Hamp1*$^{-/-}$ mice did not lose weight at any point throughout the study, consistent with there being no differences in bacterial burden between groups. Moreover, in the post-infection murine gene expression analyses, no differences in hepatic mRNA levels of pro-inflammatory cytokines were observed, which may indicate a lack of effect of hepcidin 1 deletion on immune function relevant for *M.tb* infection, despite the fact iron status has been shown to affect innate immune responses [213]. However, since hepatic gene expression may not be reflective of circulating cytokine levels, further analyses, such as cytometric assays quantifying $CD4^+$ and $CD8^+$ cells secreting IFN-$\gamma$, post infection would confirm whether hepcidin deletion has affected the immune function of these mice. This apparent lack of effect of hepcidin deletion on susceptibility to mycobacterial infection contrasts greatly with the fatal outcome of some blood borne infections in hepcidin knockout mice [214]. Hepcidin deficient mice succumb rapidly to infection with the siderophilic bacterium *Vibrio vulnificus*, which is a common cause of death in human haemochromatosis. The stark differences in outcome of infection with these two pathogens in hepcidin deficient mice highlights that hepcidin deficiency-mediated iron redistribution has distinct effects depending on the type of pathogen and where it resides in the host. In this case, outcome of

infection with macrophage-tropic bacteria such as *M.tb* contrasts with the outcome of blood-borne infections, which may well be due to distinct differences in iron availability in the macrophage and blood in these hepcidin deficient mice. Infection of hepcidin deficient mice with *M.tb* via the *i.v.* route may result in a different outcome, although the relevance of this could be debated as this is not a natural route of infection for *M.tb*.

*Hamp1*$^{-/-}$ mice have iron sparing in their splenic macrophages and kupffer cells, but it is not known whether the same is the case in alveolar macrophages. A possible explanation for the lack of effect of hepcidin1 knockout on bacterial burden is that the alveolar macrophage iron content does not differ between *Hamp1*$^{-/-}$ and control mice. Alternatively, as in splenic macrophages and kupffer cells, iron stores are reduced, but increased ferroportin leads to increased throughput of iron in these cells, which may overall have no effect on bacterial burden (this could also explain the lack of difference in splenic bacterial burden). Another hypothesis could be that alveolar macrophage iron content is reduced, impacting on mycobacterial growth but at the same time, the severe iron overload elsewhere also impairs immune responses, counterbalancing any inhibitory effect of reduced iron on bacterial burden. In support of this hypothesis, iron exerts inhibitory effects on IFN-γ-mediated immune pathways such as the production of NOS2, TNF-α and IL-6, which are vital in the immune response against *M.tb* [215-217]. Measurement of nitrate in a Greiss assay might help elucidate whether there is reduced NO production in *Hamp1*$^{-/-}$ mice. Moreover, iron has also been shown to stimulate formation of IL-10, which de-activates macrophages [218], and impaired macrophage effector

functionality has been associated with iron loading [155]. Quantification of mycobacterial gene expression could also elucidate whether the bacterium senses any changes in iron availability in the *Hamp1*$^{-/-}$ mice.

Post-infection gene expression analysis suggests that *Hamp1*$^{-/-}$ mice still attempt regulation of hepcidin expression via BMP/SMAD signalling, since markers of BMP/SMAD signalling correlated inversely with *Hamp1* mRNA. Moreover, expression of *Fpn1* mRNA was significantly higher in the *Hamp1*$^{-/-}$ mice than in controls, which was expected since they are hepcidin 1-deficient. The iron overload observed in *Hamp1*$^{-/-}$ mice due to over-expression of ferroportin is likely to have induced signalling through BMP/SMAD pathways in an attempt to reduce iron uptake and release from macrophages. Although *Hamp1*$^{-/-}$ mice are severely iron overloaded, peak *Fpn1* mRNA expression was no higher than that observed in the time course studies discussed in Chapter 3, indicating either that it has reached maximum level, it is regulated post-transcriptionally, or that hepcidin-independent mechanisms might be limiting its expression. In support of this, one study found that *Hamp1*$^{-/-}$ mice are still able to alter their iron metabolism (particularly ferroportin expression) to some degree in response to an iron-deficient diet, through local control of iron metabolism via the IRE/IRP network, independent of hepcidin [219]. In a study by Johnson et al, over-expression of ferroportin in a macrophage cell line impaired *M.tb* growth, presumably by reducing macrophage iron content and availability to the pathogen [213]. This is consistent with findings that iron depletion inhibits growth of intracellular bacteria in macrophages [162]. Interestingly, another study found that ferroportin expression was increased in RAW264.7 mouse

macrophages infected with *M.tb*, and that ferroportin localized to the *M.tb*-containing phagosome, thereby depriving the mycobacteria of iron [163]. Ferroportin has also been found to inhibit the growth of *Salmonella enterica* [157]. Therefore, even though the high expression of ferroportin here is likely just a consequence of lack of hepcidin, it mirrors protective mechanisms to restrict iron from intracellular pathogens. However, the higher *Fpn1* gene expression observed here (as a result of hepcidin deletion) did not confer any protection against *M.tb*. It might be interesting to compare *Fpn1* levels in both uninfected and infected *Hamp1*$^{-/-}$ mice to determine whether infection further induces *Fpn1,* independently of hepcidin.

Interestingly, *Tfrc* mRNA expression was higher in the *Hamp1*$^{-/-}$ mice. *Tfrc* has been shown to correlate inversely with intracellular iron concentrations [220]. Therefore, the increased *Tfrc* observed in the *Hamp1*$^{-/-}$ mice is the converse of what was expected, since livers of *Hamp1*$^{-/-}$ mice are severely iron overloaded, and most cell types, with the exception of the kupffer cells, will be iron overloaded. However, high mRNA may not result in high TfR protein since the mRNA may be relatively unstable. The observed increase in *Ftl* mRNA in the *Hamp1*$^{-/-}$ mice is consistent with these mice being iron overloaded. An explanation for this could be that iron overload in these hepcidin-deficient mice leads to increased ROS production, activating the transcription factor Nrf2, which is able to drive *Ftl* transcription, resulting in higher *Ftl* mRNA expression. Since most cell types are iron overloaded, it is also unlikely that there will be post-transcriptional modification of *Ftl* mRNA since IRPs are unable to block ribosomes in iron-loaded cells and block translation. This could

be confirmed by quantified of ferritin by a more appropriate method, such as a serum ELISA. Quantification of intramacrophage iron levels could also confirm this. Should there have been an effect of *Hamp1* deletion on disease outcome, my aim would have been to further characterise this model by quantifying differences in iron availability in the macrophages in the lungs, spleens and livers of hepcidin-deficient versus wild type mice, since it is not known whether alveolar macrophage iron content is affected by hepcidin deficiency. Gene expression analyses of *M.tb* in these mice could also determine whether the bacteria sensed altered iron availability. Perhaps they did, but they may have been able to circumvent this via the production of siderophores, for example.

Surprisingly, I observed what could be an intermediate phenotype in the heterozygous mice. Heterozygous mice had significantly raised mean cell haemoglobin than the wild type controls, with mean cell volume trending towards being significant, potentially highlighting raised blood iron levels. This could also be confirmed by quantification of serum iron by ELISA. In addition, in the post-infection gene expression data, I observed variations in the expression of genes involved in iron metabolism between heterozygous and control mice. In the heterozygous mice, *Id1* expression was significantly higher than in the wild type controls, and significantly lower than in the *Hamp1*$^{-/-}$ mice. Furthermore, although not significant, the expression of *Fpn1* and *Bmp6* was slightly higher in the heterozygous animals than in the controls. This is in contrast with a previous study by Lesbordes-Brion et al that showed no differences in hematological parameters between heterozygous and wild type animals and in which they therefore used heterozygous animals as controls [113].

It is unclear at what age the parameters were measured, but since the animals that I quantified haematological parameters in were 5 months old, it might be that the intermediate phenotype is only evident in older animals, with more pronounced iron overload, and that this was missed in the previous study. In addition, my group sizes were small (n=5), so ideally a larger group size taken at a range of ages is required to confirm this.

Although *Hamp1*$^{-/-}$ mice are iron overloaded, they have dysfunctional iron metabolism resulting in reduced intramacrophage iron concentrations as ferroportin is highly expressed. Most other cell types are iron overloaded. By feeding mice iron rich or iron deficient diets, we may be able to decrease or increase intramacrophage iron content and ultimately confirm whether increasing or decreasing intramacrophage iron availability affects susceptibility to *M.tb.* It would also be interesting to determine whether *Hamp1*$^{-/-}$ mice are more susceptible to *M.tb* when infected via an intravenous, rather than an aerosol route, since their serum iron parameters are higher, although of course human infection is via the aerosol route.

To summarise this chapter, in keeping with previous studies, I have confirmed that *Hamp1*$^{-/-}$ mice have an iron-overloaded phenotype, with increased haemoglobin and increased tissue iron deposition, resulting in a haemochromatosis-like phenotype. Despite this iron overload, *Hamp1*$^{-/-}$ mice have iron sparing in macrophages in the spleen and liver, due to over expression of ferroportin as a result of hepcidin deletion. Reduction of macrophage iron has previously been shown to inhibit mycobacterial growth [162, 213], and high hepcidin has been associated with poorer disease outcome [141]. However, here,

deletion of *Hamp1* did not have an obvious effect on susceptibility to *M.tb.* It is therefore unlikely that hepcidin itself is a major factor in the control of murine mycobacterial infection, however further studies are needed to understand the implications of this work for the role of hepcidin in human infection.

# Chapter 5

# 5 Consequences of dietary iron restriction on susceptibility to mycobacteria in mice

## 5.1 Introduction

In the previous chapter, it was established that *Hamp1* gene deletion does not affect the outcome of *M.tb* infection, suggesting that there may not be a significant role of hepcidin and iron homeostasis in *M.tb* infection mice. However, there are other ways to manipulate changes in iron distribution that could confirm this, such as by altering dietary iron availability. A number of human and animal studies have looked at the effect of altering dietary iron availability on susceptibility to mycobacterial infection. Increasing dietary iron availability has been shown to increase susceptibility to mycobacterial infection in a murine model [135, 136, 181]. Consistent with these findings, chelation of iron limits mycobacterial growth *in vitro* [181, 221]. Moreover, a number of human studies have found associations between higher dietary iron availability and increased risk of TB disease [145, 180, 222, 223]. However, the effect of restricting dietary iron on the growth of *M.tb* or BCG *in vivo* has not previously been explored.

Mice require around 35ppm of dietary iron, but the standard diet in animal facilities worldwide contains over 200ppm, which is iron overloaded in comparison to their natural iron requirements [224]. In the experiments described in this chapter, mice were fed an iron-deficient diet containing 4ppm of iron in the form of ferric citrate, or a control diet containing 200ppm, which

matches standard mouse dietary iron content. Mice were fed their respective diets *ad libitum* for 2 weeks prior to infection with either BCG by intranasal (*i.n.)* route or *M.tb* via aerosol. Mice remained on the respective diets throughout the duration of the experiments, except in the case of the pilot experiments where mice on the iron-deficient diet were switched to a 'maintenance' diet containing 18ppm of iron at the time of challenge, since the risks of high dose *M.tb* infection combined with iron deficiency were unknown at the time.

The aims of this chapter were to:

- Determine whether mycobacterial growth can be manipulated *in vitro* by altering iron availability
- Determine the effect of restricting dietary iron on mycobacterial infection *in vivo*

## 5.2 The effect of altering iron availability on growth of BCG *in vitro*

### *5.2.1 Optimisation of mycobacterial growth inhibition assays*

It is well documented that mycobacterial growth can be manipulated by altering iron availability [225-227]. However, I wanted to confirm this myself *in vitro*, to test my model systems. I grew BCG Pasteur in murine splenocytes, in differentiated THP-1 monocytes, or alone in culture medium in a 6 day time course study. BCG grew better with splenocytes than without, and growth was significantly increased in the cells treated with FAC, an exogenous iron salt,

than in the untreated controls (p=0.0286 with splenocytes and without; Figure 5.2.1A). In the splenocytes, addition of the iron chelator, DFO, reduced bacterial growth (p=0.0286 compared to controls). However, addition of hepcidin peptide did not affect bacterial growth. Consistent with these findings, a similar trend was observed in THP-1 cells (Figure 5.2.1B). In THP-1 cells, treatment with iron or chelator had a significant effect on bacterial growth, and time post-infection also affected growth in all groups (p=<0.0001 for both). Bacterial growth was significantly increased in the FAC-treated cells by D6 (p=<0.0001 compared to controls at the same timepoint). Interestingly, at 4 hours post-infection, cells treated with FAC had significantly reduced bacterial burden, perhaps indicating that it may affect the cell's ability to uptake BCG. Inhibition of bacterial growth in DFO-treated cells compared to untreated controls was evident from 3 days post-infection (p=0<0.0001), and was significantly reduced by 6 days compared to 4 hours post-infection (p=0.0362).

These data indicate, in keeping with the literature, that addition of exogenous iron stimulates bacterial growth, and addition of chelator inhibits bacterial growth [145]. Addition of hepcidin, however did not effect growth.

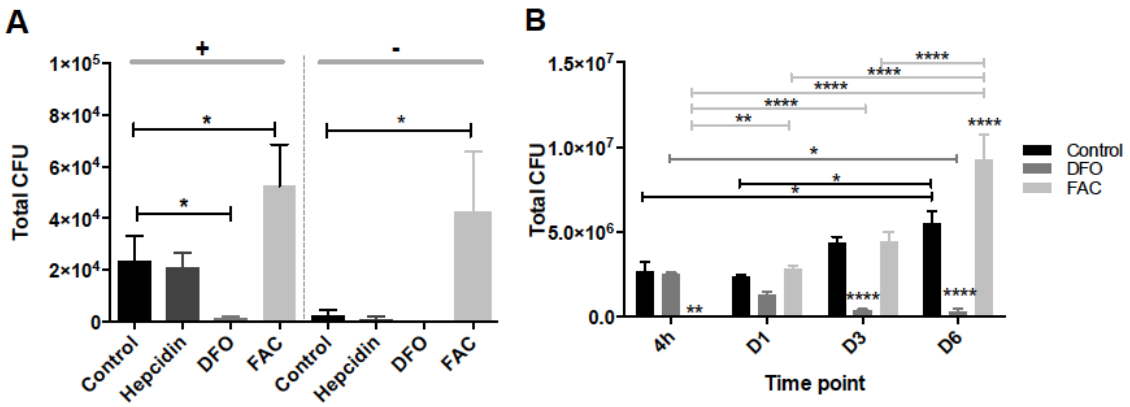


**Figure 5.2.1 *In vitro* BCG killing assays.** BCG was cultured either with (+) or without (-) murine splenocytes (A) or co-cultured in differentiated THP-1 cells (B) in a range of conditions. In A, BCG was cultured with or without splenocytes with hepcidin (0.5μM), FAC (250μg/ml) or DFO (50μM) and rotated for 96h at 37°C. Bacterial burden was quantified by counting CFU in the cell lysates. In B, differentiated THP-1 cells were pre-treated with FAC or DFO at the same concentrations as in A, for 24h prior to BCG infection. Bacterial burden was quantified by micro CFU in the cell lysates at 4h, 1 day, 3 days and 6 days post-infection. Error bars represent the mean ± SEM. Mann-Whitney tests were performed for A, and 2-way ANOVA with Bonferroni post hoc tests for multiple comparisons were performed in B. *, ** and **** represent p=<0.05, p=<0.01 and p=<0.0001 respectively. N=4 replicates per group in A, n=6 in B.

### *5.2.2 Mycobacterial growth inhibition tube (MGIT) assay*

I then wanted to evaluate the MGIT assay as an alternative method to quantify bacterial burden. In this assay, after a 4 day co-culture with host-derived cells, these cells were lysed (leaving the mycobacteria intact) and placed in the supplemented mycobacterial growth tubes, and placed in the MGIT BACTEC (BD) machine which quantifies growth in each sample relative to a positive control tube. I added BCG directly into MGIT tubes with FAC at a range of concentrations, and saw increased growth with increasing concentrations of FAC (r=1, p=0.0167; Figure 5.2.2A). A similar trend was observed after THP-1-BCG co-culture for 96 hours prior to inoculation into MGIT tubes (r=0.8810, p=0.0072, Figure 5.2.2B). I also tested whether THP-1 cell concentration might affect BCG growth, and found an inverse correlation between THP-1 cell

concentration and subsequent growth of co-cultured BCG (r=-0.9286, p=0.0022, Figure 5.2.2C). I then tested whether the MGIT assay was sensitive enough to quantify growth differences between splenocytes from unvaccinated and BCG-vaccinated mice, as has been shown before [228]. Splenocytes from vaccinated mice controlled BCG growth better than splenocytes from unvaccinated mice (p=0.0087; Figure 5.2.2D), as expected. This provides some biological validity for this assay, which therefore might be a suitable assay to determine whether alteration of dietary iron availability in mice affects susceptibility to mycobacterial infection, as an alternative to *in vivo M.tb* infection which can be more costly and time-consuming.

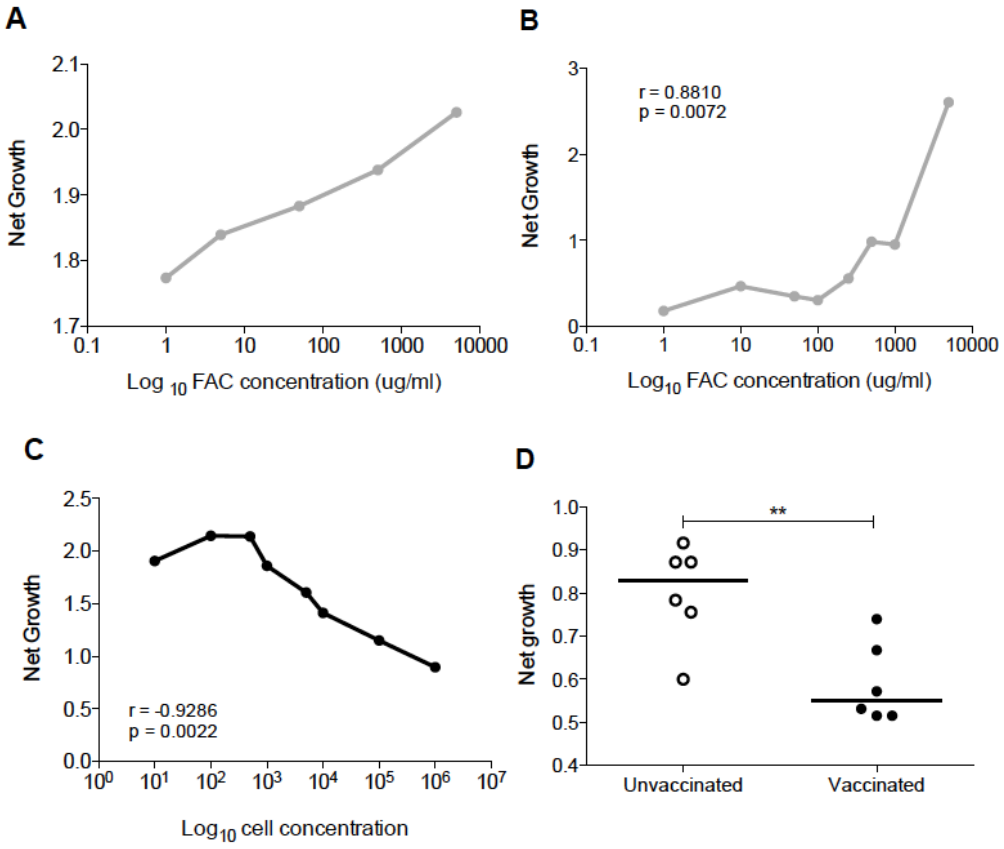


**Figure 5.2.2** ***In vitro*** **mycobacterial growth inhibition assays**. Net growth of BCG was measured in response to increasing doses of FAC directly added to MGIT tubes with no cells (A), after co-culture for 96h in THP-1 cells with increasing doses of FAC (B), when co-cultured for 96h with increasing concentrations of THP-1 cells (C) and when co-cultured for 96h with splenocytes from either unvaccinated or BCG-vaccinated mice (D). Spearman correlations were done for A, B and C. A Mann-Whitney test was done for D where ** represents p=<0.01

## 5.3 Haematological characterisation of the iron-deficient mouse model

Next, I wanted to determine whether reducing iron availability in mice alters their iron parameters, and therefore whether this is a useful model for investigating whether restricting iron *in vivo* affects susceptibility to mycobacteria.

I quantified haematological parameters, gene expression, and tissue iron accumulation in mice maintained on an iron-deficient diet compared with controls. In these experiments, 6-8 week old female C57BL/6 mice were maintained on an iron-deficient (4ppm) or control (200ppm) diet for a total of 2, 6 or 10 weeks before being bled by cardiac puncture. Lungs, liver and spleen were taken for histological analyses and liver for gene expression analyses.

### *5.3.1 Dietary iron restriction alters haematological parameters*

Some haematological parameters were affected by dietary iron restriction (Figure 5.3.1). Differences in MCV, MCH, RDW, platelets, lymphocyte counts, and basophil counts were observed between mice fed the iron-deficient diet and controls. MCV was reduced in mice fed the iron-deficient diet at 6 and 10 weeks ($p=0.0065$ and $p=0.0022$, respectively; Figure 5.3.1D), which indicates that these mice have iron deficient erythropoiesis, although haemoglobin concentration was unaffected by diet so they may not have iron deficiency anaemia. MCH was also significantly reduced at all timepoints in the mice fed the iron-deficient diet (2 weeks $p=0.0368$, 6 and 10 weeks $p=0.0022$, Figure 5.3.1E) and MCHC was reduced at 10 weeks in the mice fed the iron-deficient

diet (p=0.0152, Figure 5.3.1F). RDW and platelets were significantly higher at 6 weeks in the mice fed the iron-deficient diet (p=0.0108 and p=0.0152, respectively, Figure 5.3.1G+H). At 10 weeks, mice fed the 4ppm diet had a decreased lymphocyte count (p=0.0216, Figure 5.3.1J), and a higher basophil count (p=0.0087, Figure 5.3.1N) compared with controls, highlighting a possible effect of iron-deficient diet after 10 weeks on white blood cell functions or proportions. No other white cell parameters were affected. Overall, these haematological data indicate that the mice on the 4ppm diet are showing signs of iron deficiency, and this becomes more severe after longer on the diet.

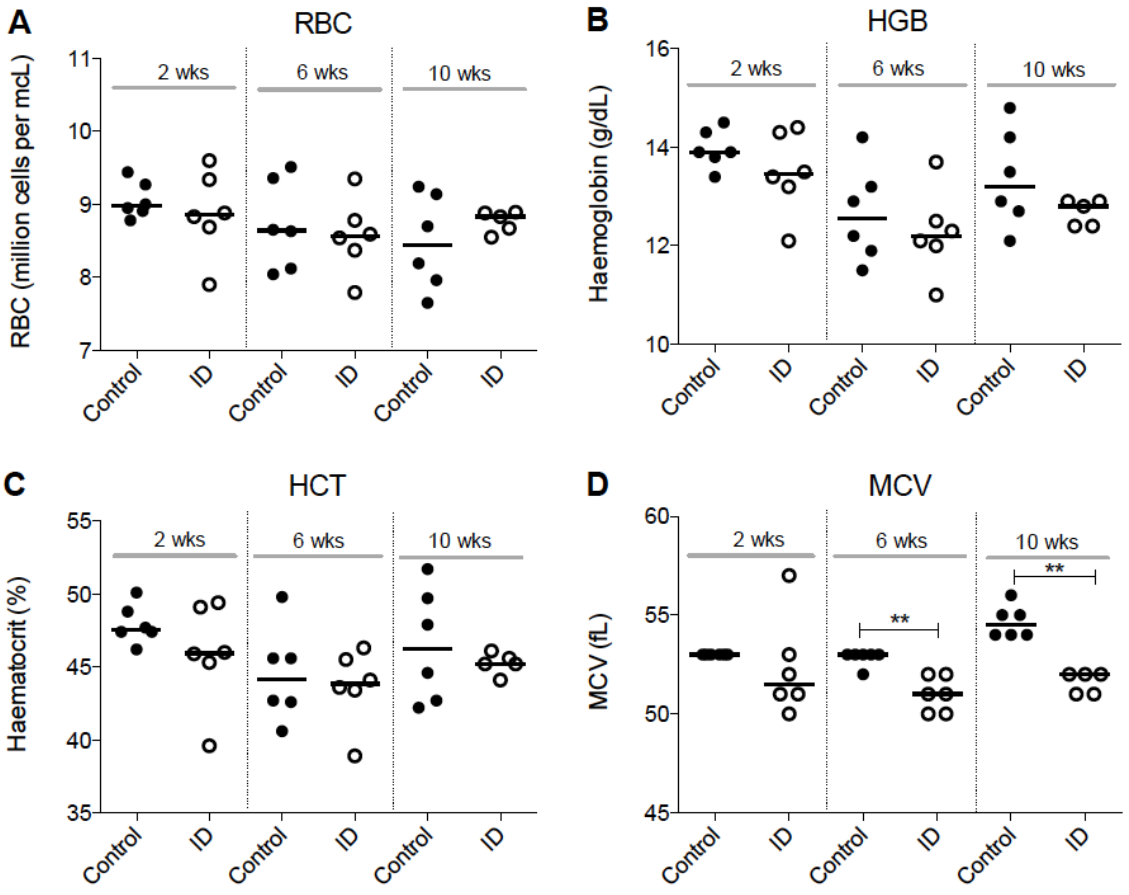

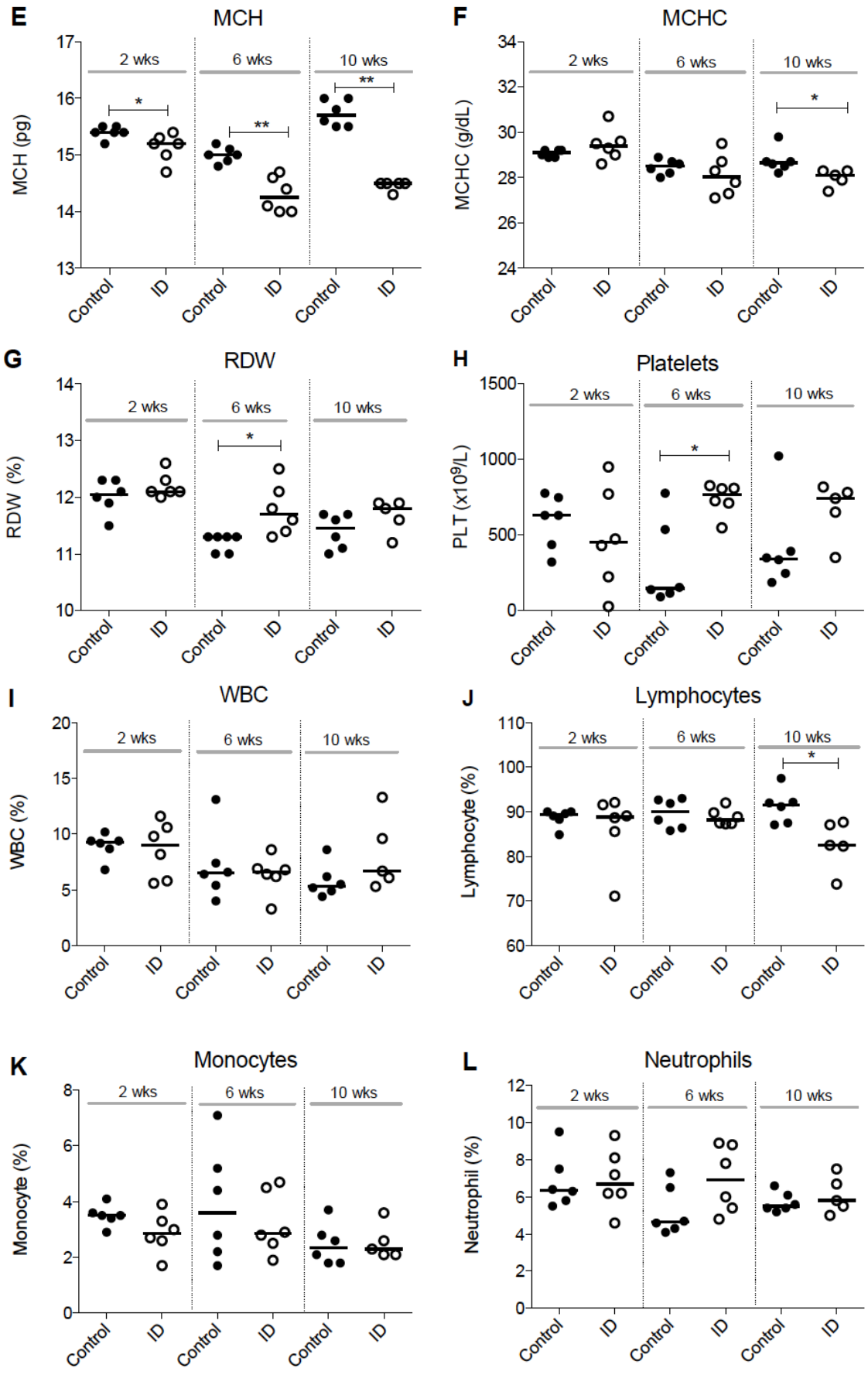
E
MCH
MCH (pg)
17
16
15
14
13
2 wks
6 wks
10 wks
*
**
**
Control
ID
F
MCHC
MCHC (g/dL)
34
32
30
28
26
24
*
G
RDW
RDW (%)
14
13
12
11
10
*
H
Platelets
PLT (x10⁹/L)
1500
1000
500
0
*
I
WBC
WBC (%)
20
15
10
5
0
J
Lymphocytes
Lymphocyte (%)
110
100
90
80
70
60
*
K
Monocytes
Monocyte (%)
8
6
4
2
0
L
Neutrophils
Neutrophil (%)
12
10
8
6
4
2
0

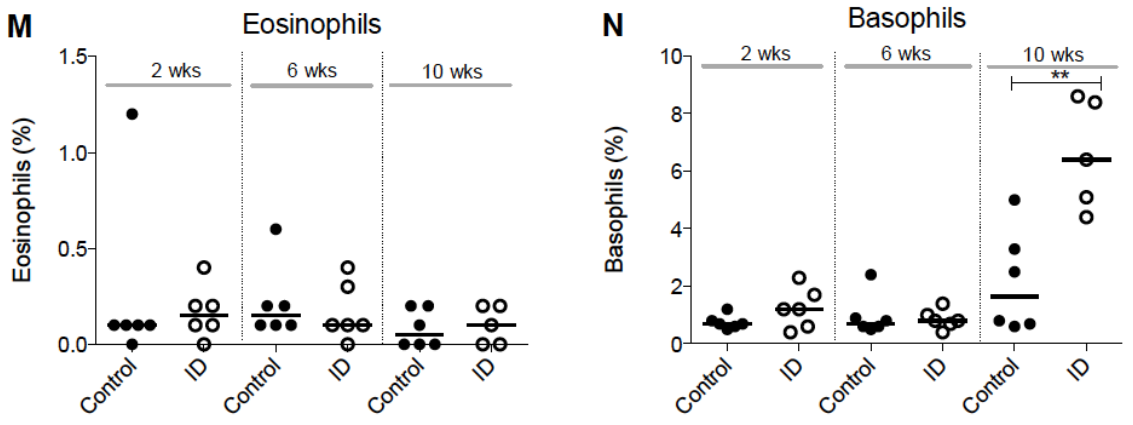


**Figure 5.3.1 Haematological parameters in mice fed an iron-deficient diet**. C57BL/6 mice were fed an iron-deficient (4ppm) or control (200ppm) diet for a total of 2, 6 or 10 weeks. Mice were bled and each endpoint and haematological parameters were quantified by an ABX Pentra 60 haematological analyser. Mann-Whitney tests were done to determine statistical differences between groups at each timepoint where *, **, *** and **** indicate p=<0.05, p=<0.01, p=<0.001 and p=<0.0001, respectively.

### *5.3.2 Dietary iron restriction affects the expression of genes involved in iron homeostasis*

Differences were observed in the expression of genes involved in iron metabolism in animals fed the iron-deficient diet compared with controls (Figure 5.3.2). Firstly, *Hamp1* expression was significantly down-regulated in mice fed the iron-deficient diet, at all timepoints (p=0.0087 at 2 weeks, p=0.002 at 6 and 10 weeks; Figure 5.3.2A). Inhibition of hepcidin production reduces the post-translational degradation of ferroportin by hepcidin, thus increasing both iron absorption from the diet and release of iron from intracellular iron stores, in order to increase iron availability. Surprisingly, *Fpn1* was also significantly down-regulated in the mice fed the iron-deficient diet, which may be due to post-transcriptional modulation by the IRE/IRP network in response to low intracellular iron concentrations. Alternatively, low iron availability leading to

reduced haem may also affect downstream pathways ultimately leading to reduction of Nrf2 and subsequent repression of *Fpn1* transcription.

In order to investigate whether the suppression of *Hamp1* during iron deficiency was via the BMP/SMAD signalling pathway, I quantified the expression of *Id1* and *Bmp6.* Consistent with the observed down regulation of *Hamp1*, *Id1* and *Bmp6* were both down regulated in the mice fed the iron-deficient diet (Figure 5.3.2 A, C+E), although these differences were not significant until after the 2 week timepoint for *Bmp6*, and later for *Id1*, indicating that longer time on the diet results in more severe iron deficiency. *Id1* and *Bmp6* both correlated positively with *Hamp1* expression, confirming regulation of *Hamp1* in iron deficiency is likely via the BMP/SMAD signalling pathway (Figure 5.3.2D+F). When *Hamp1* and *Id1* were correlated in the control mice only, no significance was observed (data not shown), suggesting that BMP/SMAD signalling is probably just regulating *Hamp1* in response to iron deficiency. I also quantified the expression of *Tfrc*, the gene encoding transferrin receptor 1, which is usually increased via IRE/IRP signalling in iron restricted conditions and is inversely proportional to intracellular iron availability [220]. I found that *Tfrc* was higher in the mice fed the iron-deficient diet, although this was not significant until mice had ben fed the 4ppm diet for 10 weeks (Figure 5.3.2I).

I also quantified the hepatic expression of genes encoding the pro-inflammatory cytokines IFN-γ, TNF-α and IL-6 (*Ifng*, *Tnfa* and *Il6*, respectively) which are usually up-regulated following mycobacterial infection, in order to investigate whether iron restriction affects their hepatic mRNA expression. No difference was observed in *Ifng* between groups (Figure 5.3.2J), however, liver *Tnfa* mRNA

was lower in the mice fed the iron-deficient diet, although this was not statistically significant (Figure 5.3.2K). Liver *Il6* mRNA expression was significantly higher in the iron-deficient mice at 6 weeks on the diet, indicating iron deficiency may have some influence on the expression of this pro-inflammatory cytokine in the liver. This may be reflected in true circulating cytokine levels, in which case may be relevant in control of mycobacterial infection (p=0.0260; Figure 5.3.2L), although this should be confirmed by immune profiling of this iron deficient mouse model. I also quantified the expression of *Saa1*, a marker of inflammation, which was not affected by the iron-deficient diet (Figure 5.3.2G), nor did it correlate with *Hamp1* (Figure 5.3.2H), supporting the idea that there is no role of JAK/STAT signalling in regulation of *Hamp1* expression by iron deficiency. These data indicate that maintenance of mice on an iron-deficient diet significantly inhibits hepcidin expression, and this is likely regulated by BMP/SMAD signalling.

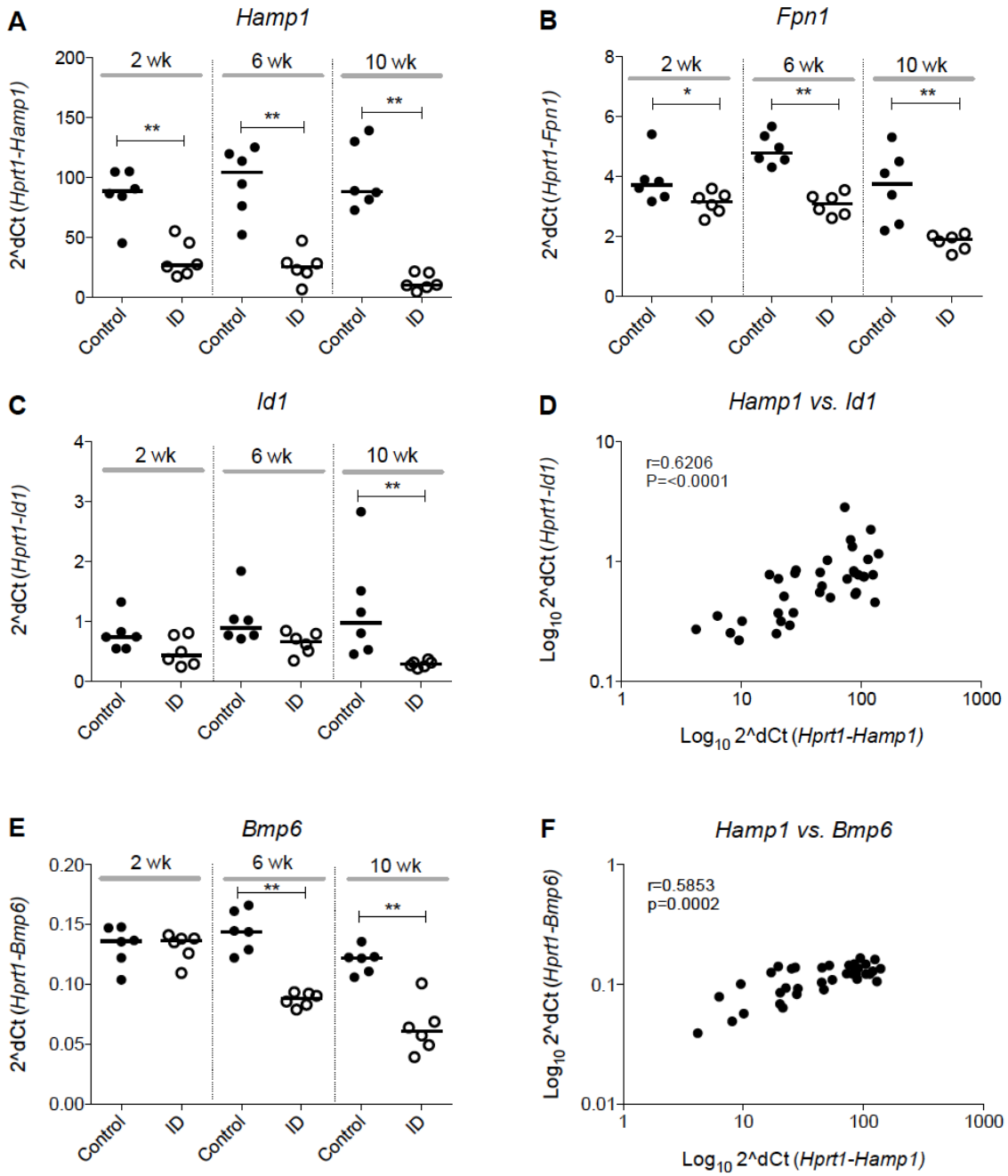
A
Hamp1
2^dCt (Hprt1-Hamp1)
2 wk
6 wk
10 wk
Control
ID
B
Fpn1
2^dCt (Hprt1-Fpn1)
C
Id1
2^dCt (Hprt1-Id1)
D
Hamp1 vs. Id1
r=0.6206
P=<0.0001
Log10 2^dCt (Hprt1-Id1)
Log10 2^dCt (Hprt1-Hamp1)
E
Bmp6
2^dCt (Hprt1-Bmp6)
F
Hamp1 vs. Bmp6
r=0.5853
p=0.0002
Log10 2^dCt (Hprt1-Bmp6)
Log10 2^dCt (Hprt1-Hamp1)

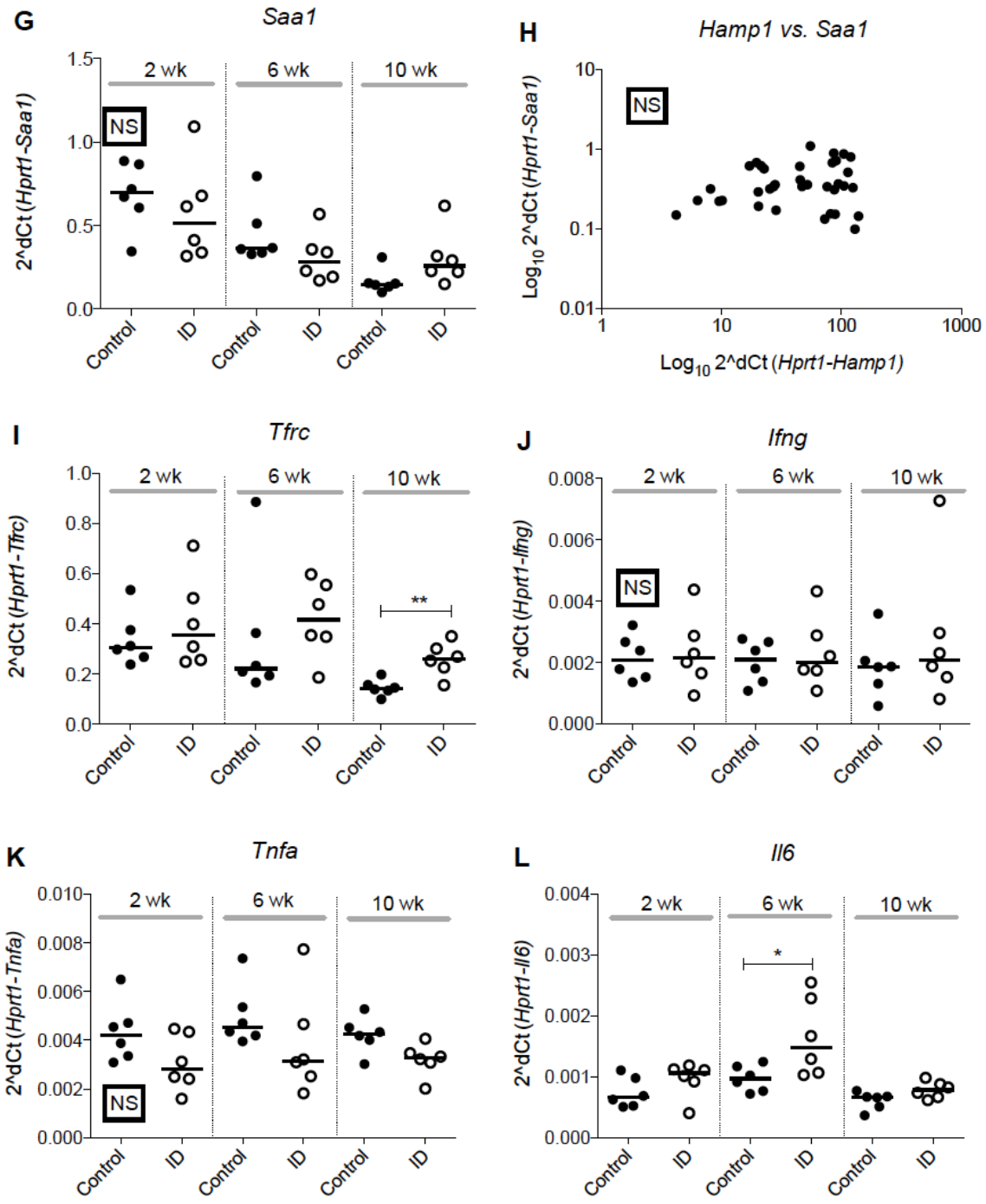


**Figure 5.3.2 The effect of dietary iron restriction on gene expression.** Female C57BL/6 mice were maintained on an iron-deficient (4ppm) or control (200ppm) diet for 2, 6 or 10 weeks. Hepatic mRNA expression was quantified by qRT-PCR for *Hamp1* (A), *Fpn1* (B), *Id1* (C), *Bmp6* (E), *Saa1* (G), *Tfrc* (I), *Ifng* (J), *Tnfa* (K) and *Il6* (L). Correlations are also shown between *Hamp1* and *Id1* (J), *Hamp1* and *Bmp6* (F) and *Hamp1* and *Saa1* (H). Controls are represented by closed circles, iron-deficient diet by open circles. Mann-Whitney tests were performed to compare groups at each timepoint where *, **, *** and **** represent p=<0.05, p<0.01, p<0.001 and p<0.0001, respectively.

### *5.3.3 Dietary iron restriction affects splenic iron accumulation*

Six to eight week old female C57BL/6 mice were fed the iron-deficient or control diet for a total of 4 weeks. Lungs, liver and spleen were removed and processed for histological analyses as described in the materials and methods chapter. No differences were observed in lung and liver non-haem iron between the two diets, but a reduction of splenic iron could be seen in the red pulp of mice fed the iron-deficient diet (Figure 5.3.3).

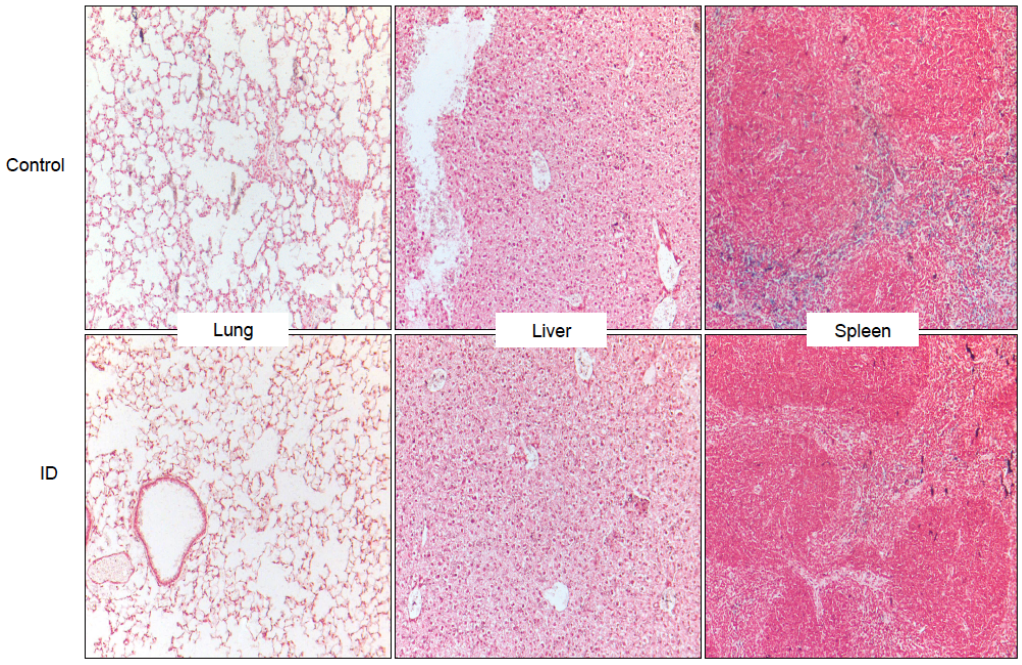


**Figure 5.3.3 Perls' staining of lungs, liver and spleen sections of mice fed an iron-deficient or control diet.** Female C57BL/6 mice were fed an iron-deficient (4ppm) or control (200ppm) diet for 4 weeks. Typical sections at an original magnification of x10 are shown. Non-haem iron stains blue.

## 5.4 The effect of dietary iron restriction on BCG infection

### *5.4.1 Experimental outline*

To determine the effect of dietary iron restriction on susceptibility to BCG infection, 8 week old C57BL/6 mice were fed an iron-deficient or control diet for 2 weeks prior to *i.n.* infection with $5x10^6$ CFU of BCG Pasteur, as described in the materials and methods chapter. Mice remained on the respective diets until they were taken down at 4 weeks post-infection, after a total of 6 weeks on the diet.

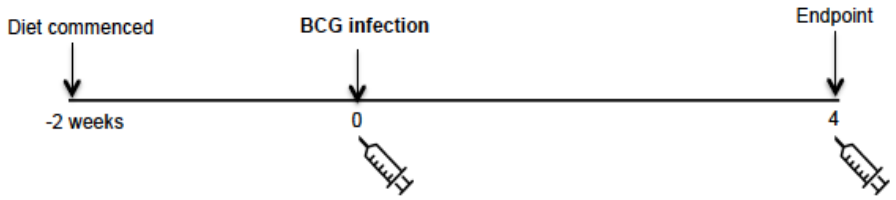


**Figure 5.4.1 Experimental design: BCG infection in iron-deficient mice.** C57BL/6 mice were fed an iron-deficient (4ppm) or control (200ppm) diet *ad libitum* 2 weeks prior to *i.n.* infection with $5x10^6$ CFU of BCG. Mice were then left for a total of 4 weeks. Age-matched uninfected controls on matched diets were also taken down at 4 weeks. Cardiac bleeds were performed at 4 weeks post-infection for haematological analyses. Lungs and spleen were removed for quantification of bacterial burden via CFU and liver for qRT-PCR. n=5 mice/group

### *5.4.2 Dietary iron restriction does not affect growth of BCG in this in vitro infection model*

Bacterial burden in lungs and spleen did not differ significantly between mice fed an iron-deficient or control diet, indicating that severe dietary iron restriction does not affect growth of BCG in this murine infection model (Figure 5.4.2).

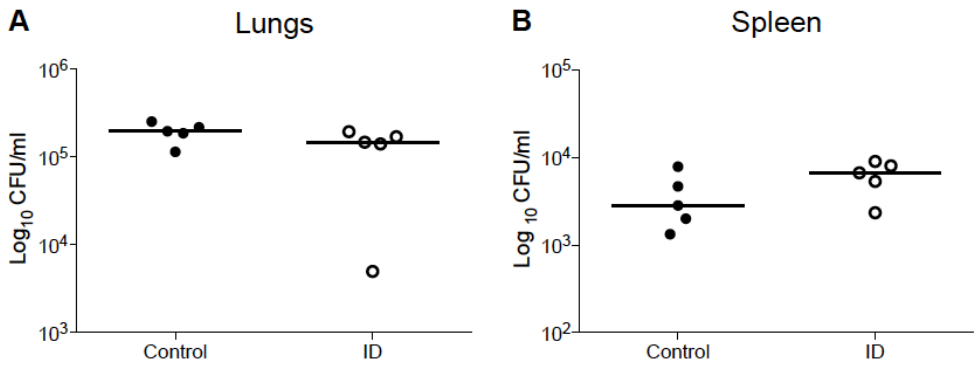


**Figure 5.4.2 Bacterial burden in iron-deficient mice infected with BCG.** C57BL/6 mice were fed an iron-deficient (4ppm) or control (200ppm) diet prior to *i.n.* infection with BCG, as described in Figure 5.4.1. Mice were taken down 4 weeks post-infection and spleen and lung homogenates were plated out for quantification of bacterial burden (CFU). Liver was also taken for qRT-PCR analyses. Mann-Whitney tests were performed to compare groups. n=4-5 mice/group

### *5.4.3 Haematological parameters are altered by BCG infection*

To determine the effect of host iron deficiency in BCG infection on haematological parameters, full blood counts were performed on all mice at the termination of the experiment, after a total of 6 weeks on the diet. In the uninfected controls, MCV and MCH were significantly reduced in the mice fed the iron-deficient diet compared with controls (p=0.0316 and p=0.0159, respectively; Figure 5.4.3D+E). The iron-deficient diet had no effect on any of the other haematological parameters. In the BCG infected mice, HGB, HCT, MCV, MCH, and MCHC were all significantly reduced (p=0.0079 for all) in mice fed the iron-deficient diet, compared with those on the control diet. Platelets and RDW were also increased in the iron-deficient infected mice (p=0.0317 and p=0.0079, respectively). White cell differentials were not affected by the iron-deficient diet, or by BCG infection (Figure 5.4.3I-N). Changes in parameters that were indicative of iron deficiency, such as MCV and MCH, became significant or more significant in the iron-deficient BCG infected

animals compared with iron-deficient uninfected controls. Moreover, significant decreases were observed in MCH in both iron-deficient and control diets when comparing uninfected and infected animals (p=0.0317 iron-deficient mice, p=0.0238 control mice, when comparing uninfected vs. BCG infected). Therefore, it is likely that BCG infection increased the severity of iron deficiency.

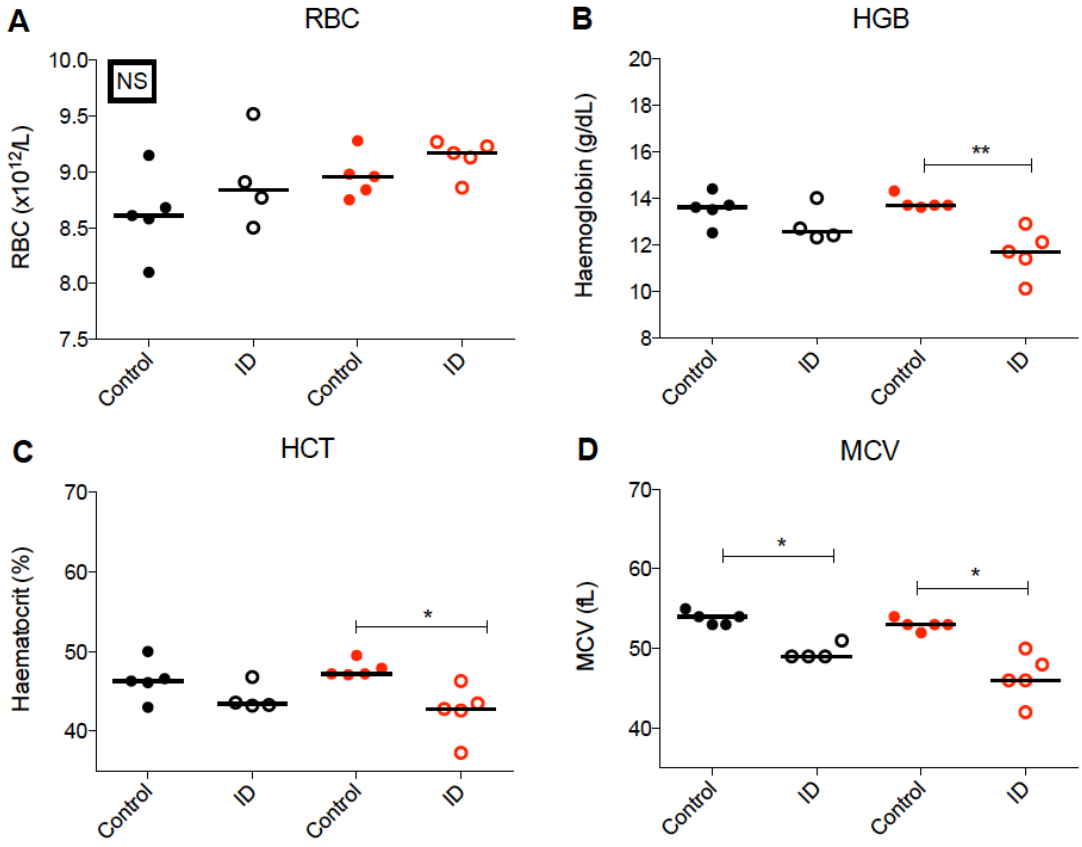

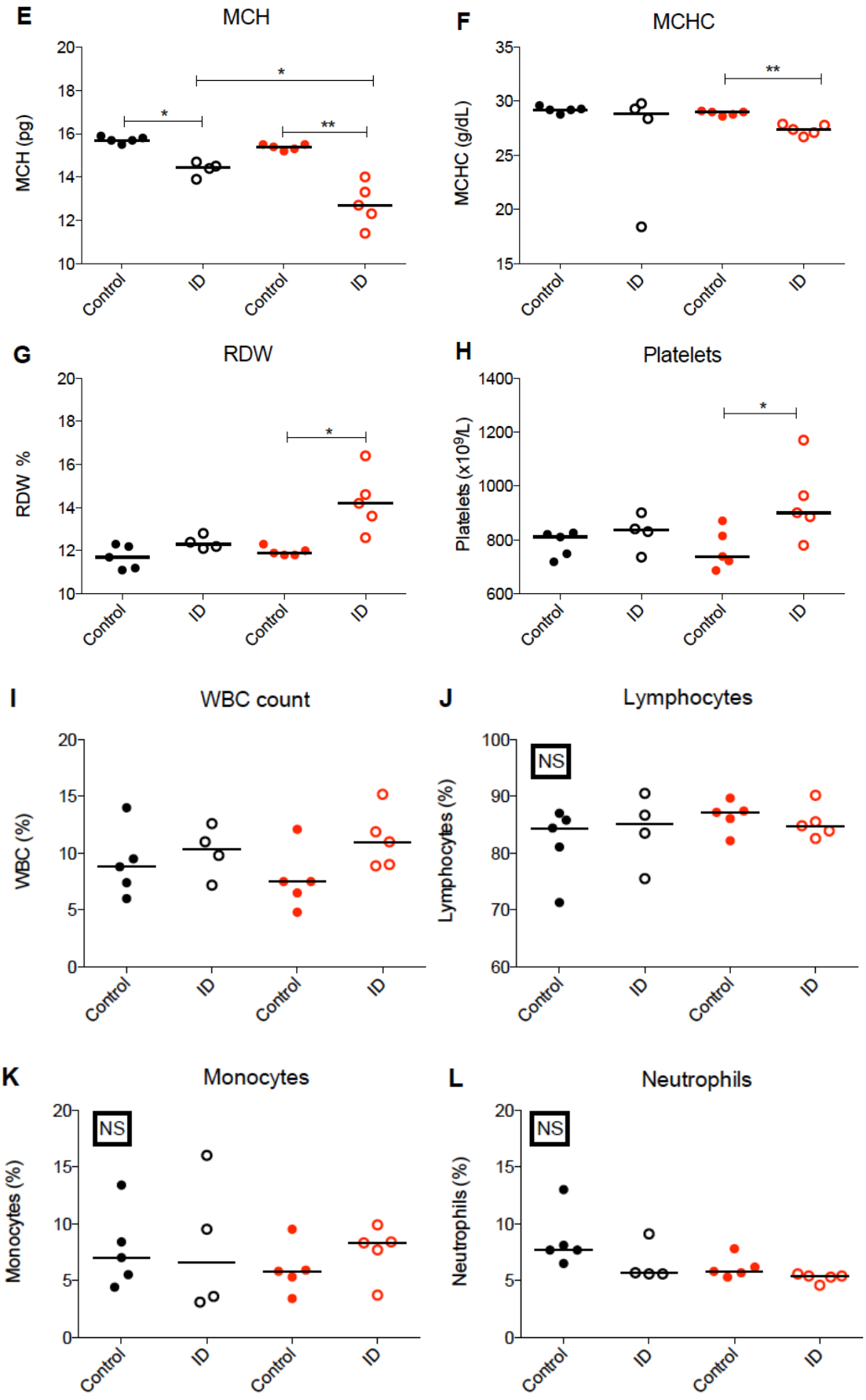
E
MCH
MCH (pg)
20
18
16
14
12
10
*
*
**
Control
ID
Control
ID
F
MCHC
MCHC (g/dL)
35
30
25
20
15
**
Control
ID
Control
ID
G
RDW
RDW %
20
18
16
14
12
10
*
Control
ID
Control
ID
H
Platelets
Platelets (x10⁹/L)
1400
1200
1000
800
600
*
Control
ID
Control
ID
I
WBC count
WBC (%)
20
15
10
5
0
Control
ID
Control
ID
J
Lymphocytes
Lymphocytes (%)
100
90
80
70
60
NS
Control
ID
Control
ID
K
Monocytes
Monocytes (%)
20
15
10
5
0
NS
Control
ID
Control
ID
L
Neutrophils
Neutrophils (%)
20
15
10
5
0
NS
Control
ID
Control
ID

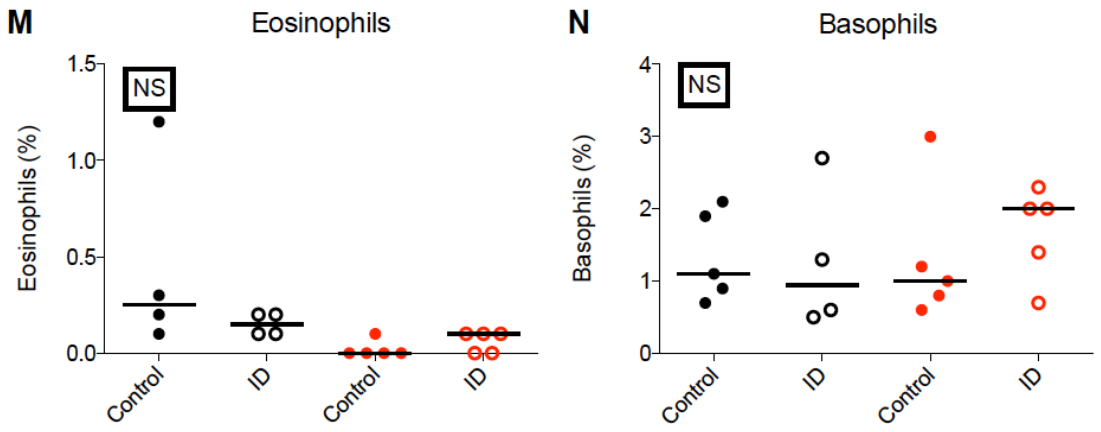


**Figure 5.4.3 The effect of dietary iron restriction in BCG infection on haematological parameters**. C57BL/6 mice were fed either an iron-deficient (4ppm) or control (200ppm) diet for 2 weeks prior to *i.n.* infection with BCG, and were maintained on these diets until termination of the experiment 4 weeks later. Mice were bled by cardiac puncture and haematological parameters were measured on a Pentra AbX machine. Mann-Whitney tests were performed to compare groups with Bonferroni post tests for multiple comparisons where required. N=5 mice per group. *, **, *** and **** represent $p<0.05$, $p<0.01$, $p<0.001$ and $p<0.0001$, respectively. Black circles represent uninfected animals, red represents infected animals

### *5.4.4 Gene expression analyses*

In the uninfected controls, *Hamp1* expression was significantly down-regulated in mice fed the iron-deficient diet, consistent with them being iron-deficient (Figure 5.4.4A). No differences were observed between uninfected controls and BCG infected mice. Ferroportin is regulated post-transcriptionally by the IRE/IRP network, which regulates cellular iron homeostasis, as well as post-translationally by hepcidin, and transcriptionally by haem [78, 126]. Feeding mice an iron-deficient diet resulted in a significant down-regulation of hepatic *Fpn1* in both the uninfected and infected animals ($p=0.0316$ for both) (Figure 5.4.4B), similar to findings earlier in this chapter. BCG infection did not affect *Fpn1* expression.

Since iron regulates hepcidin expression via BMP/SMAD signalling [78], I quantified the expression of *Bmp6* and the BMP/SMAD-dependent gene *Id1*, and found both of these genes were down-regulated in the mice fed the iron-deficient diet (Figure 5.4.4C+D), compared with controls. *Id1* and *Bmp6* were also down-regulated in the infected mice, with no differences observed between infected mice and uninfected controls, and this was significant (p=0.0316). Consistent with these findings, both *Id1* and *Bmp6* correlated positively with *Hamp1* expression in both the uninfected and infected animals Figure 5.4.4E-H), indicating that regulation of *Hamp1* by alteration of dietary iron availability is via BMP/SMAD signalling.

*Nramp1* mRNA expression was higher in infected mice, compared to uninfected controls (Figure 5.4.4I). This finding is consistent with data from Chapter 3, highlighting the possibility that mycobacterial infection increases expression of *Nramp1* as a mechanism of withholding iron from the pathogen. I also quantified the expression of *Tfrc*, the gene encoding transferrin receptor 1 protein, which transports iron bound transferrin and therefore iron into cells, thereby regulating cellular iron homeostasis [123]. There is some evidence that *Tfrc* is transcriptionally regulated by iron [229, 230]. Accordingly, I found that *Tfrc* mRNA was increased in the mice fed the iron-deficient diet compared with those on the control diet, and in the infected mice, this was significant (p=0.0316; Figure 5.4.4J), suggesting homeostatic mechanisms to increase iron uptake have been induced, indicative of iron deficiency. No differences were observed between BCG infected mice and uninfected controls.

The expression of the iron storage protein ferritin light chain (encoded by *Ftl*) was reduced in the BCG-infected mice fed the iron-deficient diet, as I expected in iron-restricted conditions, since IRE/IRP network represses the expression of ferritins under iron depletion in order to release stored iron, although this was not significant (Figure 5.4.4K) [231]. However, an opposing trend can be seen for ferritin heavy chain (encoded by *Fth*) (Figure 5.4.4L), although again, this was not significant. The expression of *Ifng* and *Tnfa* (genes encoding IFN-γ and TNF-α) were not affected by dietary iron restriction (Figure 5.4.4 M+N).

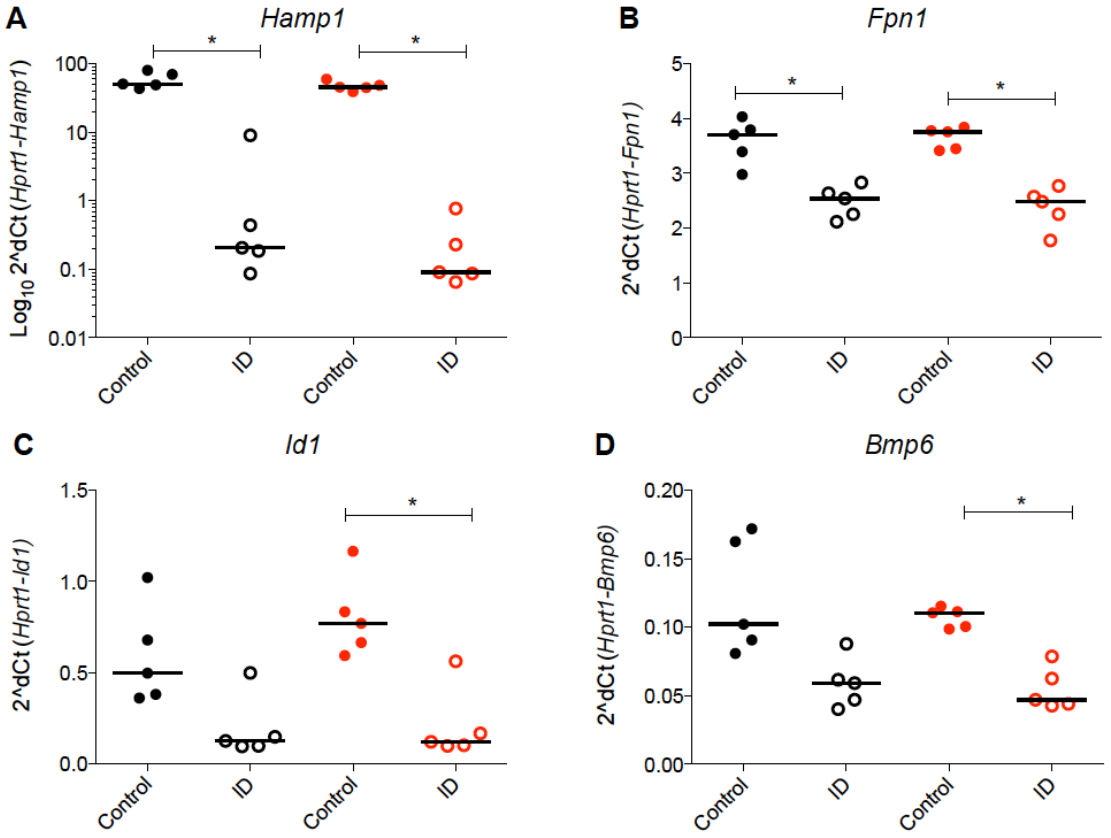

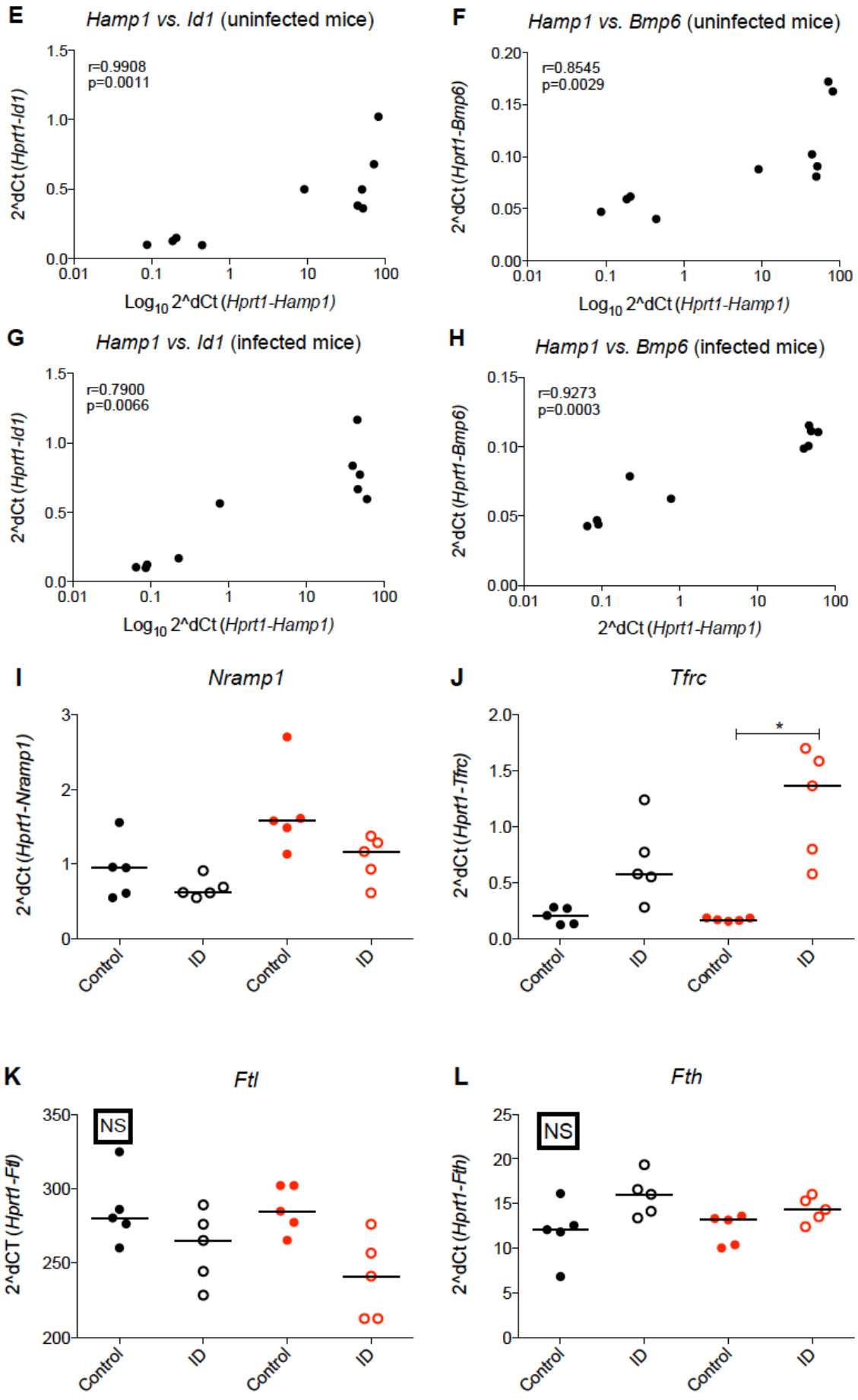
E
Hamp1 vs. Id1 (uninfected mice)
r=0.9908
p=0.0011
2^dCt (Hprt1-Id1)
Log10 2^dCt (Hprt1-Hamp1)
F
Hamp1 vs. Bmp6 (uninfected mice)
r=0.8545
p=0.0029
2^dCt (Hprt1-Bmp6)
Log10 2^dCt (Hprt1-Hamp1)
G
Hamp1 vs. Id1 (infected mice)
r=0.7900
p=0.0066
2^dCt (Hprt1-Id1)
Log10 2^dCt (Hprt1-Hamp1)
H
Hamp1 vs. Bmp6 (infected mice)
r=0.9273
p=0.0003
2^dCt (Hprt1-Bmp6)
2^dCt (Hprt1-Hamp1)
I
Nramp1
2^dCt (Hprt1-Nramp1)
Control
ID
Control
ID
J
Tfrc
2^dCt (Hprt1-Tfrc)
*
Control
ID
Control
ID
K
Ftl
NS
2^dCT (Hprt1-Ftl)
Control
ID
Control
ID
L
Fth
NS
2^dCt (Hprt1-Fth)
Control
ID
Control
ID

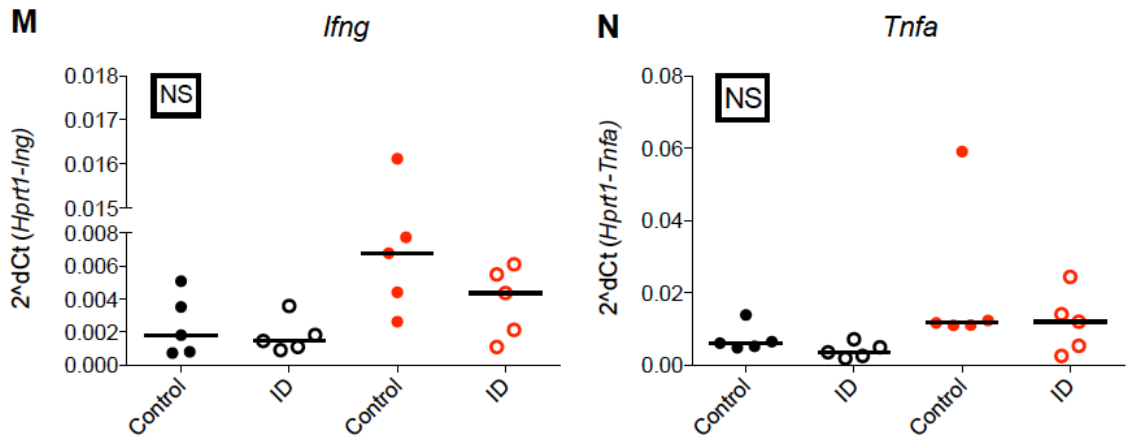


**Figure 5.4.4 Expression of genes involved in regulation of iron homeostasis, post BCG i.n. infection.** Expression of mRNA in livers taken from iron-deficient or control mice infected intranasally with $5x10^6$ CFU of BCG Pasteur. Uninfected animals are represented by black circles, infected animals by red circles. Open circles represent iron-deficient diet and closed circles represent control diet. N=5 per group. Mann-Whitney tests were done with Bonferroni corrections for multiple comparisons where *, **, *** and **** represent p=<0.05, p=<0.01, p=<0.001 and p=<0.0001, respectively.

## 5.5 The effect of dietary iron restriction on *M.tb* infection – pilot experiment

### *5.5.1 Experimental outline*

It was unknown for how long mice could remain healthy on an iron-deficient diet and also whether mice fed an iron-deficient diet could survive the usual 4 weeks post-*M.tb* infection. Therefore, a pilot experiment was planned as shown in Figure 5.5.1. Eight week old C57BL/6 mice fed either an iron-deficient or control diet for 2 weeks were infected with ~100 CFU of *M.tb* Erdman by aerosol. At the point of infection, mice on the iron-deficient diet were switched to a 'maintenance' diet containing 18ppm of ferric iron, which still contains much less iron than the usual mouse diet. A group on the standard diet given in

our animal facility was also included to compare to our custom made control diet for the iron-deficient diet.

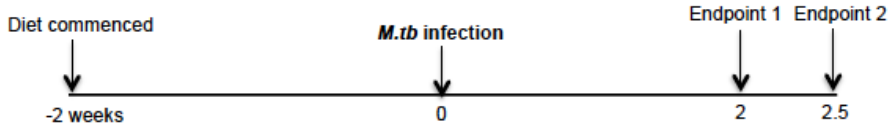


**Figure 5.5.1 Pilot iron diet experimental design.** C57BL/6 mice were split into groups of 8 and fed an iron-deficient (4ppm ferric citrate), control (200ppm) or standard (200ppm) diet *ad libitum* for 2 weeks prior to infection with ~100 CFU of *M.tb* Erdman via aerosol. At the time of infection, mice on the 4ppm diet were switched to a diet containing 18ppm iron. All other diets remained unchanged until the end of the experiment. Lungs and spleen were removed for quantification of bacterial burden via CFU and liver was snap frozen or stored in RNALater for processing for qRT-PCR

Due to unforeseen circumstances, some animals in the iron deficient diet group became sick and had to be taken down at 2 weeks post-infection, and although the remaining animals were healthy, the experiment had to be cut short. Therefore, for all data shown for this experiment, animals were taken down at 2.5 weeks post-infection. Data from sick animals are not shown and 8 healthy animals remained per group.

### *5.5.2 Mice fed an iron-restricted diet control M.tb as well as mice fed a control diet*

Dietary iron content did not affect susceptibility to *M.tb* infection (Figure 5.5.2). No differences in susceptibility were observed between the standard animal facility diet and our control diet either. Consistent with these findings, weight was also unaffected by dietary iron restriction (p=0.2484; Figure 5.5.2C).

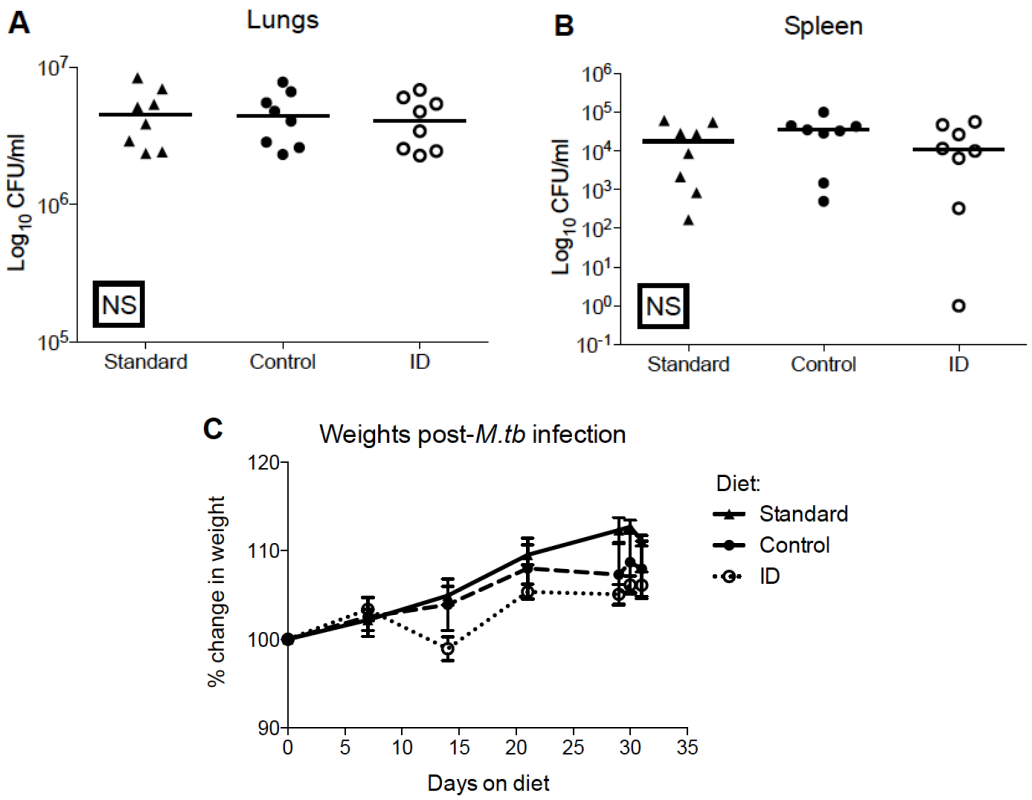


**Figure 5.5.2. Effect of restricting dietary iron availability on susceptibility to *M.tb* – pilot experiment.** C57BL/6 mice were split into groups of 8 and fed an iron restricted (4ppm) or control (200ppm) or standard animal facility diet for 2 weeks prior to infection with ~100 CFU of aerosolised *M.tb* Erdman. Animals on the 4ppm diet were switched to an 18ppm diet on the day of challenge and all mice remained on respective diets until they were culled 2.5 weeks later. Lungs (A) and spleen (B) were homogenised for quantification of bacterial burden (CFU) Mann-Whitney tests were performed to compare groups. n=8 per group. Percentage change in weight is illustrated in C, and analysed by 2-way repeated measures ANOVA.

### *5.5.3 The effect of dietary iron restriction on post-M.tb infection gene expression analyses*

I have already shown that liver *Hamp1* message is reduced after 2 weeks on the iron-deficient (4ppm) diet. Since mice require ~35ppm of iron [224], it was hypothesised that the mice switched from the 4ppm to the 18ppm 'maintenance' diet should maintain a degree of iron deficiency. However, no differences in *Hamp1* expression were observed between mice fed the iron-deficient diet and

controls, suggesting that these mice were no longer iron deficient. Interestingly, however, mice fed the standard facility diet had significantly higher *Hamp1* expression than those on the control and iron-deficient diet (p=0.0210 and p=0.0006, respectively, Figure 5.5.3A). The nutritional content of the standard facility diet differs from that of our iron-deficient and control diets. It is higher in fat, carbohydrates, and lower in protein than our custom diets, so it is probable that this could impact on iron homeostasis. These data highlight the importance of having controls with a matched diet.

*Fpn1* expression was significantly reduced in the mice fed the iron-deficient diet compared with controls, consistent with findings in the BCG infection study (p=0.0090, Figure 5.5.3B). To investigate whether regulation of *Hamp1* via iron is through the BMP/SMAD signalling pathway, I once again measured *Id1* and *Bmp6*. Similar to *Hamp1*, *Id1* was significantly reduced in the iron-deficient mice compared with the standard facility diet, but not when compared with our control diet (p=0.0141, Figure 5.5.3C). *Bmp6* expression was significantly reduced in the iron-deficient mice compared to both the control and the standard diet (p=0.0312, p=0.0057, respectively, Figure 5.5.3D). Moreover, *Id1* and *Bmp6* correlated positively with *Hamp1*, indicating that the BMP/SMAD signalling pathway may be regulating *Hamp1* expression in this context (Figure 5.5.3 G+H).

Consistent with findings in the BCG infection experiment, diet did not have an effect on hepatic expression of the genes encoding pro-inflammatory cytokines IL-6 and IFN-γ (Figure 5.5.3 E+F).

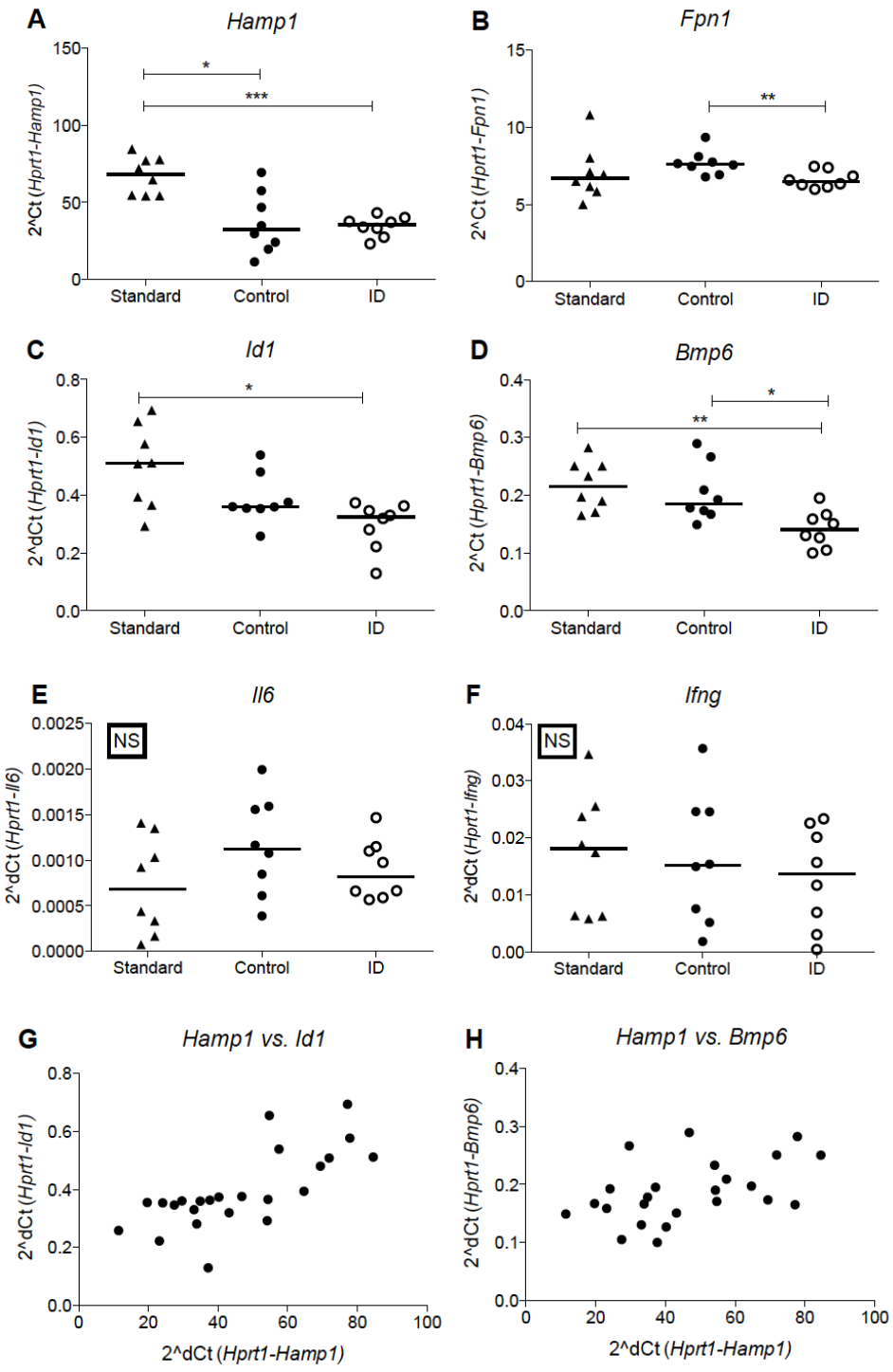


**Figure 5.5.3 Effect of restricting dietary iron availability on gene expression post-*M.tb* infection.** C57BL/6 mice were fed an iron restricted (4ppm ferric citrate, then switched to 18ppm on day of infection) or control (200ppm) diet, prior to infection with ~100 CFU of *M.*tb, as described in Figure 5.5.1. Hepatic gene expression analyses for *Hamp1* (A), *Fpn1* (B), *Id1* (C), *Bmp6* (D), *Il6* (E), and *Ifng* (F), were performed using qRT-PCR. Correlations were performed between *Hamp1* vs. *Id1* (G), and *Hamp1* vs. *Bmp6* (H). Statistical analysis was performed in Prism using Mann-Whitney tests adjusted for multiple comparisons with Bonferroni correction. Correlations were Pearson correlations after Kolmogorov-Smirnov tests for normality. *, **, *** and **** indicate p=<0.05, p=<0.01, p=<0.001 and p=<0.0001, respectively. N=8 animals per group

## 5.6 Does a diet containing 18ppm of ferric iron induce iron deficiency?

### *5.6.1 Experimental outline*

Based on data from the previous experiment, it is likely that mice switched to the 18ppm maintenance diet were no longer extremely iron-deficient.

To test this, I fed mice the 4ppm diet for 2 weeks to induce iron deficiency before switching them to the 18ppm diet. The aim was to see if there was sufficient iron in the 18ppm diet to reverse the deficiency seen with the 4ppm diet. Mice were taken down at D0 (for baseline), D3, D9 and D16 and liver was taken to quantify gene expression (Figure 5.6.1)

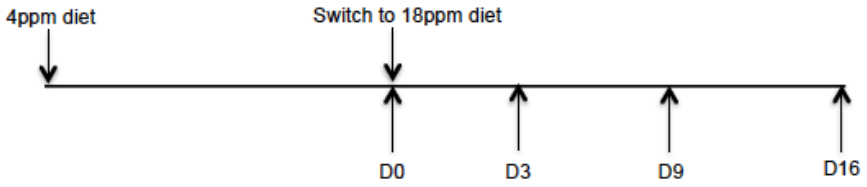


**Figure 5.6.1 Diet switching experimental outline.** C57BL/6 mice were fed an iron-deficient diet for 2 weeks, to induce iron deficiency. They were then changed to a diet containing 18ppm and culled at D0 (baseline), D3, D9 and D16. Liver was taken for qRT-PCR analyses. n=5 per group

### *5.6.2 Switching mice to a diet containing 18ppm may reverse iron deficiency induced by severe dietary iron restriction*

Expression of both *Hamp1* and *Id1* was significantly higher at D16 than at D0 (p=0.0106 and p=0.0145, respectively; Figure 5.6.2). This suggests that the iron deficiency induced by the 4ppm diet is being reversed, as *Hamp1* is starting to return to normal levels. Moreover, *Id1* and *Bmp6* correlated positively with

*Hamp1*, again in line with regulation of *Hamp1* expression being via BMP/SMAD signalling (r=0.6079, p=0.0045 and r=0.05628, p=0.0170, respectively) (Figure 5.6.2D+F).

Switching to the diet containing 18ppm did not affect *Bmp6* or *Fpn1* expression. However, *Tfrc* expression was reduced between D0 and D16 (p=0.0063, Figure 5.6.2G) and correlates inversely with *Hamp1* (r=-0.05470, p=0.0126, Figure 5.6.2F). *Tfrc* expression is increased post-transcriptionally in iron restricted conditions [220] and correlates inversely with intracellular iron concentrations so reduction of *Tfrc* after switching to the 18ppm diet suggests that these mice are no longer as iron-deficient. It would be useful to compare expression in mice fed the 18ppm to mice fed the control diet.

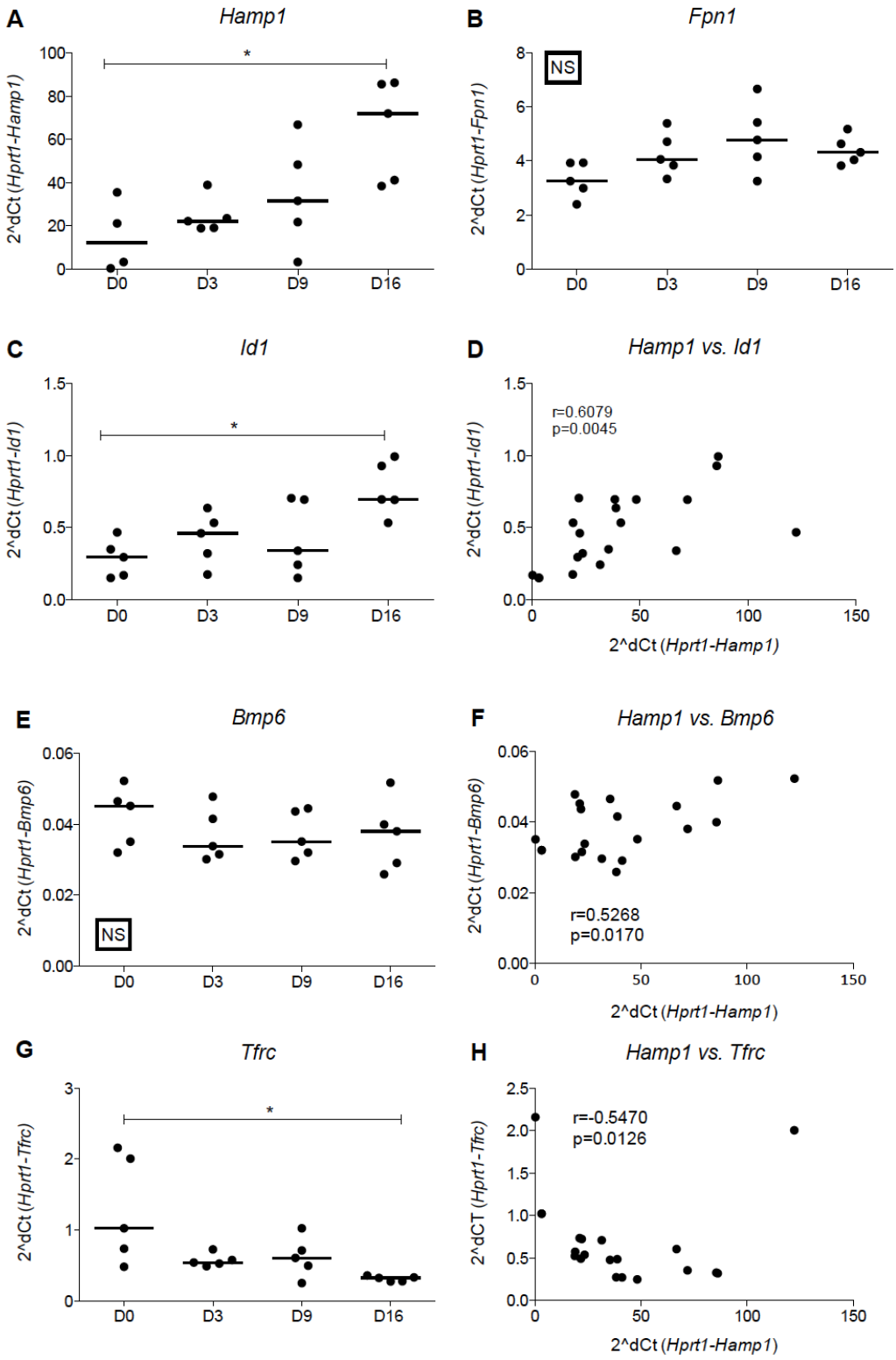


**Figure 5.6.2 The effect of switching from 4-18ppm diet on the expression of genes involved in iron metabolism.** C57BL/6 mice were fed an iron-deficient (4ppm) diet for 2 weeks prior to being switched to a diet containing 18ppm of iron. Mice were taken down at D0, D3, D9 and D16 and livers were removed for RNA extraction. qRT-PCRs were performed to quantify expression of *Hamp1* (A), *Fpn1* (B), *Id1* (C), *Bmp6* (E) and *Tfrc* (G). Correlations of *Hamp1* with *Id1*, *Bmp6* and *Tfrc* are shown in D, F and H, respectively. A Kruskal-Wallis test was performed for all timepoints, with Dunn's post tests for multiple comparisons. n = 5 per group.

## 5.7 The effect of dietary iron restriction on *M.tb* infection: experiment 1

### *5.7.1 Experimental outline*

Having established that mice are able to survive long-term on the 4ppm diet and are able to survive BCG infection on this diet, the effect of iron deficiency on *M.tb* infection was investigated again at both 4 and 8 weeks post-infection with a lower dose of *M.tb,* since mice previously became sick with a higher dose (although it is unknown whether this was related to diet or *M.tb* infection).

Eight week old female C57BL/6 mice were placed on the iron-deficient (4ppm) or control (200ppm) diet for 2 weeks prior to infection with ~50-100 CFU of aerosolised *M.tb* Erdman (Figure 5.7.1). They were maintained on their respective diets until takedown, which took place at 4 and 8 weeks post-infection. Lungs and spleen were taken for quantification of bacterial burden (CFU) and liver for gene expression analyses by qRT-PCR. All mice were 8 weeks old at the start of the experiment, and uninfected controls were included for both endpoints.

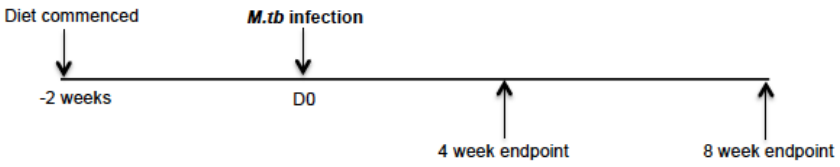


**Figure 5.7.1 Infection of iron-deficient mice with *M.tb* – experimental outline.** 8 week old female C57BL/6 mice were maintained on an iron-deficient (4ppm) or control (200ppm) diet for 2 weeks prior to infection with 50-100 CFU of aerosolised *M.tb* Erdman. Mice were taken down at 4 weeks and 8 weeks post-infection. Lungs and spleen were taken for quantification of bacterial burden (CFU) and liver for gene expression analyses. Uninfected controls were included for each timepoint. n = 6 for uninfected groups and n = 8 for infected groups

### *5.7.2 Dietary iron restriction reduces M.tb growth*

Growth of *M.tb* was significantly affected by dietary iron restriction, with reduced CFU observed in lungs (A) and spleens (B) of the mice on the iron-deficient diet compared with controls, at the 4 week time point. This reduction was significant at the 4-week time point (Figure 5.7.2). Growth was also reduced in control animals between 4 and 8 weeks, as expected since bacterial burden tends to plateau around 4 weeks post-infection (p=0.0019 for lungs and p=0.0104 for spleen).

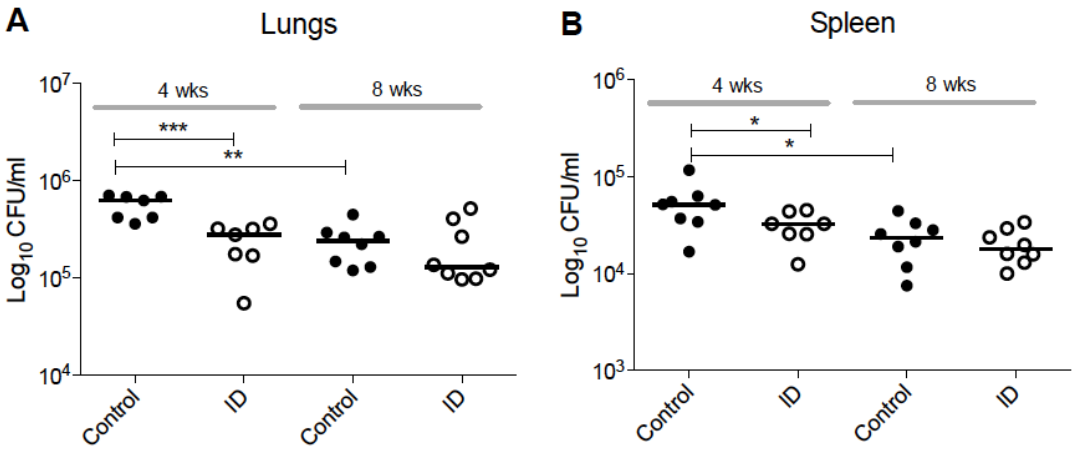


**Figure 5.7.2 Infection of iron-deficient mice with aerosolised *M.tb*.** Female C57BL/6 mice were maintained on an iron-deficient (4ppm) or control (200ppm) diet for 2 weeks prior to infection with *M.tb*. Mice were taken down at 4 and 8 weeks post-infection. Lungs and spleen were taken for quantification of bacterial burden by CFU. Full circles represent animals fed the control diet and open circles represent those on the iron-deficient diet. Significance was calculated using the Mann-Whitney tests where *, **, *** and **** signify p values of <0.05, <0.01, <0.001 and <0.0001, respectively. n = 8 per group

### *5.7.3 Gene expression analyses*

Consistent with data from earlier experiments in this chapter, *Hamp1* gene expression was significantly reduced in all groups in the iron-deficient mice, compared with controls (Figure 5.7.3A). At the 4 week timepoint, *Hamp1*

expression in the mice on both the control and iron-deficient mice dropped further after challenge (p=0.0056 and p=0.0056, respectively). This down-regulation of hepcidin is consistent with findings at 4 weeks post-infection presented in Chapter 3. The same was also seen at 8 weeks, where *Hamp1* expression was further suppressed in the infected mice compared to iron-deficient uninfected mice (p=0.0376), but the same was not seen in the control mice. Moreover, *Hamp1* did not correlate with lung CFU (Figure 5.7.3G). These data indicate that the iron-deficient diet reduces *Hamp1* expression and that *Hamp1* is down-regulated 4 weeks post-infection even in control mice, as a result of infection.

In terms of *Fpn1* expression, as before, *Fpn1* was reduced in all animals fed the iron-deficient diet (Figure 5.7.3B). No differences were observed between infected animals and uninfected controls at 4 weeks, but at 8 weeks, *Fpn1* was further reduced in the iron-deficient mice, compared to their uninfected controls (p=0.0216).

I again looked at the expression of *Id1* to determine whether BMP/SMAD correlated with the *Hamp1* suppression seen in the iron-deficient mice. As expected, *Id1* expression was significantly lower in all animals maintained on the iron-deficient diet, compared to their respective controls (Figure 5.7.3C). Furthermore, *Id1* correlated positively with *Hamp1* in the infected animals, suggesting that BMP/SMAD signalling might regulate *Hamp1* in response to reduced iron availability (r=0.9465, p=<0.0001, Figure 5.7.3F). However, when groups were split into mice fed the control diet and those fed the iron-deficient diet, *Hamp1* and *Id1* only correlated in animals fed the iron-deficient

diet, suggesting that BMP/SMAD signalling might regulate the down-regulation of *Hamp1* induced by dietary iron deficiency. However, as no significant changes were seen in *Hamp1* expression in the control mice between infected mice and uninfected controls, it is difficult to determine what might be regulating hepcidin, but we cannot rule out that the BMP/SMAD pathway may play a role.

To gain further insights into what might be regulating hepcidin, and to investigate whether the inflammatory pathway could be influencing regulation of *Hamp1* in this context, I also looked at the expression of *Saa1*, the gene encoding serum amyloid A1 protein. Serum amyloid A1 protein is highly expressed in response to inflammation [232]. *Saa1* was not significantly different between mice fed an iron-deficient or control diet at any timepoint (Figure 5.7.3D). Although not significant, *Saa1* expression was slightly lower in the mice on the iron-deficient diet. Unsurprisingly, *Saa1* expression increased post-challenge, as it is triggered by pro-inflammatory cytokines IL-6 and TNF-α, which are induced by *M.tb* infection [233, 234]. Interestingly, I found that *Saa1* correlated weakly with *Hamp1* expression (r=0.4714, p=0.0065, Figure 5.7.3H). However, the data looked to be clustering into 2 groups which I thought might be causing a false correlation, so when looking separately at each diet, I found that *Saa1* only correlated with *Hamp1* in the iron-deficient mice (r=0.7441, p=0.0014, Figure 5.7.3J) and not control animals (Figure 5.7.3I). Therefore, it is likely that the positive correlation seen between *Hamp1* and *Saa1* was due to iron deficiency, and is not related to infection, or that perhaps the iron deficient animals are more inflamed than controls.

Expression of *Tfrc* mRNA is normally higher in iron restricted conditions as the IRE/IRP regulatory pathway post-transcriptionally increases it in order to increase cellular iron uptake [231]. Although not always significant, increases can be seen in mice fed the iron-deficient diet, respective to their controls, in both uninfected and infected animals (Figure 5.7.3E). Interestingly, *Tfrc* mRNA expression was higher in the infected animals, indicating induction of *Tfrc* expression by *M.tb* infection, contrary to findings in previous studies that intracellular infection reduces *Tfrc* expression, probably in order to inhibit intracellular iron availability to inhibit bacterial growth [80] [235].

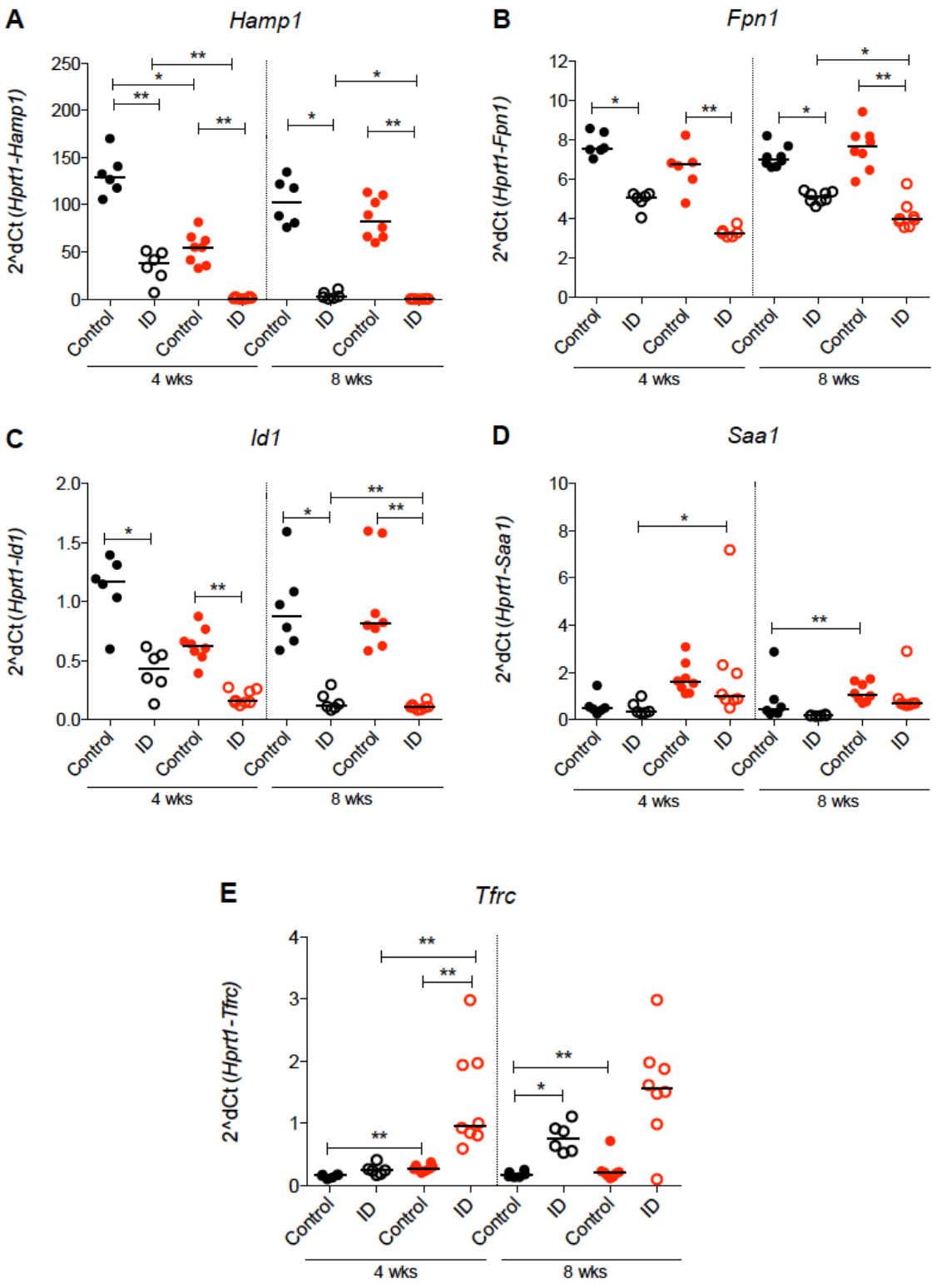
A
Hamp1
2^dCt (Hprt1-Hamp1)
250
200
150
100
50
0
Control
ID
Control
ID
Control
ID
Control
ID
4 wks
8 wks
B
Fpn1
2^dCt (Hprt1-Fpn1)
12
10
8
6
4
2
0
C
Id1
2^dCt (Hprt1-Id1)
2.0
1.5
1.0
0.5
0.0
D
Saa1
2^dCt (Hprt1-Saa1)
10
8
6
4
2
0
E
Tfrc
2^dCt (Hprt1-Tfrc)
4
3
2
1
0

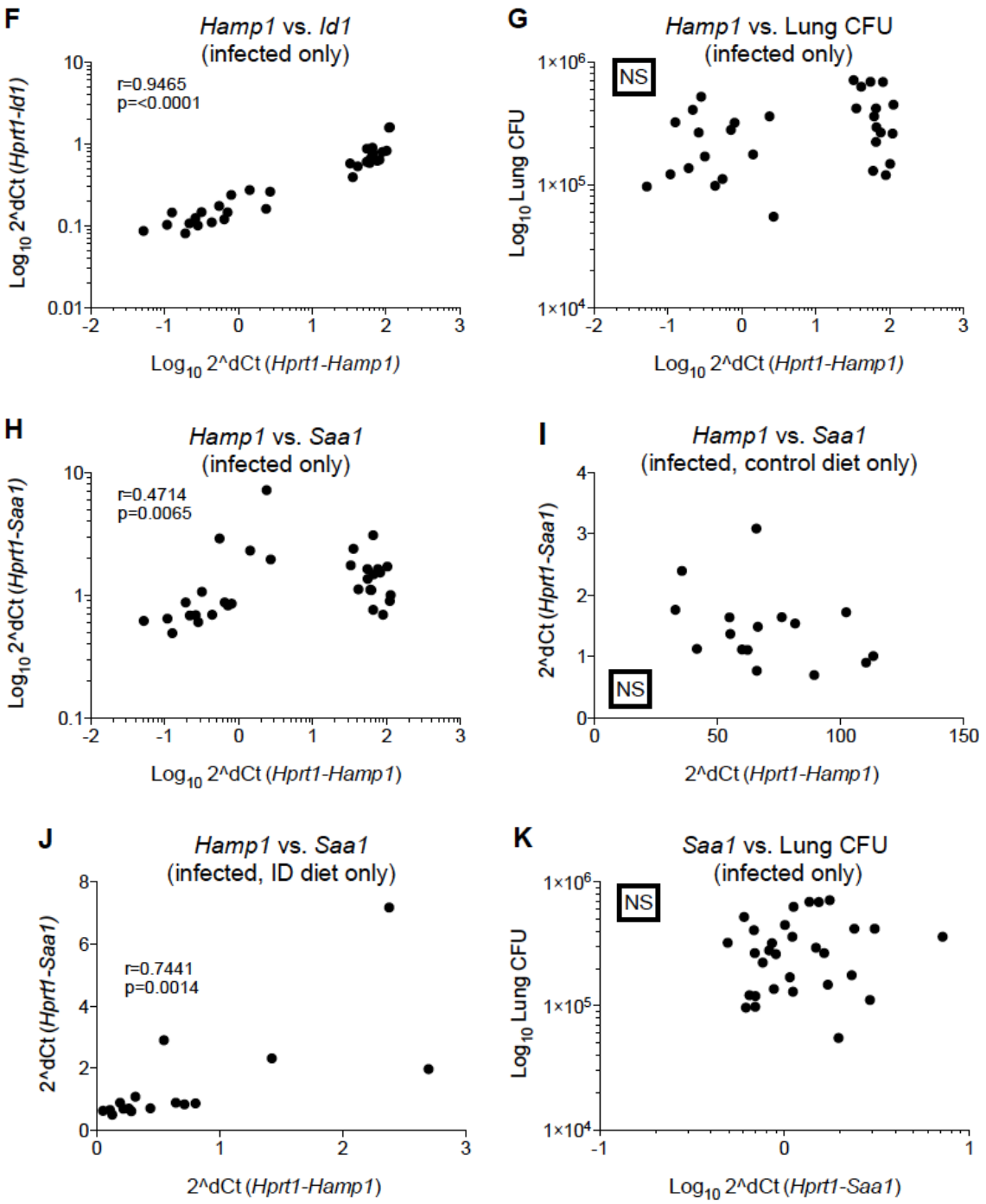


**Figure 5.7.3 The effect of restricting dietary iron availability in *M.tb* infection on the expression of genes involved in iron homeostasis.** Female C57BL/6 mice were fed either an iron-restricted (4ppm ferric iron) or control (200ppm) diet for 2 weeks prior to infection with 50-100CFU of aerosolised *M.tb*. Mice were maintained on their respective diets until takedown at 4 or 8 weeks post-infection. Lungs and spleen were removed to quantify bacterial burden (CFU) and liver for qRT-PCR. Uninfected controls were included for each takedown and are represented by black circles. Red circles indicate infected animals. Mann-Whitney tests with Bonferroni corrections for multiple comparisons were perfumed to compare groups where *, **, **, and *** indicate $p<0.05$, $p<0.01$, $p<0.001$ and $p<0.0001$, respectively. n=6 per group for uninfected controls and n=8 for infected groups.

### *5.7.4 Gene expression analyses: genes involved in immune response*

As expected, the hepatic expression of genes encoding pro-inflammatory cytokines TNF-α, IL-6 and IFN-γ (*Tnfa*, *Il6* and *Ifng*) was significantly increased post-infection, in both diets (Figure 5.7.4A, B and C, respectively), confirming that *M.tb* infection induces hepatic expression of genes encoding pro-inflammatory cytokines. This was consistent with findings in earlier chapters. No differences were observed between the iron-deficient and control diets, in uninfected or infected mice, at either timepoint, showing that severe dietary iron restriction does not affect the expression of the main pro-inflammatory cytokines induced in the innate immune responses against *M.tb,* although this should be confirmed by other immune analyses.

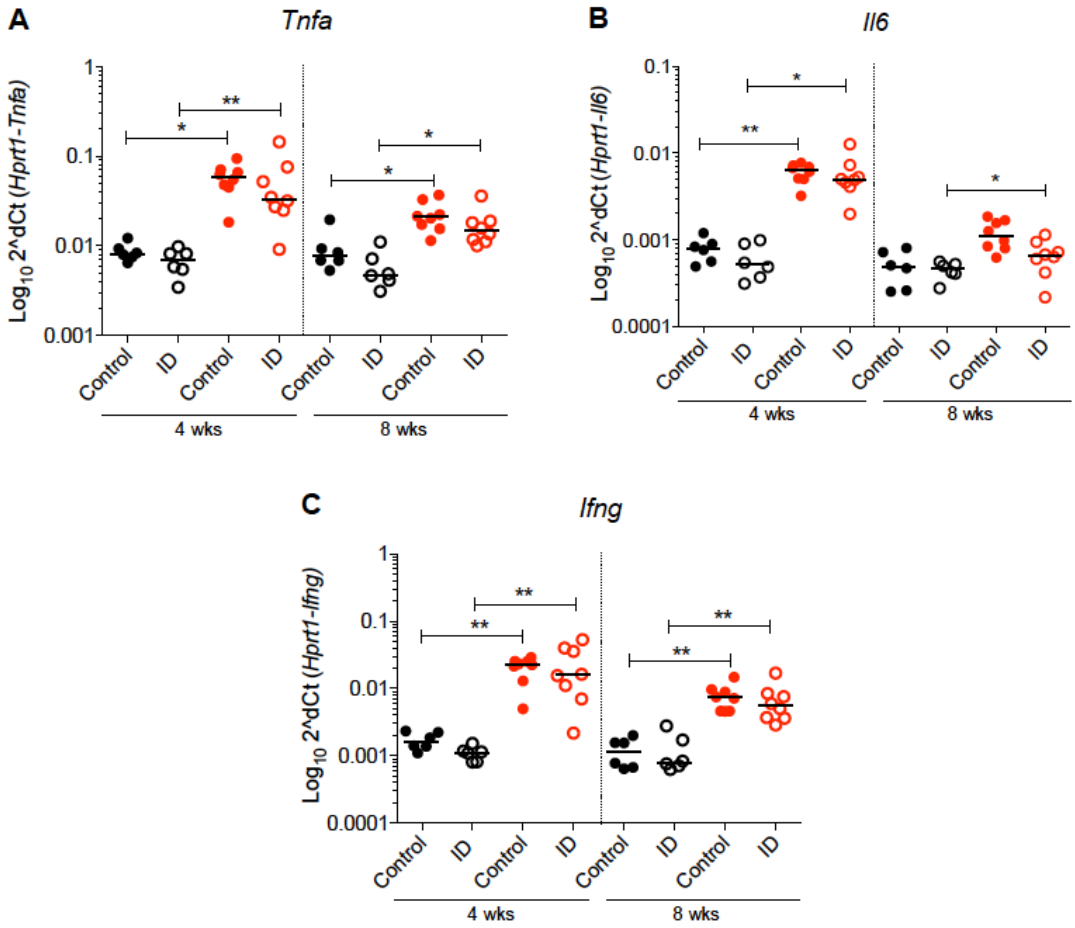


**Figure 5.7.4 Effect of restricting dietary iron availability in *M.tb* infection on the expression of genes encoding pro-inflammatory cytokines.** Female C57BL/6 mice were fed an iron restricted (4ppm ferric iron) or control (200ppm) diet for 2 weeks prior to infection with 50-100 CFU of aerosolised *M.tb*. Mice remained on the respective diets until take down at 4 weeks and 8 weeks post-infection. Liver was taken for qRT-PCR. Uninfected controls were included at both timepoints and are represented by black circles. Red circles represent infected animals. Gene expression is shown for *Tnfa* (A), *Il6* (B) and *Ifng* (C). A Kruskal Wallis test was performed on all groups, followed by Mann-Whitney with Bonferroni corrections for multiple comparisons to compare groups where *, **, **, and *** indicate $p<0.05$, $p<0.01$, $p<0.001$ and $p<0.0001$, respectively. n = 6 for uninfected controls and n = 8 for infected groups.

## 5.8 The effect of dietary iron restriction on *M.tb* infection: repeat

### *5.8.1 Experimental outline*

In the previous experiment, reduced bacterial burden was observed in the lungs and spleens of mice fed an iron-deficient diet for six weeks (two weeks before infection and four weeks after), compared with those fed a control diet, suggesting that restricting dietary iron availability affects the growth of *M.tb in vivo.* In order to determine the reproducibility of this data, I repeated this experiment with larger groups.

Eight week old female C57BL/6 mice were placed on an iron restricted (4ppm ferric iron) or control (200ppm ferric iron) diet for 2 weeks prior to infection with ~50-100 CFU of aerosolised *M.tb* Erdman (Figure 5.8.1). Mice were maintained on their respective diets until takedown, which took place at 4 and 8 weeks post-infection. Lungs and spleen were taken for quantification of bacterial burden (CFU) and liver for gene expression analyses by qRT-PCR. All mice were 8 weeks old at the start of the experiment, and uninfected controls were included for both endpoints.

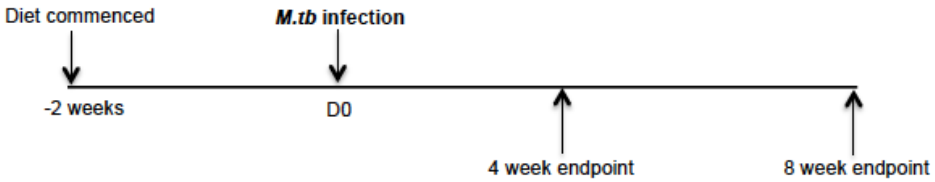


**Figure 5.8.1 Infection of iron-deficient mice with *M.tb* – experimental outline.** 8 week old female C57BL/6 mice were maintained on an iron-deficient (4ppm) or control (200ppm) diet for 2 weeks prior to infection with 50-100 CFU of aerosolised *M.tb* Erdman. Mice were taken down at 4 weeks and 8 weeks post-infection. Lungs and spleen were taken for quantification of bacterial burden (CFU) and liver for gene expression analyses. Uninfected controls were included for each timepoint. n = 6 for uninfected groups and n = 10 for infected groups

### *5.8.2 Dietary iron restriction did not affect the growth of M.tb in vivo*

In contrast with data from the previous experiment (Figure 5.7.2), no differences were observed between bacterial burdens of mice fed the iron-deficient diet and those fed the control diet, suggesting that severe dietary iron restriction does not effect susceptibility to *M.tb* infection (Figure 5.8.2). CFU counts in both lungs and spleen were reduced at the 8 week timepoint as *M.tb* growth plateaus around 4 weeks post-infection ($p=<0.0001$ for lungs, for spleen $p=0.0023$ between timepoints for mice on the iron-deficient diet, $p=0.0009$ between timepoints for mice on the control diet) (Figure 5.8.2).

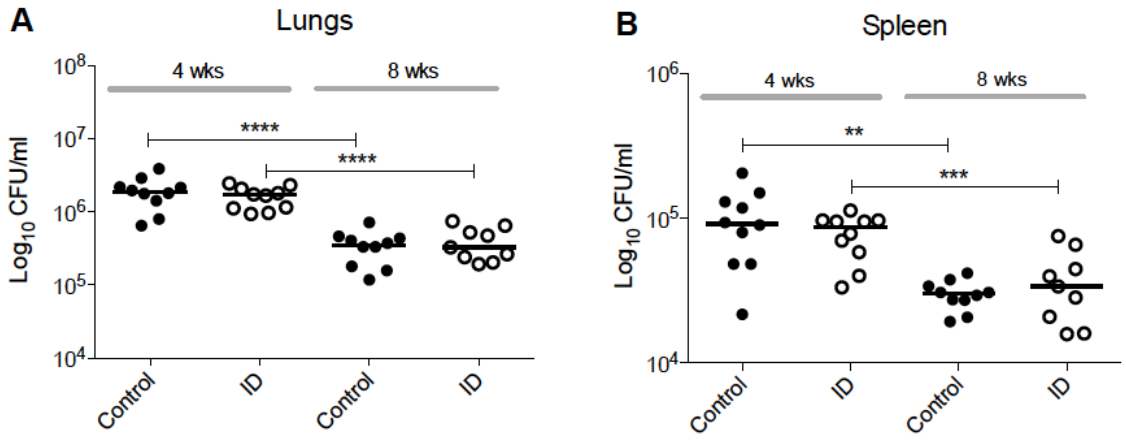


**Figure 5.8.2 Infection of iron-deficient mice with aerosolised *M.tb* - repeat.** Female C57BL/6 mice were maintained on an iron-deficient (4ppm) or control (200ppm) diet for 2 weeks prior to infection with *M.tb*. Mice were taken down at 4 and 8 weeks post-infection. Lungs and spleen were taken for quantification of bacterial burden by CFU. Full circles represent control diet and open circles represent iron-deficient diet. Significance was calculated using unpaired t-tests after testing for normality *, **, *** and **** signify p values of $<0.05$, $<0.01$, $<0.001$ and $<0.0001$, respectively. n = 10 per group

### *5.8.3 Post-M.tb infection gene expression analyses*

In the previous experiment, changes in the expression of genes involved in iron homeostasis were observed between iron-deficient and control mice. Consistent with these findings, in this experiment, *Hamp1* was significantly reduced in the iron-deficient mice, confirming that *Hamp1* expression is reduced by dietary iron restriction (Figure 5.8.3A). In addition, *M.tb* infected iron-deficient mice had reduced *Hamp1* compared to their uninfected controls ($p=0.004$ at 4 weeks, and $p=0.0128$ at 8 weeks). This suggests that particularly in the iron-deficient mice, *Hamp1* is further suppressed post-challenge.

Consistent with findings from the previous experiment, iron-deficient mice had significantly reduced *Id1* expression than their controls at the 8 week timepoint (p=0.0176 for uninfected controls, p=0.0008 for infected animals (Figure 5.8.3C) and although not significant at 4 weeks, a similar trend was observed. Moreover, a strong positive correlation was again observed between *Hamp1* and *Id1* (r=0.7992, p=<0.0001; Figure 5.8.3G). However, when splitting groups into uninfected and infected groups, and by diet, correlations were only observed for iron-deficient animals, and were not affected by infection, consistent with BMP/SMAD signalling influencing the observed suppression of hepcidin in response to dietary iron restriction. Furthermore, the expression of *Bmp6* was reduced in all groups in the iron-deficient mice, but was unaffected by infection (Figure 5.8.3D), following a similar trend to *Hamp1*. *Bmp6* also correlated positively with *Hamp1* (r=0.8685, p=<0.0001; Figure 5.8.3K). Therefore, it is likely that BMP/SMAD signalling is regulating the suppression of *Hamp1* in response to iron deficiency in the mice fed the iron deficient diet.

I also quantified expression of the gene *Saa1* and found no differences in expression between iron-deficient and control mice (Figure 5.8.3E). However, *Saa1* expression was significantly increased 4 weeks post-infection in both iron-deficient mice and controls (p=0.004 and p=0.0016, respectively). At 8 weeks, it was also increased in mice fed the control diet in comparison to uninfected controls (p=0.0016). These findings are consistent with the induction of inflammation post-*M.tb* infection, but do not highlight a role for the inflammatory pathway in regulation of hepcidin in iron deficiency. Moreover, I found *Saa1* correlated positively with lung CFU, confirming that this

inflammatory marker increases with increased bacterial burden (r=0.6853, p=<0.0001, Figure 5.8.3J). No correlations were observed between *Hamp1* and *Saa1* (Figure 5.8.3I) or *Ifng (*Figure 5.8.3H), however. These data highlight that despite there being evidence of chronic inflammation post-infection, in the context of *M.tb* infection, it is unlikely that hepcidin is being influenced by inflammatory pathways.

The gene encoding transferrin receptor 1, *Tfrc*, was significantly increased in iron-deficient mice by 4 weeks post-infection, consistent with data from the previous experiment (Figure 5.8.3F).

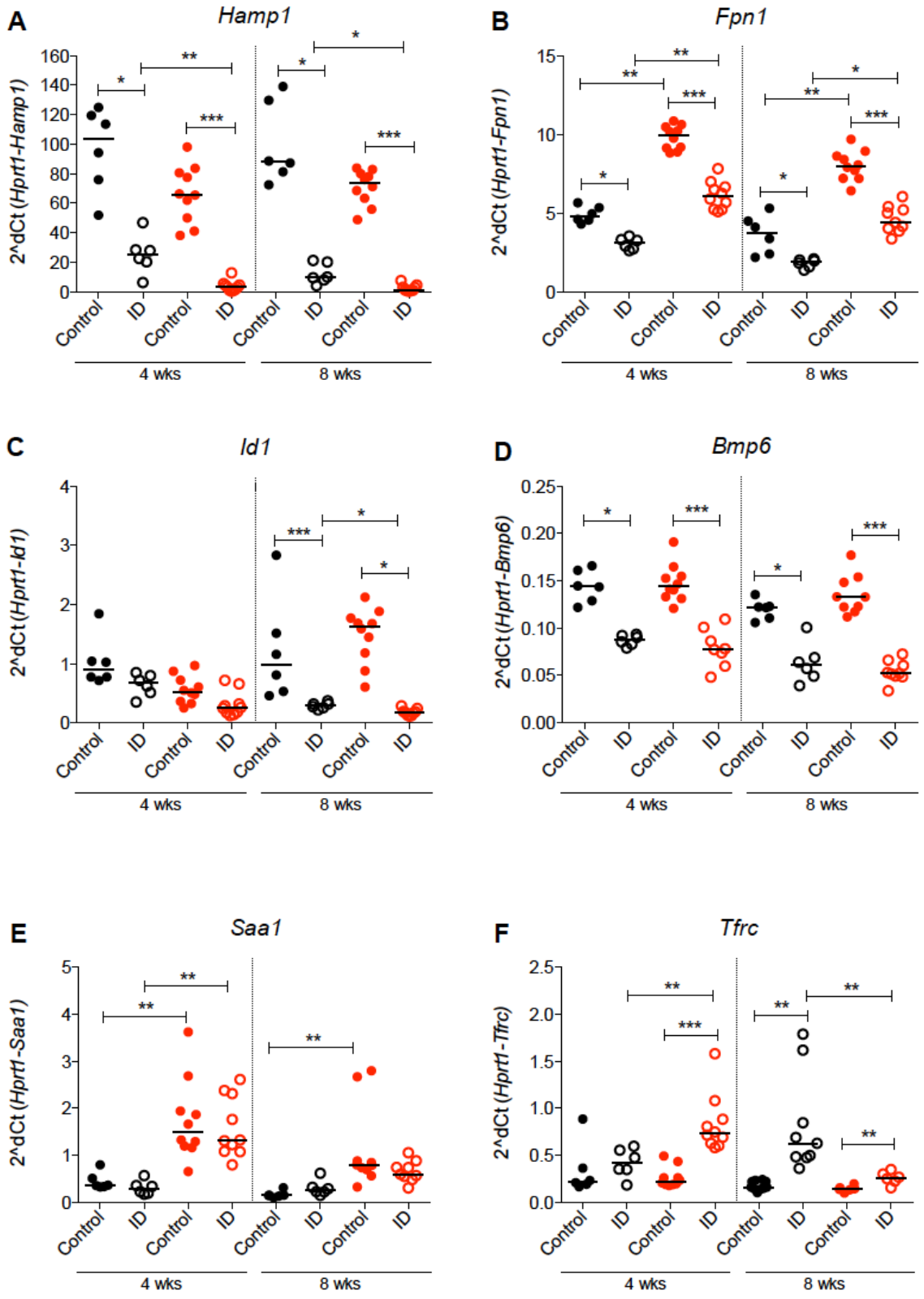
A
Hamp1
2^dCt (Hprt1-Hamp1)
B
Fpn1
2^dCt (Hprt1-Fpn1)
C
Id1
2^dCt (Hprt1-Id1)
D
Bmp6
2^dCt (Hprt1-Bmp6)
E
Saa1
2^dCt (Hprt1-Saa1)
F
Tfrc
2^dCt (Hprt1-Tfrc)
Control
ID
4 wks
8 wks

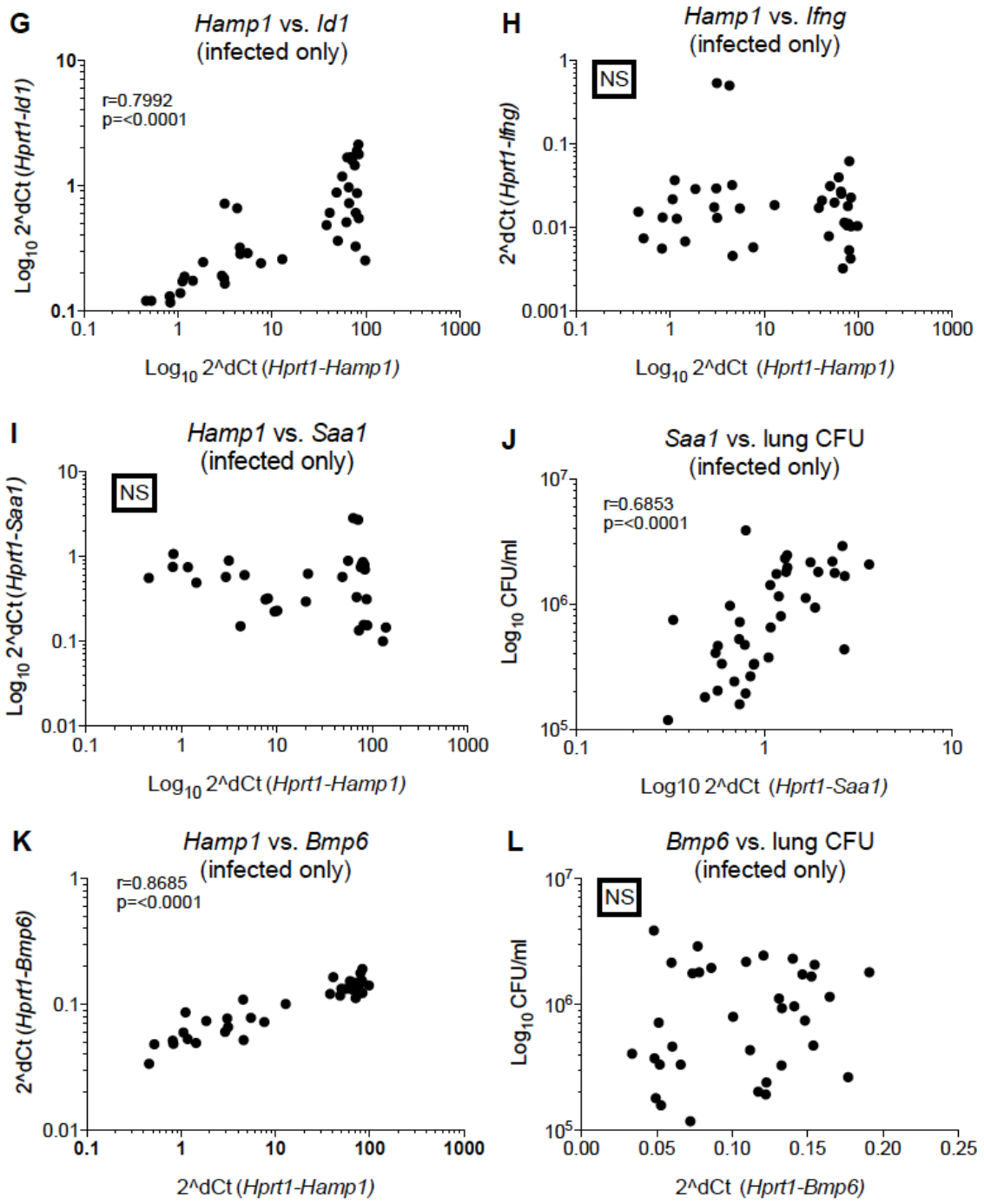


**Figure 5.8.3 Gene expression analyses in iron-deficient mice infected with *M.tb*.** C57BL/6 mice were fed an iron-deficient (4ppm) or control (200ppm) diet for 2 weeks prior to *M.tb* infection. Mice were culled after 4 and 8 weeks and hepatic gene expression was quantified by qRT-PCR. Uninfected controls were also culled at both timepoints. Gene expression is shown for *Hamp1* (A), *Fpn1* (B), *Id1* (C), *Bmp6* (D), *Saa1* (E), *Tfrc* (F) and correlations for *Hamp1* vs. *Id1* (G), *Hamp1* vs. *Ifng* (H), *Hamp1* vs. *Saa1* (I), *Saa1* vs. Lung CFU (J), *Hamp1* vs. *Bmp6* (K) and *Bmp6* vs. Lung CFU (L). Red points represent infected animals, closed circles indicate control diet and open circles iron-deficient diet. Mann-Whitney tests were done to compare groups with Bonferroni adjustment for multiple comparisons where *, **, *** and **** represent $p<0.05$, $p<0.01$, $p<0.001$ and $p<0.0001$, respectively. Correlations were Spearman correlations. N=10 per group for infected groups and n=6 for uninfected controls.

### *5.8.4 Proinflammatory cytokine expression in M.tb-infected iron deficient mice*

Iron deficiency did not affect the expression of *Ifng* or *Tnfa* pre or post-infection. However, expression of *Il6* was higher in the uninfected iron-deficient mice at 4 weeks post-infection (p=0.0260, Figure 5.8.4E). This was not significant in any other group, however, indicating that iron deficiency is unlikely to effect the hepatic expression of genes encoding these proinflammatory cytokines important in the control of *M.tb*. Expression of *Ifng* and *Tnfa* was increased post-challenge in both iron-deficient and control mice (Figure 5.8.4A+C) and both *Ifng* and *Tnfa* correlated significantly with lung CFU, as expected (r=0.5640, p=0.0002, and r=0.3519, p=0.0302, respectively, Figure 5.8.4B+D).

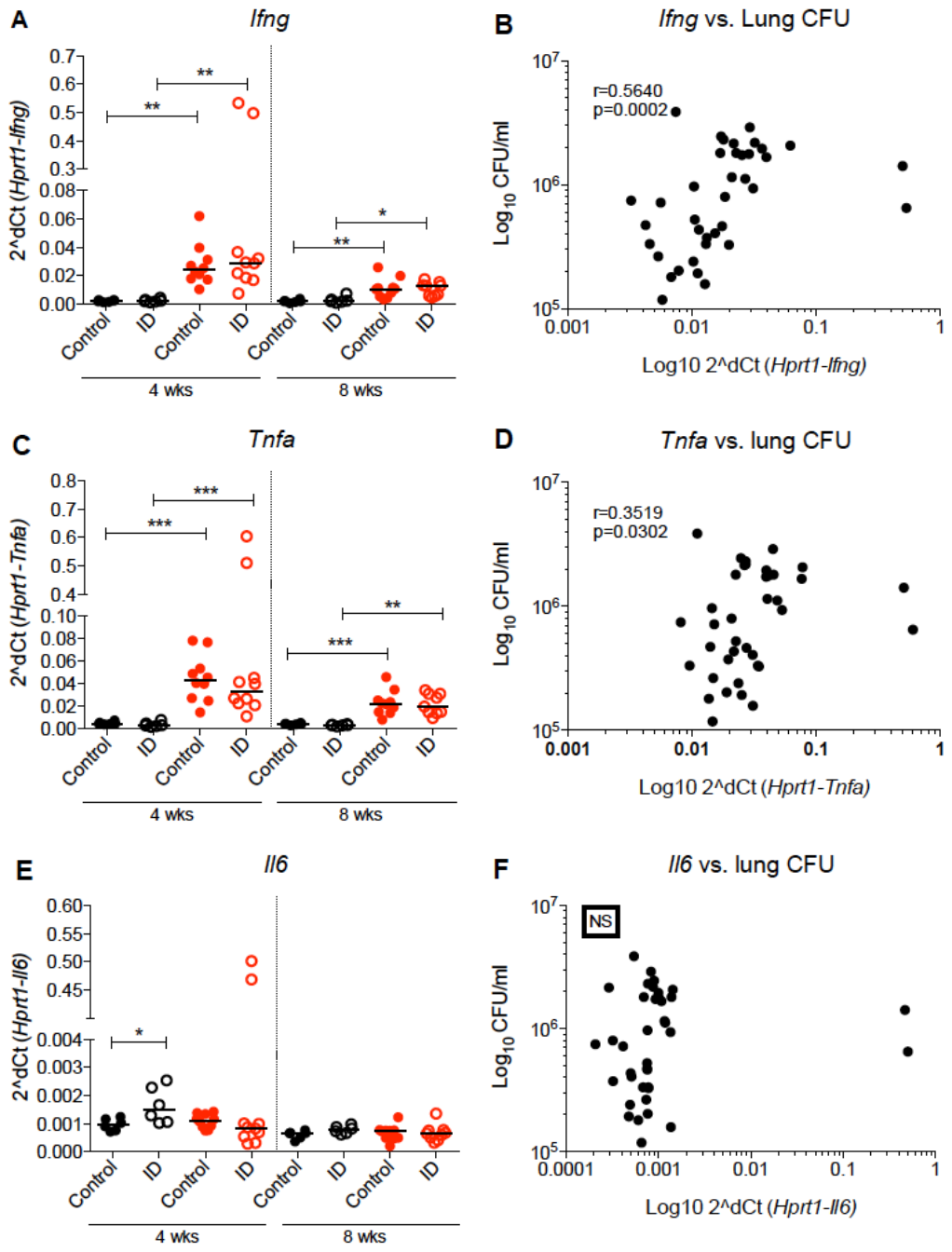


**Figure 5.8.4 Effect of restricting dietary iron availability in *M.tb* infection on the expression of genes encoding pro-inflammatory cytokines: repeat.** C57BL/6 mice were fed an iron restricted (4ppm ferric iron) or control (200ppm) diet for 2 weeks prior to infection with 50-100 CFU of aerosolised *M.tb*. Mice remained on the respective diets until they were taken down at 4 and 8 weeks post-infection. Uninfected controls were included at both timepoints. Gene expression is shown for *Ifng* (A), *Tnfa* (C), and *Il6* (D), while Spearman correlations between lung CFU and *Ifng*, *Tnfa*, and *Il6* are shown in B, D and F, respectively. Closed circles represent control diet, open circles represent iron-deficient diet with black circles representing uninfected animals and red circles infected animals. Mann-Whitney tests with Bonferroni corrections for multiple comparisons were done to compare groups where *, **, *** and **** represent $p<0.05$, $p<0.01$, $p<0.001$ and $p<0.0001$,. n= 6 for uninfected controls and n = 10 for infected groups.

## 5.9 Discussion

Key findings of this chapter:

- Chelation or addition of iron *in vitro* results in reduced or increased mycobacterial growth, respectively
- Maintenance of mice on an iron deficient diet containing 2-6ppm of iron results in iron deficiency with evidence of iron deficient erythropoiesis, but not severe anaemia.
- Iron deficiency did not affect susceptibility to BCG given by *i.n.* route
- Iron deficiency did not reproducibly affect susceptibility to *M.tb*

The aim of the experiments I have described in this chapter was to determine the effect of dietary iron restriction on mycobacterial growth *in vivo,* as well as to try to manipulate growth of mycobacteria *in vitro* by altering exogenous iron availability.

Firstly, I briefly looked at the effect of addition of exogenous iron, or iron chelator, on mycobacterial growth *in vitro* quantified both by plating out for CFU and by MGIT assays. Results highlighted an increase in bacterial growth with increasing concentrations of the iron salt FAC, and decreased growth after treatment with iron chelator DFO, consistent with previous findings [181].

I then characterised my iron-deficient mouse model and showed that changes in haematological parameters indicative of iron deficiency were evident from as early as 2 weeks after mice are switched to an iron-deficient diet (4ppm ferric

iron). As expected, signs of iron-deficiency became more evident after longer on the iron-deficient diet. The expression of genes involved in iron metabolism was also significantly affected by dietary iron restriction, consistent with previous findings [219, 236]. In particular, *Hamp1* was dramatically reduced in mice fed the iron-deficient diet, confirming that these mice are altering their iron metabolism in response to iron restriction. To investigate whether BMP/SMAD signalling might be influencing the suppression of hepcidin expression observed in the mice fed the iron-deficient diet, the expression of *Id1* and *Bmp6* was quantified. Both *Id1* and *Bmp6* correlated positively with *Hamp1* expression in the iron deficient mice, suggesting that the down regulation of *Hamp1* in response to reduced dietary iron is likely influenced by BMP/SMAD signalling. Furthermore, correlations were not observed when solely looking at mice fed the control diet, indicating that changes in *Hamp1* expression are likely in response to the iron-deficient diet, consistent with the literature [114, 237].

In addition, the expression of *Saa1*, a marker of inflammation, was quantified in order to confirm that the changes in hepcidin were not due to inflammation (although inflammation usually induces hepcidin expression), and was unaffected by diet. Interestingly, hepatic *Fpn1* expression was also significantly reduced in the iron-deficient mice even though *Hamp1* was also reduced I thought this may be due to post-transcriptional regulation of *Fpn1* by the IRE/IRP network in response to iron-restriction, or more likely a result of transcriptional regulation as a consequence of reduced haem. In this scenario, decreased dietary iron availability leads to a reduction of haem, resulting in the stabilisation of basic leucine zipper (Bach1), a transcriptional repressor. This

reduces the degradation of kelch-like ECH-associated protein 1 (Keap1), which is responsible for the sequestration of the transcriptional activator Nrf2 into the cytoplasm. Therefore in iron-deficient conditions where Keap1 is not degraded, Nrf2 is removed from the nucleus into the cytoplasm, resulting in repression of *Fpn1* mRNA [238]. These data confirm that the iron-deficient diet induces iron deficiency. However, more rigorous analyses of serum, liver and splenic iron content would be useful in order to further characterise this model.

A number of studies have already shown that murine iron overload results in enhanced mycobacterial growth [135, 136, 147, 239-241]. On the contrary, chelation of iron has been shown to inhibit bacterial growth *in vivo* [135], but there appears to be little information regarding the effect of iron deficiency on mycobacterial growth *in vivo.* In order to determine whether iron deficiency affects susceptibility to mycobacteria, I infected mice fed an iron-deficient diet with BCG. However, BCG growth was unaffected by dietary iron restriction. This did not rule out that infection with a more virulent mycobacterium, such as *M.tb*, might be affected by reduced iron availability. Therefore, I also infected iron-deficient mice with *M.tb.* Interestingly, in the first *M.tb* infection experiment, iron-deficient mice had significantly reduced bacterial growth in lungs and spleen at the 4 week time point, suggesting that iron-deficiency reduced bacterial growth as it restricted iron availability to the bacteria, or that iron deficiency improves immune function of these mice. However, when this was repeated with larger groups of animals, no differences were observed. This was surprising since such large differences were observed in the first challenge ($p<0.001$ between groups in the lungs). Gene expression analyses in the

infected animals as well as uninfected controls confirmed that the mice fed the iron-deficient diet were indeed iron-deficient in both experiments. When looking at the raw data for bacterial burden, in the first *M.tb* infection experiment, control mice taken down 4 weeks after infection had a median CFU of $6.3x10^5$ in their lungs and $5.1x10^4$ in their spleens. In the repeat experiment, these values were $1.9x10^6$ and $9.2x10^4$, respectively, indicating that mice in the second experiment received a higher dose of *M.tb* than in the previous experiment. Variations in challenge doses are often common due to the complexity of *M.tb* preparation and other factors such as time taken to set up the challenge equipment, as well as fluctuations in the temperature in the lab, which is why we can only give an estimated challenge dose. Infection with a higher *M.tb* dose may explain the disparity in results observed between these two experiments. In our *M.tb* challenge experiments, a lower challenge dose is often used to detect differences between vaccine candidates since it does not overburden the mice with *M.tb* and is therefore often more sensitive. In this case, the higher dose of *M.tb* given to mice in the second experiment may have overburdened their lungs, and therefore slight differences in bacterial growth influenced by alterations in dietary iron availability may not be evident. One way to confirm this could be to plan another experiment with a range of doses of *M.tb*. However, one could question the clinical relevance of these findings if effects of altering dietary iron availability are only evident in infection with a lower bacillary burden. Another important point to make is that human infection is very different from controlled murine aerosol infection, with close household contacts being exposed more frequently than more casual social contact, so if dietary iron availability does affect susceptibility, it is likely also dependent on a

number of other factors, such as the number of CFU a person is exposed to. Since dietary iron restriction also affects serum iron parameters, infection via *i.v.* route may also be interesting to look at, however this is not a natural route of infection.

Other factors such as the age of the mice before exposure to *M.tb*, the age of mice before being fed an iron-deficient diet, as well as the time the mice were fed the diet before challenge, could also impact on the outcome of infection. Iron deficiency was more severe after longer on the diet, so it would also be interesting to compare outcomes in mice fed the diet for a range of times prior to exposure to *M.tb,* as it is possible that iron stores were not sufficiently depleted to observe any changes in bacterial burden after 2 weeks on an iron-deficient diet. Of note, the mice used in the first iron diet infection experiment were considerably smaller than those in the second experiment, so it is possible that these were 1-2 weeks younger. Younger mice would have reduced iron stores from being fed the usual high iron diet prior to being switched to the iron deficient diet, and so may become severely iron deficient more quickly than older mice, which could explain the disparity in results seen between these two challenges. An important point to make is that the iron deficiency observed in these mice may not be comparable to severe iron deficiency that is often observed in humans, where haemoglobin is significantly reduced and anaemia occurs. More severe forms of iron deficiency, such as can be seen in humans, may have a more significant impact on mycobacterial growth, so the outcomes of the mouse studies described here may not be reflected in human infection.

Another angle to investigate would be look at gene expression analyses in the *M.tb* itself in iron-deficient and control mice in order to determine whether the bacteria itself are acting in an iron-starved manner, for example, does *M.tb* increase the expression of its iron acquisition genes in the iron-deficient mice? It would have been ideal to compare bacterial gene expression in the first experiment and the second experiment but unfortunately bacterial RNA was only collected from mice in the second experiment, when no differences in disease outcome between groups were observed. Since *M.tb* is such a slow-growing pathogen, it may be able to adjust to mild iron deficiency so its growth is unaffected. Gene expression analyses of the *M.tb* in this second experiment could confirm whether *M.tb* has upregulated iron acquisition genes such as those involved in siderophore biosynthesis (the *mbt* genes), as well as the *irtAB* operon, (which is involved in uptake of siderophores), and therefore whether it is iron-starved.

Host immune function can also be affected by iron availability. It is well documented that iron deficiency may inhibit host immune responses, and may impact on T cell proliferation, as it is an essential co-factor for cellular activities [242, 243]. On the contrary, reduced intracellular iron has been associated with stimulation of release of anti-microbial cytokines such as TNF-α and iNOS [166]. To investigate whether iron deficiency affects the immune response required for defence against *M.tb*, I quantified the hepatic expression of genes encoding pro-inflammatory cytokines involved in the immune response against *M.tb:* IFN-γ, TNF-α, and IL-6. No differences were observed in the expression of genes encoding IFN-γ or TNF-α between iron-deficient and control mice. Interestingly,

hepatic *Il6* expression was significantly higher in the iron-deficient mice after 6 weeks on the diet. However, this was not consistent across experiments, and was no longer significant after 10 weeks on the diet, even though still trending the same way. Increases in the expression of these cytokines were observed post-infection, which is consistent across all *M.tb* infection experiments in my thesis, so hepatic expression of these genes is sensitive enough to pick up big inductions of these cytokines. Although no differences were observed in hepatic expression of these cytokines, this does not rule out the possibility that the immune response is impaired in the iron-deficient mice. Further analyses, such as flow cytometric analyses or Luminex cytokine bead assays are required to investigate this. If the immune response is negatively affected in the iron-deficient mice, it is possible that any mild inhibition of mycobacterial growth as a result of reduced iron availability is effectively neutralised by the iron-deficient host being less able to control infection, and therefore the final bacterial burden does not differ between iron-deficient mice and controls. In addition, it might be useful to confirm that the alveolar macrophages and DCs, which are the primary host cells of *M.tb,* are actually iron deficient in the mice fed the iron-deficient diet, in comparison to controls. It is possible that they are not, and this could explain why bacterial burden was unaffected by feeding mice the iron-deficient diet.

In conclusion, data presented in this chapter confirm that an iron-deficient diet containing 4ppm of ferric iron induces iron deficiency in a mouse, but increasing the iron content to 18ppm soon reverses this phenotype. BCG infection was unaffected in mice fed the iron-deficient diet, and in one *M.tb* infection experiment, growth was also unaffected. However, it is possible that dietary

iron restriction mildly inhibited mycobacterial proliferation in concert with impairing host immune function and therefore no overall effect on bacterial burden was evident. A lower dose of *M.tb* such as that given in the first infection experiment where iron-deficient mice had reduced bacterial burden may have been easier for iron-deficient mice with slightly impaired immune function to control than the dose in the second experiment, where no differences in bacterial burden were observed between groups. Therefore, further work needs to be done to elucidate whether immune function is affected in the iron-deficient mice and whether the mycobacteria are acting in an iron starved manner. Since iron deficiency did affect bacterial burden in one of my experiments, we cannot rule out that iron status of the host may be of clinical relevance in the context of human *M.tb* infection but further work needs to be done to clarify this.

# Conclusions and future directions

# 6 Conclusions and future directions

The role of iron in infectious disease has long been the focus of a number of scientific studies, since the virulence of many pathogens, as well as the host immune response, may be affected by iron availability. The role of iron in mycobacterial growth has been studied extensively, and there is some evidence for a role of iron, in particular a role for hepcidin, in susceptibility to TB disease [138, 142]. However, research into whether the iron status of the murine host affects disease pathogenesis, and how *M.tb* infection affects host iron homeostasis, is scarce. A limited number of murine studies have looked at the effect of altering dietary iron availability on susceptibility to mycobacterial infection, as well as at how genetic disorders resulting in dysfunctional iron metabolism affect disease outcome. However, further research needs to be done to increase our understanding of this field for the development of new therapies, and to inform iron replacement strategies in the developing world. Therefore, this thesis aimed to:

a) Determine the effect of *in vivo M.tb* and BCG infection on the expression of hepcidin and other genes involved in iron homeostasis in BALB/c and C57BL/6 mice
b) Determine the effect of BCG vaccination on the expression of hepcidin and other genes involved in iron homeostasis
c) Determine the effect of hepcidin deficiency on susceptibility to *in vivo M.tb* infection using a hepcidin-deficient mouse model

d) Determine the effect of dietary iron deficiency on susceptibility to *in vivo* *M.tb* infection

There is evidence in the literature that immune and infectious stimuli induce expression of hepcidin, resulting in the locking of iron inside cells, which is thought to be a host mechanism to limit iron availability to blood-borne pathogens [140]. However, it is becoming increasingly likely that regulation of host iron homeostasis during infection depends on the location of the pathogen, and paradoxically, whilst hepcidin may be protective against extracellular pathogens [138, 214], it may be detrimental in intracellular infection. Hepcidin has been associated with TB disease in a number of studies [244]. However, in these studies, increased disease severity was associated with higher hepcidin levels. Therefore, it is possible that hepcidin is not protective in TB infection. The experiments in this thesis provide evidence that hepcidin is down-regulated post-*M.tb* infection. This is contrary to what was hypothesised, and contrasts with *in vitro* studies in macrophages in which hepcidin was induced to a high-level post-infection [104]. In this thesis, the observed down-regulation of hepcidin gene expression 4 weeks post-*M.tb* infection was consistent over a number of experiments. Hepcidin expression was not significantly reduced in infected BCG-vaccinated mice, possibly due to the vaccine reducing bacterial burden. Ideally, this should be confirmed at the protein level by serum hepcidin ELISAs, which have only recently become available, although this was not done in this project due to restrictions in BSL3 containment.

I also found that expression of *Nramp1* increased post-infection. Since there is increasing evidence that *Nramp1* functions to pump iron out of the *M.tb*-

containing phagosome [166, 226], my hypothesis is that the host response to infection with *M.tb* is to down-regulate hepcidin and other genes involved in iron homeostasis such that macrophage iron content is reduced, in order to deprive the intracellular pathogen of an iron source. In support of this, *in vitro* growth of the intracellular pathogen *S.typhi* is reduced when hepcidin levels are lower. This is likely as a result of increased ferroportin expression reducing intracellular iron for the pathogen [157]. The down-regulation of ferritin observed in my experiments post-infection may also represent a host mechanism of reducing intracellular iron stores, since *M.tb* is able to access iron from ferritin [145].

Upon further analyses of the post-infection time course studies, I found that hepcidin expression correlated with markers of BMP/SMAD signalling, suggesting that it may be regulated by inhibition of the BMP/SMAD signalling pathway through an unknown mechanism. This could be confirmed, however, perhaps at the protein level. Moreover, it was interesting to find a potential involvement of hypoxia in the observed suppression of hepcidin post-infection. Further investigations and quantification of HIFs or other markers of hypoxia such as EPO, are required in order to confirm a role for hypoxia in the regulation of hepcidin post-infection. Determining the exact molecular mechanisms involved in the regulation of hepcidin post-*M.tb* infection requires further analyses.

If the reduced hepcidin expression I observed post-infection is an attempt to control *M.tb* infection by reducing macrophage iron content, one might expect that a hepcidin-deficient mouse would be more protected against *M.tb* than wild

type controls, since these mice also have reduced spleen and liver macrophage iron content due to high ferroportin expression [113]. However, one major finding of this thesis was that hepcidin deletion did not affect outcome of *M.tb* infection, nor did it affect the expression of genes encoding pro-inflammatory cytokines required for control of *M.tb*. This lack of effect of hepcidin deletion on disease outcome contrasts greatly with the increased susceptibility of hepcidin deficient mice to extracellular pathogens such as *V.vulnificus,* highlighting that hepcidin deficiency-mediated iron redistribution has very different effects depending on the type of pathogen in terms of its preferred niche in the host.

Further analyses are required to elucidate whether immune function is affected in the *Hamp1*$^{-/-}$ mice, since iron overload can impair macrophage function as well as synthesis of ROS, thereby affecting host immune response. Although splenic macrophages and kupffer cells in *Hamp1*$^{-/-}$ mice have reduced iron content, we do not know if the same is true of alveolar macrophages. Histology data confirms that the lungs are iron overloaded but the exact location of this iron and its effect on alveolar macrophage iron content need to be confirmed. If the iron content of the alveolar macrophages is unaffected, this could explain the lack of effect of hepcidin deletion on bacterial burden. Another possibility is that macrophage iron content is decreased in *Hamp1*$^{-/-}$ mice, which could impact on mycobacterial growth, but in parallel, systemic iron overload impairs host immune function, counterbalancing any effect of reduced iron availability on mycobacterial growth. However, we also quantified bacterial burden in the spleen, in which we know the macrophages are iron-deficient, and no differences were observed here either. A hepcidin over-expressing mouse model or

administration of exogenous hepcidin might help to clarify this, since hepcidin-overloaded mice would have reduced ferroportin expression and therefore higher macrophage iron content than mice with normal iron metabolism.

I further investigated the role of iron in mycobacterial infection by infecting iron-deficient mice with BCG or *M.tb.* BCG growth was unaffected by dietary iron content. Therefore, it was surprising to find that *M.tb* bacterial burden was significantly reduced in iron-deficient mice, corresponding with studies showing that chelation of iron reduces bacterial growth [181]. However, when this experiment was repeated, no significant differences between groups were observed. Gene expression data confirms that the mice were iron deficient to the same extent as in the previous experiment. The only factor that appears to have changed was that the dose of *M.tb* given in the second experiment was slightly higher, probably due to variations in experimental conditions. If increasing the dose overburdens the host with *M.tb* such that restricting dietary iron no longer affects disease outcome, then host iron availability appears not to be a critical factor in disease pathogenesis and may not be of clinical relevance for human disease. However, a set of *M.tb* infection experiments at a range of doses might confirm whether iron availability having an effect on bacterial burden post-infection is dose-dependent. I did not observe any effect of iron deficiency on the hepatic expression of proinflammatory cytokines relevant for control of *M.tb* infection, but it is possible that reduction of dietary iron negatively affected the immune response, effectively counterbalancing any inhibitory effect that iron deficiency might have on mycobacterial growth. More

rigorous immune analyses such as flow cytometric analyses and quantification of immune effectors such as iNOS might clarify this.

Although the data presented in this thesis point to a lack of significant role of iron and hepcidin in control of *M.tb* infection in mice, several key experiments might support these findings. Firstly, in terms of the *M.tb* hepcidin time course experiments, larger groups of animals could confirm the down-regulation of hepcidin post-infection, although this has already been observed over a number of experiments. Secondly, rigorous immune analyses could be done in the iron-deficient and *Hamp1*$^{-/-}$ mouse models, to elucidate whether their immune responses have been affected by iron deficiency and hepcidin knockout, respectively. *M.tb* gene expression analyses in these two models could determine whether it is iron starved and up-regulating its iron acquisition genes i.e. whether the phenotypes are strong enough to affect mycobacterial gene expression. In terms of iron diet experiments, it might be worth looking at differing degrees of iron deficiency, by feeding mice an iron-deficient diet for a range of times before infection, since it is possible that mice still had iron reserves after only 2 weeks on the diet, and therefore mycobacterial growth was unaffected. A range of doses of *M.tb* could also be used in the iron diet experiments, to confirm whether the effect of iron deficiency on disease outcome observed in the first infection study was dose-dependent. Thirdly, to confirm that murine iron availability does not affect *M.tb* growth *in vivo*, mice could be fed a high iron diet to induce iron overload. The hepcidin-deficient mice that I used in this project were severely iron overloaded with a haemochromatosis-like phenotype due to overexpression of ferroportin leading to uncontrolled release of

iron from macrophages. This results in decreased macrophage iron content, although the effect of hepcidin deletion on alveolar macrophage iron is yet to be determined. A high iron diet would increase iron stores, and potentially macrophage iron, a phenotype that I have not looked at in this project. Another interesting angle to investigate would be whether BCG vaccine efficacy could be manipulated *in vivo* by administering it with iron chelators, or additional iron. In addition, does cellular immune response to BCG vaccination relate to iron status in humans? Finally, it would also be interesting to look at what is happening at the cellular level post-infection, for example, and whether this is altered by iron deficiency. Although the murine *M.tb* infection model is useful as it is cheap and relatively easy to manipulate, the relevance of high dose murine challenge to human infection is unclear. Other animals, such as NHPs may be more suitable since their infection is more comparable to human infection, and regulation of iron homeostasis is more comparable to that in humans.

Today, TB is still a devastating disease, and it remains clear that there is a pressing need for new diagnostic tests, therapeutic interventions and an improved vaccine. Since efforts to develop an effective vaccine are still ongoing, it is evident that novel research into host responses post-infection is necessary to gain a better understanding of disease pathogenesis and therefore how we might prevent disease. In this thesis, I explored the role of iron homeostasis, in particular the role of hepcidin, in mycobacterial infection. I have shown that in a murine model of mycobacterial infection, there does not appear to be a significant role for hepcidin or iron homeostasis in *M.tb* infection. Hepcidin

gene expression was affected post-infection, but neither deletion of hepcidin1 or induction of iron deficiency by restricting dietary iron strongly affected disease outcome. Recently, a strain of *M.tb* with mutant bacterioferritin was found to be susceptible to antibiotics as well as by host effector mechanisms, and was therefore unable to establish chronic infection in mice [151]. This same strain also provided protection against virulent *M.tb* comparable to that of BCG [245]. Drugs that target mycobacterial iron acquisition are also showing promise [173, 174]. In light of these findings, perhaps targeting mycobacterial iron acquisition systems to create avirulent strains suitable for vaccines, or targeting them therapeutically in people infected with *M.tb,* is a better area to focus iron-related TB research on. To conclude, in this thesis I have shown that host iron homeostasis is altered post-*M.tb* infection, but neither manipulation of iron homeostasis by inducing iron deficiency nor deleting the hepcidin gene compromised the host's ability to control infection. Although we still have a lot to learn about TB disease pathogenesis, novel findings such as those highlighted in this thesis are an important step towards determining which areas to focus TB research on. Based on the findings discussed here, it may be more beneficial in future to focus on manipulating the iron status of the bacterium itself (be that for a vaccine, or therapeutically) rather than the host, in order to control *M.tb* infection and prevent disease.

# 7 Appendix

| Reagent | Supplier | Product Code |
|---|---|---|
| 10% Neutral Buffered Formalin | Sigma Aldrich Company Ltd. | HT5011 |
| 7H9 Broth Base | Becton Dickinson Ltd. | 271310 |
| ADC growth supplement | Becton Dickinson Ltd. | 212352 |
| Agarose | Sigma Aldrich Company Ltd. | A9539-500G |
| BD Bactec 7ml MGIT tubes | Becton Dickinson Ltd. | 245122 |
| BD Bactec MGIT 960 Supplement Kit | Becton Dickinson Ltd. | 245124 |
| BD Microtainer tube with Dipotassium EDTA | Becton Dickinson Ltd. | 365974 |
| Deferoxamine mesylate salt (DFO) | Sigma Aldrich Company Ltd. | D9533 |
| Dimethylsulphoxide (DMSO) | Sigma Aldrich Company Ltd. | D2650-100ML |
| Ferric ammonium citrate (FAC) | Sigma Aldrich Company Ltd. | F-5879 |
| Foetal Calf Serum (FCS) | Sigma Aldrich Company Ltd. | F2442 |
| Gene Ruler 1Kbp DNA ladder | Fisher Scientific | 115 71595 |
| Glycerol | Sigma Aldrich Company Ltd. | 49767 |
| GoTaq Flexi DNA Polymerase Kit | Promega | M929 |
| Hepcidin/LEAP-1 (human) | Peptide Institute Inc | 4392-S |
| High Capacity cDNA Reverse Transcription Kit | Life Technologies | 4368814 |
| Igepal | Sigma Aldrich Company | I8896 |
| Iron-adjusted diet (18ppm) | Harlan Teklad | TD.130757 |
| Iron-adjusted diet (200ppm) | Harlan Teklad | TD.07801 |
| Iron-deficient diet (2-6ppm) | Harlan Teklad | TD.99397 |
| IsoFlurane | Oxford University Veterinary Services | |
| L-Glutamine | Sigma Aldrich | G7513 |

| | | |
|---|---|---|
| | Company Ltd. | |
| Middlebrook 7H10 agar base | Sigma Aldrich Company Ltd. | M0303 |
| Middlebrook 7H11 agar base | Sigma Aldrich Company Ltd. | M0428 |
| *Mycobacterium tuberculosis* | BEI Resources | NR-15404 |
| MicroAmp Fast Optical 96-well Reaction Plate 0.1mL | Life Technologies | |
| OADC enrichment | Becton Dickinson Ltd. | 212240 |
| Penicillin/Streptomycin | Sigma Aldrich Company Ltd. | P0781 |
| PFTE Tubing 0.3mm x 0.6mm | Sigma Aldrich Company Ltd. | Z609692 |
| Phorbol 12-myristate 13-acetate (PMA) | Sigma Aldrich Company Ltd. | P1585 |
| Phosphate buffered saline (PBS) | Sigma Aldrich Company Ltd. | D8537 |
| Precellys CK28R reinforced 2ml tubes containing 2.8mm ceramic beads | Stretton Scientific | 03961-1-007 |
| Proteinase K | Qiagen | 19131 |
| RNAlater RNA Stabilisation Reagent | Qiagen | 76104 |
| RNeasy Plus Mini Kit | Qiagen | 74136 |
| RPMI 1640 | Sigma Aldrich Company Ltd. | R0883-500ML |
| RPMI 1640 HEPES modification with 25nM HEPES | Sigma Aldrich Company Ltd. | R5886-500ML |
| SYBR Safe DNA Gel Stain | Fisher Scientific | S33102 |
| TAE buffer | Fisher Scientific | 10490264 |
| TaqMan Gene Expression Assays | Life Technologies | 4331182 |
| TaqMan Gene Expression Mastermix | Life Technologies | 4369016 |
| Trypan Blue 0.4% | Sigma Aldrich Company Ltd. | T8151-100ML |
| Tween80 | Becton Dickinson Ltd. | 231181 |

**Table 2 Table of Reagents**

| Solution | Recipe |
|---|---|
| ACK | 8.29g NaCl (0.15M)<br>1g $KHCO_3$ (1mM)<br>37.2g $Na_2EDTA$ in 800ml $dH_2O$<br>pH adjusted to 7.2-7.4 with 1M HCl<br>made up to 1L with $dH_2O$ |
| Freezing solution for cells | 50% FBS<br>40% RPMI 1640<br>10% DMSO |
| Middlebrook Agar | 900ml $dH_2O$<br>19.47g Middlebrook agar base<br>5ml glycerol<br>Autoclave<br>Add 100ml OADC enrichment after autoclaving while still warm |
| RO medium | RPMI 1640<br>2mM L-Glutamine<br>100U/ml Penicillin<br>100µg/ml Streptomycin sulphate |
| R10 medium | RPMI 1640<br>10% FBS<br>2mM L-Glutamine<br>100U/ml Penicillin<br>100µg/ml Streptomycin sulphate |

**Table 3 Table of solutions**

# 8 References


1. WHO, Tuberculosis. 2013: Available from: http://www.who.int/tb/publications/factsheets/en/index.html.
2. McShane, H., Tuberculosis vaccines: beyond bacille Calmette-Guerin. Philos Trans R Soc Lond B Biol Sci, 2011. 366(1579): p. 2782-9.
3. Ahmad, S., Pathogenesis, immunology, and diagnosis of latent Mycobacterium tuberculosis infection. Clin Dev Immunol, 2011. 2011: p. 814943.
4. Kleinnijenhuis, J., et al., Innate immune recognition of Mycobacterium tuberculosis. Clin Dev Immunol, 2011. 2011: p. 405310.
5. O'Garra, A., et al., The immune response in tuberculosis. Annu Rev Immunol, 2013. 31: p. 475-527.
6. Pawlowski, A., et al., Tuberculosis and HIV co-infection. PLoS Pathog, 2012. 8(2): p. e1002464.
7. WHO, Global tuberculosis report 2014. 2014.
8. Lienhardt, C., et al., Global tuberculosis control: lessons learnt and future prospects. Nat Rev Microbiol, 2012. 10(6): p. 407-16.
9. Nunes-Alves, C., et al., In search of a new paradigm for protective immunity to TB. Nat Rev Microbiol, 2014. 12(4): p. 289-99.
10. Flynn, J.L. and J. Chan, Immunology of tuberculosis. Annu Rev Immunol, 2001. 19: p. 93-129.
11. Kaufmann, S.H., How can immunology contribute to the control of tuberculosis? Nat Rev Immunol, 2001. 1(1): p. 20-30.
12. Zuñiga, J., et al., Cellular and humoral mechanisms involved in the control of tuberculosis. Clin Dev Immunol, 2012. 2012: p. 193923.
13. Mishra, A.K., et al., Lipoarabinomannan and related glycoconjugates: structure, biogenesis and role in Mycobacterium tuberculosis physiology and host-pathogen interaction. FEMS Microbiol Rev, 2011. 35(6): p. 1126-57.
14. Bafica, A., et al., TLR9 regulates Th1 responses and cooperates with TLR2 in mediating optimal resistance to Mycobacterium tuberculosis. J Exp Med, 2005. 202(12): p. 1715-24.
15. Poltorak, A., et al., Defective LPS signaling in C3H/HeJ and C57BL/10ScCr mice: mutations in Tlr4 gene. Science, 1998. 282(5396): p. 2085-8.

16. Scanga, C.A., et al., MyD88-deficient mice display a profound loss in resistance to Mycobacterium tuberculosis associated with partially impaired Th1 cytokine and nitric oxide synthase 2 expression. Infect Immun, 2004. 72(4): p. 2400-4.
17. Fremond, C.M., et al., Fatal Mycobacterium tuberculosis infection despite adaptive immune response in the absence of MyD88. J Clin Invest, 2004. 114(12): p. 1790-9.
18. Vergne, I., et al., Mycobacterium tuberculosis phagosome maturation arrest: mycobacterial phosphatidylinositol analog phosphatidylinositol mannoside stimulates early endosomal fusion. Mol Biol Cell, 2004. 15(2): p. 751-60.
19. Gutierrez, M.G., et al., Autophagy is a defense mechanism inhibiting BCG and Mycobacterium tuberculosis survival in infected macrophages. Cell, 2004. 119(6): p. 753-66.
20. Tiwari, B., U.M. Ramakrishnan, and T.R. Raghunand, The Mycobacterium tuberculosis protein pair PE9 (Rv1088)-PE10 (Rv1089) forms heterodimers and induces macrophage apoptosis through Toll-like receptor 4. Cell Microbiol, 2015. 17(11): p. 1653-69.
21. Flynn, J.L., et al., Tumor necrosis factor-alpha is required in the protective immune response against Mycobacterium tuberculosis in mice. Immunity, 1995. 2(6): p. 561-72.
22. Kindler, V., et al., The inducing role of tumor necrosis factor in the development of bactericidal granulomas during BCG infection. Cell, 1989. 56(5): p. 731-40.
23. Newport, M.J., et al., A mutation in the interferon-gamma-receptor gene and susceptibility to mycobacterial infection. N Engl J Med, 1996. 335(26): p. 1941-9.
24. Chackerian, A.A., et al., Dissemination of Mycobacterium tuberculosis is influenced by host factors and precedes the initiation of T-cell immunity. Infect Immun, 2002. 70(8): p. 4501-9.
25. Murphy, K., M. Walport, and C. Janeway, Janeway's Immunobiology. 2012, New York: Garland Science.
26. Ladel, C.H., S. Daugelat, and S.H. Kaufmann, Immune response to Mycobacterium bovis bacille Calmette Guérin infection in major histocompatibility complex class I- and II-deficient knock-out mice: contribution of CD4 and CD8 T cells to acquired resistance. Eur J Immunol, 1995. 25(2): p. 377-84.
27. van der Wel, N., et al., M. tuberculosis and M. leprae translocate from the phagolysosome to the cytosol in myeloid cells. Cell, 2007. 129(7): p. 1287-98.

28. Ottenhoff, T.H. and S.H. Kaufmann, Vaccines against tuberculosis: where are we and where do we need to go? PLoS Pathog, 2012. 8(5): p. e1002607.
29. Churchyard, G.J., et al., Mycobacterial disease in South African gold miners in the era of HIV infection. Int J Tuberc Lung Dis, 1999. 3(9): p. 791-8.
30. Reiley, W.W., et al., ESAT-6-specific CD4 T cell responses to aerosol Mycobacterium tuberculosis infection are initiated in the mediastinal lymph nodes. Proc Natl Acad Sci U S A, 2008. 105(31): p. 10961-6.
31. Kamath, A.B., et al., Cytolytic CD8+ T cells recognizing CFP10 are recruited to the lung after Mycobacterium tuberculosis infection. J Exp Med, 2004. 200(11): p. 1479-89.
32. Lazarevic, V. and J. Flynn, CD8+ T cells in tuberculosis. Am J Respir Crit Care Med, 2002. 166(8): p. 1116-21.
33. Cooper, A.M., et al., Disseminated tuberculosis in interferon gamma gene-disrupted mice. J Exp Med, 1993. 178(6): p. 2243-7.
34. Peters, W. and J.D. Ernst, Mechanisms of cell recruitment in the immune response to Mycobacterium tuberculosis. Microbes Infect, 2003. 5(2): p. 151-8.
35. Saunders, B.M. and W.J. Britton, Life and death in the granuloma: immunopathology of tuberculosis. Immunol Cell Biol, 2007. 85(2): p. 103-11.
36. Ramakrishnan, L., Revisiting the role of the granuloma in tuberculosis. Nat Rev Immunol, 2012. 12(5): p. 352-66.
37. Boehme, C.C., et al., Rapid molecular detection of tuberculosis and rifampin resistance. N Engl J Med, 2010. 363(11): p. 1005-15.
38. Fogel, N., Tuberculosis: A disease without boundaries. Tuberculosis (Edinb), 2015.
39. Organisation, W.H., Treatment of tuberculosis: guidelines. 4th Edition ed, ed. W.H. Organisation. Vol. WHO/HTM/TB/2009.420. 2009, Geneva, Switzerland: WHO Press.
40. Combs, D.L., R.J. O'Brien, and L.J. Geiter, USPHS Tuberculosis Short-Course Chemotherapy Trial 21: effectiveness, toxicity, and acceptability. The report of final results. Ann Intern Med, 1990. 112(6): p. 397-406.
41. Organisation, W.H. Tuberculosis Fact Sheet. WHO global TB programme c1948 [cited 2015 August].
42. Comas, I. and S. Gagneux, The past and future of tuberculosis research. PLoS Pathog, 2009. 5(10): p. e1000600.
43. WHO, Tuberculosis. 2013. Available from: http://www.who.int/tb/challenges/mdr/tdrfaqs/en/.

44. McShane, H., Vaccine strategies against tuberculosis. Swiss Med Wkly, 2009. 139(11-12): p. 156-60.
45. Colditz, G.A., et al., Efficacy of BCG vaccine in the prevention of tuberculosis. Meta-analysis of the published literature. JAMA, 1994. 271(9): p. 698-702.
46. Trunz, B.B., P. Fine, and C. Dye, Effect of BCG vaccination on childhood tuberculous meningitis and miliary tuberculosis worldwide: a meta-analysis and assessment of cost-effectiveness. Lancet, 2006. 367(9517): p. 1173-80.
47. Rodrigues, L.C., et al., Effect of BCG revaccination on incidence of tuberculosis in school-aged children in Brazil: the BCG-REVAC cluster-randomised trial. Lancet, 2005. 366(9493): p. 1290-5.
48. Sterne, J.A., L.C. Rodrigues, and I.N. Guedes, Does the efficacy of BCG decline with time since vaccination? Int J Tuberc Lung Dis, 1998. 2(3): p. 200-7.
49. Ahsan, M.J., Recent advances in the development of vaccines for tuberculosis. Ther Adv Vaccines, 2015. 3(3): p. 66-75.
50. Grode, L., et al., Increased vaccine efficacy against tuberculosis of recombinant Mycobacterium bovis bacille Calmette-Guérin mutants that secrete listeriolysin. J Clin Invest, 2005. 115(9): p. 2472-9.
51. Arbues, A., et al., Construction, characterization and preclinical evaluation of MTBVAC, the first live-attenuated M. tuberculosis-based vaccine to enter clinical trials. Vaccine, 2013. 31(42): p. 4867-73.
52. Goonetilleke, N.P., et al., Enhanced immunogenicity and protective efficacy against Mycobacterium tuberculosis of bacille Calmette-Guérin vaccine using mucosal administration and boosting with a recombinant modified vaccinia virus Ankara. J Immunol, 2003. 171(3): p. 1602-9.
53. Williams, A., et al., Boosting with poxviruses enhances Mycobacterium bovis BCG efficacy against tuberculosis in guinea pigs. Infect Immun, 2005. 73(6): p. 3814-6.
54. Verreck, F.A., et al., MVA.85A boosting of BCG and an attenuated, phoP deficient M. tuberculosis vaccine both show protective efficacy against tuberculosis in rhesus macaques. PLoS One, 2009. 4(4): p. e5264.
55. McShane, H., et al., Enhanced immunogenicity of CD4(+) t-cell responses and protective efficacy of a DNA-modified vaccinia virus Ankara prime-boost vaccination regimen for murine tuberculosis. Infect Immun, 2001. 69(2): p. 681-6.
56. Williams, A., et al., Evaluation of vaccines in the EU TB Vaccine Cluster using a guinea pig aerosol infection model of tuberculosis. Tuberculosis (Edinb), 2005. 85(1-2): p. 29-38.

57. Sharpe, S.A., et al., Establishment of an aerosol challenge model of tuberculosis in rhesus macaques and an evaluation of endpoints for vaccine testing. Clin Vaccine Immunol, 2010. 17(8): p. 1170-82.
58. Vordermeier, H.M., et al., Viral booster vaccines improve Mycobacterium bovis BCG-induced protection against bovine tuberculosis. Infect Immun, 2009. 77(8): p. 3364-73.
59. Tameris, M.D., et al., Safety and efficacy of MVA85A, a new tuberculosis vaccine, in infants previously vaccinated with BCG: a randomised, placebo-controlled phase 2b trial. Lancet, 2013. 381(9871): p. 1021-8.
60. Acosta, A., et al., The importance of animal models in tuberculosis vaccine development. Malays J Med Sci, 2011. 18(4): p. 5-12.
61. Young, D., Animal models of tuberculosis. Eur J Immunol, 2009. 39(8): p. 2011-4.
62. Gupta, U.D. and V.M. Katoch, Animal models of tuberculosis. Tuberculosis (Edinb), 2005. 85(5-6): p. 277-93.
63. Dharmadhikari, A.S. and E.A. Nardell, What animal models teach humans about tuberculosis. Am J Respir Cell Mol Biol, 2008. 39(5): p. 503-8.
64. Collins, F.M., The immunology of tuberculosis. Am Rev Respir Dis, 1982. 125(3 Pt 2): p. 42-9.
65. Apt, A.S., Are mouse models of human mycobacterial diseases relevant? Genetics says: 'yes!'. Immunology, 2011. 134(2): p. 109-15.
66. Dannenberg, A.M. and F.M. Collins, Progressive pulmonary tuberculosis is not due to increasing numbers of viable bacilli in rabbits, mice and guinea pigs, but is due to a continuous host response to mycobacterial products. Tuberculosis (Edinb), 2001. 81(3): p. 229-42.
67. Rhoades, E.R., A.A. Frank, and I.M. Orme, Progression of chronic pulmonary tuberculosis in mice aerogenically infected with virulent Mycobacterium tuberculosis. Tuber Lung Dis, 1997. 78(1): p. 57-66.
68. Medina, E., B.J. Rogerson, and R.J. North, The Nramp1 antimicrobial resistance gene segregates independently of resistance to virulent Mycobacterium tuberculosis. Immunology, 1996. 88(4): p. 479-81.
69. Forget, A., et al., Differences in response among inbred mouse strains to infection with small doses of Mycobacterium bovis BCG. Infect Immun, 1981. 32(1): p. 42-7.
70. Chackerian, A.A. and S.M. Behar, Susceptibility to Mycobacterium tuberculosis: lessons from inbred strains of mice. Tuberculosis (Edinb), 2003. 83(5): p. 279-85.
71. Apt, A. and I. Kramnik, Man and mouse TB: contradictions and solutions. Tuberculosis (Edinb), 2009. 89(3): p. 195-8.

72. Koch, R., Aetiologie der Tuberculose. Vol. 19. 1882: Berl Klin Wochenschr.
73. Ladefoged, A., K. Bunch-Christensen, and J. Guld, Tuberculin sensitivity in guinea-pigs after vaccination with varying doses of BCG of 12 different strains. Bull World Health Organ, 1976. 53(4): p. 435-43.
74. Calmette, A., ANegre, L, Essais de vaccination contre l infection tuberculeuse par voie buccale chez les petits animaux de laboratorie. Vol. 38. 1924: Annales de l'Institut Pasteur.
75. Manabe, Y.C., et al., Different strains of Mycobacterium tuberculosis cause various spectrums of disease in the rabbit model of tuberculosis. Infect Immun, 2003. 71(10): p. 6004-11.
76. Capuano, S.V., et al., Experimental Mycobacterium tuberculosis infection of cynomolgus macaques closely resembles the various manifestations of human M. tuberculosis infection. Infect Immun, 2003. 71(10): p. 5831-44.
77. Lin, P.L., et al., Early events in Mycobacterium tuberculosis infection in cynomolgus macaques. Infect Immun, 2006. 74(7): p. 3790-803.
78. Muckenthaler, M.U., B. Galy, and M.W. Hentze, Systemic iron homeostasis and the iron-responsive element/iron-regulatory protein (IRE/IRP) regulatory network. Annu Rev Nutr, 2008. 28: p. 197-213.
79. Ganz, T., Systemic iron homeostasis. Physiol Rev, 2013. 93(4): p. 1721-41.
80. Thom, R.E., et al., The expression of ferritin, lactoferrin, transferrin receptor and solute carrier family 11A1 in the host response to BCG-vaccination and Mycobacterium tuberculosis challenge. Vaccine, 2012. 30(21): p. 3159-68.
81. Rodriguez, M., G., Control of iron metabolism in Mycobacterium tuberculosis. Trends in Microbiology, 2006. 14(7): p. 320-327.
82. Canonne-Hergaux, F., et al., Cellular and subcellular localization of the Nramp2 iron transporter in the intestinal brush border and regulation by dietary iron. Blood, 1999. 93(12): p. 4406-17.
83. Gunshin, H., et al., Cloning and characterization of a mammalian proton-coupled metal-ion transporter. Nature, 1997. 388(6641): p. 482-8.
84. Gunshin, H., et al., Cybrd1 (duodenal cytochrome b) is not necessary for dietary iron absorption in mice. Blood, 2005. 106(8): p. 2879-83.
85. Gunshin, H., et al., Slc11a2 is required for intestinal iron absorption and erythropoiesis but dispensable in placenta and liver. J Clin Invest, 2005. 115(5): p. 1258-66.
86. Iolascon, A. and L. De Falco, Mutations in the gene encoding DMT1: clinical presentation and treatment. Semin Hematol, 2009. 46(4): p. 358-70.

87. Harrison, P.M. and P. Arosio, The ferritins: molecular properties, iron storage function and cellular regulation. Biochim Biophys Acta, 1996. 1275(3): p. 161-203.
88. Torti, F.M. and S.V. Torti, Regulation of ferritin genes and protein. Blood, 2002. 99(10): p. 3505-16.
89. Ferreira, C., et al., Early embryonic lethality of H ferritin gene deletion in mice. J Biol Chem, 2000. 275(5): p. 3021-4.
90. Darshan, D., et al., Conditional deletion of ferritin H in mice induces loss of iron storage and liver damage. Hepatology, 2009. 50(3): p. 852-60.
91. Aziz, N. and H.N. Munro, Both subunits of rat liver ferritin are regulated at a translational level by iron induction. Nucleic Acids Res, 1986. 14(2): p. 915-27.
92. Cook, J.D., C.H. Flowers, and B.S. Skikne, The quantitative assessment of body iron. Blood, 2003. 101(9): p. 3359-64.
93. Jacobs, A. and M. Worwood, Ferritin in serum. Clinical and biochemical implications. N Engl J Med, 1975. 292(18): p. 951-6.
94. Kosman, D.J., Redox cycling in iron uptake, efflux, and trafficking. J Biol Chem, 2010. 285(35): p. 26729-35.
95. Cherukuri, S., et al., Unexpected role of ceruloplasmin in intestinal iron absorption. Cell Metab, 2005. 2(5): p. 309-19.
96. Donovan, A., et al., The iron exporter ferroportin/Slc40a1 is essential for iron homeostasis. Cell Metab, 2005. 1(3): p. 191-200.
97. Gozzelino, R. and M.P. Soares, Coupling heme and iron metabolism via ferritin H chain. Antioxid Redox Signal, 2014. 20(11): p. 1754-69.
98. Bartnikas, T.B., N.C. Andrews, and M.D. Fleming, Transferrin is a major determinant of hepcidin expression in hypotransferrinemic mice. Blood, 2011. 117(2): p. 630-7.
99. Bartnikas, T.B., Known and potential roles of transferrin in iron biology. Biometals, 2012. 25(4): p. 677-86.
100. Krause, A., et al., LEAP-1, a novel highly disulfide-bonded human peptide, exhibits antimicrobial activity. FEBS Lett, 2000. 480(2-3): p. 147-50.
101. Park, C.H., et al., Hepcidin, a urinary antimicrobial peptide synthesized in the liver. J Biol Chem, 2001. 276(11): p. 7806-10.
102. Nemeth, E., et al., Hepcidin regulates cellular iron efflux by binding to ferroportin and inducing its internalization. Science, 2004. 306(5704): p. 2090-3.
103. Drakesmith, H. and A.M. Prentice, Hepcidin and the iron-infection axis. Science, 2012. 338(6108): p. 768-72.

104. Sow, F.B., et al., Expression and localization of hepcidin in macrophages: a role in host defense against tuberculosis. J Leukoc Biol, 2007. 82(4): p. 934-45.
105. Roetto, A., et al., Mutant antimicrobial peptide hepcidin is associated with severe juvenile hemochromatosis. Nat Genet, 2003. 33(1): p. 21-2.
106. Papanikolaou, G., et al., Mutations in HFE2 cause iron overload in chromosome 1q-linked juvenile hemochromatosis. Nat Genet, 2004. 36(1): p. 77-82.
107. Nicolas, G., et al., The gene encoding the iron regulatory peptide hepcidin is regulated by anemia, hypoxia, and inflammation. J Clin Invest, 2002. 110(7): p. 1037-44.
108. Ilyin, G., et al., Comparative analysis of mouse hepcidin 1 and 2 genes: evidence for different patterns of expression and co-inducibility during iron overload. FEBS Lett, 2003. 542(1-3): p. 22-6.
109. Gutschow, P., et al., A competitive enzyme-linked immunosorbent assay specific for murine hepcidin-1: correlation with hepatic mRNA expression in established and novel models of dysregulated iron homeostasis. Haematologica, 2015. 100(2): p. 167-77.
110. Lou, D.Q., et al., Functional differences between hepcidin 1 and 2 in transgenic mice. Blood, 2004. 103(7): p. 2816-21.
111. Roy, C.N., et al., Hepcidin antimicrobial peptide transgenic mice exhibit features of the anemia of inflammation. Blood, 2007. 109(9): p. 4038-44.
112. Nicolas, G., et al., Severe iron deficiency anemia in transgenic mice expressing liver hepcidin. Proc Natl Acad Sci U S A, 2002. 99(7): p. 4596-601.
113. Lesbordes-Brion, J.C., et al., Targeted disruption of the hepcidin 1 gene results in severe hemochromatosis. Blood, 2006. 108(4): p. 1402-5.
114. Ganz, T. and E. Nemeth, Hepcidin and iron homeostasis. Biochim Biophys Acta, 2012.
115. Babitt, J.L., et al., Bone morphogenetic protein signaling by hemojuvelin regulates hepcidin expression. Nat Genet, 2006. 38(5): p. 531-9.
116. Babitt, J.L., et al., Modulation of bone morphogenetic protein signaling in vivo regulates systemic iron balance. J Clin Invest, 2007. 117(7): p. 1933-9.
117. Wang, R.H., et al., A role of SMAD4 in iron metabolism through the positive regulation of hepcidin expression. Cell Metab, 2005. 2(6): p. 399-409.
118. Meynard, D., et al., Lack of the bone morphogenetic protein BMP6 induces massive iron overload. Nat Genet, 2009. 41(4): p. 478-81.
119. Andriopoulos, B., et al., BMP6 is a key endogenous regulator of hepcidin expression and iron metabolism. Nat Genet, 2009. 41(4): p. 482-7.

120. Huang, F.W., et al., A mouse model of juvenile hemochromatosis. J Clin Invest, 2005. 115(8): p. 2187-91.
121. Nemeth, E., et al., IL-6 mediates hypoferremia of inflammation by inducing the synthesis of the iron regulatory hormone hepcidin. J Clin Invest, 2004. 113(9): p. 1271-6.
122. Kautz, L., et al., Identification of erythroferrone as an erythroid regulator of iron metabolism. Nat Genet, 2014. 46(7): p. 678-84.
123. Ganz, T. and E. Nemeth, Iron homeostasis in host defence and inflammation. Nat Rev Immunol, 2015. 15(8): p. 500-10.
124. Ravasi, G., et al., Circulating factors are involved in hypoxia-induced hepcidin suppression. Blood Cells Mol Dis, 2014. 53(4): p. 204-10.
125. Hintze, K.J. and J.P. McClung, Hepcidin: A Critical Regulator of Iron Metabolism during Hypoxia. Adv Hematol, 2011. 2011: p. 510304.
126. Muckenthaler, M., N.K. Gray, and M.W. Hentze, IRP-1 binding to ferritin mRNA prevents the recruitment of the small ribosomal subunit by the cap-binding complex eIF4F. Mol Cell, 1998. 2(3): p. 383-8.
127. Campillos, M., et al., SIREs: searching for iron-responsive elements. Nucleic Acids Res, 2010. 38(Web Server issue): p. W360-7.
128. Sanchez, M., et al., Iron-regulatory proteins limit hypoxia-inducible factor-2alpha expression in iron deficiency. Nat Struct Mol Biol, 2007. 14(5): p. 420-6.
129. Wallander, M.L., E.A. Leibold, and R.S. Eisenstein, Molecular control of vertebrate iron homeostasis by iron regulatory proteins. Biochim Biophys Acta, 2006. 1763(7): p. 668-89.
130. Papanikolaou, G., et al., Mutations in HFE2 cause iron overload in chromosome 1q-linked juvenile hemochromatosis. Nat Genet, 2004. 36(1): p. 77-82.
131. Gan, E.K., L.W. Powell, and J.K. Olynyk, Natural history and management of HFE-hemochromatosis. Semin Liver Dis, 2011. 31(3): p. 293-301.
132. Gordeuk, V.R., et al., Associations of iron overload in Africa with hepatocellular carcinoma and tuberculosis: Strachan's 1929 thesis revisited. Blood, 1996. 87(8): p. 3470-6.
133. Gangaidzo, I.T., et al., Association of pulmonary tuberculosis with increased dietary iron. J Infect Dis, 2001. 184(7): p. 936-9.
134. Isanaka, S., et al., Iron deficiency and anemia predict mortality in patients with tuberculosis. J Nutr, 2012. 142(2): p. 350-7.
135. Schaible, U.E., et al., Correction of the iron overload defect in beta-2-microglobulin knockout mice by lactoferrin abolishes their increased susceptibility to tuberculosis. J Exp Med, 2002. 196(11): p. 1507-13.

136. Lounis, N., et al., Impact of iron loading on the activity of isoniazid or ethambutol in the treatment of murine tuberculosis. Int J Tuberc Lung Dis, 2003. 7(6): p. 575-9.
137. RATLEDGE, C. and F.G. WINDER, The accumulation of salicylic acid by mycobacteria during growth on an iron-deficient medium. Biochem J, 1962. 84: p. 501-6.
138. Armitage, A.E. and E. Moran, HIV-Associated Tuberculosis: Does the Iron-Regulatory Hormone Hepcidin Connect Anemia With Poor Prognosis? J Infect Dis, 2016. 213(1): p. 3-5.
139. Sow, F.B., et al., Mycobacterium tuberculosis components stimulate production of the antimicrobial peptide hepcidin. Tuberculosis (Edinb), 2011. 91(4): p. 314-21.
140. Armitage, A.E., et al., Hepcidin regulation by innate immune and infectious stimuli. Blood, 2011. 118(15): p. 4129-39.
141. Kerkhoff, A.D., et al., Relationship Between Blood Concentrations of Hepcidin and Anemia Severity, Mycobacterial Burden, and Mortality Among Patients With HIV-Associated Tuberculosis. J Infect Dis, 2015.
142. Minchella, P.A., et al., Iron homeostasis and progression to pulmonary tuberculosis disease among household contacts. Tuberculosis (Edinb), 2015. 95(3): p. 288-93.
143. Minchella, P.A., et al., Elevated hepcidin at HIV diagnosis is associated with incident tuberculosis in a retrospective cohort study. Int J Tuberc Lung Dis, 2014. 18(11): p. 1337-9.
144. Gobin, J. and M.A. Horwitz, Exochelins of Mycobacterium tuberculosis remove iron from human iron-binding proteins and donate iron to mycobactins in the M. tuberculosis cell wall. J Exp Med, 1996. 183(4): p. 1527-32.
145. Boelaert, J.R., et al., The effect of the host's iron status on tuberculosis. J Infect Dis, 2007. 195(12): p. 1745-53.
146. Clemens, D.L. and M.A. Horwitz, The Mycobacterium tuberculosis phagosome interacts with early endosomes and is accessible to exogenously administered transferrin. J Exp Med, 1996. 184(4): p. 1349-55.
147. Kochan, I., The role of iron in bacterial infections, with special consideration of host-tubercle bacillus interaction. Curr Top Microbiol Immunol, 1973. 60: p. 1-30.
148. Barclay, R. and C. Ratledge, Participation of iron on the growth inhibition of pathogenic strains of mycobacterium avium and M. paratuberculosis in serum. Zentralbl Bakteriol Mikrobiol Hyg A, 1986. 262(2): p. 189-94.

149. De Voss, J.J., et al., The salicylate-derived mycobactin siderophores of Mycobacterium tuberculosis are essential for growth in macrophages. Proc Natl Acad Sci U S A, 2000. 97(3): p. 1252-7.
150. Ratledge, C., Iron, mycobacteria and tuberculosis. Tuberculosis (Edinb), 2004. 84(1-2): p. 110-30.
151. Pandey, R. and G.M. Rodriguez, A ferritin mutant of Mycobacterium tuberculosis is highly susceptible to killing by antibiotics and is unable to establish a chronic infection in mice. Infect Immun, 2012. 80(10): p. 3650-9.
152. Subbian, S., et al., Vaccination with an Attenuated Ferritin Mutant Protects Mice against Virulent Mycobacterium tuberculosis. Journal of Immunology Research, 2015. 2015: p. 12.
153. Ganz, T., Iron in innate immunity: starve the invaders. Curr Opin Immunol, 2009. 21(1): p. 63-7.
154. Portugal, S., et al., Host-mediated regulation of superinfection in malaria. Nat Med, 2011. 17(6): p. 732-7.
155. Nairz, M., et al., Iron at the interface of immunity and infection. Front Pharmacol, 2014. 5: p. 152.
156. Nairz, M., et al., The co-ordinated regulation of iron homeostasis in murine macrophages limits the availability of iron for intracellular Salmonella typhimurium. Cell Microbiol, 2007. 9(9): p. 2126-40.
157. Chlosta, S., et al., The iron efflux protein ferroportin regulates the intracellular growth of Salmonella enterica. Infect Immun, 2006. 74(5): p. 3065-7.
158. Botella, H., et al., Metallobiology of host-pathogen interactions: an intoxicating new insight. Trends Microbiol, 2012. 20(3): p. 106-12.
159. Olakanmi, O., L.S. Schlesinger, and B.E. Britigan, Hereditary hemochromatosis results in decreased iron acquisition and growth by Mycobacterium tuberculosis within human macrophages. J Leukoc Biol, 2007. 81(1): p. 195-204.
160. Nairz, M., et al., Slc11a1 limits intracellular growth of Salmonella enterica sv. Typhimurium by promoting macrophage immune effector functions and impairing bacterial iron acquisition. Cell Microbiol, 2009. 11(9): p. 1365-81.
161. Ben-Othman, R., et al., Leishmania-mediated inhibition of iron export promotes parasite replication in macrophages. PLoS Pathog, 2014. 10(1): p. e1003901.
162. Paradkar, P.N., et al., Iron depletion limits intracellular bacterial growth in macrophages. Blood, 2008. 112(3): p. 866-74.
163. Van Zandt, K.E., et al., The iron export protein ferroportin 1 is differentially expressed in mouse macrophage populations and is present

in the mycobacterial-containing phagosome. J Leukoc Biol, 2008. 84(3): p. 689-700.
164. Nairz, M., et al., Nitric oxide-mediated regulation of ferroportin-1 controls macrophage iron homeostasis and immune function in Salmonella infection. J Exp Med, 2013. 210(5): p. 855-73.
165. Sohn, Y.S., et al., Rescuing iron-overloaded macrophages by conservative relocation of the accumulated metal. Br J Pharmacol, 2011. 164(2b): p. 406-18.
166. Weiss, G. and U.E. Schaible, Macrophage defense mechanisms against intracellular bacteria. Immunol Rev, 2015. 264(1): p. 182-203.
167. Li, X., et al., SLC11A1 (NRAMP1) polymorphisms and tuberculosis susceptibility: updated systematic review and meta-analysis. PLoS One, 2011. 6(1): p. e15831.
168. Chakraborty, S., et al., The multifaceted roles of neutrophil gelatinase associated lipocalin (NGAL) in inflammation and cancer. Biochim Biophys Acta, 2012. 1826(1): p. 129-69.
169. Johnson, E.E. and M. Wessling-Resnick, Iron metabolism and the innate immune response to infection. Microbes Infect, 2012. 14(3): p. 207-16.
170. Holmes, M.A., et al., Siderocalin (Lcn 2) also binds carboxymycobactins, potentially defending against mycobacterial infections through iron sequestration. Structure, 2005. 13(1): p. 29-41.
171. Byrd, T.F. and M.A. Horwitz, Interferon gamma-activated human monocytes downregulate transferrin receptors and inhibit the intracellular multiplication of Legionella pneumophila by limiting the availability of iron. J Clin Invest, 1989. 83(5): p. 1457-65.
172. Olakanmi, O., et al., Intraphagosomal Mycobacterium tuberculosis acquires iron from both extracellular transferrin and intracellular iron pools. Impact of interferon-gamma and hemochromatosis. J Biol Chem, 2002. 277(51): p. 49727-34.
173. Ratledge, C. and K.A. Brown, Inhibition of mycobactin formation in Mycobacterium smegmatis by p-aminosalicylate. A new proposal for the mode of action of p-aminosalicylate. Am Rev Respir Dis, 1972. 106(5): p. 774-6.
174. Ferreras, J.A., et al., Small-molecule inhibition of siderophore biosynthesis in Mycobacterium tuberculosis and Yersinia pestis. Nat Chem Biol, 2005. 1(1): p. 29-32.
175. Somu, R.V., et al., Rationally designed nucleoside antibiotics that inhibit siderophore biosynthesis of Mycobacterium tuberculosis. J Med Chem, 2006. 49(1): p. 31-4.
176. Weiss, G., Iron and immunity: a double-edged sword. Eur J Clin Invest, 2002. 32 Suppl 1: p. 70-8.

177. Fang, F.C. and G. Weiss, Iron ERRs with Salmonella. Cell Host Microbe, 2014. 15(5): p. 515-6.
178. Chan, Y.R., et al., Lipocalin 2 is required for pulmonary host defense against Klebsiella infection. J Immunol, 2009. 182(8): p. 4947-56.
179. Trousseau, A., True and false Chlorosis, in Lectures on Clinical Medicine, L.a. Blakiston, Editor. 1872: Philadelphia, PA.
180. Moyo, V.M., et al., Tuberculosis and iron overload in Africa: a review. Cent Afr J Med, 1997. 43(11): p. 334-9.
181. Lounis, N., et al., Iron and Mycobacterium tuberculosis infection. J Clin Virol, 2001. 20(3): p. 123-6.
182. Champy, M.F., et al., Genetic background determines metabolic phenotypes in the mouse. Mamm Genome, 2008. 19(5): p. 318-31.
183. Cavey, T., et al., Mouse genetic background impacts both on iron and non-iron metals parameters and on their relationships. Biometals, 2015. 28(4): p. 733-43.
184. Détivaud, L., et al., Hepcidin levels in humans are correlated with hepatic iron stores, hemoglobin levels, and hepatic function. Blood, 2005. 106(2): p. 746-8.
185. Cooper, A.M., K.D. Mayer-Barber, and A. Sher, Role of innate cytokines in mycobacterial infection. Mucosal Immunol, 2011. 4(3): p. 252-60.
186. Leung, P.S., et al., Increased duodenal iron uptake and transfer in a rat model of chronic hypoxia is accompanied by reduced hepcidin expression. Gut, 2005. 54(10): p. 1391-5.
187. Peyssonnaux, C., et al., Regulation of iron homeostasis by the hypoxia-inducible transcription factors (HIFs). J Clin Invest, 2007. 117(7): p. 1926-32.
188. Saiga, H., et al., Lipocalin 2-dependent inhibition of mycobacterial growth in alveolar epithelium. J Immunol, 2008. 181(12): p. 8521-7.
189. Blackwell, J.M., et al., Understanding the multiple functions of Nramp1. Microbes Infect, 2000. 2(3): p. 317-21.
190. Govoni, G., et al., Cell-specific and inducible Nramp1 gene expression in mouse macrophages in vitro and in vivo. J Leukoc Biol, 1997. 62(2): p. 277-86.
191. Fritsche, G., et al., Slc11a1 (Nramp1) impairs growth of Salmonella enterica serovar typhimurium in macrophages via stimulation of lipocalin-2 expression. J Leukoc Biol, 2012. 92(2): p. 353-9.
192. Garcia-Pelayo, M.C., et al., BALB/c mice display more enhanced BCG vaccine induced Th1 and Th17 response than C57BL/6 mice but have equivalent protection. Tuberculosis (Edinb), 2015. 95(1): p. 48-53.

193. Besson-Fournier, C., et al., Induction of activin B by inflammatory stimuli up-regulates expression of the iron-regulatory peptide hepcidin through Smad1/5/8 signaling. Blood, 2012. 120(2): p. 431-9.
194. Moisan, J., et al., Role of SLC11A1 (formerly NRAMP1) in regulation of signal transduction induced by Toll-like receptor 7 ligands. FEMS Immunol Med Microbiol, 2006. 47(1): p. 138-47.
195. Vallon, R., et al., Serum amyloid A (apoSAA) expression is up-regulated in rheumatoid arthritis and induces transcription of matrix metalloproteinases. J Immunol, 2001. 166(4): p. 2801-7.
196. Thorn, C.F., Z.Y. Lu, and A.S. Whitehead, Regulation of the human acute phase serum amyloid A genes by tumour necrosis factor-alpha, interleukin-6 and glucocorticoids in hepatic and epithelial cell lines. Scand J Immunol, 2004. 59(2): p. 152-8.
197. de Seny, D., et al., Acute-phase serum amyloid a in osteoarthritis: regulatory mechanism and proinflammatory properties. PLoS One, 2013. 8(6): p. e66769.
198. Mwandumba, H.C., et al., Mycobacterium tuberculosis resides in nonacidified vacuoles in endocytically competent alveolar macrophages from patients with tuberculosis and HIV infection. J Immunol, 2004. 172(7): p. 4592-8.
199. Nguyen, N.B., et al., Hepcidin expression and iron transport in alveolar macrophages. Am J Physiol Lung Cell Mol Physiol, 2006. 291(3): p. L417-25.
200. Mulvey, M.R., L.C. Kühn, and D.G. Scraba, Induction of ferritin synthesis in cells infected with Mengo virus. J Biol Chem, 1996. 271(16): p. 9851-7.
201. Bellamy, R., et al., Variations in the NRAMP1 gene and susceptibility to tuberculosis in West Africans. N Engl J Med, 1998. 338(10): p. 640-4.
202. Zhang, W., et al., Variants of the natural resistance-associated macrophage protein 1 gene (NRAMP1) are associated with severe forms of pulmonary tuberculosis. Clin Infect Dis, 2005. 40(9): p. 1232-6.
203. Harada, T., et al., Ferritin selectively suppresses delayed-type hypersensitivity responses at induction or effector phase. Cell Immunol, 1987. 109(1): p. 75-88.
204. Wrighting, D.M. and N.C. Andrews, Interleukin-6 induces hepcidin expression through STAT3. Blood, 2006. 108(9): p. 3204-9.
205. Armitage, A.E., et al., Hepcidin regulation by innate immune and infectious stimuli. Blood, 2011.
206. Haase, V.H., Hypoxic regulation of erythropoiesis and iron metabolism. Am J Physiol Renal Physiol, 2010. 299(1): p. F1-13.

207. Flynn, J.L., et al., IL-12 increases resistance of BALB/c mice to Mycobacterium tuberculosis infection. J Immunol, 1995. 155(5): p. 2515-24.
208. Behar, S.M., et al., Susceptibility of mice deficient in CD1D or TAP1 to infection with Mycobacterium tuberculosis. J Exp Med, 1999. 189(12): p. 1973-80.
209. Sow, F.B., et al., Mycobacterium tuberculosis components stimulate production of the antimicrobial peptide hepcidin. Tuberculosis (Edinb), 2011. 91(4): p. 314-21.
210. Ganz, T., Hepcidin and iron regulation, 10 years later. Blood, 2011. 117(17): p. 4425-33.
211. Rogers, J. and H. Munro, Translation of ferritin light and heavy subunit mRNAs is regulated by intracellular chelatable iron levels in rat hepatoma cells. Proc Natl Acad Sci U S A, 1987. 84(8): p. 2277-81.
212. MacKenzie, E.L., K. Iwasaki, and Y. Tsuji, Intracellular iron transport and storage: from molecular mechanisms to health implications. Antioxid Redox Signal, 2008. 10(6): p. 997-1030.
213. Johnson, E.E., et al., Role of ferroportin in macrophage-mediated immunity. Infect Immun, 2010. 78(12): p. 5099-106.
214. Arezes, J., et al., Hepcidin-induced hypoferremia is a critical host defense mechanism against the siderophilic bacterium Vibrio vulnificus. Cell Host Microbe, 2015. 17(1): p. 47-57.
215. Weiss, G., et al., Iron regulates nitric oxide synthase activity by controlling nuclear transcription. J Exp Med, 1994. 180(3): p. 969-76.
216. Nairz, M., et al., The struggle for iron - a metal at the host-pathogen interface. Cell Microbiol, 2010. 12(12): p. 1691-702.
217. Weiss, G., et al., Iron modulates interferon-gamma effects in the human myelomonocytic cell line THP-1. Exp Hematol, 1992. 20(5): p. 605-10.
218. Fritsche, G., et al., Nramp1-functionality increases iNOS expression via repression of IL-10 formation. Eur J Immunol, 2008. 38(11): p. 3060-7.
219. Masaratana, P., et al., Regulation of iron metabolism in Hamp (-/-) mice in response to iron-deficient diet. Eur J Nutr, 2013. 52(1): p. 135-43.
220. Herbison, C.E., et al., The role of transferrin receptor 1 and 2 in transferrin-bound iron uptake in human hepatoma cells. Am J Physiol Cell Physiol, 2009. 297(6): p. C1567-75.
221. Cronjé, L., et al., Iron and iron chelating agents modulate Mycobacterium tuberculosis growth and monocyte-macrophage viability and effector functions. FEMS Immunol Med Microbiol, 2005. 45(2): p. 103-12.
222. Trousseau, A., True or false chlorosis, in Lectures in Clinical Medicine. 1872, Lindsay and Blakiston: Philadelphia, PA. p. 95-117.

223. Kasvosve, I., et al., African iron overload. Acta Clin Belg, 2000. 55(2): p. 88-93.
224. Nutrition, S.o.L.A. and B.o.A. Committee on Animal Nutrition, National Research Council, Nutrient requirements of laboratory animals. Fourth revised edition ed. Nutrient requirements of laboratory animals. 1995, Washington, D.C.: National Academy Press. 190.
225. Douvas, G.S., M.H. May, and A.J. Crowle, Transferrin, iron, and serum lipids enhance or inhibit Mycobacterium avium replication in human macrophages. J Infect Dis, 1993. 167(4): p. 857-64.
226. Zwilling, B.S., et al., Role of iron in Nramp1-mediated inhibition of mycobacterial growth. Infect Immun, 1999. 67(3): p. 1386-92.
227. Gomes, M.S., et al., Effects of iron deprivation on Mycobacterium avium growth. Tuber Lung Dis, 1999. 79(5): p. 321-8.
228. Marsay, L., et al., Mycobacterial growth inhibition in murine splenocytes as a surrogate for protection against Mycobacterium tuberculosis (M. tb). Tuberculosis (Edinb), 2013. 93(5): p. 551-7.
229. Theil, E.C., Regulation of ferritin and transferrin receptor mRNAs. J Biol Chem, 1990. 265(9): p. 4771-4.
230. Rao, K., et al., Transcriptional regulation by iron of the gene for the transferrin receptor. Mol Cell Biol, 1986. 6(1): p. 236-40.
231. Pantopoulos, K., Iron metabolism and the IRE/IRP regulatory system: an update. Ann N Y Acad Sci, 2004. 1012: p. 1-13.
232. Urieli-Shoval, S., R.P. Linke, and Y. Matzner, Expression and function of serum amyloid A, a major acute-phase protein, in normal and disease states. Curr Opin Hematol, 2000. 7(1): p. 64-9.
233. Ganapathi, M.K., et al., Effect of combinations of cytokines and hormones on synthesis of serum amyloid A and C-reactive protein in Hep 3B cells. J Immunol, 1991. 147(4): p. 1261-5.
234. Ito, A., et al., Augmentation of type I IL-1 receptor expression and IL-1 signaling by IL-6 and glucocorticoid in murine hepatocytes. J Immunol, 1999. 162(7): p. 4260-5.
235. Nairz, M., et al., Interferon-gamma limits the availability of iron for intramacrophage Salmonella typhimurium. Eur J Immunol, 2008. 38(7): p. 1923-36.
236. Krijt, J., et al., Effect of iron overload and iron deficiency on liver hemojuvelin protein. PLoS One, 2012. 7(5): p. e37391.
237. Ganz, T., Hepcidin, a key regulator of iron metabolism and mediator of anemia of inflammation. Blood, 2003. 102(3): p. 783-8.
238. Marro, S., et al., Heme controls ferroportin1 (FPN1) transcription involving Bach1, Nrf2 and a MARE/ARE sequence motif at position -7007 of the FPN1 promoter. Haematologica, 2010. 95(8): p. 1261-8.

239. Dhople, A.M., M.A. Ibanez, and T.C. Poirier, Role of iron in the pathogenesis of Mycobacterium avium infection in mice. Microbios, 1996. 87(351): p. 77-87.
240. Gomes, M.S. and R. Appelberg, Evidence for a link between iron metabolism and Nramp1 gene function in innate resistance against Mycobacterium avium. Immunology, 1998. 95(2): p. 165-8.
241. Lepper, A.W., R.G. Jarrett, and V.M. Lewis, The effect of different levels of iron intake on the multiplication of Mycobacterium paratuberculosis in C57 and C3H mice. Vet Microbiol, 1988. 16(4): p. 369-83.
242. Mainou-Fowler, T. and J.H. Brock, Effect of iron deficiency on the response of mouse lymphocytes to concanavalin A: the importance of transferrin-bound iron. Immunology, 1985. 54(2): p. 325-32.
243. Walter, T., et al., Iron, anemia, and infection. Nutr Rev, 1997. 55(4): p. 111-24.
244. Armitage, A.E. and E. Moran, HIV-Associated Tuberculosis: Does the Iron-Regulatory Hormone Hepcidin Connect Anemia With Poor Prognosis? J Infect Dis, 2015.
245. Subbian, S., et al., Vaccination with an attenuated ferritin mutant protects mice against virulent Mycobacterium tuberculosis. Journal of Immunology Research, 2015. 2015: p. 12.